

**AD-A255 071**



WL-TR-92-3009



**EVALUATION OF ALTERNATIVES FOR INCREASING A-7D  
REARWARD VISIBILITY**

G. J. Frank  
G. J. Stenger  
University of Dayton Research Institute  
300 College Park  
Dayton, Ohio 45469-0110

**DTIC**  
**ELECTE**  
**SEP 08 1992**  
**S A D**

April 1992

Interim Report for Period Aug 88 to May 90

Approved for public release; distribution is unlimited.

FLIGHT DYNAMICS DIRECTORATE  
WRIGHT LABORATORY  
AIR FORCE SYSTEMS COMMAND  
WRIGHT-PATTERSON AIR FORCE BASE, OHIO 45433-6553

**92 9 02 257**

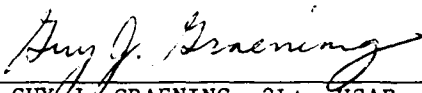
105400 **92-24548**  
  
15498

## NOTICE

When Government drawings, specifications, or other data are used for any purpose other than in connection with a definitely Government-related procurement, the United States Government incurs no responsibility or any obligation whatsoever. The fact that the government may have formulated or in any way supplied the said drawings, specifications, or other data, is not to be regarded by implication, or otherwise in any manner construed, as licensing the holder, or any other person or corporation; or as conveying any rights or permission to manufacture, use, or sell any patented invention that may in any way be related thereto.

This report is releasable to the National Technical Information Service (NTIS). At NTIS, it will be available to the general public, including foreign nations.

This technical report has been reviewed and is approved for publication.



GUY J. GRAENING, 2Lt, USAF  
Project Engineer



RALPH J. SPEELMAN, Chief  
Aircrew Protection Branch  
Vehicle Subsystems Division



RICHARD E. COLCLOUGH, JR.  
Chief  
Vehicle Subsystems Division

If your address has changed, if you wish to be removed from our mailing list, or if the addressee is no longer employed by your organization please notify WL/FIVR, WPAFB, OH 45433-6553 to help us maintain a current mailing list.

Copies of this report should not be returned unless return is required by security considerations, contractual obligations, or notice on a specific document.

UNCLASSIFIED

SECURITY CLASSIFICATION OF THIS PAGE

REPORT DOCUMENTATION PAGE				Form Approved OMB No. 0704-0188	
1a. REPORT SECURITY CLASSIFICATION UNCLASSIFIED			1b. RESTRICTIVE MARKINGS		
2a. SECURITY CLASSIFICATION AUTHORITY			3. DISTRIBUTION / AVAILABILITY OF REPORT Approved for public release; distribution is unlimited.		
2b. DECLASSIFICATION / DOWNGRADING SCHEDULE					
4. PERFORMING ORGANIZATION REPORT NUMBER(S) UDR-TR-90-121			5. MONITORING ORGANIZATION REPORT NUMBER(S) WL-TR-92-3009		
6a. NAME OF PERFORMING ORGANIZATION University of Dayton Research Institute		6b. OFFICE SYMBOL (If applicable)	7a. NAME OF MONITORING ORGANIZATION Flight Dynamics Dir. (WL/FIVR) Wright Laboratory		
6c. ADDRESS (City, State, and ZIP Code) 300 College Park Dayton OH 45469-0110			7b. ADDRESS (City, State, and ZIP Code) Wright-Patterson AFB OH 45433-6553		
8a. NAME OF FUNDING / SPONSORING ORGANIZATION		8b. OFFICE SYMBOL (If applicable)	9. PROCUREMENT INSTRUMENT IDENTIFICATION NUMBER F33615-84-C-3404		
8c. ADDRESS (City, State, and ZIP Code)			10. SOURCE OF FUNDING NUMBERS		
			PROGRAM ELEMENT NO. 64212F	PROJECT NO. 1926	TASK NO. 01
11. TITLE (Include Security Classification) EVALUATION OF ALTERNATIVES FOR INCREASING A-7D REARWARD VISIBILITY					
12. PERSONAL AUTHOR(S) G. J. Frank and G. J. Stenger					
13a. TYPE OF REPORT Interim		13b. TIME COVERED FROM 88AUG TO 90MAY	14. DATE OF REPORT (Year, Month, Day) 1992 April		15. PAGE COUNT 154
16. SUPPLEMENTARY NOTATION					
17. COSATI CODES			18. SUBJECT TERMS (Continue on reverse if necessary and identify by block number)		
FIELD	GROUP	SUB-GROUP			
19. ABSTRACT (Continue on reverse if necessary and identify by block number) Experience has shown that the present A-7D canopy provides poor rearward visibility for defensive maneuvering against an adversary behind the A-7. Alternatives were identified and evaluated for increasing rearward visibility, including: increasing the length of the canopy transparency; adding external mirrors; modifying the existing internal mirrors; using a refractive lens; and altering the canopy profile. This evaluation showed that increasing the transparency length would provide the greatest increase in rearward visibility with the least distortion. The feasibility of extending the transparency was analyzed using a finite element model which showed that the transparency could be extended without increasing the maximum stress levels. Advanced composites were used to design an alternate canopy frame to allow the transparency to be extended by five inches. This frame was designed to be as stiff and strong as the current aft frame. The design required no modification to the surrounding fuselage and did not change the overall canopy weight.					
20. DISTRIBUTION / AVAILABILITY OF ABSTRACT <input checked="" type="checkbox"/> UNCLASSIFIED/UNLIMITED <input type="checkbox"/> SAME AS RPT. <input type="checkbox"/> DTIC USERS			21. ABSTRACT SECURITY CLASSIFICATION Unclassified		
22a. NAME OF RESPONSIBLE INDIVIDUAL Russell E. Urzi			22b. TELEPHONE (Include Area Code) (513) 229-2916		22c. OFFICE SYMBOL WL/FIVR

DD Form 1473, JUN 86

Previous editions are obsolete.

SECURITY CLASSIFICATION OF THIS PAGE

UNCLASSIFIED

## FOREWORD

The work documented in this report was performed by the Aerospace Mechanics Division of the University of Dayton Research Institute, Dayton, Ohio, under contract no. F33615-84-C-3404 for the Flight Dynamics Laboratory, Wright-Patterson Air Force Base, Ohio. Air Force administrative direction and technical support was provided by Capt. Paul J. Kolodziejski and Lt. Duncan Dversdall, WL/FIVR.

The work described herein was conducted during the period August 1988 to May 1990. Project supervision and technical assistance were provided through the Aerospace Mechanics Division of the University of Dayton Research Institute with Dale H. Whitford, Supervisor, and Blaine S. West, Head, Structures Group. Principal investigators for this program were Gregory J. Stenger and Geoffrey J. Frank. The authors wish to thank Lt. Dversdall for his assistance and insight in this project.

Accession For:	
NTIS CRA&I	<input checked="checked" type="checkbox"/>
DTIC TAB	<input type="checkbox"/>
Unannounced	<input type="checkbox"/>
Justification	
By	
Distribution /	
Availability Codes	
Dist	Avail and/or Special
A-1	

DTIC QUALITY INSPECTED 1

## TABLE OF CONTENTS

SECTION	PAGE
1 INTRODUCTION AND SUMMARY	1
1.1 Design Guidelines and Constraints	1
1.2 Summary	1
2 DEFINITION AND EVALUATION OF ALTERNATIVES FOR INCREASING REARWARD VISIBILITY	3
2.1 Technical Approach	3
2.2 Evaluation of Alternatives	6
2.2.1 Canopy Acrylic Extension	6
2.2.2 Mirrors	14
2.2.3 Refractive Lenses	19
2.2.4 Bubbled Canopy	28
2.3 Recommended Alternative	28
3 DETAILED DESIGN AND ANALYSIS OF SELECTED ALTERNATIVE	31
3.1 Canopy Stress Evaluation	31
3.1.1 Model Development	31
3.1.2 Model Validation	42
3.1.3 Analysis of Extended Transparency	52
3.2 Modified Canopy Aft Frame Design	62
3.3 Inertial Property Evaluation	67
4 CONCLUSIONS AND RECOMMENDATIONS	72
REFERENCES	74
APPENDIX A: STRUCTURAL ANALYSIS OF CANOPY AFT FRAME	76
APPENDIX B: MODIFIED CANOPY AFT FRAME DRAWINGS	118

## LIST OF ILLUSTRATIONS

FIGURE		PAGE
1	Profile of Original Canopy	4
2	Region Blocked by Aft Arch of Original Canopy	5
3	Altered Viewing Angle in Vertical Plane Due to Elongation of Canopy	7
4	View Angle in Horizontal Plane as Canopy Length is Extended	8
5	Altered View Angle in Horizontal Plane Due to Elongation of Canopy	9
6	Sight Angles Available from Design Eye	11
7	Sight Angles Available for 3-inch Lateral Head Movement	11
8	Sight Angles Available for 6-inch Lateral Head Movement	12
9	Sight Angles Available for 9-inch Lateral Head Movement	12
10	Reduction Due to Lateral Head Motion of Area Blocked from View	13
11	Reduction in Blocked Area as Canopy is Extended	13
12	Location of External Mirror on F-4 Cockpit	16
13	View Using External Mirror on F-4 Cockpit	16
14	Existing and Proposed Overhead Mirrors	17
15	Intersection of Cutting Plane and Canopy Surface for Analysis of Mirrors	18
16	Sight Lines Available Using Existing Internal Mirror and Proposed External Mirror	20
17	Geometry Used for Calculation of Refracted Line of Sight	22
18	Lens with Varying Angle	22

# LIST OF ILLUSTRATIONS, continued

FIGURE		PAGE
19	Altered View Angle in Vertical Plane Due to 2.0 Degree Lens on Original Canopy	23
20	Sight Angles for Refractive Lens on Original Canopy ( $\mu_1=1.6$ , $b=2^\circ$ )	25
21	Altered View Angle in Vertical Plane Due to 10 Deg. Canopy Bubble with 5 Deg. Lens	26
22	Sight Angles for Refractive Lens on Bubbled Canopy ( $\mu_1=1.5$ , $b=5^\circ$ )	27
23	Concept for Modification of Canopy to Raise Design Eye Above Aft Arch	29
24	Geometry of Elements Used in MAGNA Model	32
25	Profile of Quadratic Shell Elements on Right-Hand Side of Initial Canopy Model	33
26	Edge Conditions for A-7 Canopy	34
27	Beam Elements Used to Approximate Boundary Conditions for Canopy Acrylic	36
28	Cross-Sections of Canopy Frame for MAGNA Model	37
29	Pressure Distribution for Critical Load Case	39
30	von Mises Stress Distribution on Right Side of Interior Surface of Initial Model of Canopy	43
31	von Mises Stress Distribution on Right Side of Exterior Surface of Initial Model of Canopy	44
32	Shell Elements for the Revised Model of Canopy	46
33	Stress Distribution Perpendicular to the Right Side Rail	48
34	Stress Distribution Perpendicular to Forward Former	49
35	Stress Distribution Perpendicular to Aft Former	49

# LIST OF ILLUSTRATIONS, continued

FIGURE		PAGE
36	von Mises Stress Distribution on Right Side of Interior Surface of Revised Model of Canopy	50
37	von Mises Stress Distribution on Right Side of Exterior Surface of Revised Canopy	51
38	Stress Distribution Perpendicular to Right Side Rail on Interior Surface	54
39	Stress Distribution Perpendicular to Aft Former on Inner Surface	55
40	von Mises Stress on Inner Surface of Canopy - Reduced Aft Frame	56
41	von Mises Stress on Outer Surface of Canopy - Reduced Aft Frame	57
42	von Mises Stress on Inner Surface of Canopy - Clamped Along Aft Edge	58
43	von Mises Stress on Outer Surface of Canopy - Clamped Along Aft Edge	59
44	von Mises Stress on Inner Surface of Canopy - Clamped Lower, Free Upper Aft Edge	60
45	von Mises Stress on Outer Surface of Canopy - Clamped Lower, Free Upper Aft Edge	61
46	Existing Aft Canopy Frame	63
47	Modified Aft Canopy Frame	65
48	Sign Convention for Inertias	70
49	Recommended Canopy Aft Arch for 5-inch Extension of Transparency	73
A-1	Models of Principal Canopy Structure	77
A-2	Cross-Sections on Model of Existing Structure	78



# LIST OF ILLUSTRATIONS, continued

FIGURE		PAGE
A-3	Cross-Sections of Modified Structure Model	80
A-4a	Displacements Due to Load Case 1	84
A-4b	Displacements Due to Load Case 2	85
A-4c	Displacements Due to Load Case 3	86
A-4d	Displacements Due to Load Case 4	87
A-4e	Displacements Due to Load Case 5	88
A-4f	Displacements Due to Load Case 6	89
A-4g	Displacements Due to Load Case 7	90
A-4h	Displacements Due to Load Case 8	91
A-4i	Displacements Due to Load Case 9	92
A-5	Symbols Used in Stress Calculation	95
A-6	Cross-Sections of Lower Pressure Panels	98
A-7	Displacements in Lower Composite Panel Under 5-psi Pressure Load	99
A-8	Longitudinal Stress in Outer Ply of Panel for 5-psi Pressure Load	100
A-9	Geometry and Boundary Conditions of Upper Composite Panel Model	102
A-10	Deflections of Upper Composite Panel for 5-psi Pressure Load	103
A-11	Longitudinal Stress in Outer Ply of Composite Panel for 5-psi Pressure Load	104
A-12	Deflections of Upper Composite Panel for 5-psi Pressure and -25-lb/in Edge Load	106

LIST OF ILLUSTRATIONS, continued

FIGURE		PAGE
A-13	Longitudinal Stress in Outer Ply of Composite Panel for 5-psi Pressure and -25-lb/in Edge Load	107
A-14	Serrated Pivot Bolt Adapter Joint	108
A-15	Analytic Model of Pivot Bolt Adapter Joint	110
A-16	Geometry and Materials for FE Model of Pivot Bolt Adapter Joint	113
A-17	Intersection of Cross-Tube and Side-Tube	114
A-18	Models for Analysis of Cross-Tube and Side-Tube Intersection	116

## LIST OF TABLES

TABLE		PAGE
1	Locations of Strain Gages in Flight Test	42
2	Stresses Normal to Side Rail at Strain Gage Locations (initial model)	45
3	Stresses Normal to Side Rail at Strain Gage Locations (revised model)	47
4	Weight of Modified Frame Components	68
5	Mass Properties of Existing and Modified Canopies	69
A.1	Material Properties	82
A.2	Load Cases	83
A.3	Summary of Displacements	93
A.4	Strength Comparison	96

## NOMENCLATURE

A	Area ( $\text{in}^2$ )
C	Pressure coefficient
E	Young's modulus ( $\text{lbf/in}^2$ )
F	Force ( $\text{lbf}$ )
G	Shear modulus ( $\text{lbf/in}^2$ )
I	Mass moment of inertia ( $\text{lbm} \cdot \text{in}^2$ ) or area moment of inertia ( $\text{in}^4$ )
J	Polar moment of inertia ( $\text{in}^4$ )
L	Length ( $\text{in}$ )
M	Moment ( $\text{in-lbf}$ ) or moment resultant ( $\text{in-lbf/in}$ )
N	In-plane force resultant ( $\text{lbf/in}$ )
S	Allowable strength ( $\text{lbf/in}^2$ )
T	Torque ( $\text{in} \cdot \text{lbf}$ )
U	Translation displacement ( $\text{in}$ )
V	Volume fraction or shear load ( $\text{lbf}$ )
a,b,c,d,g	Angles (rads) or intermediate results of equations
d	Diameter
f	Area fraction
k	Stress concentration factor
q	Dynamic pressure ( $\text{lbf/in}^2$ )
t	Thickness ( $\text{in}$ )
w	Width ( $\text{in}$ )
$\alpha$	Angular acceleration ( $\text{rad/s}^2$ ) or coefficient of thermal expansion ( $1/^\circ\text{F}$ )
$\phi$	Rotation displacement ( $\text{rad}$ )

$\nu$	Poisson's ratio
$\mu$	Index of refraction
$\rho$	Mass density (lbm/in <sup>3</sup> )
$\tau$	Shear stress (lbf/in <sup>2</sup> )
$\sigma$	Axial Stress (lbf/in <sup>2</sup> )
$\Delta P$	Pressure differential (lbf/in <sup>2</sup> )
$\gamma$	Shear strain (lbf/in <sup>2</sup> )

#### SUBSCRIPTS/SUPERSCRIPTS:

C	Compressive
T	Tensile
b	Area blocked from view
c	Centroidal
e	Elastic
f	Volume fraction based on percent fibers
i	Interlaminar shear
p	Plastic
s	Shear
x,y,z	Direction for variable definition
xx,yy,xy,etc.	Axes for property definition
$\ell$	Area bounded by thin-wall beam

## SECTION 1

### INTRODUCTION AND SUMMARY

USAF experience has shown that the present A-7D canopy provides insufficient rearward visibility for effective defensive maneuvering when engaged by an adversary behind the A-7. In 1987, as a consequence of a projected extension of A-7 service life, the National Guard Bureau requested the assistance of WRDC/FIVR in studying the application of advanced technology to this problem. Of particular interest was increasing the transparency length.

#### 1.1 DESIGN GUIDELINES AND CONSTRAINTS

The design guidelines and constraints established for the evaluation of A-7D alternatives and for determining the design details of the selected alternative were:

- maximizing the increase in rearward visibility in the A-7D aircraft as measured by the reduction in area blocked from the pilot's view,

- minimizing the modifications to the existing aircraft structure for ease of implementation and low cost,

- maintaining the current weight of the canopy assembly, and

- minimizing distortion in the area of increased visibility.

#### 1.2 SUMMARY

Alternatives identified for increasing rearward visibility for the A-7D were:

- Increasing the length of the canopy transparency,

- Adding external mirrors,

- Modifying the existing internal mirrors,

- Using a refractive lens around the aft portion of the transparency, and

- Altering (bubbling out) the canopy profile.

The concepts were evaluated to determine the reduction in the region obstructed from the pilot's view aft of the aircraft. Distortion of the pilot's view and ease of implementation were also considered. This evaluation showed that, of the alternatives considered, increasing the length of

the transparency would provide the greatest increase in rearward visibility with the least distortion.

A detailed design and analysis of the selected alternative was performed. The feasibility of extending the transparency was analyzed using a finite element model of the canopy. Stresses in the transparency were analyzed for the highest operational pressure load. Stress results for a baseline model of the existing canopy were validated with experimental test data. Stress results for canopy models with extended transparencies were compared to the baseline results to determine the effect of lengthening the transparency on the maximum stress levels. The models showed that the transparency could be extended without increasing the maximum stress levels.

An alternate canopy frame was designed to allow the transparency to be extended by 5 inches. This frame was designed to be as stiff and strong as the current aft frame. Advanced composites were used in the design to offset the weight increase of the lengthened transparency. The design used the existing canopy side rails and forward arch and required no modification to the surrounding fuselage.

## SECTION 2

### DEFINITION AND EVALUATION OF ALTERNATIVES FOR INCREASING REARWARD VISIBILITY

Several alternatives for increasing the rearward visibility of the A-7D aircraft were identified. These alternatives were:

1. increasing the length of the canopy transparency,
2. adding external mirrors (such as on the F-4),
3. modifying the internal mirrors,
4. using refractive lenses (currently used on buses),
5. altering the canopy profile (like that of the A-10, F-16, etc.).

The alternatives were evaluated to determine the reduction in the region obstructed from the pilot's view. Distortion of the pilot's view and ease of implementation were also considered.

#### 2.1 TECHNICAL APPROACH

To facilitate definition of the region blocked from the pilot's view, a three-dimensional CAD model of the canopy surface was generated. To simplify the comparison, evaluations were performed only in the region above a horizontal plane through the "design eye" position (waterline 130.1). The design eye position is shown in Figure 1. For direct view the wings enter the field of view just below waterline 130. Limiting the analysis to the region above the horizontal plane excluded the area visible to the pilot below the wings. However, the majority of the field of view which would be of interest to the pilot was evaluated. The "design eye" shown in Figure 1 was taken from assembly drawings of the canopy [1]. This position was originally used to position the mirrors in an area already blocked by the windshield and canopy arch.

Two measures were used to compare the region blocked from the pilot's view. The first is given by the angle between the longitudinal axis of the aircraft and the line of sight closest to this axis for a given configuration. For comparison of different alternatives, this angle can be calculated as a function of the distance around the canopy aft arch to give a description of the rearward visibility in different directions. The lines of sight are illustrated in Figure 2 along with the angle up from the waterline at the centerline of the aft arch. A measure of the



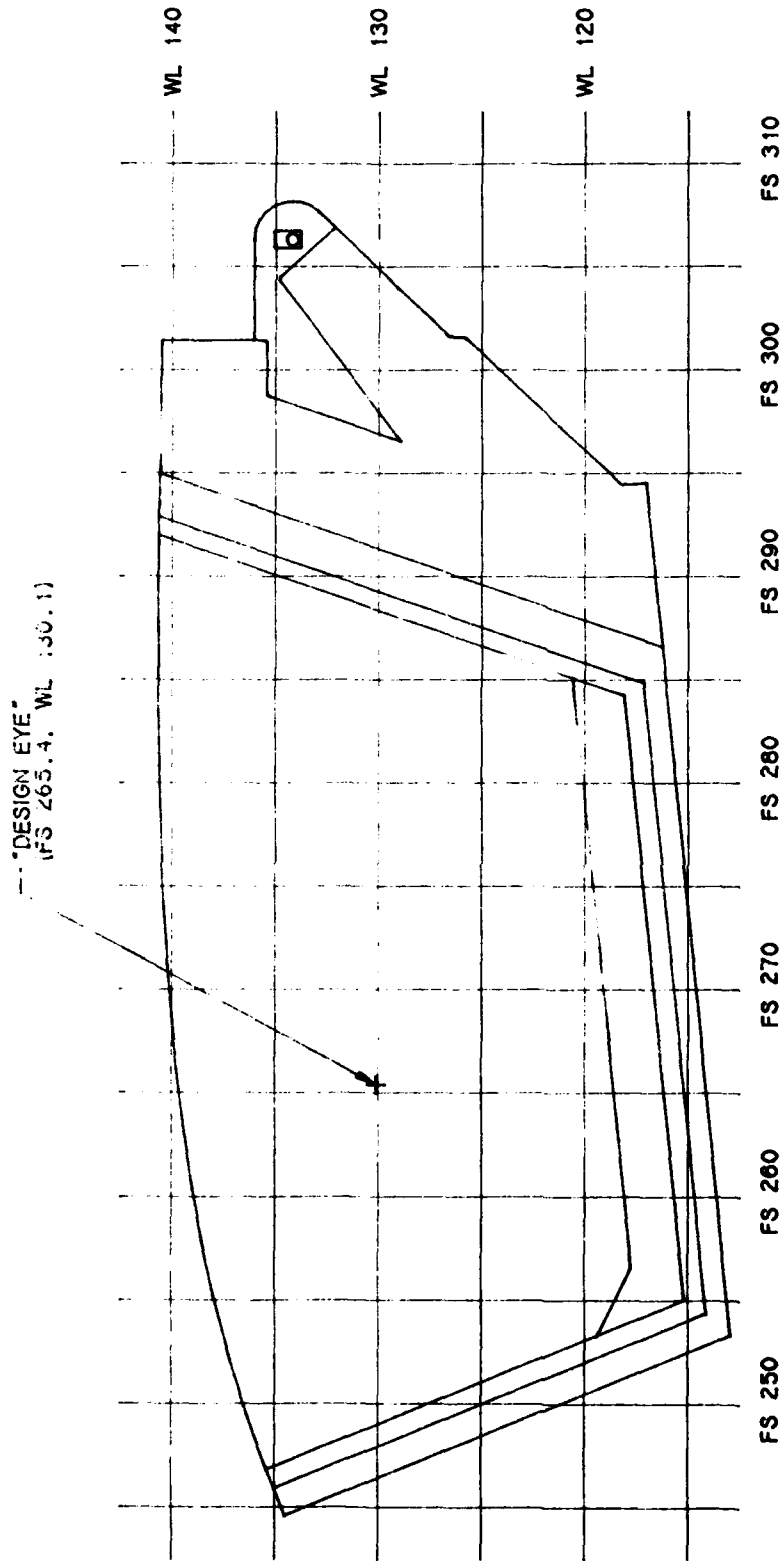


Figure 1. Profile of Original Canopy.

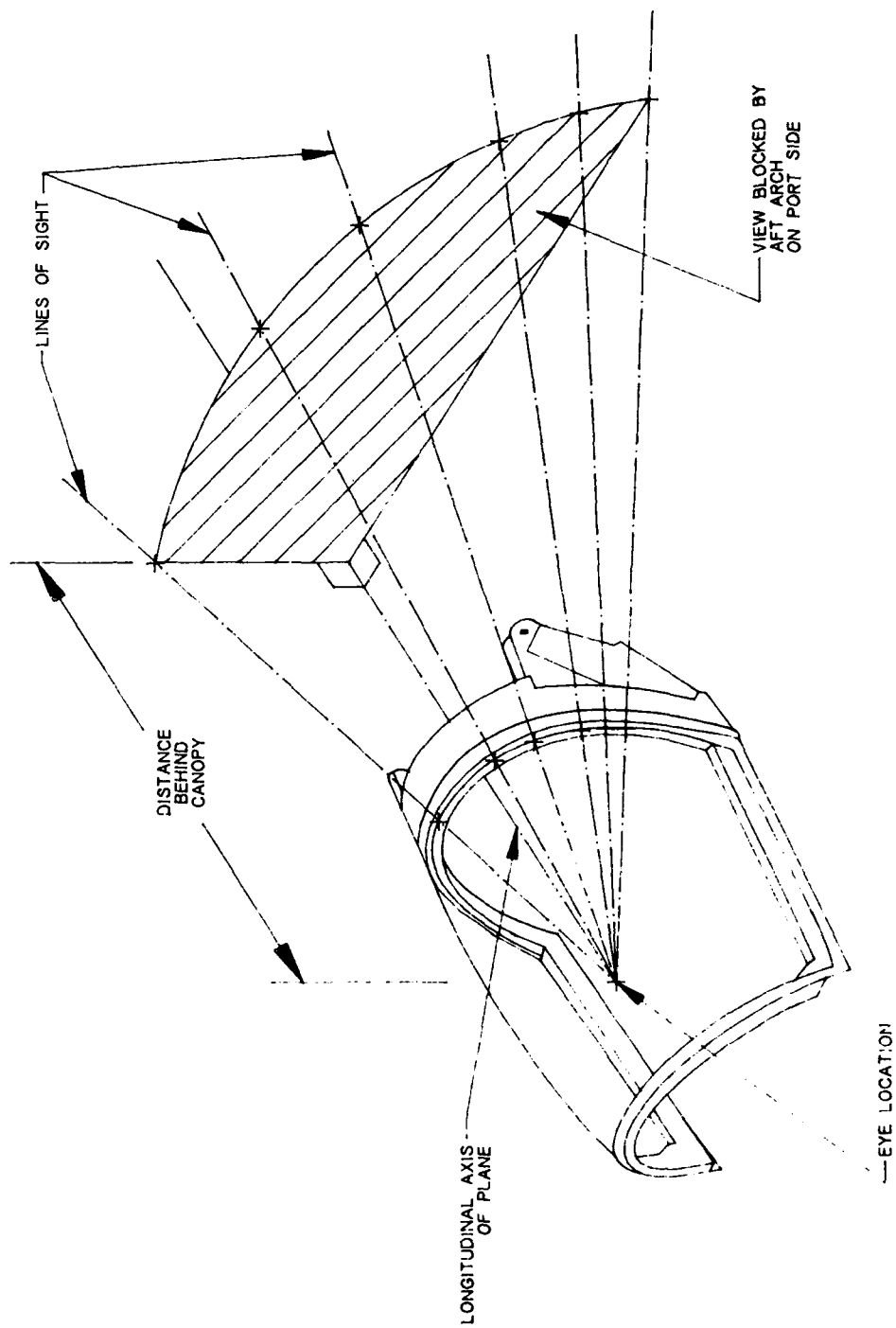


Figure 2. Region Blocked by Aft Arch of Original Canopy.

overall effect of each modification is the total area blocked by the aft arch. The area is determined by integrating the area swept out by the lines of sight at a given distance aft of the aircraft. This area is shown in Figure 2. The blocked area is proportional to the square of the distance from the aircraft.

The amount of view distortion and ease of implementation for each of the alternatives were evaluated on a qualitative basis only. Evaluation of distortion considered the effects of both manufacturing tolerances (such as nonparallel transparency surfaces) and properties of the system (such as bending of light by curved mirrors or refracting lenses). Evaluation of ease of implementation considered the amount of modification to the aircraft required to install the system.

## 2.2 EVALUATION OF ALTERNATIVES

### 2.2.1 Canopy Acrylic Extension

The effect of increasing the length of the transparency along the existing mold-line of the aircraft was investigated. To accomplish this extension, removal of some or all of the aft arch of the canopy frame would be required. The 6-inch width of the existing aft arch [1] formed the limit of the length by which the canopy transparent area could be extended without requiring modifications of the fuselage. This investigation was limited to this 6-inch increase in the canopy length.

Rearward visibility is greatly affected by the position of the pilot's "eye" in the cockpit. Although no data on the location of the eye for rearward view was available, the pilot's eye position must move laterally to allow the pilot to see past the headrest. The eye will also shift aft slightly when the pilot turns his head, but this type of motion affects rearward visibility only slightly. For comparison of designs involving direct view through the aft portion of the transparency, only the effect of lateral motion of the eye position was considered.

Figures 3 through 5 show the effect of extension of the transparency on the angle between the centerline of the aircraft and the pilot's line of sight. In these figures the lines representing the aft edge of the transparency in the original and extended configurations are shown. Figure 3 shows the effect of extending the canopy for lines of sight in the vertical plane. The figure shows that a 6-inch increase in the transparency length would result in a reduction from 21.5° to 17.9° of the angle blocked from view, a reduction of 17 percent.

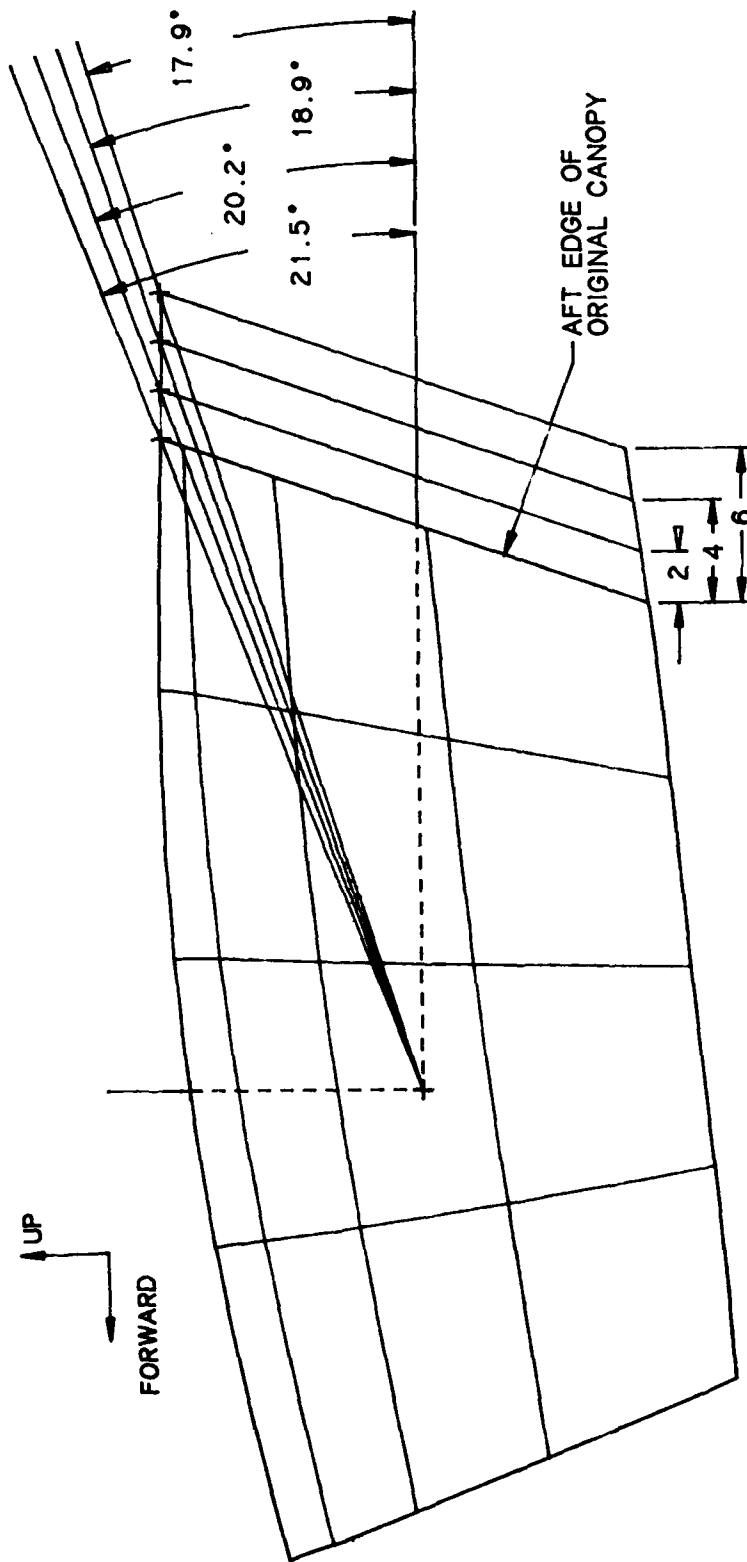


Figure 3. Altered Viewing Angle in Vertical Plane due to Elongation of Canopy (Viewpoint is Design Eye).

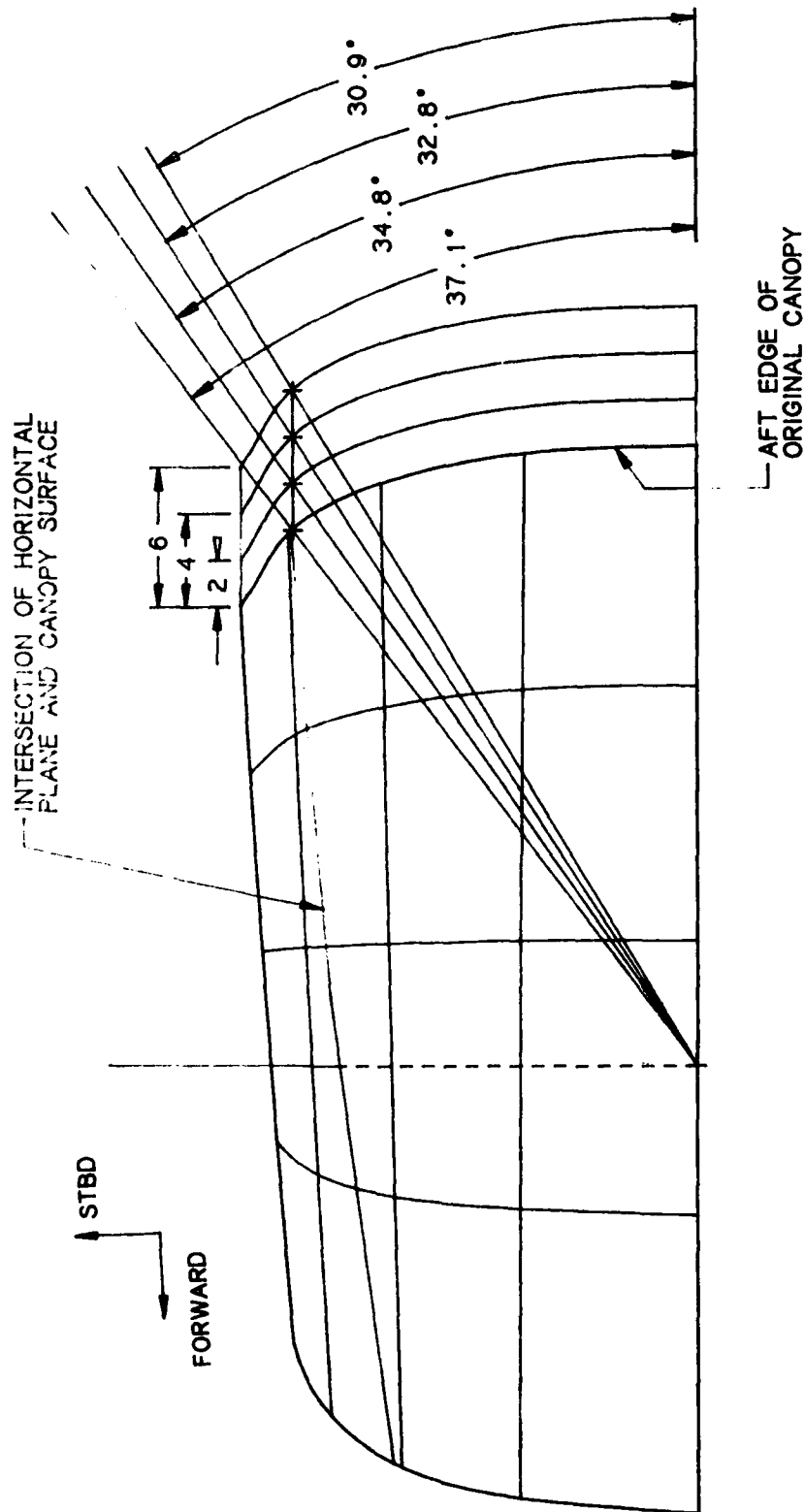


Figure 4. View Angle in Horizontal Plane as Canopy Length is Extended (Viewpoint is Design Eye).

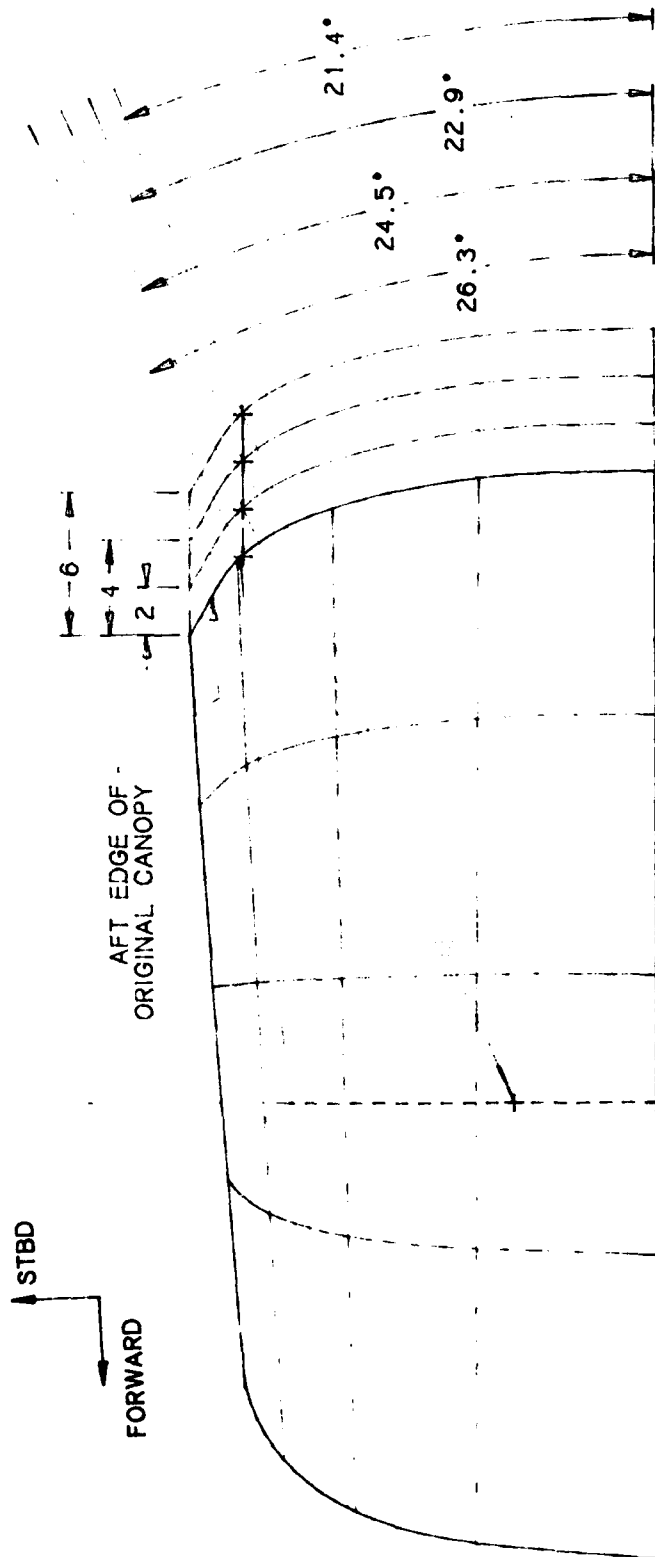


Figure 5. Altered View Angle in Horizontal Plane Due to Elongation of Canopy  
(Viewpoint is Displaced 6 inches Laterally from Design Eye).

Figures 4 and 5 show the change in the field of view in a horizontal plane at waterline 130.1 due to changes in canopy length. Comparison of the two figures shows the effect of lateral motion of the pilot's eye position on the angle blocked by the aft arch. For the original acrylic length, the 6-inch lateral displacement of the eye position shown in Figure 5 reduces the blocked angle to  $26.3^\circ$ , compared to  $37.1^\circ$  for the measurement from a centerline eye position in Figure 4. Similar improvements are seen by comparing angles in the two figures for extended configurations of the canopy.

Reduction in blocked angle due to increased canopy length at a given eye position is shown in Figures 6 through 9. These figures are based on the angle between the line of sight and the longitudinal axis of the aircraft for six positions around the aft arch. These points were distributed around one side of the aft arch from the canopy centerline to waterline 130.1. Measuring around the aft edge of the canopy, it is 22 inches from the centerline to this waterline. A polynomial curve was used to interpolate the distinct points.

Data presented on each figure show that there is a fairly constant decrease in blocked angle for a given amount of canopy extension, regardless of the eye position. Comparison of the four figures shows that there is a substantial reduction in sight angle blocked by the aft arch as the pilot moves his head further to the side. This is especially apparent for sight lines near the horizontal (20 or so inches around the aft edge of the canopy).

The figures show that the angle blocked for viewing toward the centerline increases as the eye location moves laterally from the centerline design eye. However, to see directly aft from a position which is offset from the canopy centerline, one would not look back across the centerline of the arch. Instead, one would look at a position at the aft edge of the acrylic which is also offset from the centerline of the canopy. The vertical dotted lines on Figures 7 through 9 show the position on the aft arch which is directly aft of the eye location used to generate the data in each figure. The portions of the curves to the left of these dotted lines lie in a region which the pilot would not use when looking aft. Therefore only the regions to the right of the dotted lines should be used for comparison. This shows that the visibility increases continually as the eye moves laterally from the centerline.

The total area blocked by the aft arch, as described in Section 2.1, was also calculated as a function of transparency length and eye position. Figure 10 shows the blocked area  $A_b$  as a function of eye location for the current canopy transparency length. The area  $A_b$

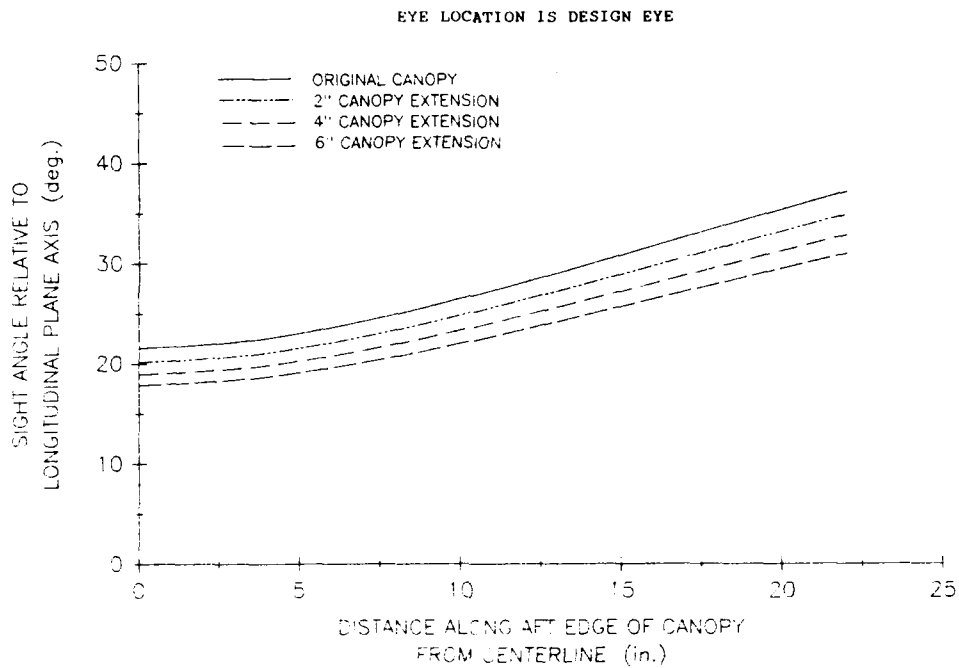


Figure 6. Sight Angles Available from Design Eye.

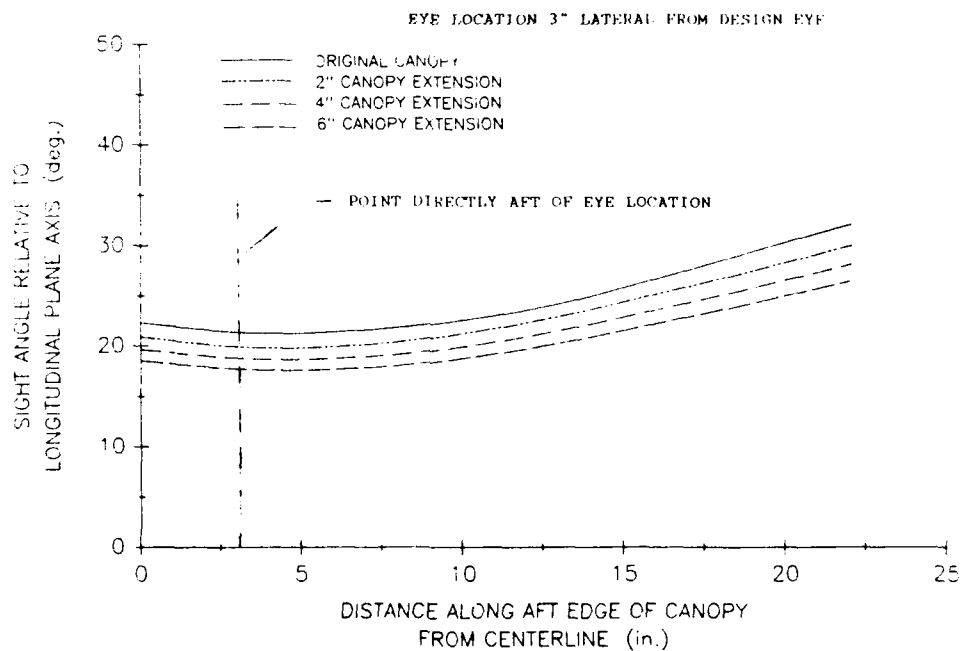


Figure 7. Sight Angles Available for 3-inch Lateral Head Movement.



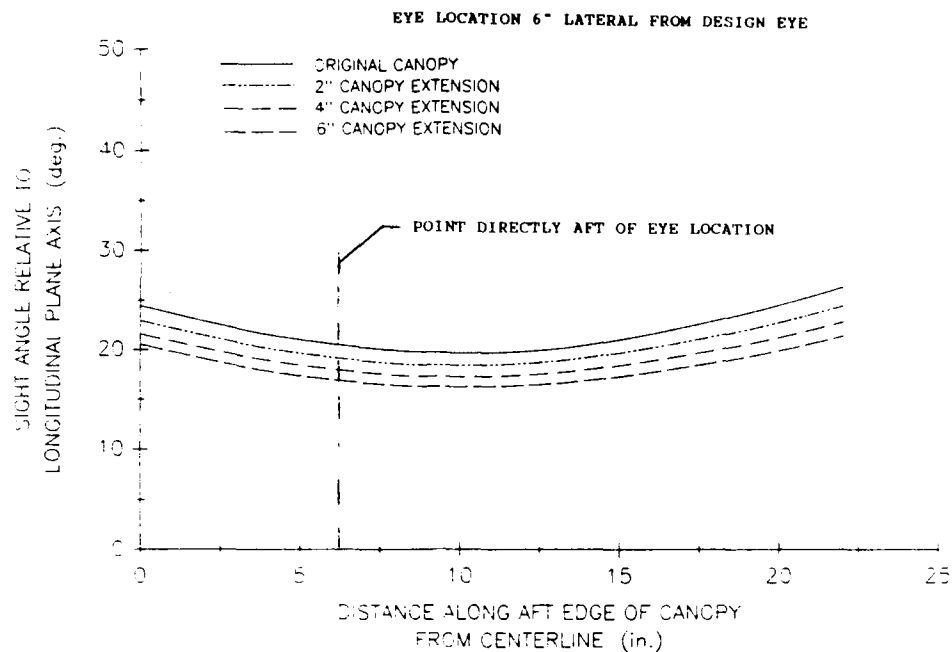


Figure 8. Sight Angles Available for 6-inch Lateral Head Movement.

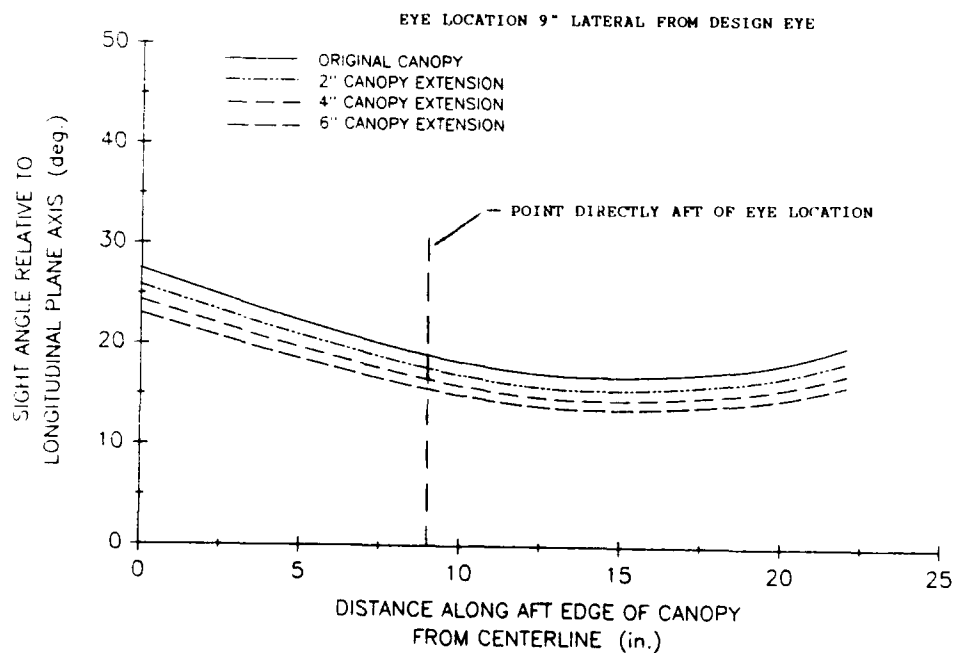


Figure 9. Sight Angles Available for 9-inch Lateral Head Movement.

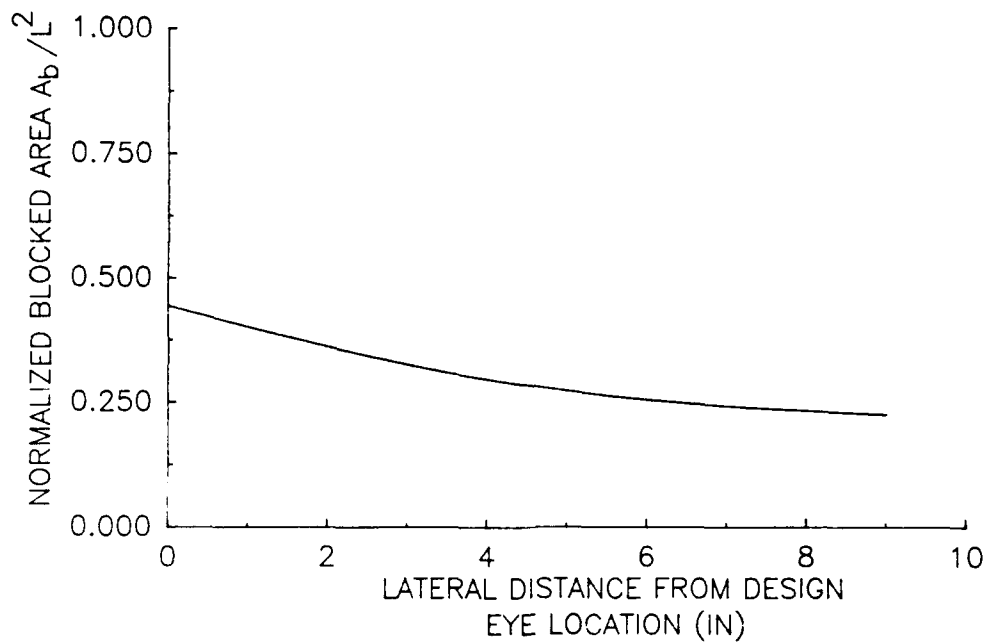


Figure 10. Reduction due to Lateral Head Motion of Area Blocked from View.

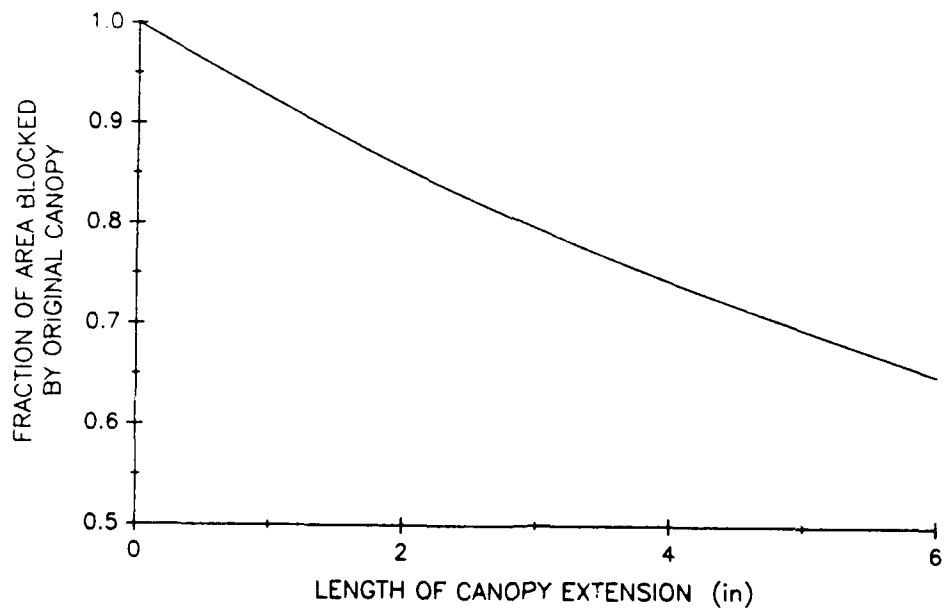


Figure 11. Reduction in Blocked Area as Canopy is Extended.

in the figure has been normalized by the square of the distance  $L$  between the aircraft and the region being viewed. The figure shows that lateral motion of the eye of 9 inches decrease the blocked area by half. Figure 11 shows the fraction of blocked area  $f$  as a function of canopy length. The fraction of blocked area was determined as the ratio of blocked area for the extended canopy to the blocked area for the original canopy. For a given increase in canopy length, the reduction in total blocked area is almost independent of eye position. The total area  $A$  which cannot be seen aft of the aircraft for a given canopy length, eye position, and distance aft of the aircraft is

$$A = f_b \cdot \frac{A_b}{L^2} \cdot L^2 \quad (1)$$

Any increase in canopy length would result in the pilot looking through the lengthened portion at a more oblique angle. This will cause some increased distortion in the extended portion. However, inspection of two canopies which had been removed from service did not show a significant distortion of the canopies' optical quality when observed at very oblique angles.

The results of this evaluation show that the extension of the canopy acrylic would increase the visible region. The 5-inch acrylic extension discussed in detail in Section 3 would provide a reduction in blocked area of slightly more than 30 percent. The analysis also shows that a further decrease in blocked area results from the pilot's ability to move his head farther to the side when looking aft. However, for a given eye position, the decrease in area hidden from view is a function of the increase in transparency length.

### 2.2.2 Mirrors

Possibilities for enhancing rearward visibility by expanding the use of internal mirrors or adding external mirrors were evaluated. The A-7D currently has three mirrors in the cockpit arranged around the front arch of the canopy frame. The overhead mirror is approximately 2 inches wide and extends along the canopy for 7 inches. The lower edge of this mirror is 3 inches below the outer surface of the canopy transparency. The side mirrors lie on

the sides of the front arch centered 4 inches below the design eye position. The side mirrors are approximately 2 1/2 inches wide and extend along the arch for 4 inches.

An external mirror which has successfully been added to the rear cockpit of F-4 fighters was used as a model for a possible external mirror for the A-7D. Figure 12 shows the location of the external mirror on the aft cockpit of an F-4. Figure 13 shows the region visible using the mirror. The mirror is approximately 3 inches high and extends along the arch for 7 inches. The convexity of the mirror allows for a field of view which extends from approximately 2° to 14° from the longitudinal axis of the aircraft. A flat mirror of the same size and location would provide a field of view over a region from 2° to 8° from the longitudinal axis.

Figure 14 illustrates the existing internal and proposed external mirrors. The 7° fields of view shown are for a 2-inch wide flat internal mirror and a 3-inch wide flat external mirror. The upper figure shows that the angle which the closest line of sight makes with the longitudinal axis is about 9° for the internal mirror. The dashed lines in the lower figure shows that the external mirror could achieve a line of sight which is 7° from the longitudinal axis. However, this would require that the image pass through the canopy surface three times.

The bright arc in Figure 13 is caused by reflections from the surface of the F-4 canopy. Similar reflections from the A-7 canopy would obscure a large portion of this field of view if the reflected light were to take the path indicated by the dashed lines. To prevent canopy surface reflections from interfering with the field of view, the external mirror must be oriented so that the line of sight closest to the aircraft is tangent to the forward canopy surface. This is shown in the lower portion of Figure 14 by the solid lines at 20° from the horizontal.

In order to evaluate the usefulness of internal and external mirrors, the angle between the line of sight and the longitudinal aircraft axis was determined as a function of position around the aft arch. Location around the aft arch, as opposed to locations around the forward arch where the mirrors are located, was used to facilitate comparison with the angles from direct view. The geometry used in the calculation of the angles is shown in Figure 15. A cutting plane containing the longitudinal axis of the aircraft and a point on the aft arch was intersected with the canopy surface. The mirrors for a given point on the aft arch were located at the intersection of the cutting plane and the forward edge of the canopy acrylic. The inner

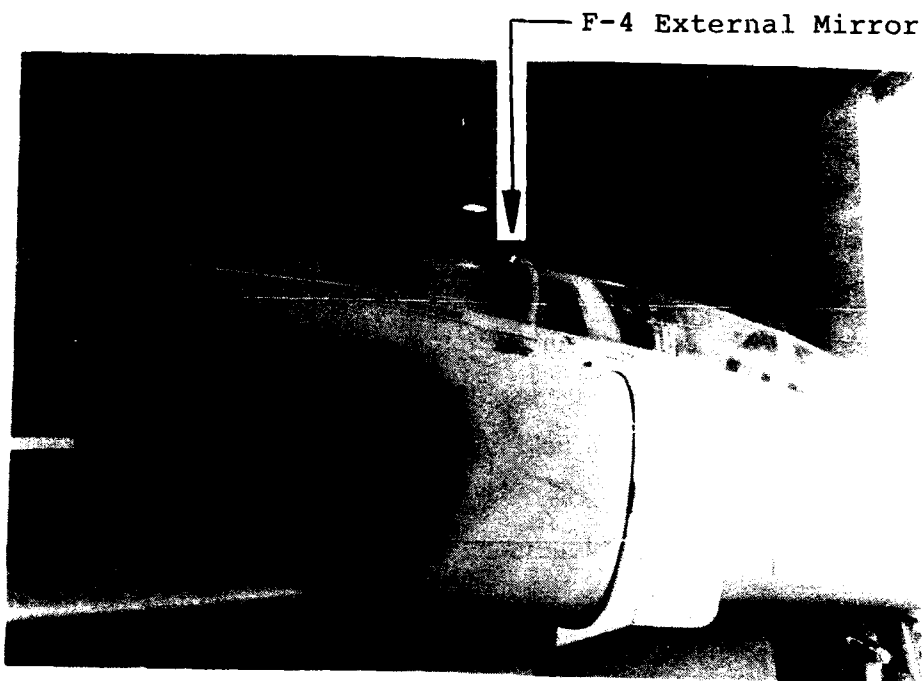
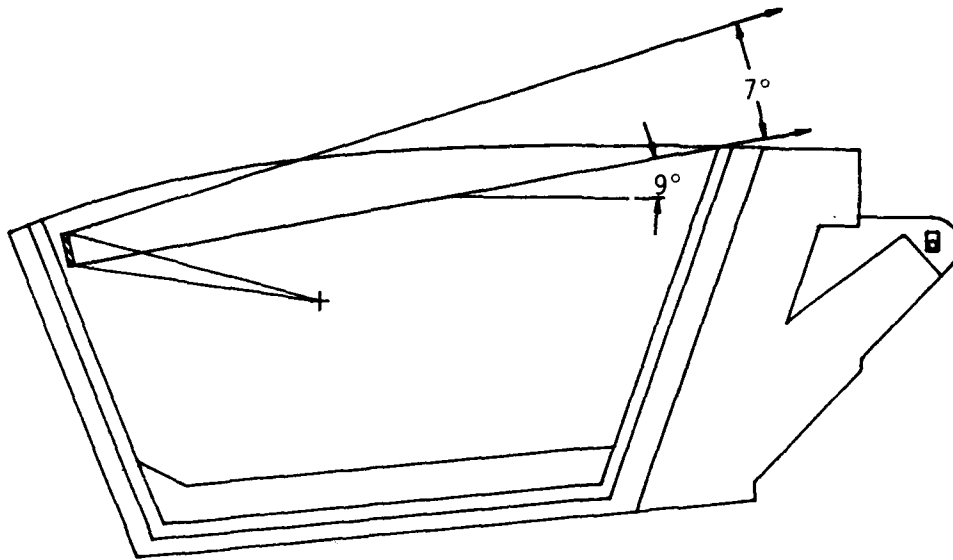


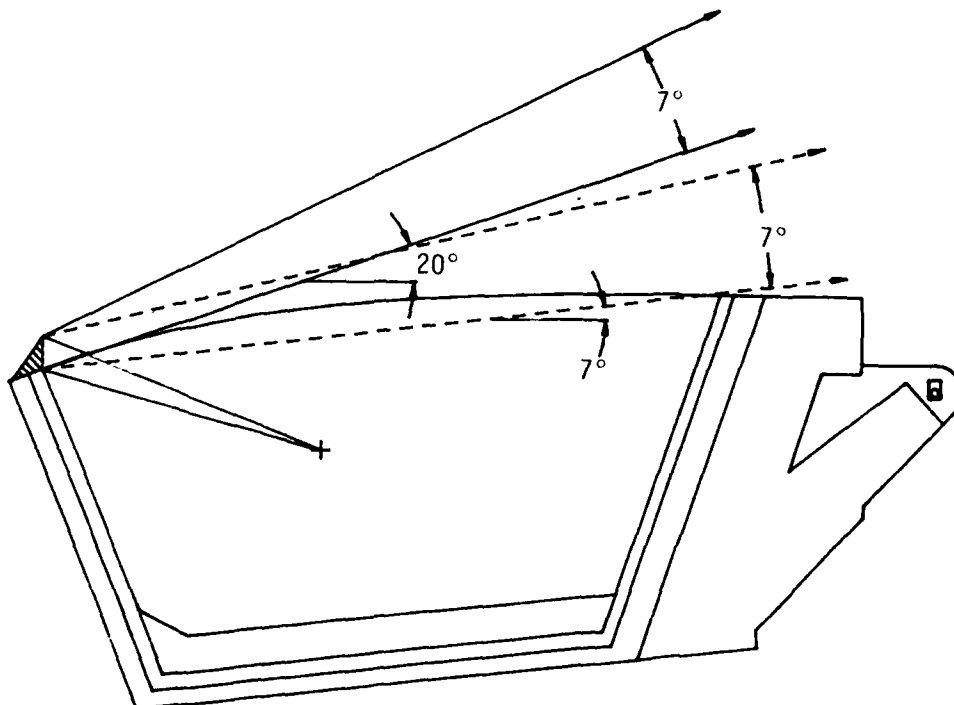
Figure 12. Location of External Mirror on F-4 Cockpit.



Figure 13. View Using External Mirror on F-4 Cockpit.  
(Note: Aircraft is in hangar)



EXISTING OVERHEAD MIRROR



PROPOSED EXTERNAL MIRROR

Figure 14. Existing and Proposed Overhead Mirrors.

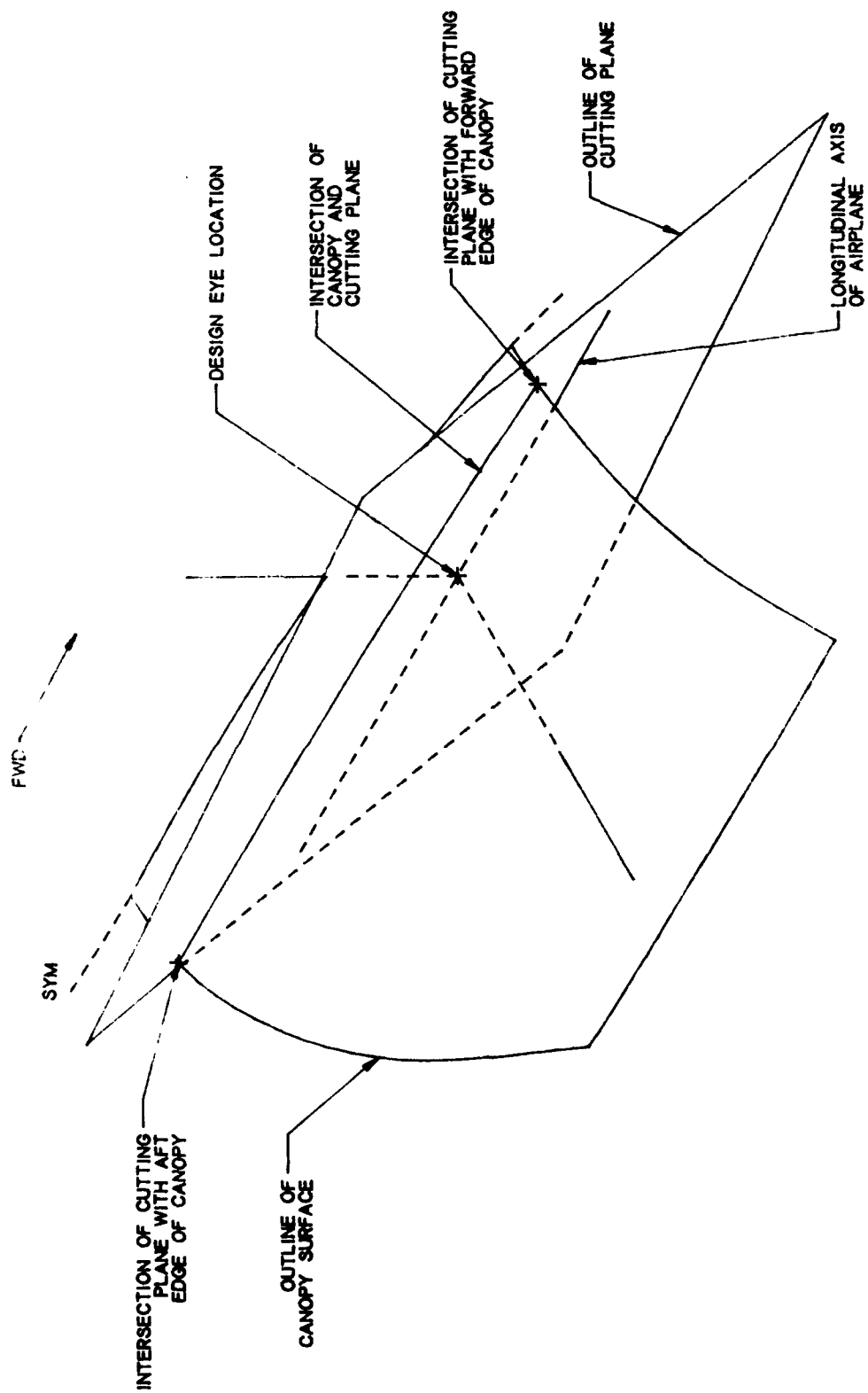


Figure 15. Intersection of Cutting Plane and Canopy Surface for Analysis of Mirrors.

edge of the internal mirror was assumed to be 3 inches inside the canopy surface and the inner edge of the external mirror was assumed to be at the canopy surface. For the internal mirror the angles were calculated between the longitudinal axis and a line connecting the inner edge of the mirror with the point of the aft edge of the canopy. The angles for the external mirror were calculated between the longitudinal axis and a tangent to the canopy surface at the forward edge.

The sight angles calculated as described above are plotted in Figure 16. The graph shows that a far greater angle is blocked using external mirrors than internal mirrors. It can also be seen that the internal mirrors provide a line of sight which is closer to the axis of the aircraft for positions all around the aft arch.

The analysis performed for evaluation of the mirrors shows that external mirrors are only effective when the forward edge of the canopy is nearly parallel to the axis of the aircraft. This occurs for the rear cockpit of the F-4, on which they are currently used. It also occurs for the rear cockpit of the A-7K, on which the addition of external mirrors would be beneficial. However, the slope of the forward portion of the A-7D canopy prevents external mirrors from being effective.

Due to the very small angle between the reflected line of sight and the canopy surface, the image reflected by internal mirrors is distorted. However, internal mirrors are very effective for providing lines of sight which are close to the axis of the aircraft. Figure 16 shows that the sight angles are nearly constant for any mirror position. Thus, altering the position of the mirrors would not significantly increase the visible area. Because of the limited fields of view of the existing internal mirrors, an area on either side of the aircraft exists for which the angle blocked is greater than the  $10^\circ$  shown in Figure 16. Most of this area could be eliminated by the addition of mirrors midway between the overhead mirror and the existing side mirrors. While additional mirrors cannot greatly decrease the region blocked from view, they do offer some improvement for rearward visibility without affecting the pilot's view and with only a minimal weight increase.

### 2.2.3 Refractive Lenses

Refractive lenses are currently used by the automotive industry to enhance the field of view on some vans and buses. These lenses give a wider field of view at the expense



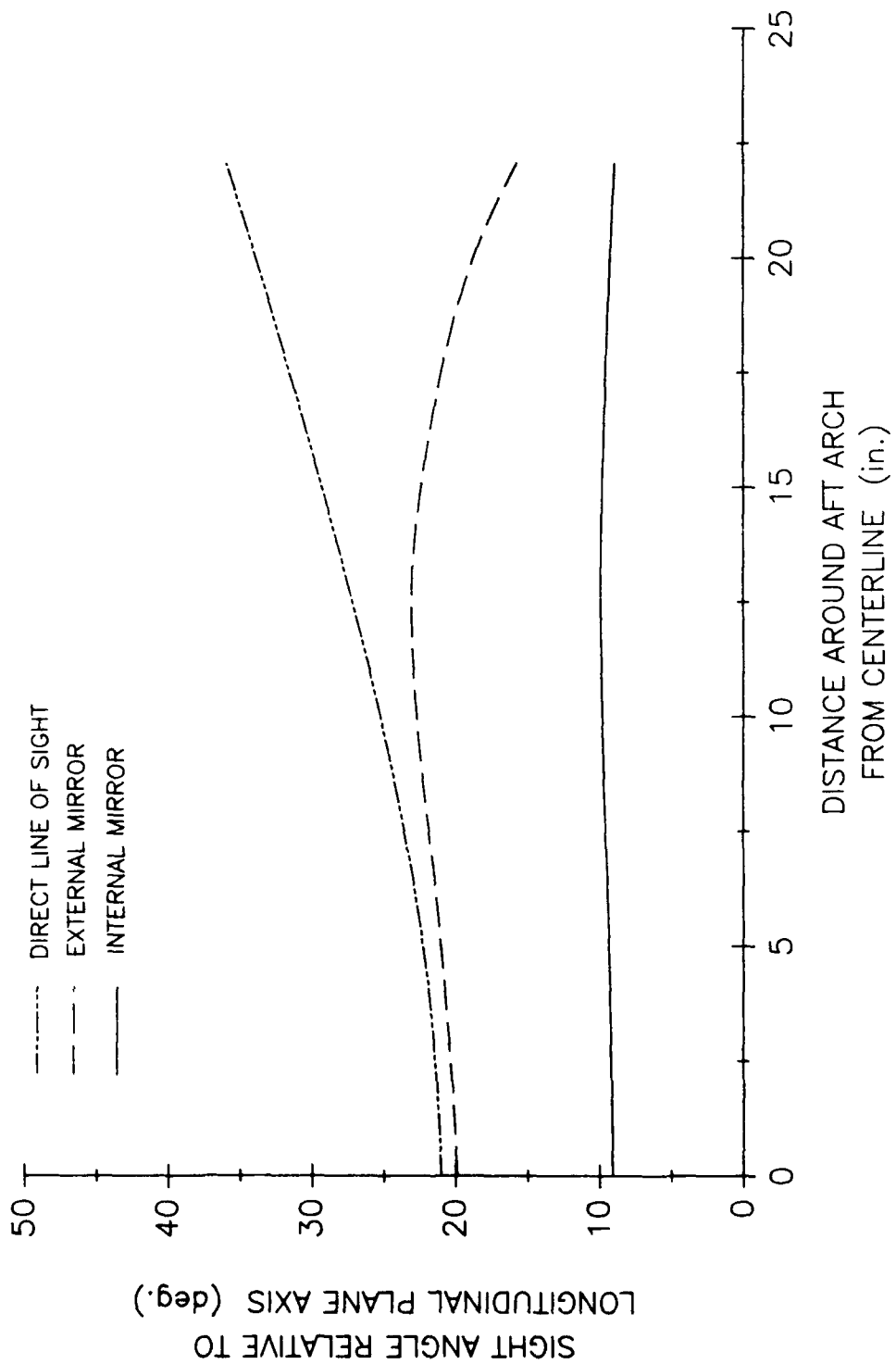


Figure 16. Sight Lines Available Using Existing Internal Mirror and Proposed External Mirror.

of distorting the viewed object's image and perceived location. For automotive applications the lenses are placed on a rear window, and the driver's line of sight is nearly normal to them. To adapt similar lenses for use on the A-7D, it would be necessary to apply them around the aft edge of the canopy. The pilot's line of sight would then strike the lenses at an oblique angle. The factors associated with the possibility of using such lenses in this manner have been investigated.

The geometry associated with determining the refracted line-of-sight for a given lens configuration is shown in Figure 17. The relationship between the pilot's direct line of sight, "a", and the refracted line of sight, "d", is:

$$d = 90 - \{ \sin^{-1} [ \mu_1 \sin (g+b) + c ] \} \quad (2)$$

where:

$$g = \sin^{-1} \{ [\sin(90 - a - b - c)] / \mu_1 \}$$

and

a = angle between pilot's line of sight and longitudinal axis of aircraft (degrees)

b = angle of lens taper (degrees)

c = angle between canopy surface and longitudinal axis of aircraft (degrees)

d = angle between refracted line of sight and longitudinal axis of aircraft (degrees)

$\mu_1$  = index of refraction of lens.

At the leading edge of the lens, it would be necessary to reduce the taper angle, "b," to zero. Otherwise, there would be a sudden change in the effective line of sight. A parabolic shape similar to that depicted in Figure 18 would be required for the lens. The lens taper angles used in the following examples are those at the aft edge of the lens, where the angle would be largest.

Figure 19 shows the one concept for applying a refractive lens to the original canopy. For this example the lens has an index of refraction  $\mu_1 = 1.6$  and a taper angle  $b = 2.0^\circ$

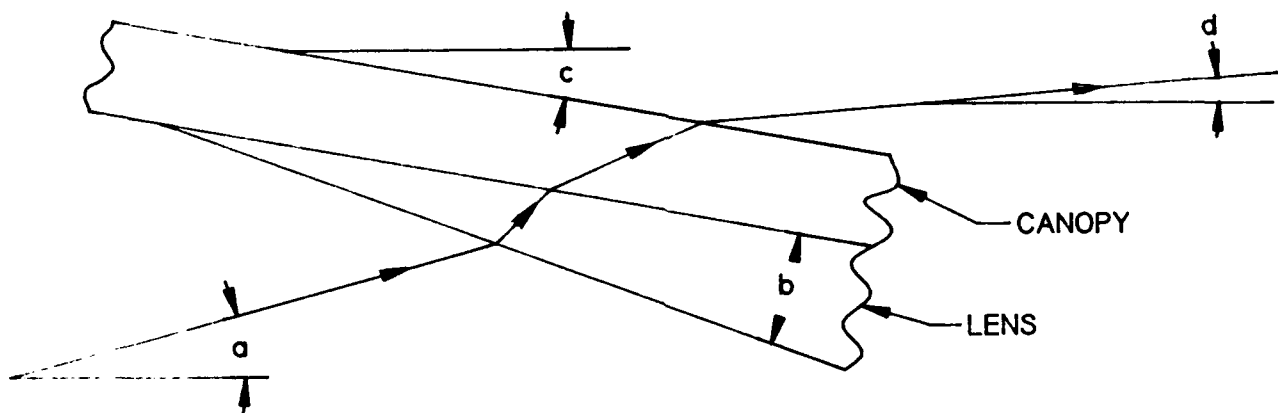


Figure 17. Geometry Used for Calculation of Refracted Line of Sight.

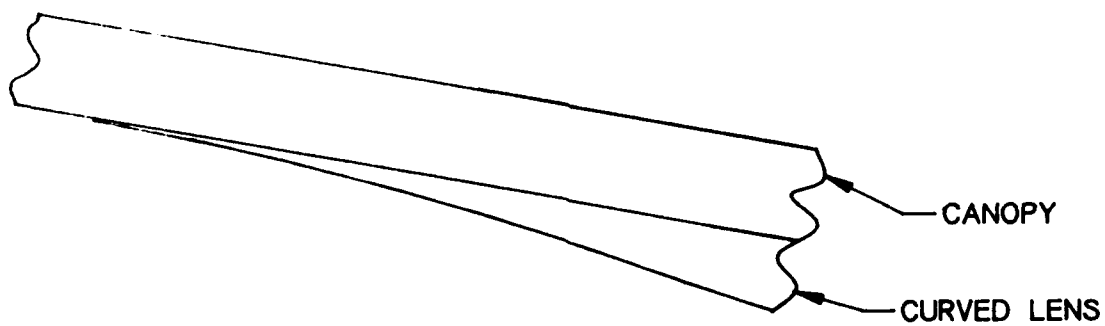


Figure 18. Lens with Varying Angle.

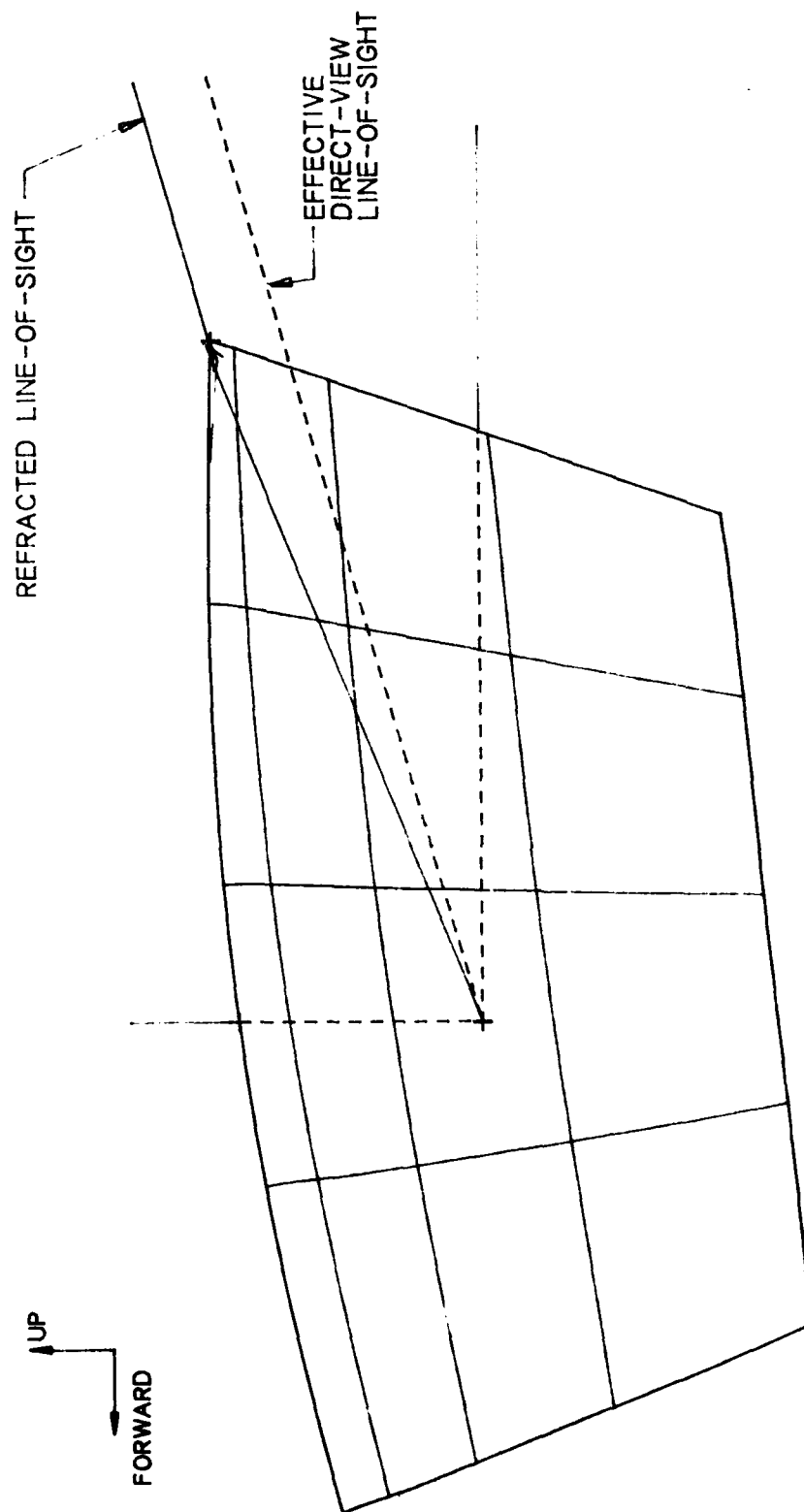


Figure 19. Altered View Angle in Vertical Plane Due to 2.0 Degree Lens on Original Canopy. Viewpoint is Design Eye ( $\mu_1=1.6$ )

at the aft edge. The figure shows the refracted line of sight in the vertical plane for an eye at the centerline design eye location. The effective line of sight at this location is the same as if the canopy acrylic could be extended by approximately 10 inches.

Figure 20 shows the refracted angle, "d," as a function of distance around the aft edge of the canopy for this lens geometry. The lines corresponding to each of the four eye positions are drawn only for positions on the aft arch where the pilot would view. That is, these curves are shown for positions on the aft arch which lie outboard of the eye position and above the horizontal plane. Comparison of these curves with those for canopy acrylic extension (Figures 6 through 9) shows that a thin lens can produce the same effect as a substantial increase in canopy length. For the design eye location viewing in the vertical and horizontal planes, this example lens configuration has the same effect as elongating the acrylic by 10 and 5 inches, respectively. For other eye positions, the effect is even greater.

Refractive lenses have great potential based solely on analysis of the reduction in the region blocked from view. However, there are some serious drawbacks to the use of lenses. One problem is that for oblique angles of incidence, the lenses reflect rather than refract the image. For example, if  $b = 2.0^\circ$  and  $\mu_1 = 1.6$  and if  $(a + c)$  is less than  $15^\circ$ , the pilot would see a reflection of the cockpit interior instead of a refracted image. Since the line of sight from the mirror intersects the aft portion of the canopy at an angle less than  $15^\circ$ , the mirrors would be unusable in this area, where they are otherwise most effective. Reflections also occur if the eye position is more than 10 inches from the centerline. A second problem is the sensitivity of the effective line of sight to head position and lens taper angle. Changes in eye position or small distortions in the shape of the lens will change the perceived location of the object being viewed.

A reduction in sensitivity to head position for both perceived location of object and reflection of image can be achieved by making the line of sight more normal to the canopy surface. An example of this concept is shown in Figure 21. For this example the lens has an index of refraction  $\mu_1 = 1.5$  and a taper angle  $b = 5.0^\circ$  at the aft edge. The principal change from the previous example is that the canopy profile is modified, producing the increase in normality between the line of sight and the canopy surface. Figure 22 shows the refracted angle "d" as a function of distance around the aft edge of the canopy for this lens geometry. Comparison of Figures 20 and 22 shows similar values for "d" for given eye and aft arch

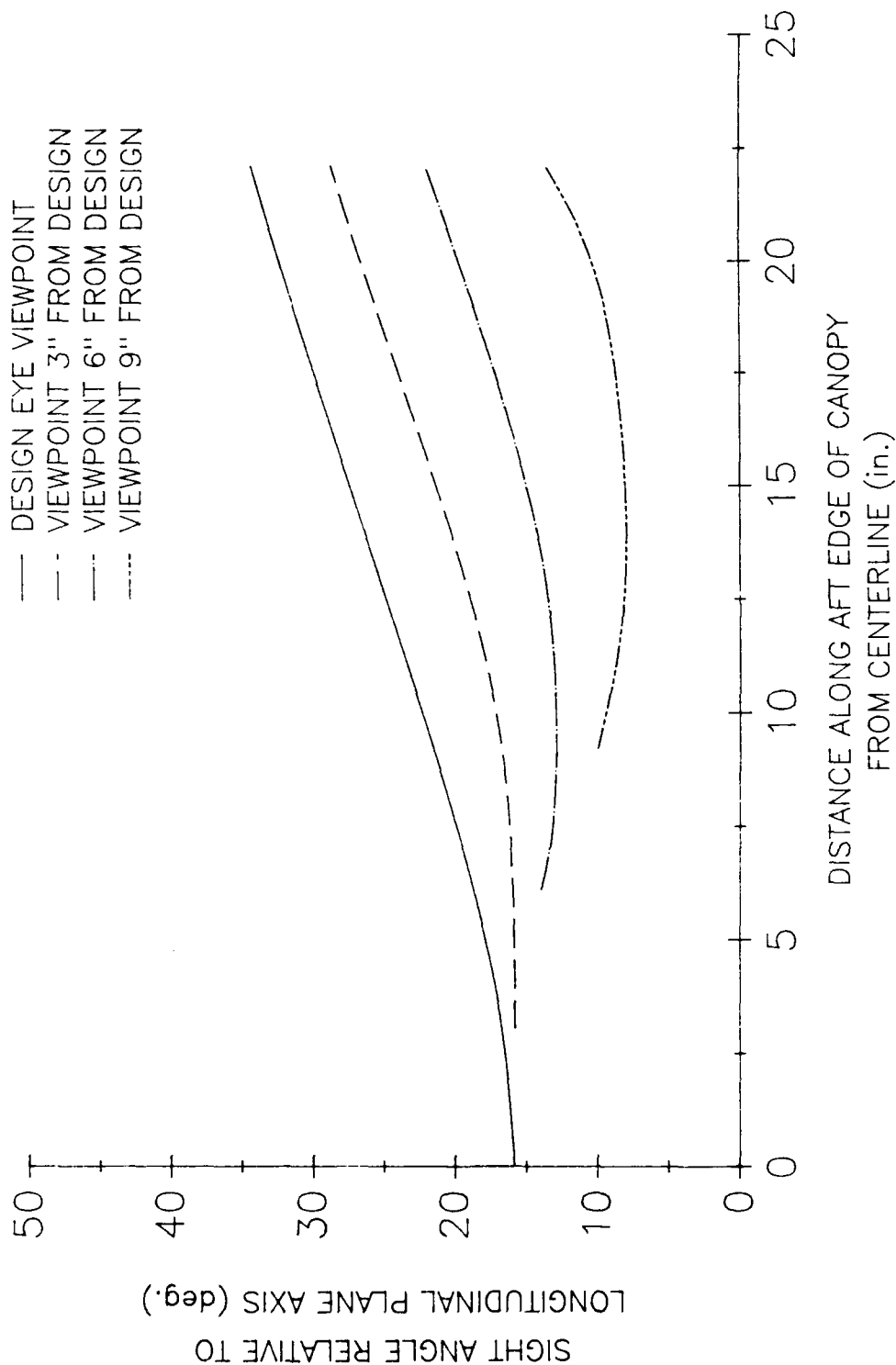


Figure 20. Sight Angles for Refractive Lens on Original Canopy  
( $\mu_1=1.6$ ,  $b=2^\circ$ )

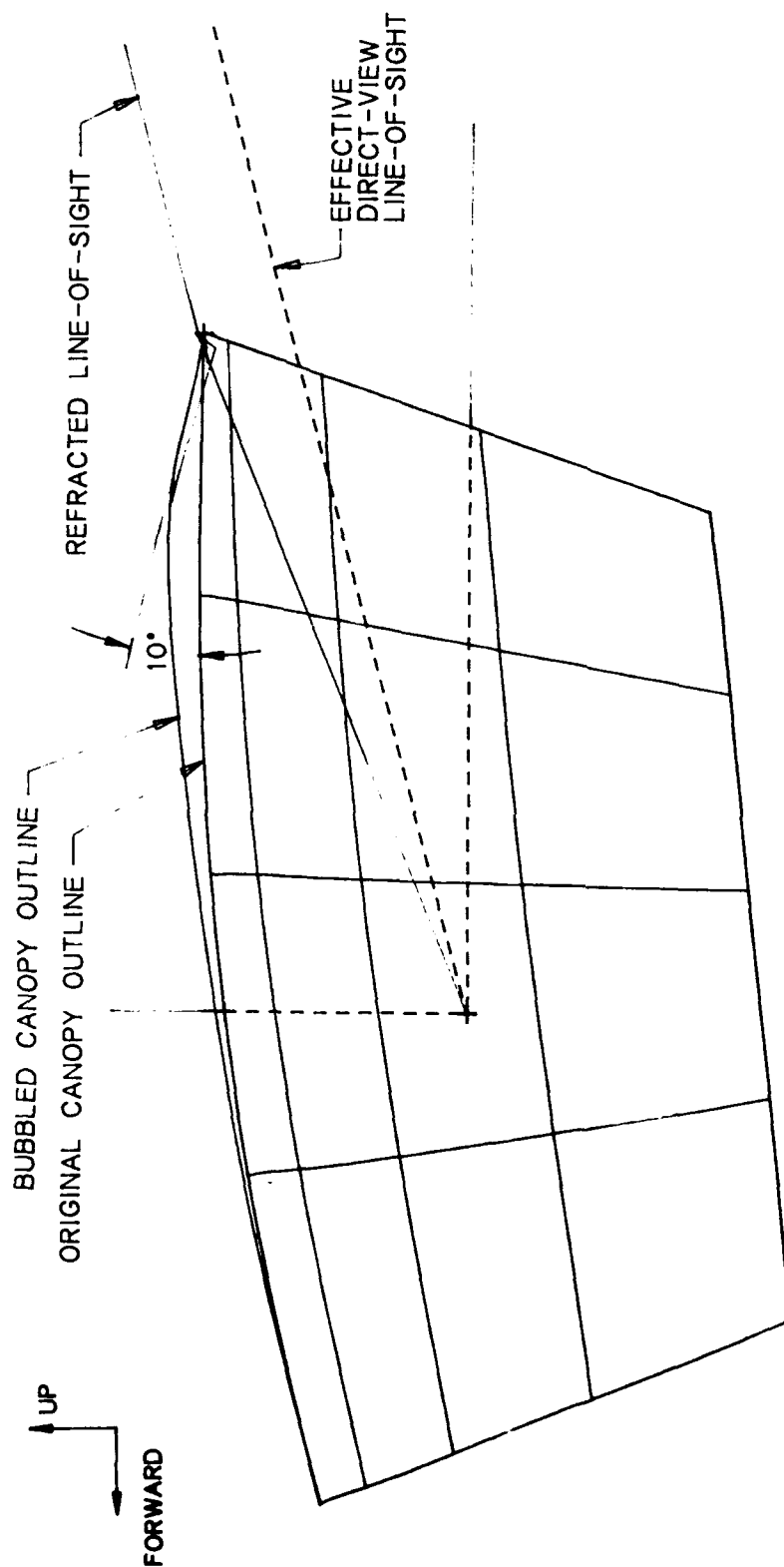


Figure 21. Altered View Angle in Vertical Plane Due to 10 Deg. Canopy Bubble with 5 Deg. Lens. Viewpoint is Design Eye ( $\mu_1=1.4$ )

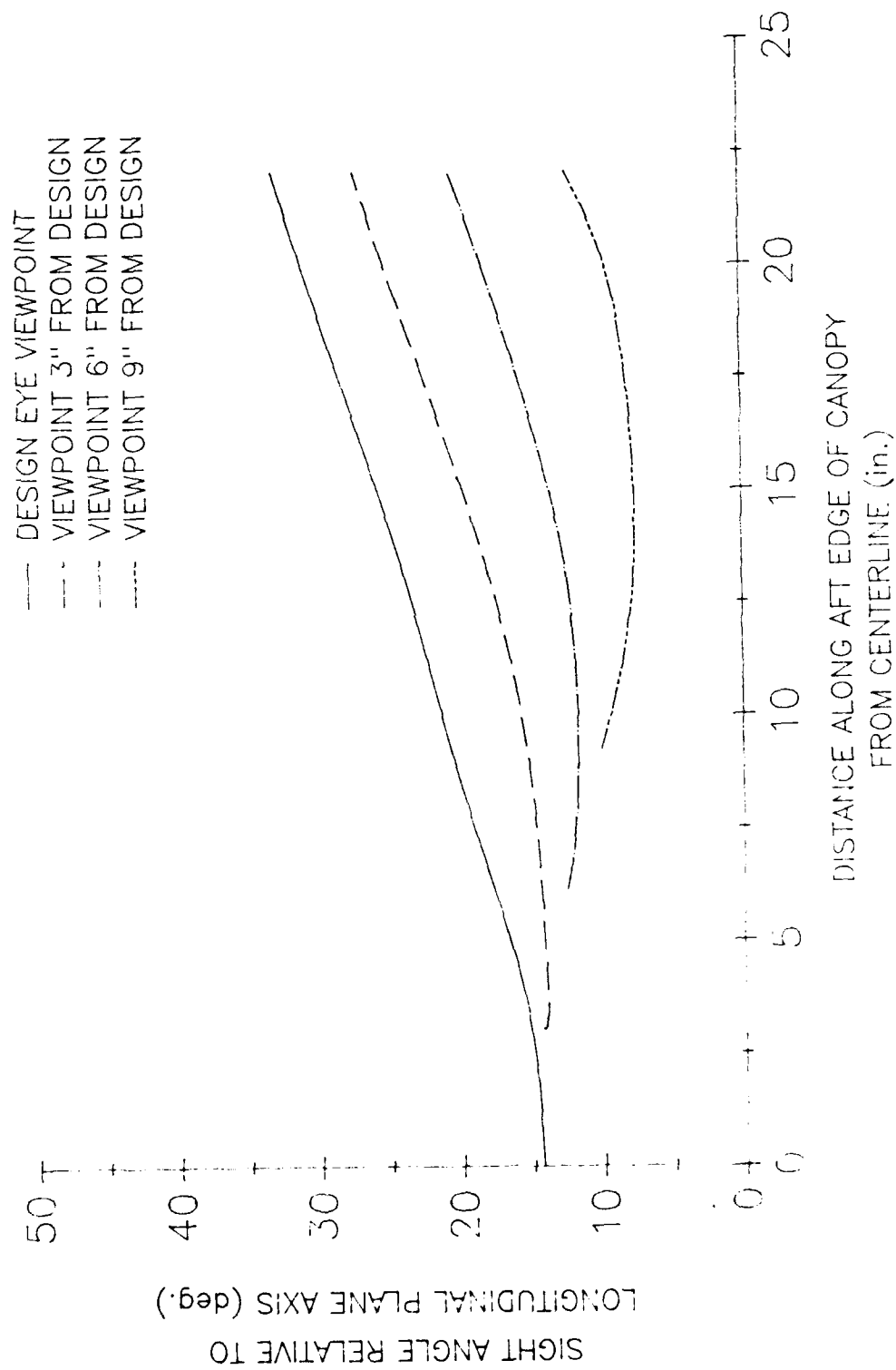


Figure 22. Sight Angles for Refractive Lens on Bubbled Canopy ( $\mu=1.5$ ,  $b=5^\circ$ ).



position. However, the angle "d" decreases less for this example for a given lateral motion of the eye, indicating the reduced sensitivity of this geometry to eye position.

Although the alteration of the canopy profile can reduce the sensitivity of the lens system to changes in eye location, it cannot make the mirrors useful in this area. If the angle "c" is large enough so that the mirror image is not obscured by lens reflections, the mirror image would be refracted so that the pilot only sees the side of the aircraft. Thus, for the A-7D alternatives, utilizing refractive lenses which produce an increase in visible area correspondingly reduce the usefulness of the mirrors.

#### 2.2.4 Bubble Canopy

A bubble canopy has been successfully used on many single-seat aircraft to enhance visibility. Examples include the AV-8, A-10, F-15, and F-16. The bubble canopies of these aircraft permit an unobstructed view of nearly the entire sky above the horizon aft of the aircraft. However, to achieve this unobstructed view, these aircraft have the design eye of the pilot above the aft arch of the canopy frame and the fuselage of the aircraft.

On the A-7D, the design eye of the pilot is 10 inches below the apex of the aft canopy arch. Figure 23 shows a concept for modifying the canopy to allow the pilot to be raised by 10 inches. Major modifications to the fuselage would be required, including:

- alterations to the windshield, canopy and fuselage moldlines,
- modifications to raise the seat, controls, and instruments by 10 inches, and
- requalification of the ejection system and windshield.

The projected high cost of this alternative did not warrant further investigation under this effort.

### 2.3 RECOMMENDED ALTERNATIVE

Alterations in the current locations of the internal mirrors would not enhance rearward visibility. However, the addition of two internal mirrors on the forward canopy arch would decrease the area blocked from the pilot's view near the axis of the aircraft without affecting the pilot's vision in other areas. External mirrors are not recommended because they would not increase the area visible to the pilot. Refractive lenses have the potential to greatly reduce the area blocked from the pilot's view. However, it would be very difficult to fabricate the lenses within acceptable limits of distortion. Also, movement of the pilot's head would change the

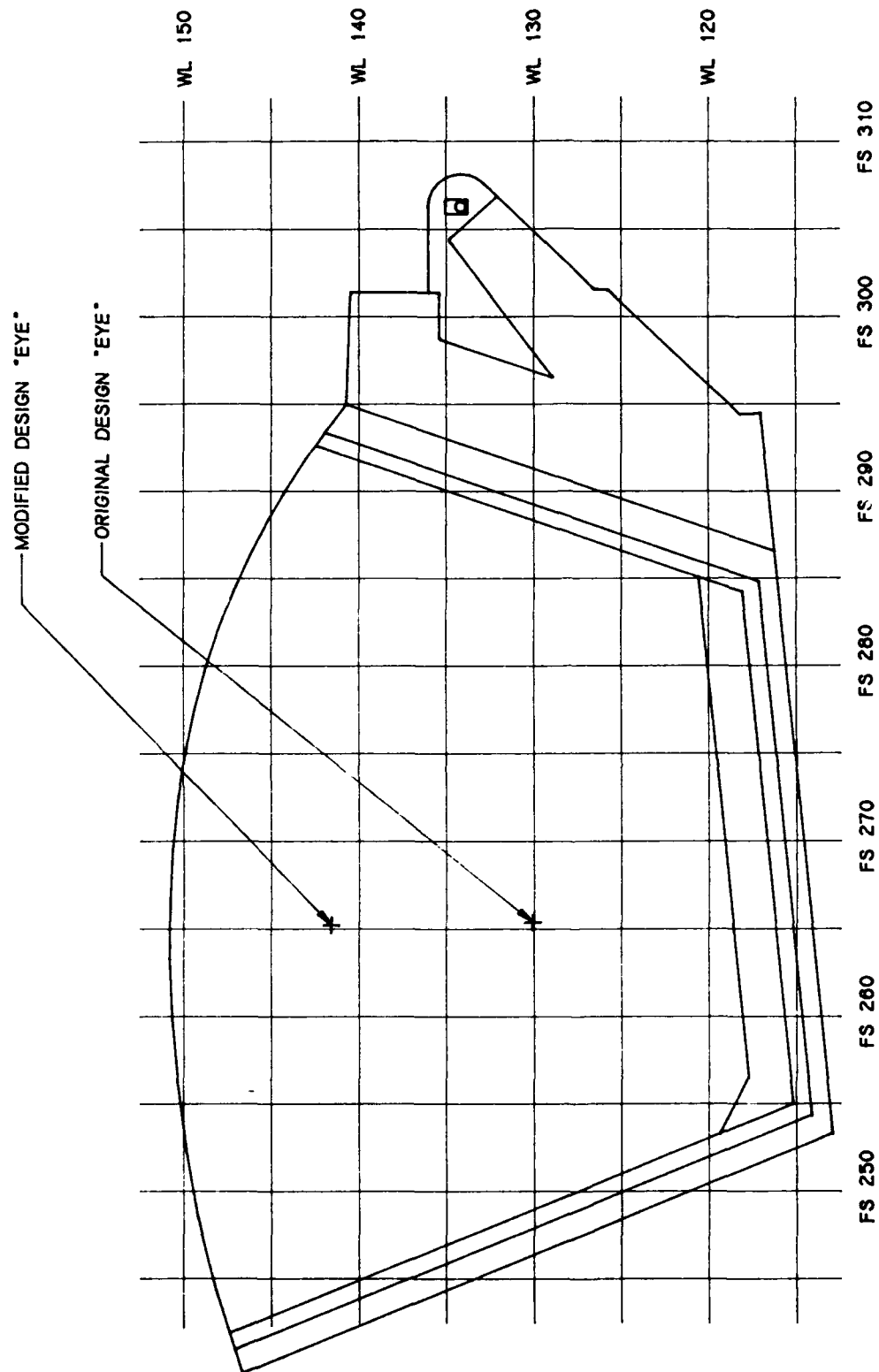


Figure 23. Concept for Modification of Canopy to Raise Design Eye Above Aft Arch.

apparent location of objects, and lenses would make the mirrors useless for viewing close to the axis of the aircraft. These drawbacks prohibit the applicability of existing refractive lenses.

A bubble canopy is not recommended because of the major changes required to the aircraft moldline and the high cost associated with major modifications to the fuselage.

The greatest increase in rearward visibility without impairing the pilot's vision in other areas and without major airframe modifications can be achieved by elongation of the canopy acrylic. A 5-inch extension of the canopy transparency would result in a 31 percent decrease in the rearward area blocked from sight. The results presented in Section 3 show that a 5-inch increase is feasible without changing the total weight of the canopy.

## SECTION 3

### DETAILED DESIGN AND ANALYSIS OF SELECTED ALTERNATIVE

A detailed design of an alternate A-7D canopy is presented in this section. This canopy increases the transparent portion of the transparency by 5 inches in length. The analysis includes a stress evaluation of the lengthened transparency and a detailed design of an alternate canopy frame.

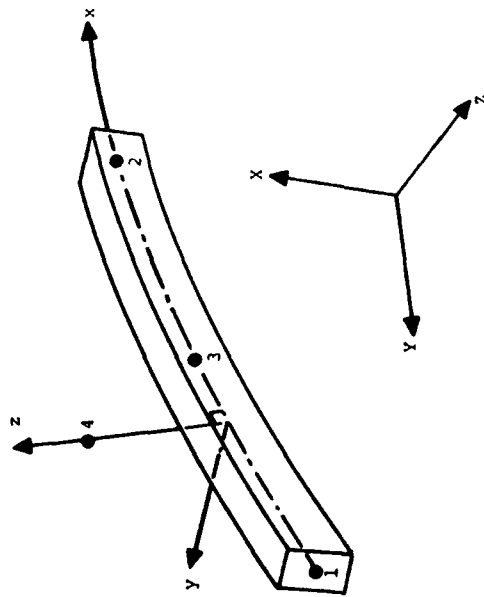
#### 3.1 CANOPY STRESS EVALUATION

The stress in the lengthened transparency was compared to the stress level in the current production canopy using finite element models. If the alternate canopy is to be feasible, the maximum stress in the extended transparency must not exceed the maximum stress in the current configuration. An increase in canopy stress for a modified configuration would require that either the canopy be made thicker or that the entire canopy frame be redesigned. An increase in canopy thickness (currently 0.25 inch) would increase the overall weight of the canopy and require requalification of the ejection system. A complete change of the canopy frame would be expensive and might require requalification of the ejection system. A finite element model was developed to determine the stress distribution in the acrylic. Results of the analysis, summarized in this section, showed that the transparency could be extended without increasing maximum stress.

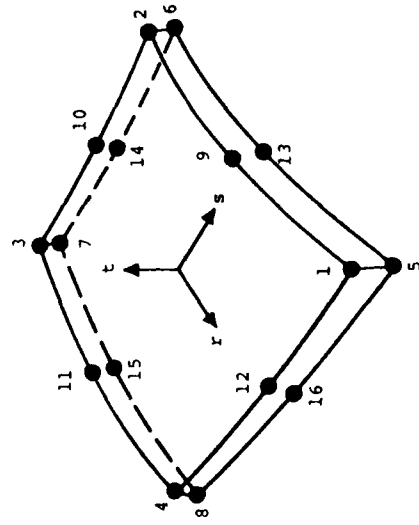
##### 3.1.1 Model Development

A finite element model was developed using the MAGNA program [2]. The canopy transparency was modeled using 16 node thick shell elements. The element orientation is shown in Figure 24. One side of the original model of the transparency is shown in Figure 25. This model was later revised to give results which agreed more closely with test data for the load conditions. The modifications are discussed in Section 3.1.2.

The actual edge conditions of the transparency are complicated. As shown in Figure 26 the canopy acrylic is bonded to a nylon edge strip. The nylon edge strip is held in place by an aluminum retainer bolted to the forward arch and side rail. At the aft edge, the



Frame - Beam Elements



Transparency - 16-node Shell Element

Figure 24. Geometry of Elements Used in MAGNA Model.

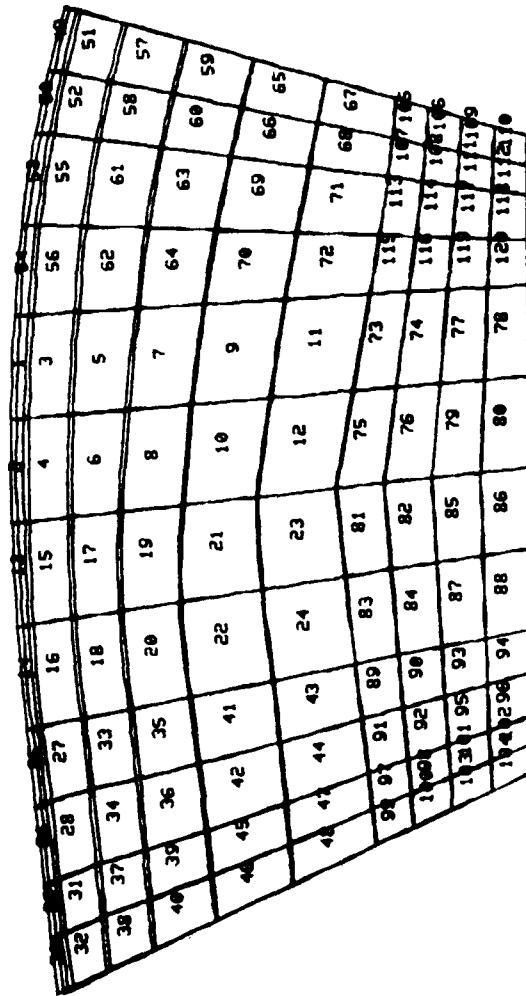


Figure 25. Profile of Quadratic Shell Elements on Right-Hand Side of Initial Canopy Model.

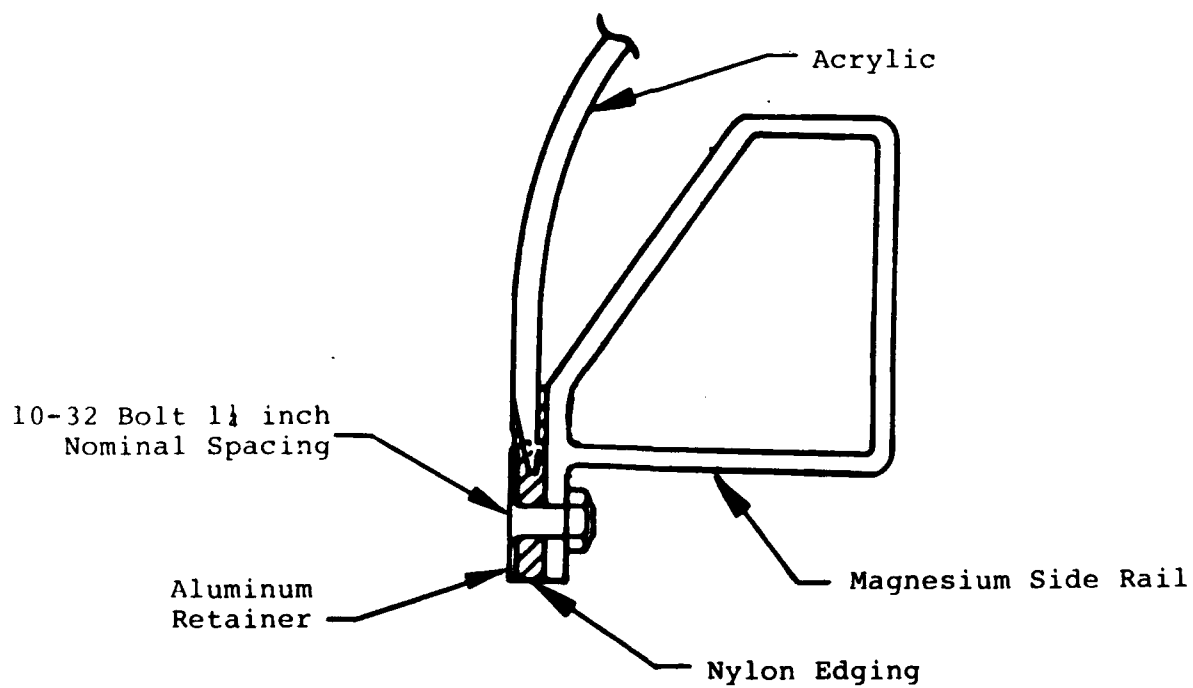
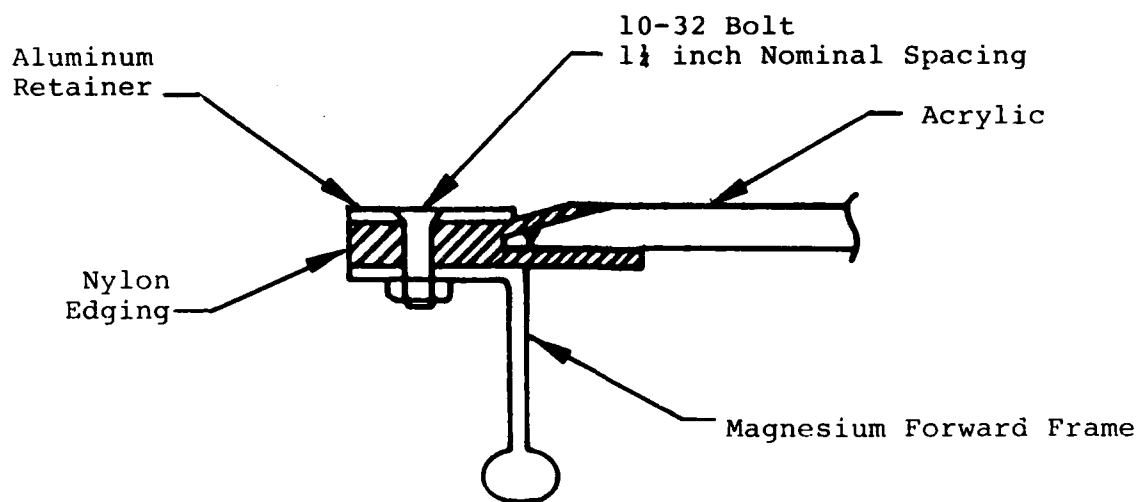


Figure 26. Edge Conditions for A-7 Canopy [3].

canopy acrylic is held in a similar fashion except the bolts go through the acrylic which extends to the edge. Quadratic beam elements were used to model the canopy frame. The element orientation is shown in Figure 24. To simplify the modeling of the boundary conditions at the transparency edge, it was assumed that the beams are rigidly fixed to the canopy acrylic along the line of bolts holding the aluminum retainer; omitting the nylon edge strip. The wire mesh model of the canopy frame is shown in Figure 27. Elements of the wire mesh were attached to the inner surface of the canopy. Constraints were used to ensure that the displacements of the shell elements match the displacements and rotations of the beams. Displacements of the entire structure were fixed at the aft hinges and side pins as shown in Figure 27. It was assumed that the hinge and pins would be free enough to allow small rotations of the canopy frame.

Due to limitations on the way beam element properties could be input to this program, the beam cross-sections were approximated by a series of rectangular sections. The cross-sections used are shown in Figure 28. These cross-sections were based on measurements from assembly drawings of the canopy [1]. It was later determined that some of the wall thicknesses used were thinner than those of the actual frame. However, the good agreement between test data [3] and finite element calculations indicated that changes in the beam cross-section would not significantly change the results.

The critical load was a static pressure distribution from the original design of the canopy [4] which corresponded to the condition which produced the highest stress during flight [3]. The load was based on the pressure developed by an aircraft at Mach number 0.95 and 22,000 feet altitude at full left rudder. This case was analyzed because of the availability of the pressure distribution [4] and the stresses from strain gage data at this flight condition [3]. The pressure distribution due to flight loads on the canopy surface is shown in Figure 29. The pressure was determined by multiplying the value shown at a given location on the canopy by 3.84 psi. Positive pressure was directed inward on the outer surface. The total pressure at a given location was a combination of a 5-psi cabin pressure pushing out on the interior canopy surface and the flight loads pulling out on the exterior canopy surface.

The theoretical temperature of the transparency for the flight condition used is 96° F [4]; however, the actual test data was taken at 54° F [3]. The material properties used in the model were chosen to match the temperature from the test data. Young's modulus for the



Forward

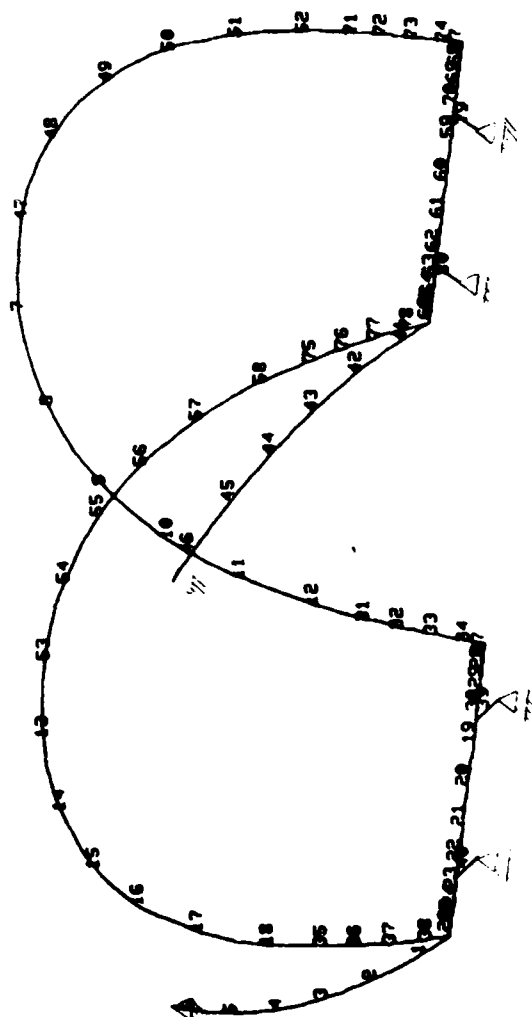
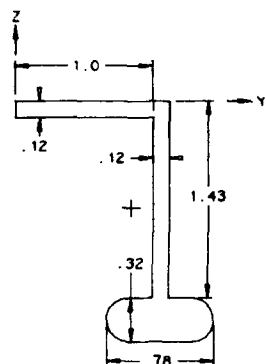


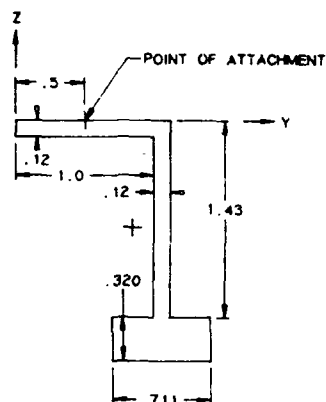
Figure 27. Beam Elements Used to Approximate Boundary Conditions for Canopy Acrylic.

Front Former:



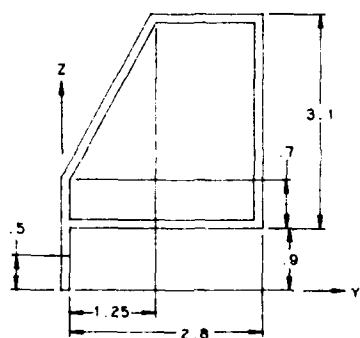
$$\begin{aligned} A &= 0.519 \text{ in}^2 \\ Y_C &= 0.931 \text{ in} \\ Z_C &= -0.947 \text{ in} \\ I_{YY} &= 0.229 \text{ in}^4 \\ I_{ZZ} &= 0.049 \text{ in}^4 \\ I_{YZ} &= -0.059 \text{ in}^4 \end{aligned}$$

MAGNA Model:



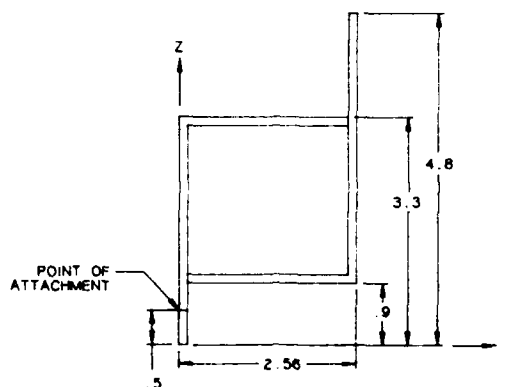
$$\begin{aligned} A &= 0.519 \text{ in}^2 \\ Y_C &= 0.931 \text{ in} \\ Z_C &= -0.947 \text{ in} \\ I_{YY} &= 0.229 \text{ in}^4 \\ I_{ZZ} &= 0.049 \text{ in}^4 \\ I_{YZ} &= -0.060 \text{ in}^4 \end{aligned}$$

Side Rail:



$$\begin{aligned} A &= 1.45 \text{ in}^2 \\ Y_C &= 1.50 \text{ in} \\ Z_C &= 2.09 \text{ in} \\ I_{YY} &= 2.19 \text{ in}^4 \\ I_{ZZ} &= 1.69 \text{ in}^4 \\ I_{YZ} &= 0.66 \text{ in}^4 \end{aligned}$$

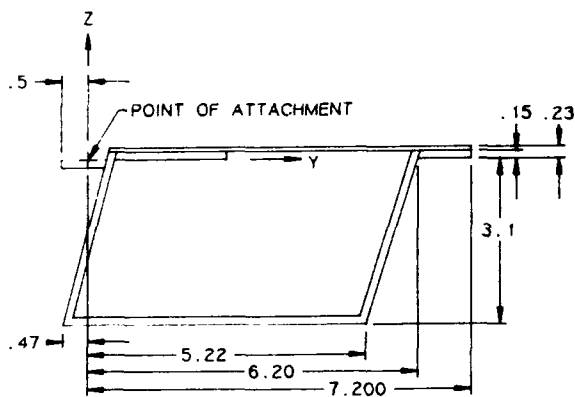
MAGNA Model:



$$\begin{aligned} A &= 1.52 \text{ in}^2 \\ Y_C &= 1.34 \text{ in} \\ Z_C &= 2.21 \text{ in} \\ I_{YY} &= 2.23 \text{ in}^4 \\ I_{ZZ} &= 1.80 \text{ in}^4 \\ I_{YZ} &= 0.67 \text{ in}^4 \end{aligned}$$

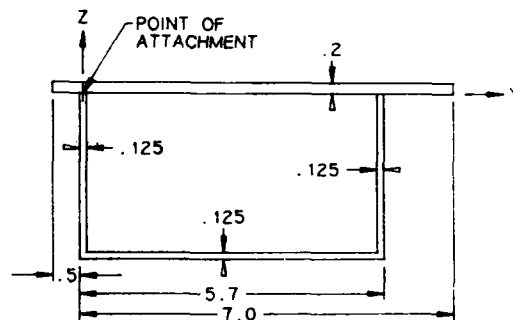
Figure 28. Cross-Sections of Canopy Frame for MAGNA Model.

Aft Former:

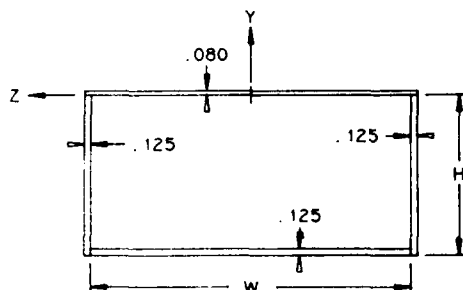


$$\begin{aligned} A &= 2.63 \text{ in}^2 \\ Y_C &= 2.85 \text{ in} \\ Z_C &= -1.27 \text{ in} \\ I_{YY} &= 5.29 \text{ in}^4 \\ I_{ZZ} &= 14.98 \text{ in}^4 \\ I_{YZ} &= 1.43 \text{ in}^4 \end{aligned}$$

MAGNA Model:



$$\begin{aligned} A &= 2.63 \text{ in}^2 \\ Y_C &= 3.02 \text{ in} \\ Z_C &= -1.26 \text{ in} \\ I_{YY} &= 5.15 \text{ in}^4 \\ I_{ZZ} &= 13.8 \text{ in}^4 \\ I_{YZ} &= 0.60 \text{ in}^4 \end{aligned}$$



Model of Box Beams Connecting Pins to Aft Former

$$H = 3 \text{ in}$$

W varies from 6 in. at forward end to 3 in. at aft pins.

Figure 28. (continued).

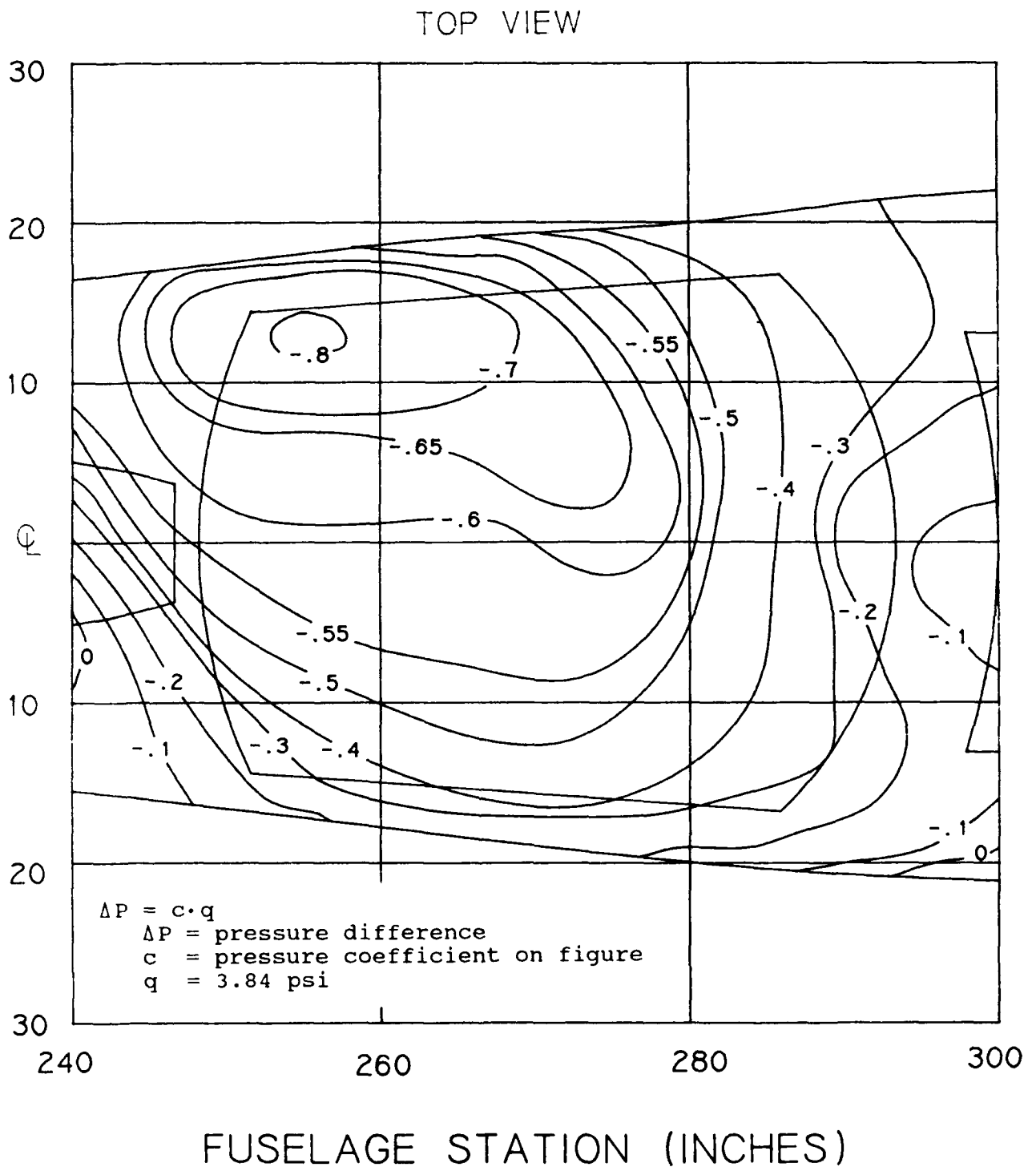


Figure 29. Pressure Distribution for Critical Load Case [4].

# LEFT PROFILE

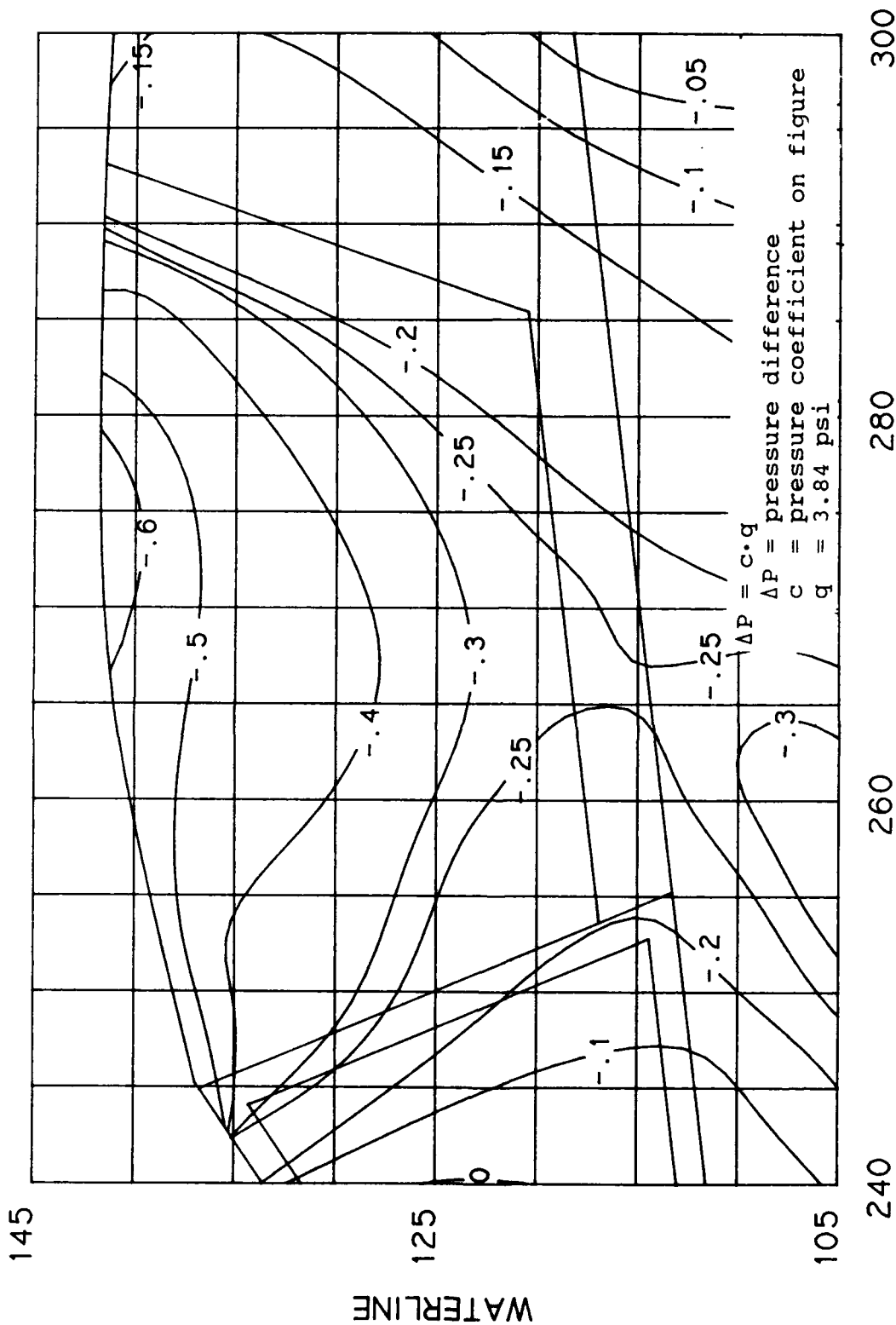


Figure 29. (continued).

RIGHT PROFILE

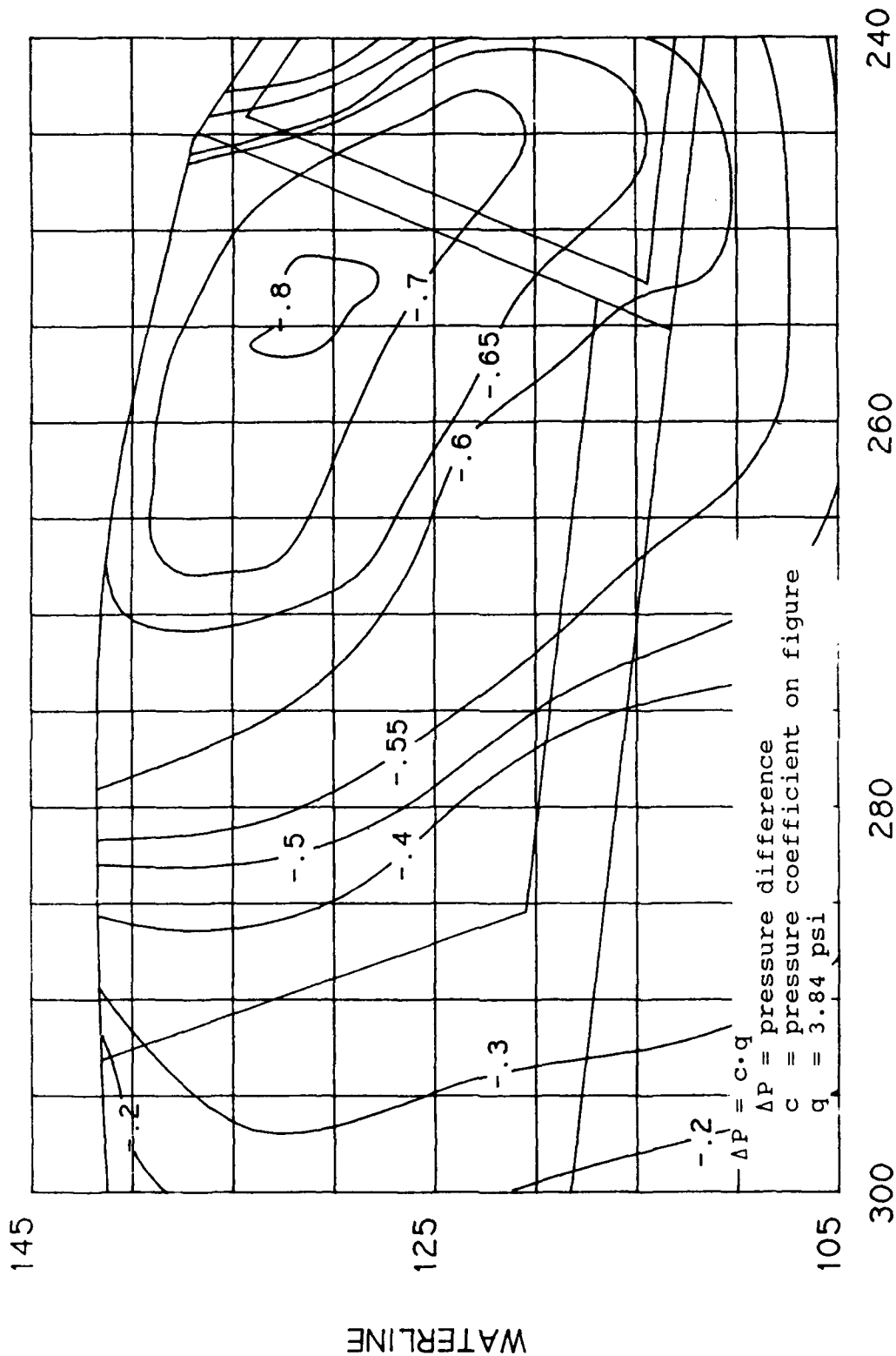


Figure 29. (continued).

acrylic was 485,000 psi and Poisson's ratio is 0.35 [3]. For the magnesium structure the Young's modulus was  $6.5 \times 10^6$  psi and the Poisson's ratio was 0.35 [5].

### 3.1.2 Model Validation

The model was validated by comparing the results of the FE analysis with flight test data. The von Mises stress on the inner and outer surfaces of the right-hand side of the canopy is shown in Figures 30 and 31. Stresses on the right-hand side were higher than those on the left-hand side for this load condition, and the highest stress occurred near the forward latch on the inside surface of the canopy. This agreed with results published by LTV for this load [3]. However, comparison of the stresses with those from test data showed that this model predicted bending stresses much higher than those measured.

The locations of the strain gages for which flight test data were available for this loading condition are shown in Figures 30 and 31. The strain gages were aligned perpendicular to the side rail. Exact locations of the gages are listed in Table 1. The distance from the forward latch listed in this table is measured along the canopy side rail. The distance from the bolt row is measured from the centerline of the row of bolts which attach the canopy to the side rail and which form the edge of the canopy for the model.

Table 1 - Locations of Strain Gauges in Flight Test [Ref 3]

Gage No.	Dist. from Fwd. Latch (in)	Dist. from Bolt Row (in)	Surface
9	9.6	2.20	inner
10	9.6	1.70	inner
11	15.8	1.70	inner
20	9.6	2.20	outer
21	9.6	1.70	outer
22	15.8	1.70	outer

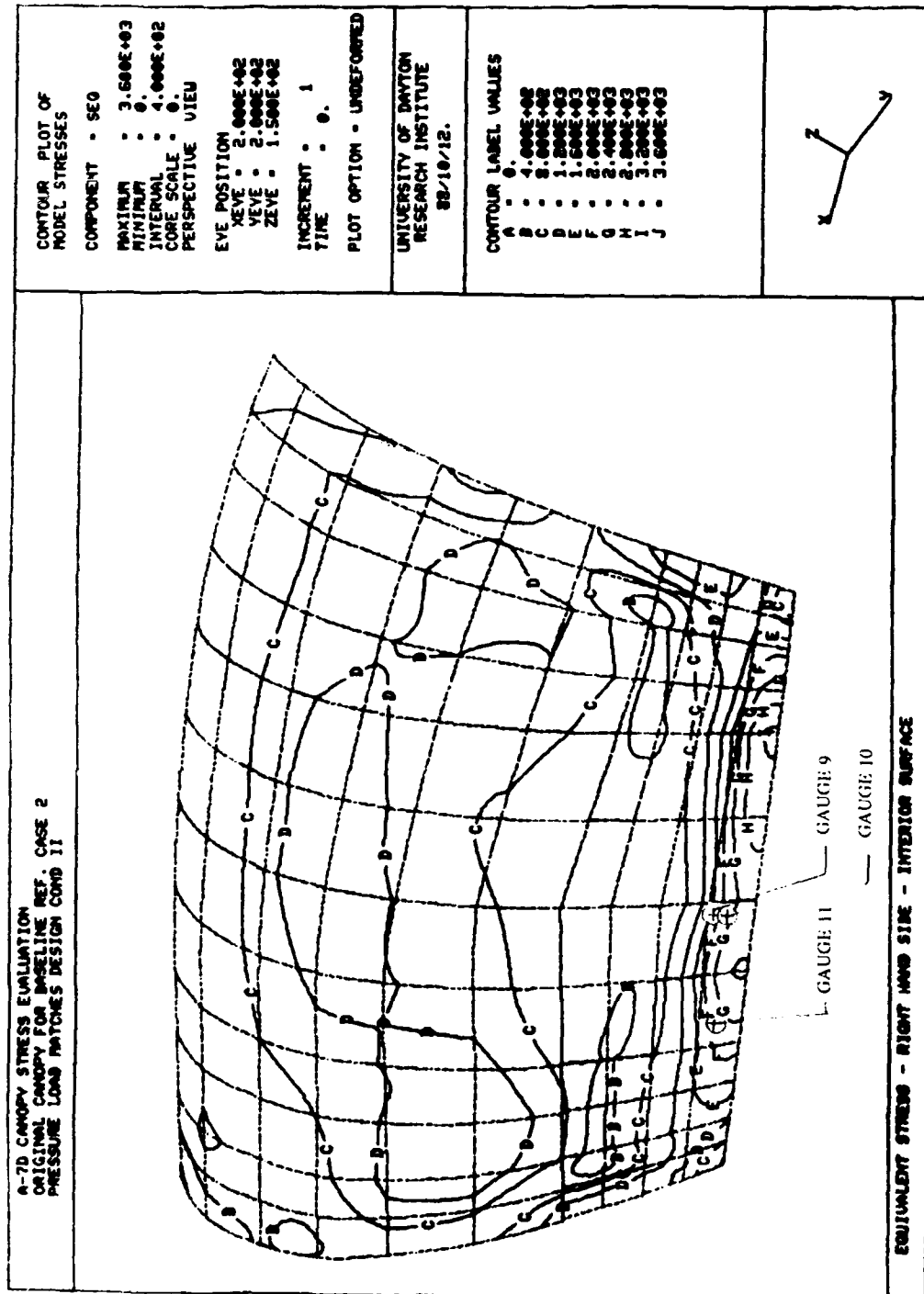


Figure 30. von Mises Stress Distribution on Right Side of Interior Surface of Initial Model of Canopy.



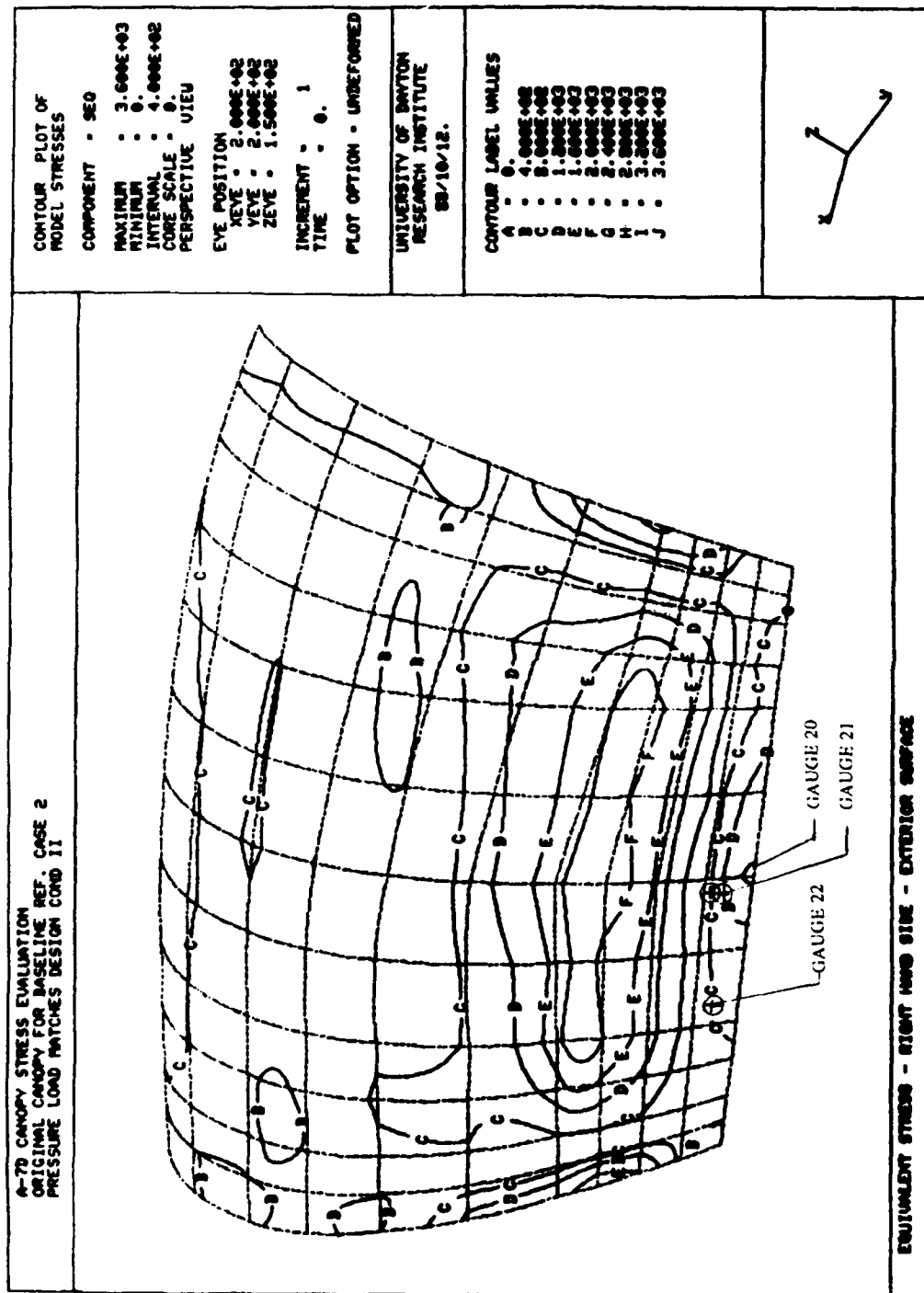


Figure 31. von Mises Stress Distribution on Right Side of Exterior Surface of Initial Model of Canopy.

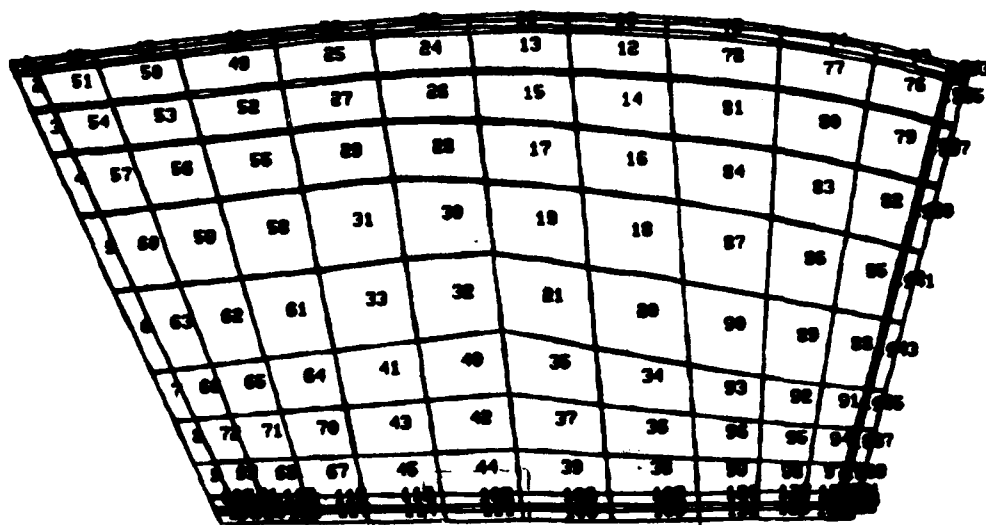
The stresses on the transparency surface directed perpendicular to the side rail from both the tests and the FE analysis are listed in Table 2. The flight test data were obtained at a canopy pressure  $\Delta P=4.9$  psi, dynamic pressure  $q=3.28$  psi, and temperature of  $54^\circ\text{ F}$  [3]. The theoretical conditions used for the model were canopy pressure  $\Delta P=5.0$  psi, dynamic pressure  $q=3.84$  psi, and temperature  $54^\circ\text{ F}$  [4].

Table 2 - Stresses Normal to Side Rail at Strain Gage Locations (initial model)

Gage Number	Measured Stress (psi)	FE Model Stress (psi)
9	1044	2600
10	1816	3400
11	2291	2900
20	40	-1300
21	-670	-2100
22	-571	-1500

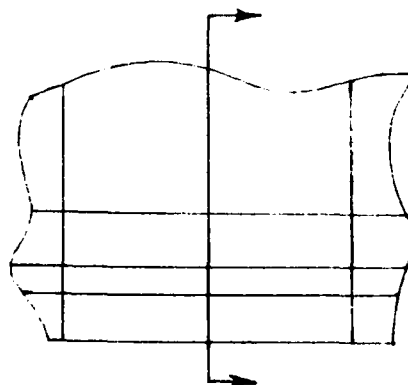
Averaging the stresses on the inner and outer surfaces gives the in-plane component of the stress. The in-plane stresses from the model were in reasonable agreement with the strain gage data. However, the stresses due to bending were much higher for the model than for test data. The high bending stresses were due to the simplified manner used to model the attachment of the canopy acrylic and the canopy frame. The lower stresses in the actual canopy indicated that the physical attachment between the transparency and the side rail had more flexibility than was allowed in the model.

Rather than attempt to model the attachment exactly, the elements near the frame were refined and tapered. A profile of the element mesh used is shown in Figure 32. The elements closest to the model's edge were tapered to increase the flexibility in this region. The tapered elements were in the region which, on the actual canopy, is actually nylon or is covered by nylon and aluminum. Thus, the tapered elements were not in the region where stresses were considered critical.



see Detail

Location of  
Beam Element Attachment



Detail of Elements at Edge

Figure 32. Shell Elements for the Revised Model of Canopy.

A comparison between the strain gage data and the results from the revised model is listed in Table 3. Good agreement exists between the test data and the results from this revised model.

Table 3 - Stresses Normal to Side Rail at Strain Gage Locations (revised model)

Gage No.	Measured Stress (psi)	FE Model Stress (psi)
9 (inside)	1044	1400
10 (inside)	1816	2050
11 (inside)	2291	2300
20 (outside)	40	20
21 (outside)	-670	-600
22 (outside)	-571	-550

LTV [3] used strain gage data in conjunction with a finite element model to determine the stresses in the transparency. Results of the MAGNA model are compared with the LTV results for the load case under consideration in Figures 33 through 35. Stresses in all of the figures are on the inside surface of the transparency at the location where the nylon and acrylic join. Stresses shown are normal to the frame. The figures show good agreement between the LTV and MAGNA results for the side rail and aft former. In particular, the peak value of 2950 psi above the forward latch agrees very well for both models. However, the stress levels predicted by the MAGNA model at the front former did not correlate well with those predicted by LTV. This was not considered significant because peak stresses do not occur in that region and no structural modifications were intended for the front former.

The good correlation between the results from the MAGNA model and the LTV data was considered sufficient to validate the use of this model as a baseline for investigating the effects of modifications to the transparency or structure. In Figures 36 and 37, von Mises stress distributions are shown for the inner and outer surfaces of the canopy respectively for the critical load case. The figures show that highest stresses occur on the inside surface above the forward

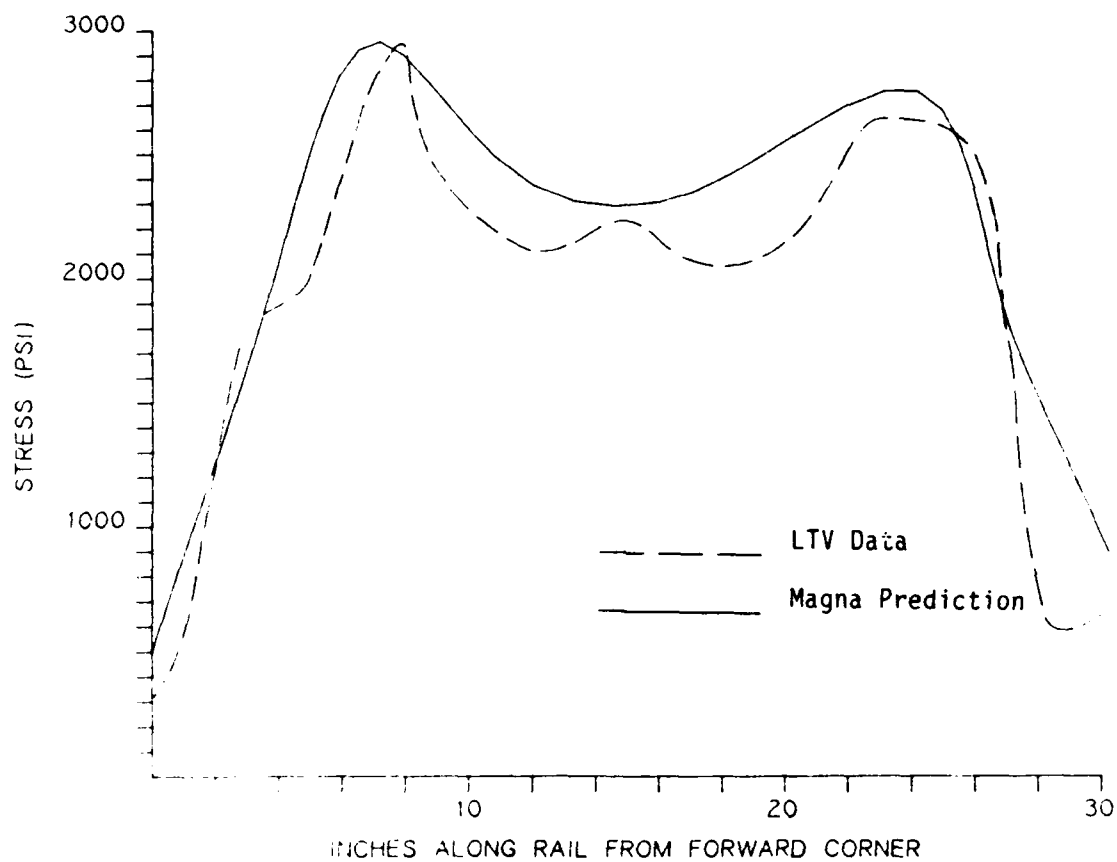


Figure 33. Stress Distribution Perpendicular to the Right Side Rail.

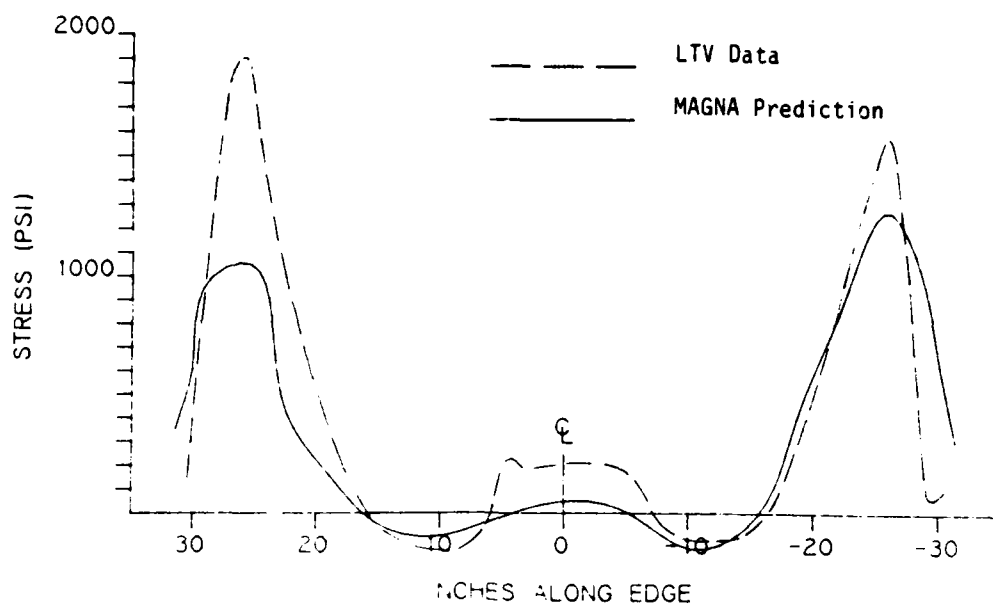


Figure 34. Stress Distribution Perpendicular to Forward Former.

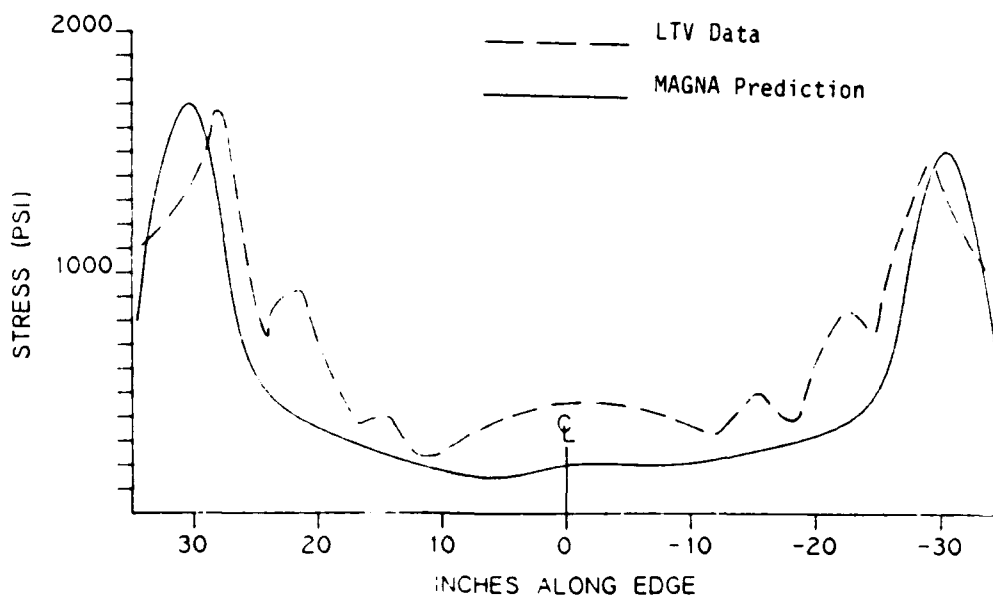


Figure 35. Stress Distribution Perpendicular to Aft Former.

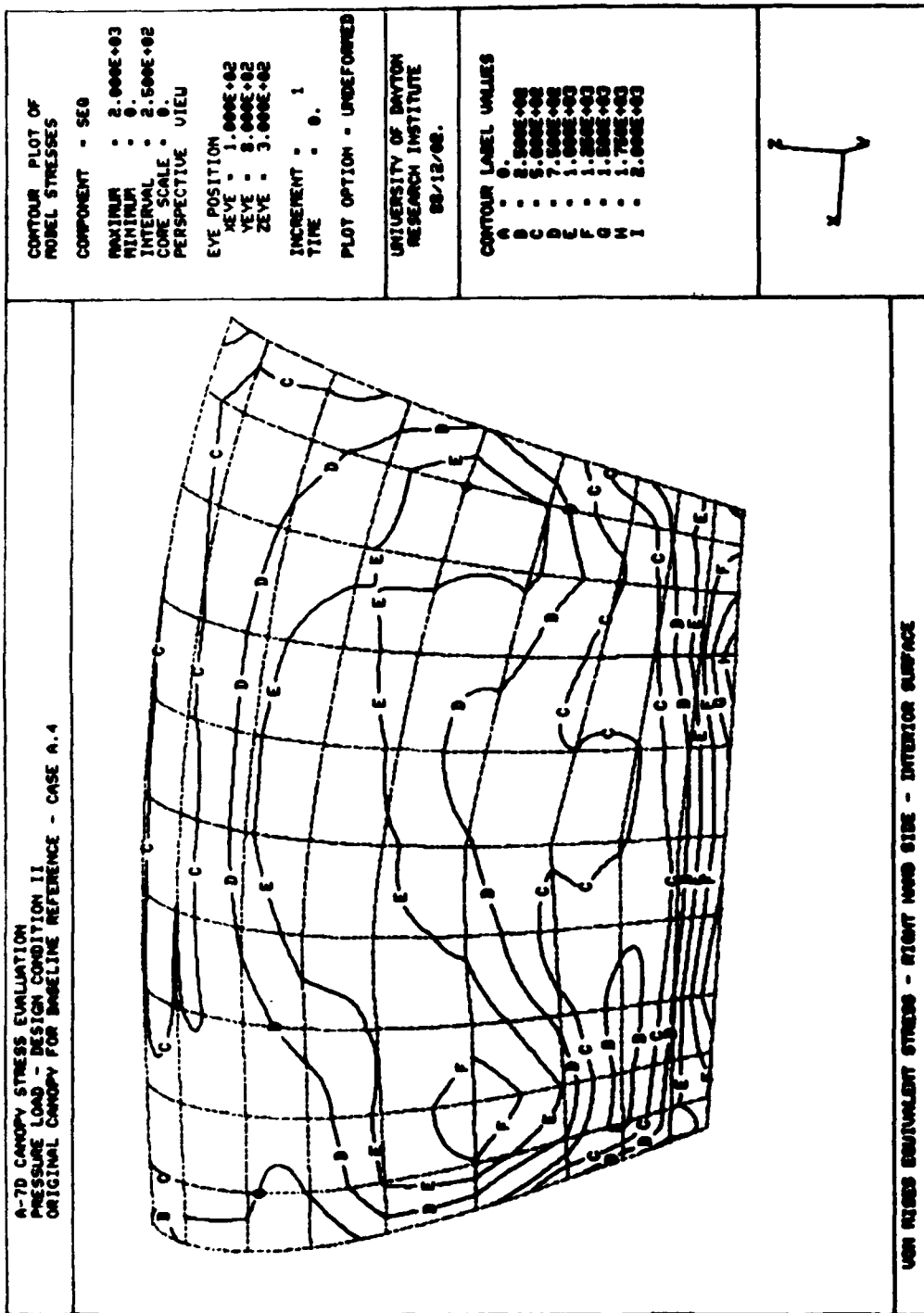


Figure 36. von Mises Stress Distribution on Right Side of Interior Surface of Revised Model of Canopy.

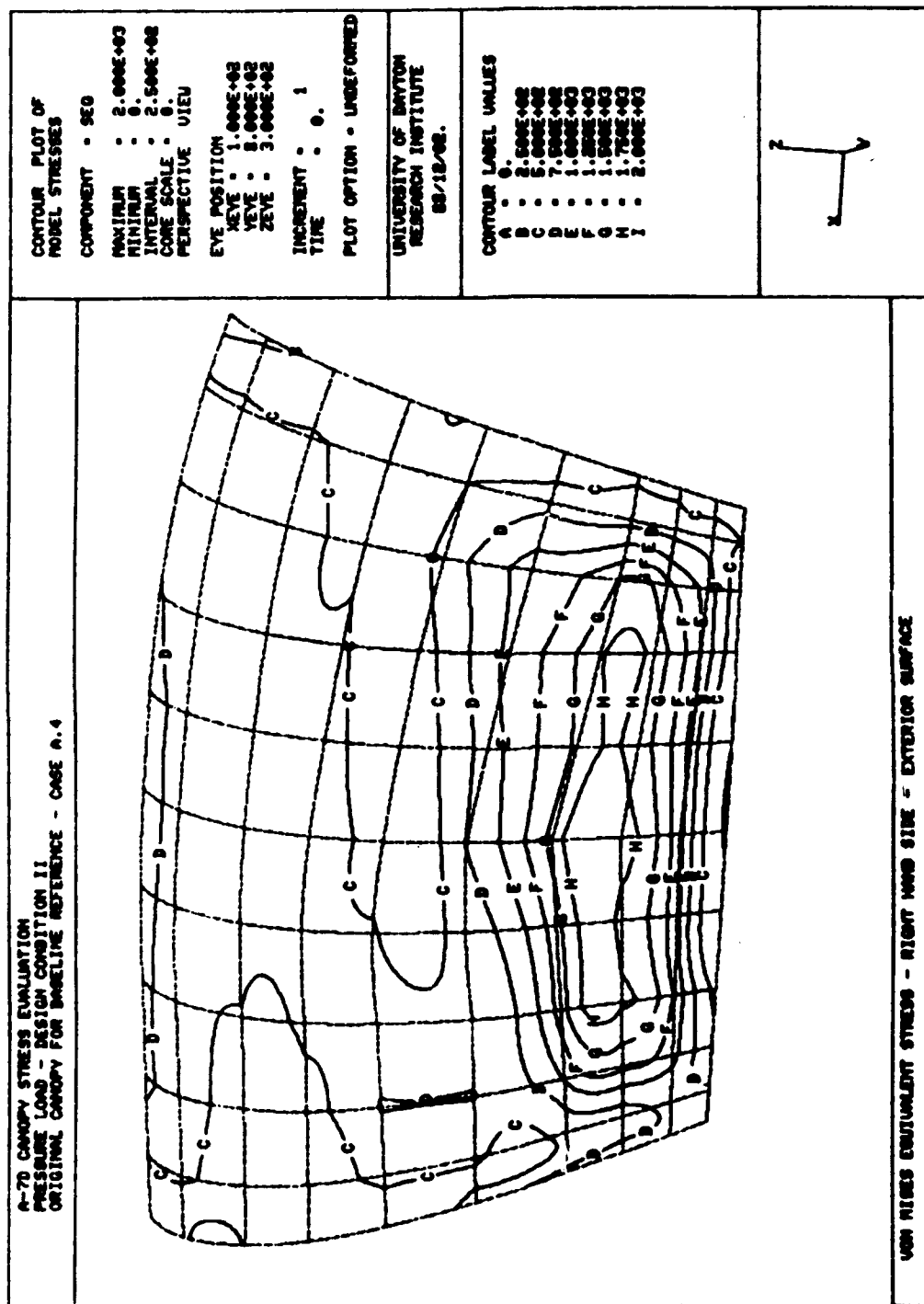


Figure 37. von Mises Stress Distribution on Right Side of Exterior Surface of Revised Canopy.



latch and on the outer surface approximately 5 inches above the side rail. These stresses are caused primarily by bending as the canopy "mushrooms" due to the pressure load.

The calculated stress levels in the transparency correlated closely with experimental data. The model of the current canopy showed that peak stresses occur on the inner surface of the transparency just above the forward latch and on the outer surface 5 inches from the side rail. These were the critical stress locations for evaluating the modifications discussed in Sections 3.1.3.

### 3.1.3 Analysis of Extended Transparency

The detailed analysis of extending the canopy transparency is described in this section. The model described in Section 3.1.2 was modified to represent extension of the transparency by 4.5 inches while maintaining the production moldline.

At the time that this analysis was performed, an extended length for the transparency had not been selected. The modifications in Section 3.2 were designed to provide a 5-inch retainer. The changes in results were not significant enough to require repeating the analysis.

Three cases were run to evaluate the effects of different aft structures on the stresses in the acrylic. The first case represented a typical aft frame structure. Cases 2 and 3 were included to evaluate the effects of extreme changes in support structure stiffness on the stress distribution in the transparency. The cases run were:

1. Replace existing aft arch with a more flexible aft arch than that currently used, but otherwise use the same aft structure. Properties of the arch used were:

$$A = 1.55 \text{ in}^4, I_{xx} = 2.27 \text{ in}^4$$

$$I_{yy} = 0.82 \text{ in}^4, I_{xy} = 0.27 \text{ in}^4$$

These properties are consistent with narrowing the existing arch by 4.5 inches.

2. Fixing the aft edge of the transparency, eliminating the aft structure. (This case represents an extremely stiff aft arch.)
3. Fixing the lower portion of the transparency and allowing the aft edge of the transparency above W.L. 132 to be free. (This case represents an extremely flexible aft arch.)

For all three cases the conditions at the side rail and front former were the same as for the model in Section 3.1.2.

Results of the three cases are compared with the analytic results for the original canopy in Figures 38 and 39. Figure 38 shows the stress normal to the side rail on the inner surface for the original canopy and for case 1. Results for cases 2 and 3 showed trends nearly identical to that of case 1, but with a slightly lower peak value. The figure shows that for the lengthened transparency the location of the peak value shifts from the forward latch to the aft latch. The peak value increases about 3 percent, from 2950 psi to 3040 psi.

Figure 39 shows the stress normal to the aft edge on the inner surface for all three cases as well as the original canopy. In all three cases the peak stress was reduced by lengthening the canopy. As expected, a stress concentration occurs for case 3 at the point where the aft edge changes from clamped to free. However, this discontinuity, which would not exist on an actual canopy, did not affect the stress outside of a small region.

Figures 40 through 45 show the von Mises stress for the inner and outer surface of the canopy for the three cases. For all three cases the distribution is nearly identical except near the aft edge, demonstrating that the aft structure does not significantly affect the overall transparency stress levels or stress distribution for closed canopy operation. The peak value of von Mises stress occurs on the outer surface of the canopy between the two latches. The elongated models predicted that this value increases by about 3 percent, from 2000 psi in the original model to 2060 psi. In all cases the peak stresses were well below the flexural fatigue strength of 4,800 psi [6] for stretched acrylic at 106 cycles. Thus, a satisfactory margin of safety can be maintained for the elongated transparency without increasing the thickness of the transparency acrylic. Although the stress level in the nylon edge was not evaluated, the small increase in stress in the acrylic should not significantly change the stress in the nylon edge.

The three boundary condition cases analyzed represented a wide range of possible aft support structures. The analysis in this section showed that changes in aft frame stiffness did not significantly affect the stress levels in the canopy transparency. In the recommended aft configuration presented in Section 3.2, the lower part of the aft structure is much stiffer than that of the current frame, while the upper part is more flexible. The proposed modifications would extend the transparency by 5.0 inches. Although the finite element cases were run for a 4.5-inch extension, the differences in results for a 5-inch extension were not

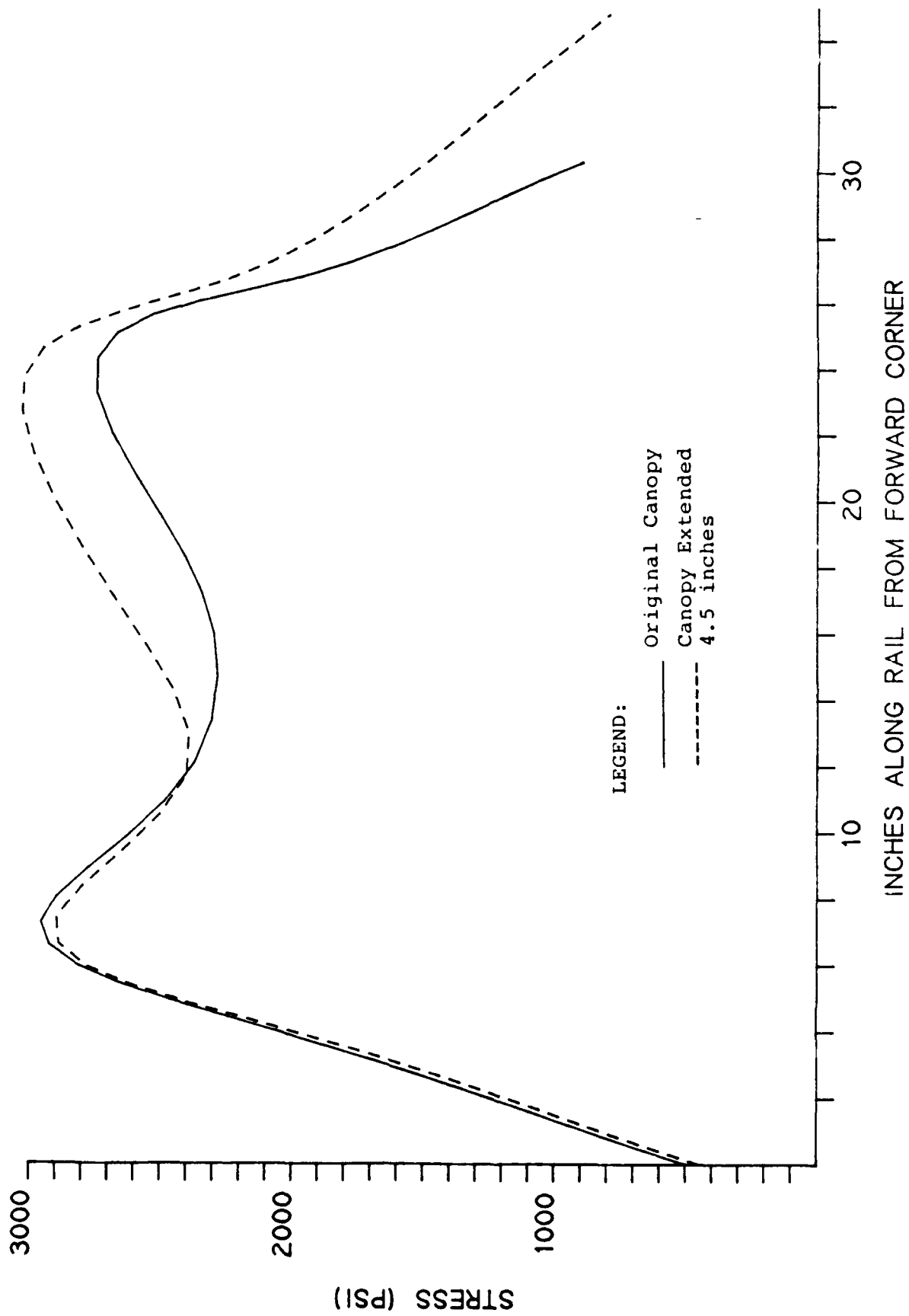


Figure 38. Stress Distribution Perpendicular to Right Side Rail on Interior Surface.

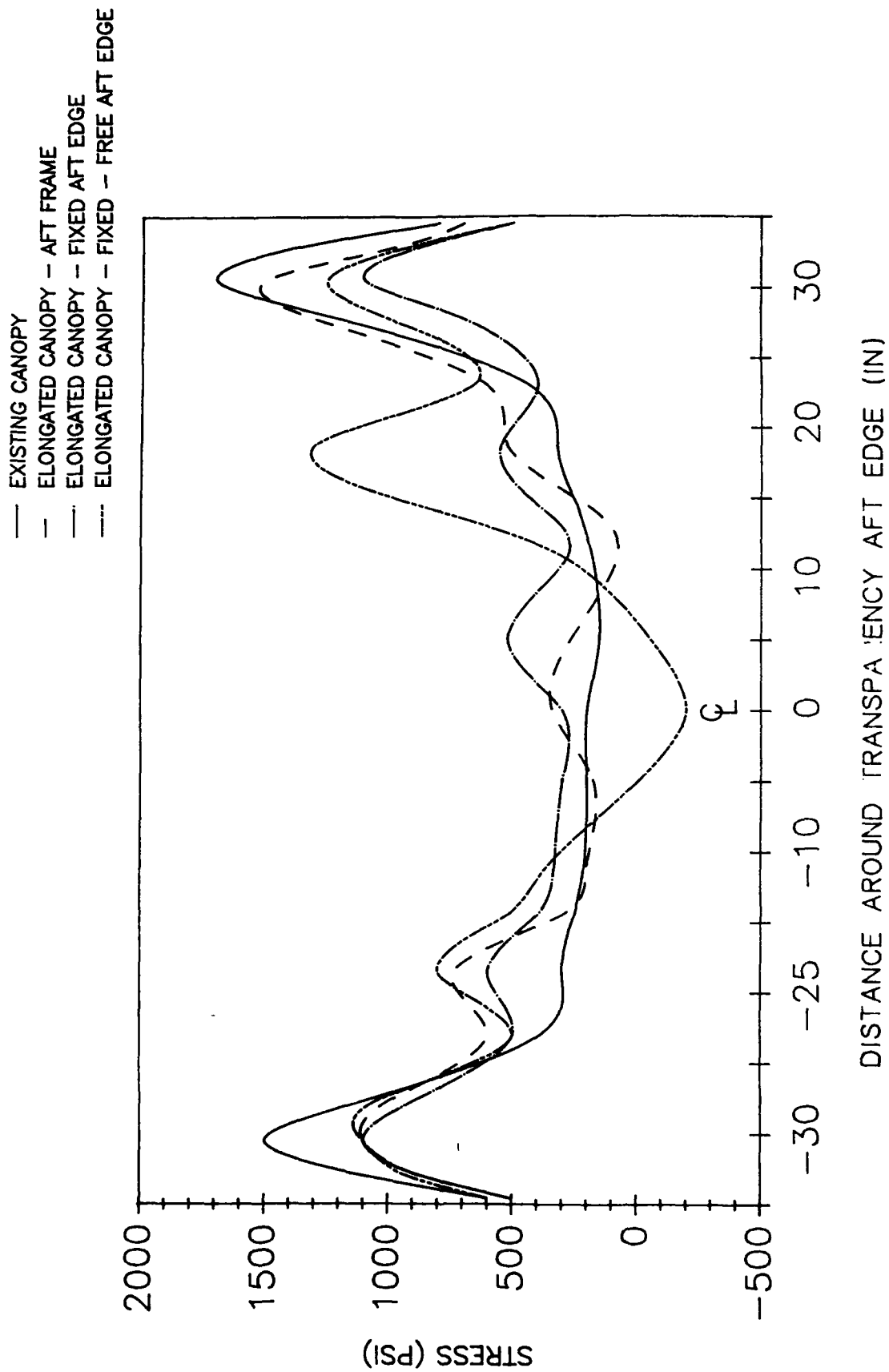


Figure 39. Stress Distribution Perpendicular to Aft Former on Inner Surface.

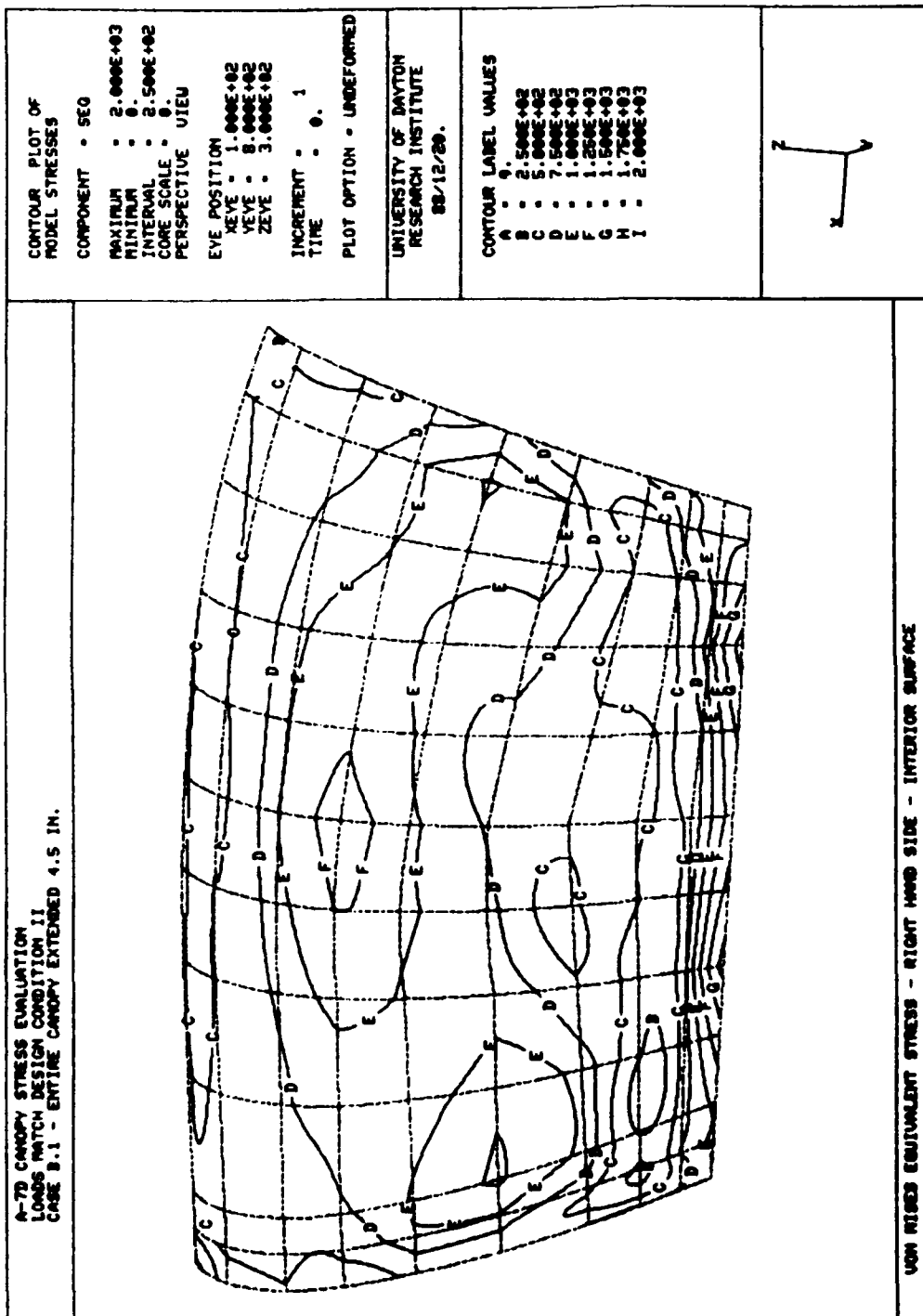


Figure 40. von Mises Stress on Inner Surface of Canopy - Reduced Aft Frame.

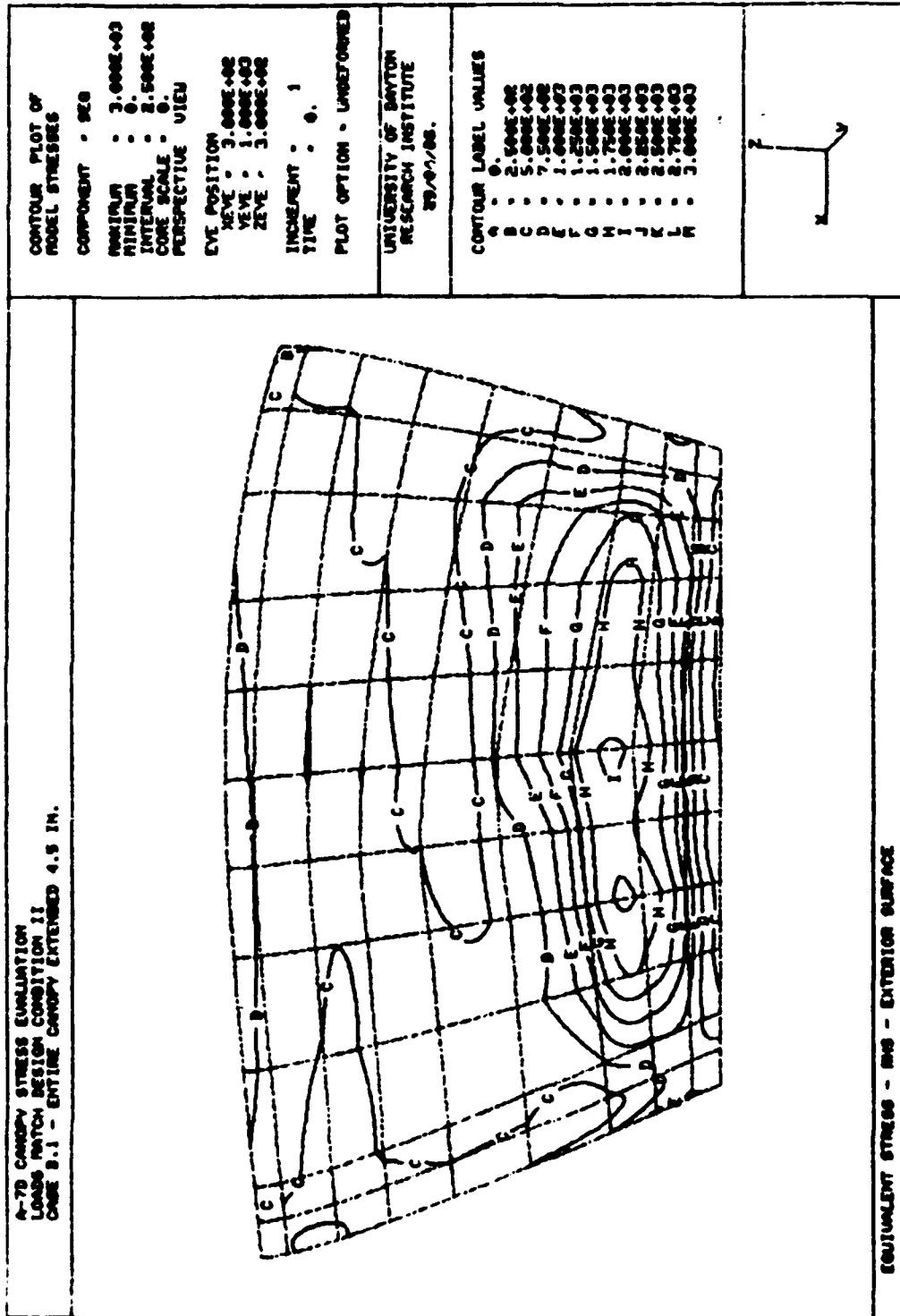


Figure 41. von Mises Stress on Outer Surface of Canopy - Reduced Aft Frame.

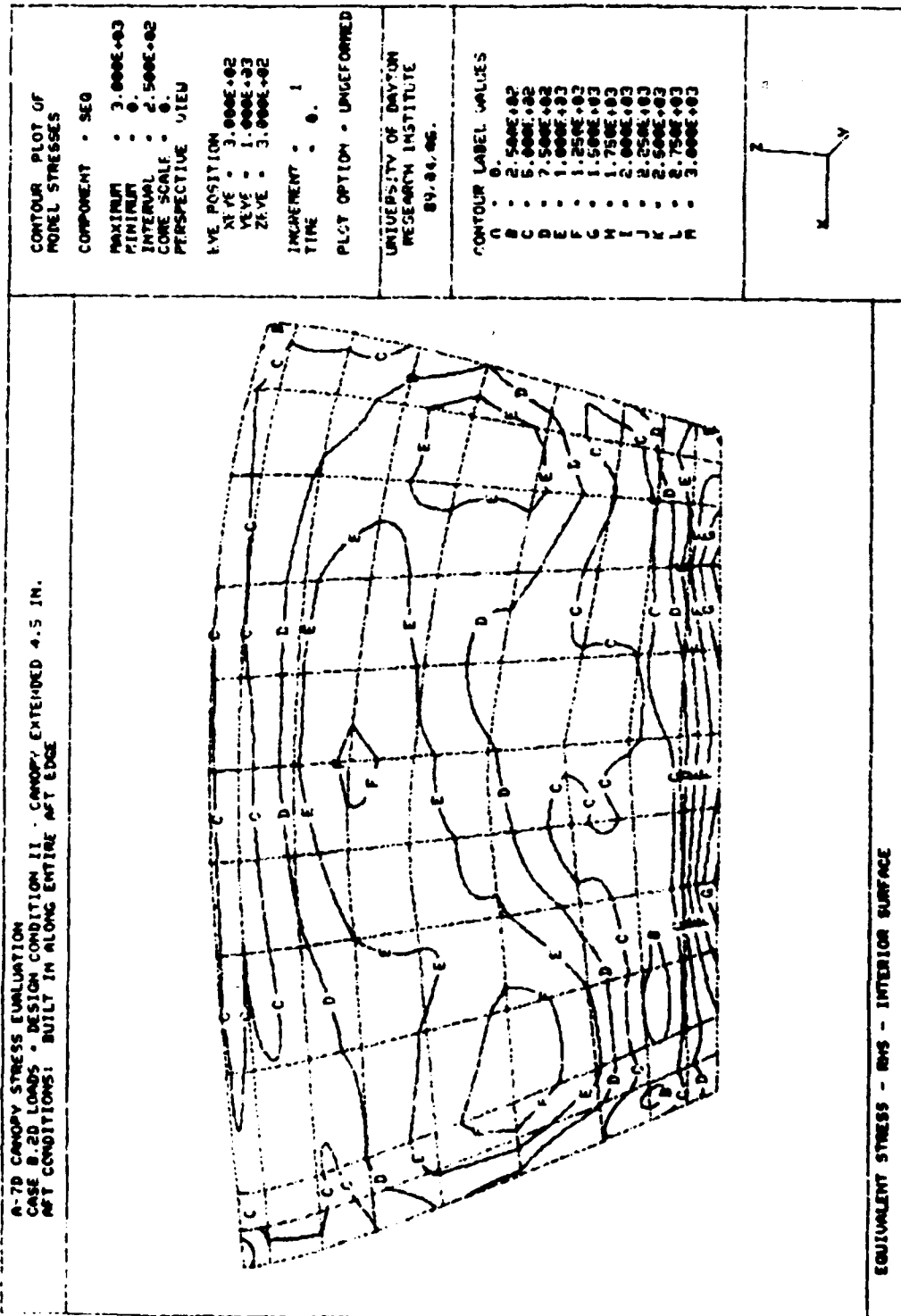


Figure 42. von Mises Stress on Inner Surface of Canopy - Clamped Along Aft Edge.

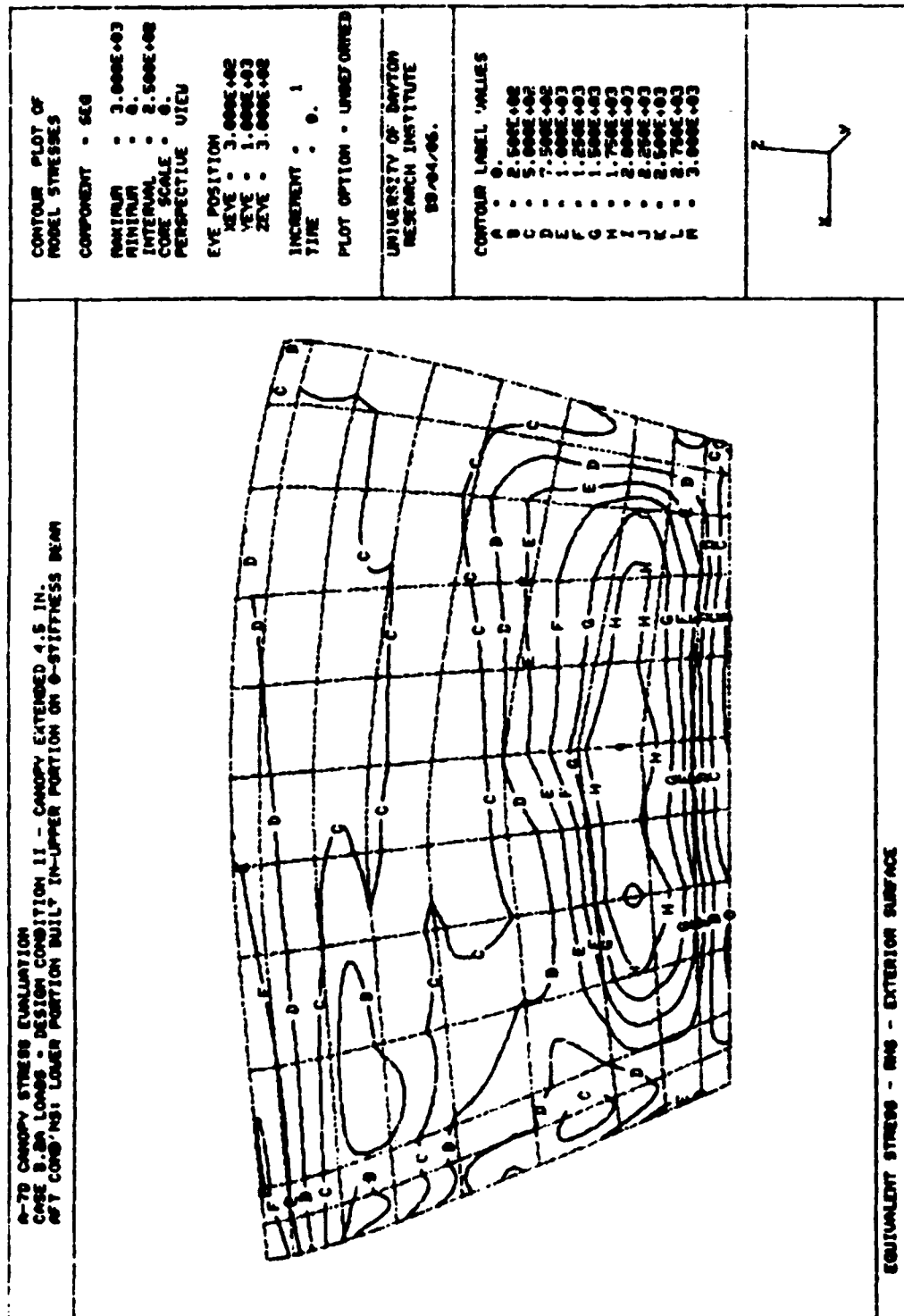


Figure 43. von Mises Stress on Outer Surface of Canopy - Clamped Along Aft Edge.



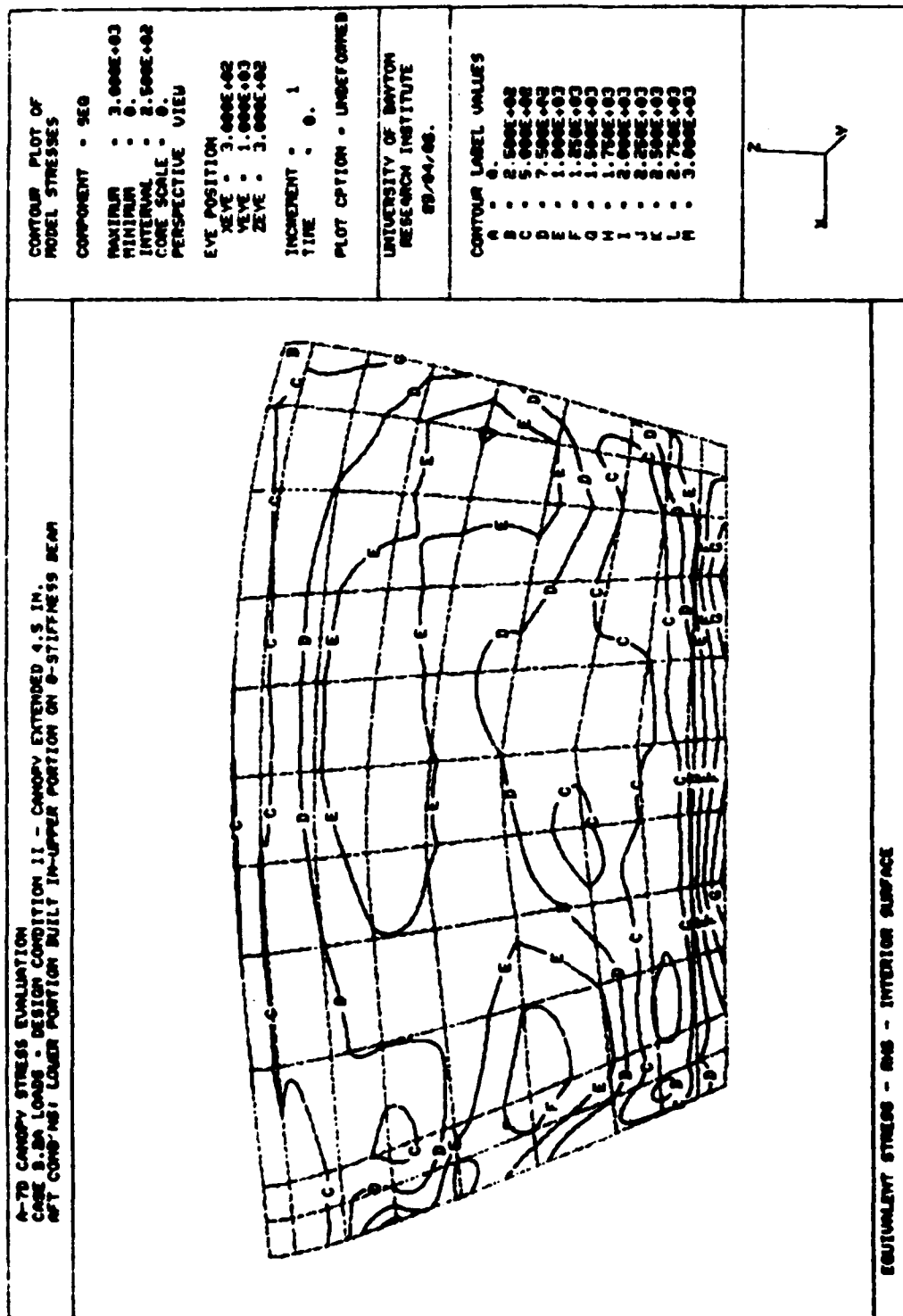


Figure 44. von Mises Stress on Inner Surface of Canopy -  
Clamped Lower, Free Upper Aft Edge.

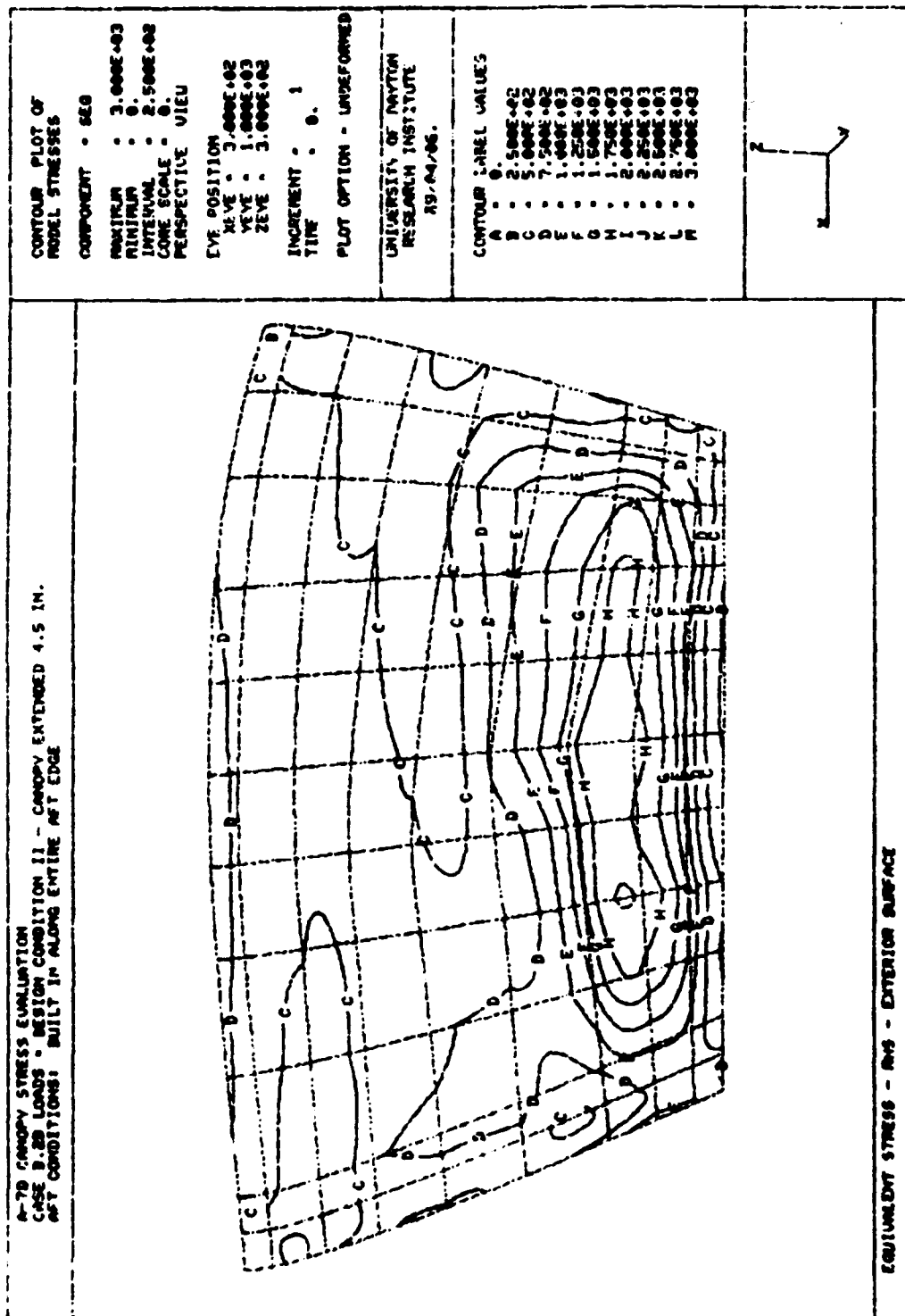


Figure 45. von Mises Stress on Outer Surface of Canopy -  
Clamped Lower, Free Upper Aft Edge.

expected to be significant enough to require repeating the analysis. Based on the results of case 3, which is the limiting case of a stiff lower section and flexible upper section, stresses due to the proposed modifications should remain in an acceptable range. Thus, the extended stretched acrylic transparency can remain 0.25 inch thick.

### 3.2 MODIFIED CANOPY AFT FRAME DESIGN

A modified aft frame for the canopy which would allow the transparency to be extended was designed. Advanced composites were selected for the modified frame because they offered the design flexibility and high stiffness-to-weight ratio necessary to allow the transparency to be extended by 5.0 inches (increasing the weight of the acrylic panel by 4.5 lb) without increasing the total weight of the canopy. Unidirectional graphite/epoxy was used in areas requiring high stiffness and/or strength. Woven Kevlar was used in selected areas to provide high impact resistance. A detailed description of the redesigned structure is presented in Appendix B.

The basic differences between the existing and modified frames are illustrated in Figures 46 and 47, which include:

1. replacing the magnesium arch (rectangular tube section) with a straight graphite/epoxy tube as the primary structure for torsional stiffness of the canopy,
2. replacing the magnesium beams along the sides of the aft frame with graphite/epoxy beams,
3. replacing the rib-stiffened aluminum pressure panels with honeycomb composite panels,
4. replacing the aluminum skin with a woven Kevlar skin of equal bending stiffness,
5. replacing the aft transparency support flange on the magnesium arch with a Kevlar support strip.

The modified structure was designed to (1) match or exceed the stiffness and strength of the existing frame, (2) require no modifications to surrounding aircraft structures, and (3) match the overall weight of the existing canopy assembly. The overall stiffness and strength of the existing and modified frames are compared in Appendix A for a variety of load cases. Loads

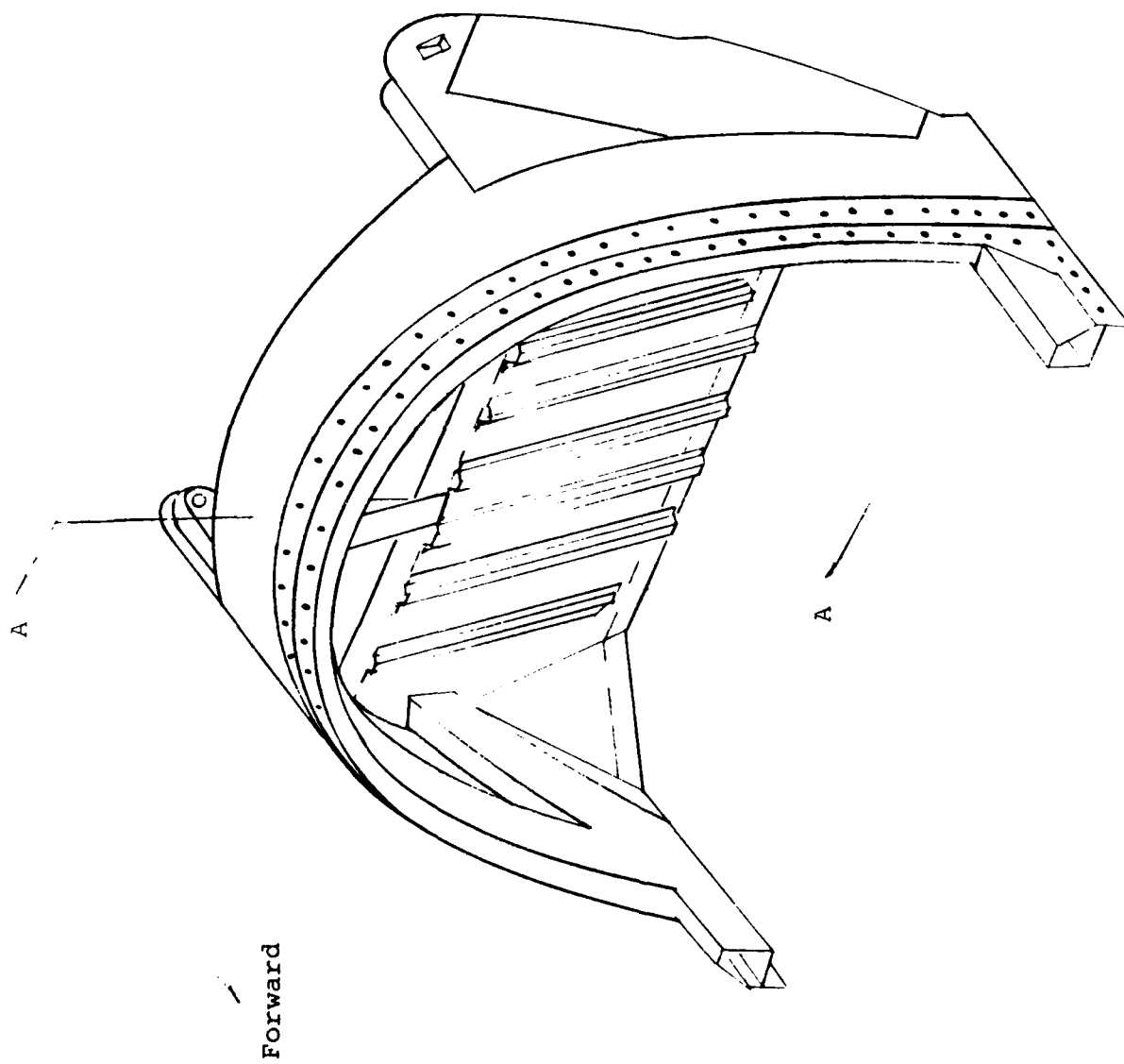


Figure 46. Existing Aft Canopy Frame [Ref. 7].

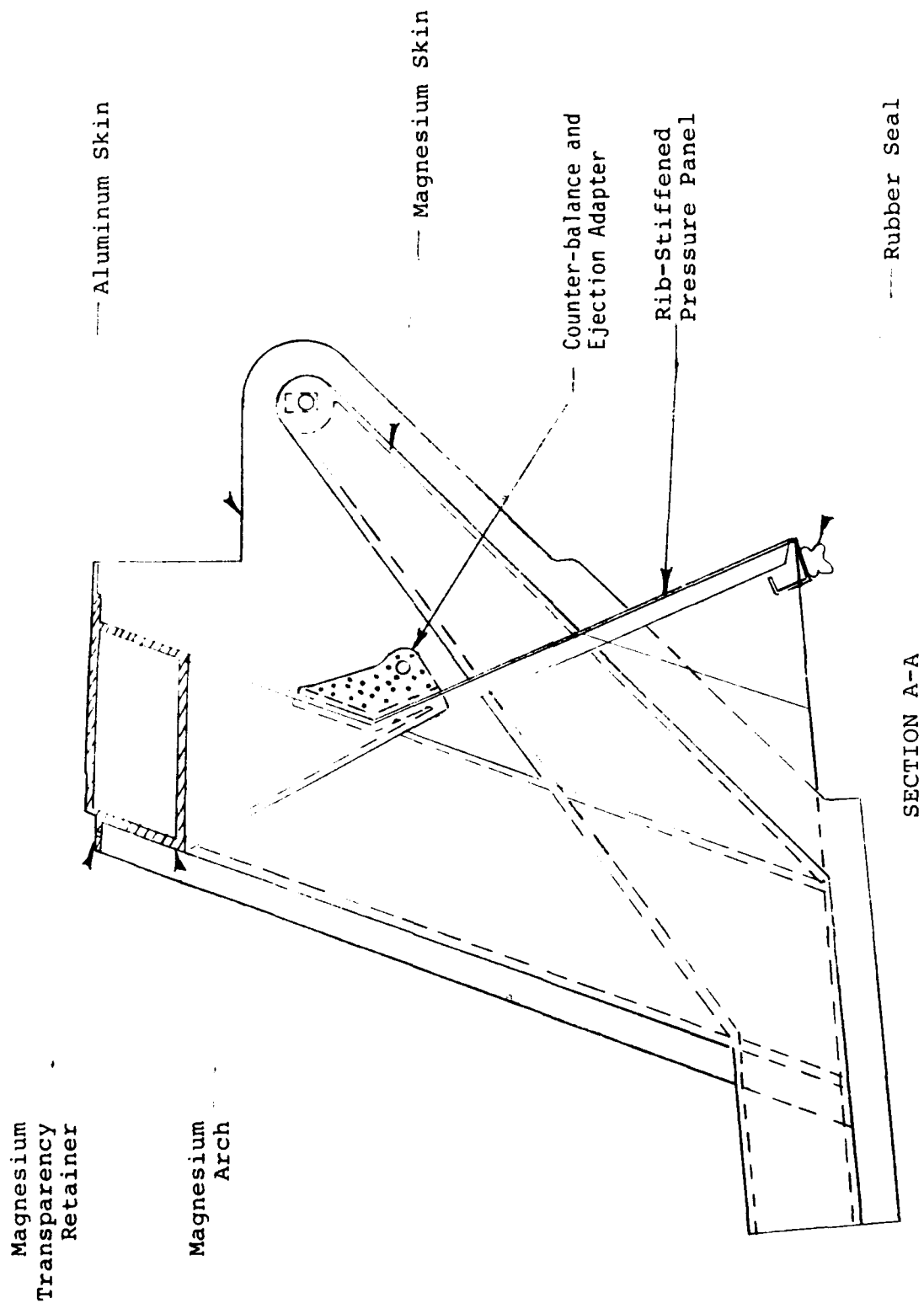


Figure 46. (continued).

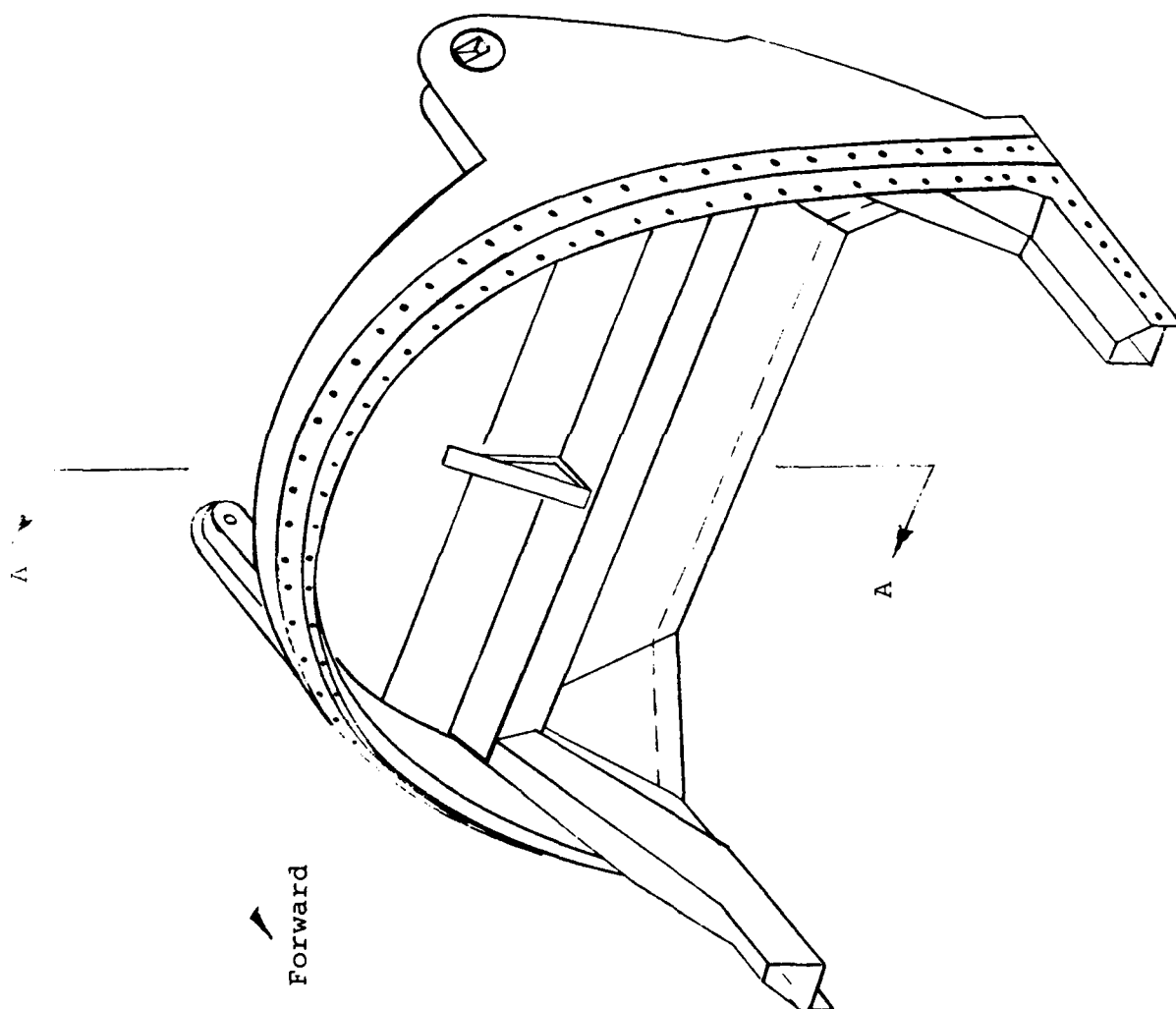


Figure 47. Modified Aft Canopy Frame.

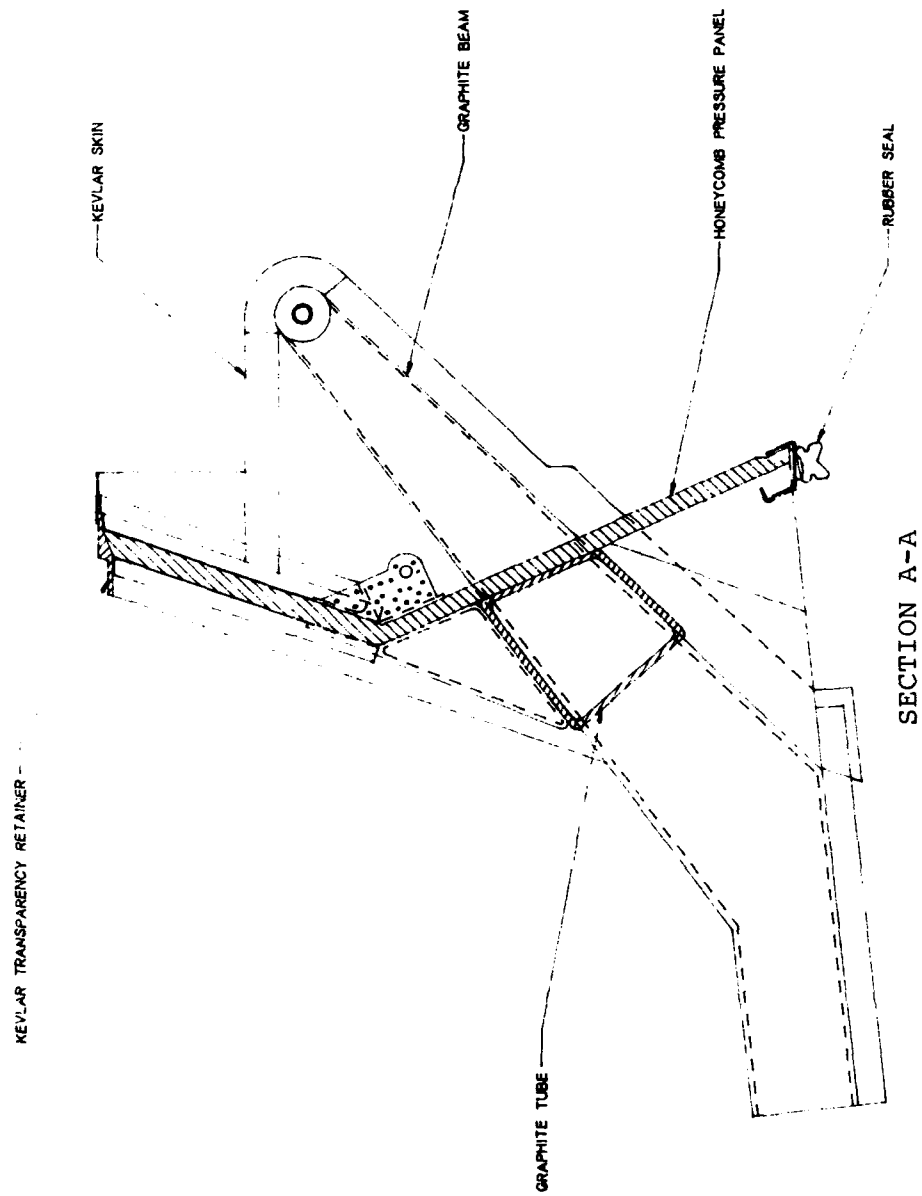


Figure 47. (continued).

encountered by the frame for both open and closed canopy operation were considered. For all cases, the modified frame equalled or exceeded the strength and stiffness of the existing frame.

To facilitate integration of the modified frame into the rest of the structure, no changes have been made in the hardware used for attaching the aft frame to the existing canopy side rails. The rubber pressure seal and seal mounting hardware are the same as on the current production canopy. The canopy counterbalance adapter assembly is also retained, as are the splice plates where the aft frame attaches to the side rails. Thus, the only modifications required are rebuilding the aft frame and extending the transparency.

The modified canopy was designed to match the weight of the existing structure. In Section 3.3 the effects of the redistribution of weight in the canopy are discussed. Table 4 summarizes the weights of the individual components of the altered structure. The total theoretical weight of the modified parts, 31.53 lb, matches almost exactly with the 31.51 lb given for the corresponding parts on the existing canopy [1].

### 3.3 INERTIAL PROPERTY EVALUATION

The structure proposed in Section 3.2 has the same mass as the existing structure, but the mass is distributed differently. The effects of the change in mass distribution on the inertia properties of the canopy were evaluated using three-dimensional CAD models of the structure. The models show that the principal inertias change by less than one percent. Thus, canopy ejection, which is affected by the inertial properties of the canopy, is essentially unaffected by the proposed structural modifications.

To evaluate the effects on inertial properties of the changes proposed in Section 3.2, a three-dimensional CAD model of the canopy was generated. This model allowed the mass moments of inertia, which govern the dynamic response of the canopy, to be calculated accurately. A modified canopy model, which included the proposed changes, was developed from the model of the existing canopy. The models used lines and surfaces with effective densities and cross-sections to approximate the mass distribution for the canopies. The weights used for modeling the existing canopy and forward portion of the modified canopy were obtained from the theoretical weights listed on LTV assembly drawings [1].

The weight of a canopy assembly based on parts lists [1] was 92.28 pounds. An actual A-7D canopy (SN A6-232), from which the mirrors and rubber seal were missing, weighed 94.5 X 0.5 pounds. The mass distribution of the model of the existing canopy was based on the



Table 4 - Weight of Modified Frame Components

Part	Quantity	Weight per Unit (lb)	Total Weight (lb)
5.0 in acrylic extension	1	4.50	4.50
Aft frame cross tube	1	6.56	6.56
Beams along aft frame sides	2	3.51	7.02
Pivot bolt adapter	2	0.38	0.76
Pressure panels	1	4.30	4.30
Skin	1	3.13	3.13
C'balance adapter support	1	0.28	0.28
Transparency edge support	1	2.48	2.48
Pressure panel edge retainer	1	0.29	0.29
Fasteners:			
Nutplates	107	0.0015	0.1605
Blind fasteners	4	0.0122	0.0488
	12	0.0071	0.0852
	4	0.0068	0.0272
	42	0.0055	0.2310
Panel Inserts	63	0.0012	0.0756
	4	0.0105	0.0420
	4	0.0092	0.0368
Gussets at tube joint	2	0.24	0.48
	2	0.11	0.22
	2	0.09	0.18
2% Adhesive allowance	-	0.62	0.62
TOTAL			31.53

theoretical component weights. However, these weights were scaled up by 2.4% to achieve a value of 94.5 pounds, matching the measured value. The computed center of gravity (CG) of the model was 0.31 inch below and 0.30 inch forward of the measured location of the CG. The difference between the measured and calculated location of the CG was within the tolerances of the measurements; the computed values were 0.18 inch below and 0.24 inch forward of the

measured values. Thus, the CAD model was acceptable for use as a baseline in determining the effects of the proposed modifications on the inertia properties of the canopy.

The model of the original canopy was modified to account for the changes proposed in Section 3.2. The modified model also had a weight of 94.5 pounds. Values for the CG and inertias of the existing and proposed canopies are listed in Table 5. Coordinates for this chart are based on a standard right-hand system aligned with the aircraft fuselage stations and waterlines. Positive directions are defined as in Figure 48. The models indicated that the CG of the modified canopy will be 0.36 inch lower than that of the existing canopy, primarily caused by the replacement of the magnesium aft arch with a composite torque tube.

Table 5 - Mass Properties of Existing and Modified Canopies

Weight	Existing Measured 94.5±0.5	Existing Calculated 94.50	Modified Calculated 94.50	Change 0.0
CG Location (in)				
X	279.1±t	278.80	278.77	-0.03
Y	0.0	0.00	0.00	0.00
Z	127.8±0.5	127.49	127.13	-0.36
Inertias with respect to CG (10 <sup>3</sup> lb-in <sup>2</sup> )				
I <sub>xx</sub>	-	25.5	25.4	-0.1
I <sub>yy</sub>	-	32.2	32.5	0.3
I <sub>zz</sub>	-	45.5	45.4	-0.1
I <sub>xz</sub>	-	1.6	1.2	-0.4
I <sub>yz</sub>	-	0.0	0.0	0.0
I <sub>xy</sub>	-	0.0	0.0	0.0
Inertia with respect to aft pins (10 <sup>3</sup> lb-in <sup>2</sup> )				
I <sub>yy</sub> <sup>o</sup>	-	106.7	107.6	0.9

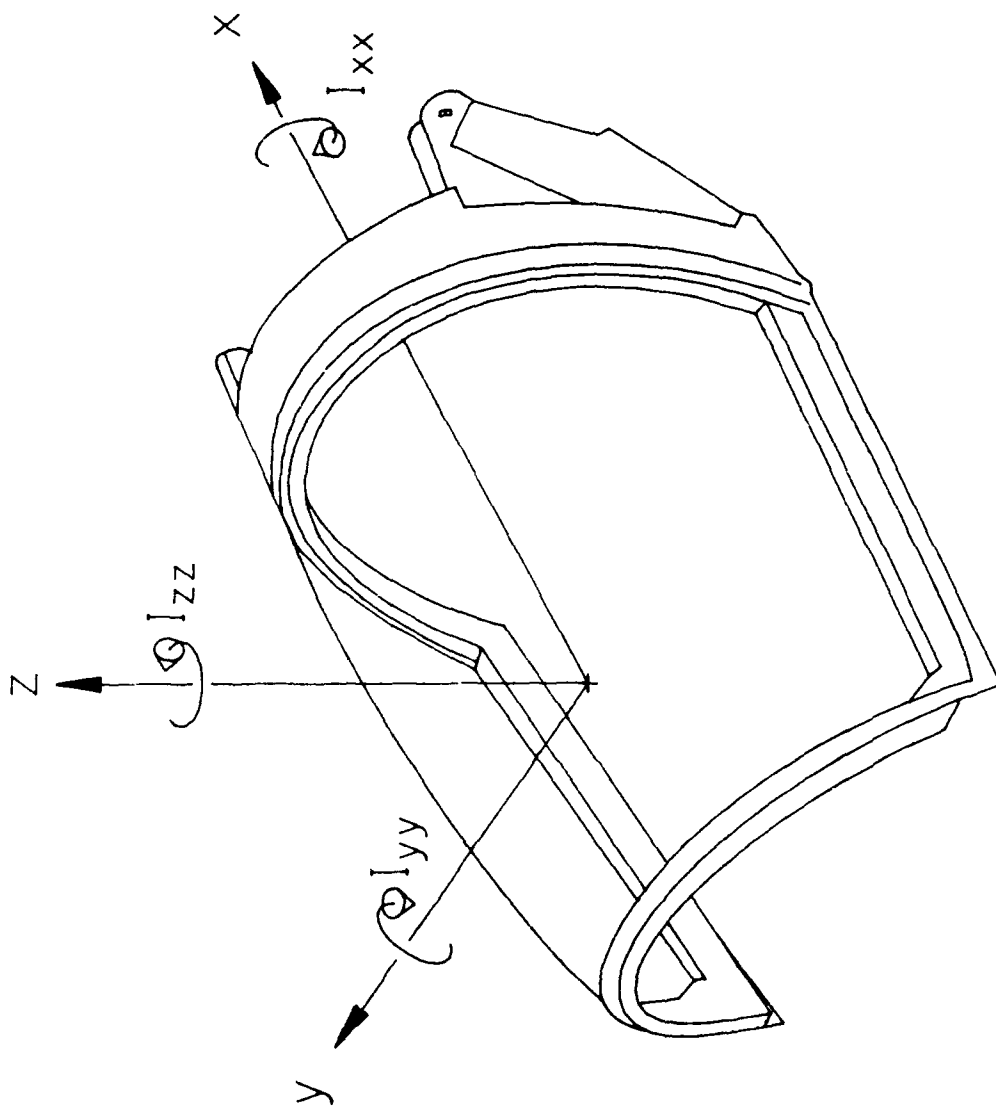


Figure 48. Sign Convention for Inertias.

The reaction of the canopy during ejection is controlled by the inertia with respect to the aft pins  $I_{yy}^o$ . If the aircraft is not accelerating, the motion of the canopy during ejection is described by

$$\Sigma M^o = I_{yy}^o \cdot \alpha. \quad (3)$$

$M^o$  are moments about the axis through the aft pins and  $\alpha$  is the angular acceleration of the canopy about the y-axis [8]. During ejection,  $M^o$  will be caused by the weight of the canopy, the pressure of the wind, and the force of the ejector. Since all of these forces are the same for both the original and modified canopy, the angular acceleration of the canopy  $\alpha$  is inversely proportional to  $I_{yy}^o$ . The models show that  $I_{yy}^o$  will increase by 0.8% due to the proposed changes. Thus, the modified canopy would accelerate about 0.8% slower during ejection than the existing canopy.

The location of the CG, the weight of the canopy, and the inertias with respect to the CG have a great effect on the motion of the canopy after it breaks free from the aircraft during ejection. These factors also have a slight effect on the overall motion and control of the aircraft. The theoretical weights of the existing and proposed versions are the same and, as shown in Table 5, the change in CG and inertias are small (less than 1%). Thus, the change in motion of the ejected canopy is negligible.

## SECTION 4

### CONCLUSIONS AND RECOMMENDATIONS

Five alternative systems were evaluated for increasing rearward visibility for the A-7D aircraft. These were increasing the canopy transparency length, adding external mirrors, modifying the internal mirrors, using refractive lenses, and altering the canopy profile. Of the alternatives evaluated, increasing the usable length of the canopy transparency is recommended. A 5-inch extension of the transparency would reduce the area currently hidden from the pilot's view aft of the aircraft by 31 percent. Additional internal mirrors could also offer some enhancement for rearward visibility. Refractive lenses could greatly increase rearward visibility, but would cause distortion and could reduce the effectiveness of the mirrors. External mirrors or modifying the profile of the canopy would not increase the area visible to the pilot.

Finite element modeling of the transparency showed that the stresses in the canopy acrylic are not significantly affected by increasing the transparency length. Thus, an extended transparency could have the same (0.25-inch) thickness as the current transparency. The modeling also showed that supporting the aft edge of the transparency with a more flexible structure than that which is currently used does not affect the maximum stress in the acrylic transparency.

The canopy aft frame was redesigned using advanced composites; as shown in Figure 49. This structure allows the transparency to be lengthened by 5 inches and was designed to be at least as stiff and strong as the current aft frame. The use of composite materials in the aft frame minimized its weight, offsetting the 4.5-pound transparency weight increase. The change in mass distribution due to the proposed modifications would not significantly alter the inertia of the canopy, and, therefore, egress and emergency jettison should be unaffected.

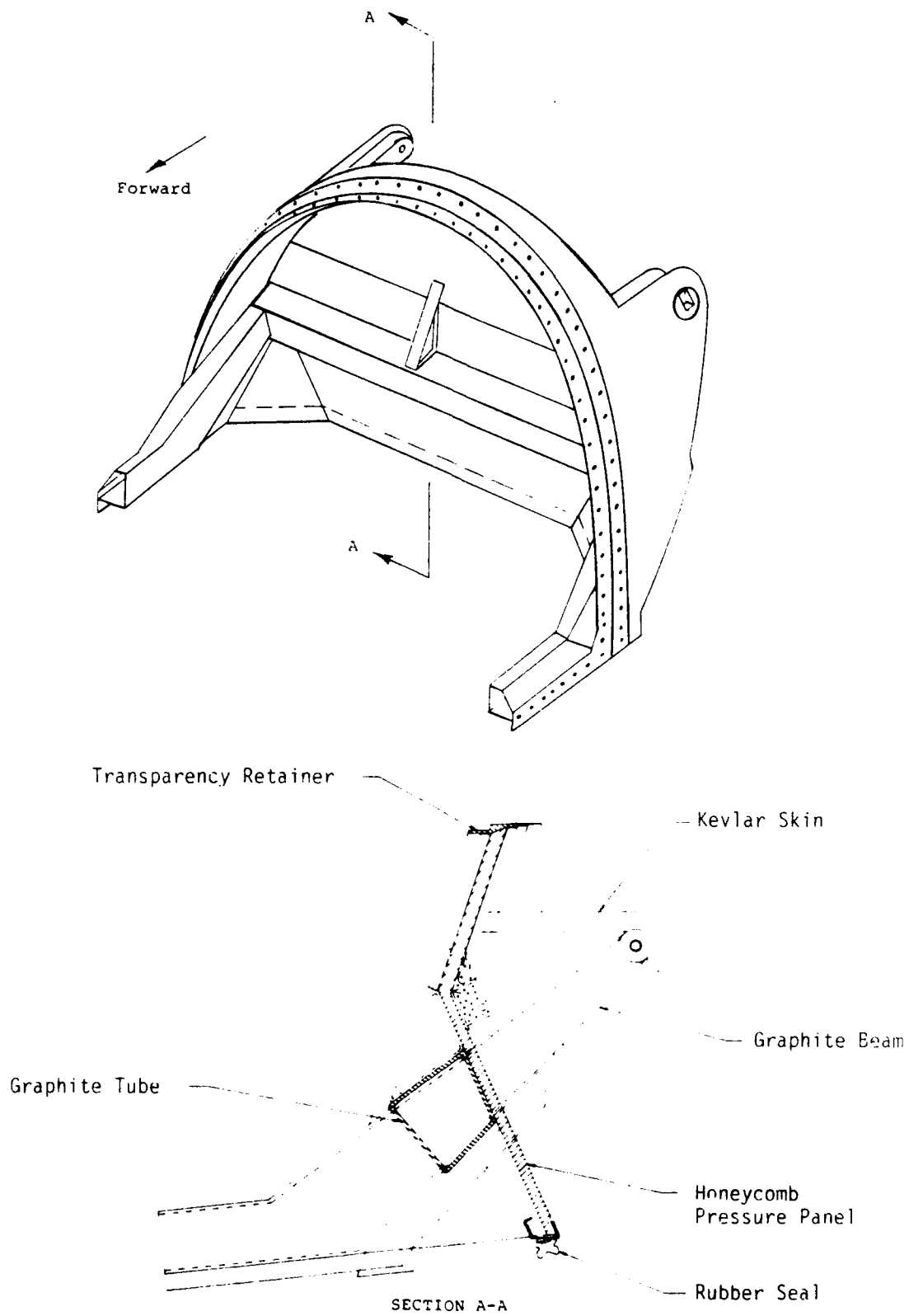


Figure 49. Recommended Canopy Aft Arch for 5-inch Extension of Transparency.

## REFERENCES

1. Drawing No. 215-20079, "Canopy Installation, Moveable Nose Fuselage Section," Vought Corp., Dallas, TX, February 1979.
2. Brockman, R. A., "MAGNA Computer Program User's Manual," UDR-TR-82-14, University of Dayton, Dayton, Ohio, December 1984.
3. "A-7 Canopy Structural Investigation," LTV TR 2-53440/GL-185, Vought Corp., Dallas, TX, 1976.
4. "Windshield and Canopy Stress Analysis Design Data," LTV TR 2-53420/ER-1969, Vought Corp., Dallas, TX, July 1965.
5. MIL-HDBK-5, "Strength of Metal Aircraft Elements," March 1961.
6. MIL-HDBK-17A, "Plastics for Aerospace Vehicles, Part II: Transparent Glazing Materials," June 1977.
7. T.O. 1A-70-4-2, "Illustrated Parts Breakdown, Airframe, A-7D," Vought Corp., Dallas, TX, August 15, 1984.
8. T. R. Kane and D. A. Levinson, Dynamics: Theory and Application. McGraw-Hill, New York, 1985.
9. S. W. Tsai, Composites Design. Think Composites, Dayton, Ohio, 1987.
10. MIL-HDBK-5, "Strength of Metal Aircraft Elements," March 1961.
11. DOD/NASA Advanced Composites Design Guide: Vol. I - Design, Air Force Wright Aeronautical Laboratories, Wright-Patterson Air Force Base, Ohio, July 1983.
12. "Data Manual for Kevlar 49," E. I. duPont de Nemours Co., Wilmington, DE, 1986.
13. M. Yoshkari, COSMOS/M User Guide, Structural Research and Analysis Corporation, Santa Monica, CA, May 1989.
14. Drawing No. 215-20403, "Canopy Aft Frame," Vought Corp., Dallas, TX, June 1971.
15. R. J. Roark and W. C. Young, Formulas for Stress and Strain. McGraw-Hill, New York, 1982.
16. J. T. Oden, Mechanics of Elastic Structures. McGraw-Hill, New York, 1967.
17. Metals Handbook, Vol. 2, American Society for Metals, Materials Park, OH, 1979.

18. Drawing No. 215-20425, "Bolt Shoulder, Serrated Canopy Pivots, Nose Fuselage Section," Vought Corp., Dallas, TX, August 1973.
19. N. J. Pagano, "Exact Moduli of Anisotropic Laminates," Mechanics of Composite Materials (Vol. 2), G. P. Sendeckyj, Ed. Academic Press, New York, 1974, pp. 23-44.
20. MIL-HDBK-17A, "Plastics for Aerospace Vehicles, Part I: Reinforced Plastics," January 1971.



## APPENDIX A

### STRUCTURAL ANALYSIS OF CANOPY AFT FRAME

This section presents the detailed analysis of the aft structure discussed in Section 4. Since LTV structural design data was unavailable, equivalent strength and stiffness design criteria were used to design the alternate structure. The equivalent stiffness design criteria required that the displacement of the proposed structure be equal to or less than that of the existing structure for any given loads. The equivalent strength design criteria required that the margin of safety of the proposed structure equalled or exceeded that of the existing structure for all load cases. The direct comparison of the two structures under various loads guaranteed that the proposed structure had safety margins which equalled or exceeded those for the original structure.

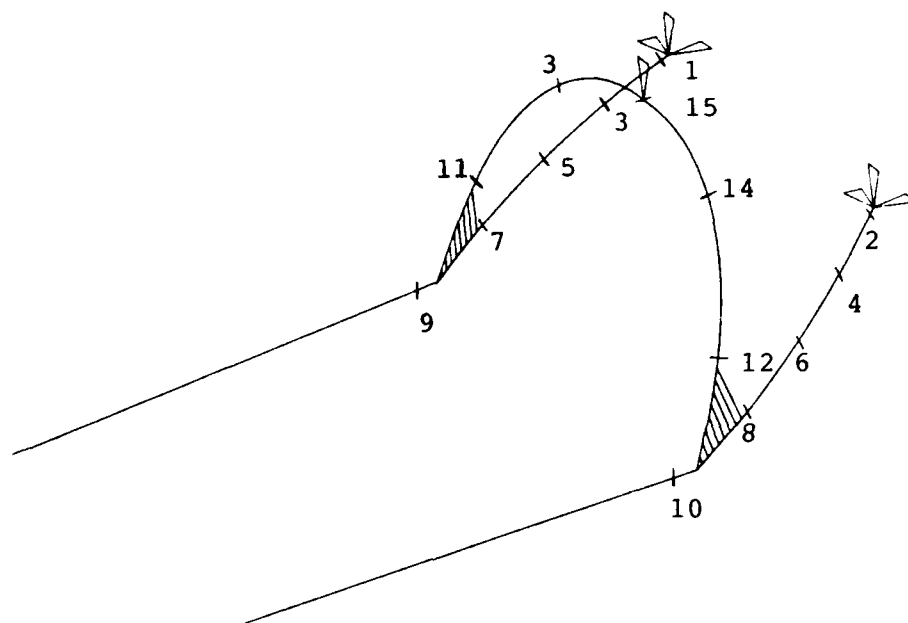
#### A.1 MATERIALS PROPERTIES AND DESIGN CRITERIA

Material properties used in the analysis are listed in Table A.1. Allowable strengths listed for the metals are yield strengths. Both the moduli and allowable strengths listed for the composite materials are values from the cited references reduced by 15% to account for manufacturing defects. The reduction in material properties provided an additional margin of safety on both strength and stiffness. For the analysis of beam type structures, effective moduli were used based on the in-plane properties of the laminate [9].

#### A.2 BEAM STRUCTURE

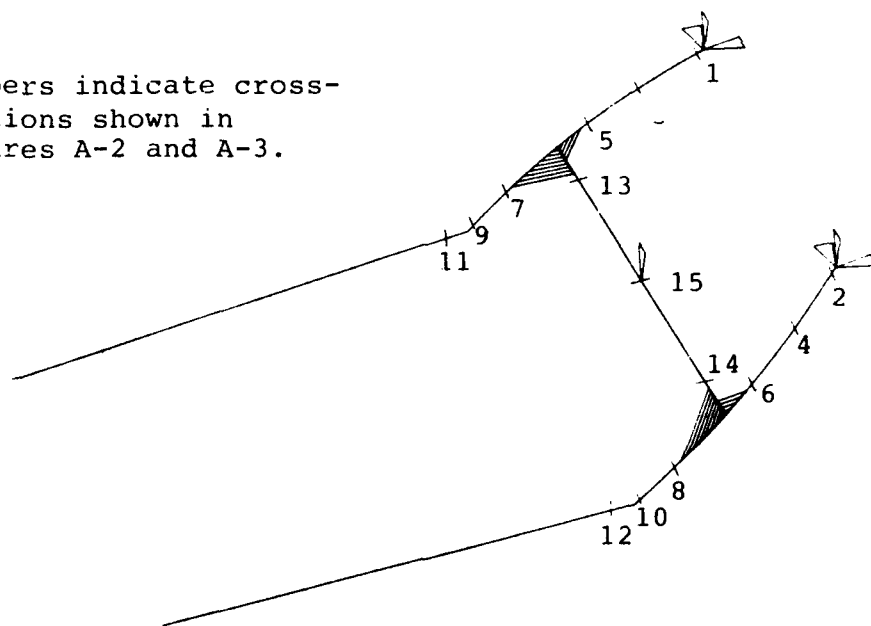
The structural analysis of the principal load-carrying aft support structure was performed using finite element (FE) analysis. It was assumed that the primary structure be treated as thin-walled beams, and that the contributions to the overall stiffness of the structure from the skin and pressure panels be neglected. The models used for this analysis are shown in Figure A-1. These models were developed using beam elements with the COSMOS FE program [13]. To model the intersections of the beams, elements in the space where the beams physically intersect were constrained to move as rigid bodies. These areas are cross-hatched in Figure A-1.

Cross-sections of interest for stress analysis are indicated on Figure A-1 by the numbered locations. Cross-sectional properties for these locations are detailed in Figures A-2 and A-3.



Original Structure

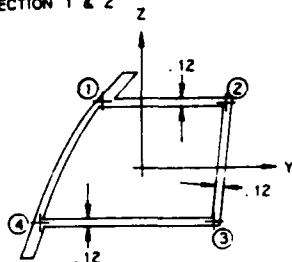
Numbers indicate cross-sections shown in Figures A-2 and A-3.



Modified Structure

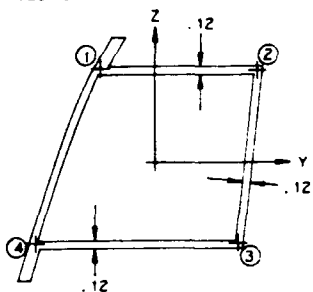
Figure A-1. Models of Principal Canopy Structure.

SECTION 1 & 2



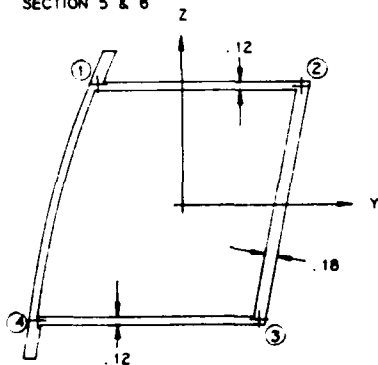
$$\begin{aligned} A &= 0.99 \text{ in}^2 \\ I_{YY} &= 0.55 \text{ in}^4 \\ I_{ZZ} &= 0.93 \text{ in}^4 \\ I_{YZ} &= 0.17 \text{ in}^4 \\ A_1 &= 4.21 \text{ in}^2 \end{aligned}$$

SECTION 3 & 4



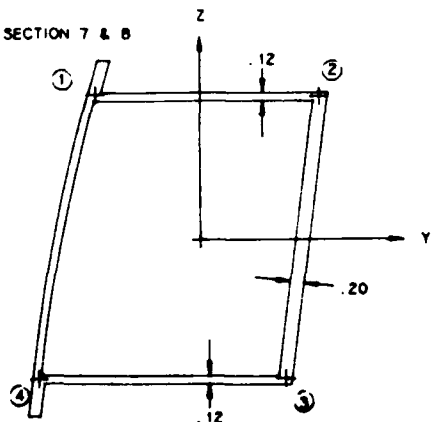
$$\begin{aligned} A &= 1.28 \text{ in}^2 \\ I_{YY} &= 1.44 \text{ in}^4 \\ I_{ZZ} &= 1.72 \text{ in}^4 \\ I_{YZ} &= 0.33 \text{ in}^4 \\ A_1 &= 7.18 \text{ in}^2 \end{aligned}$$

SECTION 5 & 6



$$\begin{aligned} A &= 1.84 \text{ in}^2 \\ I_{YY} &= 3.42 \text{ in}^4 \\ I_{ZZ} &= 3.70 \text{ in}^4 \\ I_{YZ} &= 0.77 \text{ in}^4 \\ A_1 &= 11.55 \text{ in}^2 \end{aligned}$$

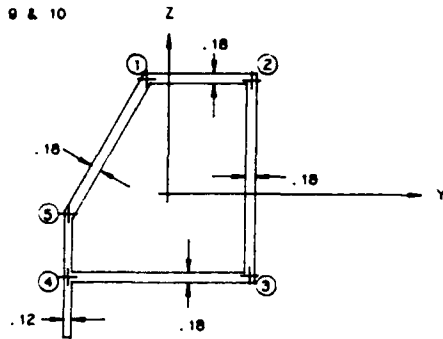
SECTION 7 & 8



$$\begin{aligned} A &= 2.20 \text{ in}^2 \\ I_{YY} &= 5.68 \text{ in}^4 \\ I_{ZZ} &= 5.21 \text{ in}^4 \\ I_{YZ} &= -0.84 \text{ in}^4 \\ A_1 &= 15.1 \text{ in}^2 \end{aligned}$$

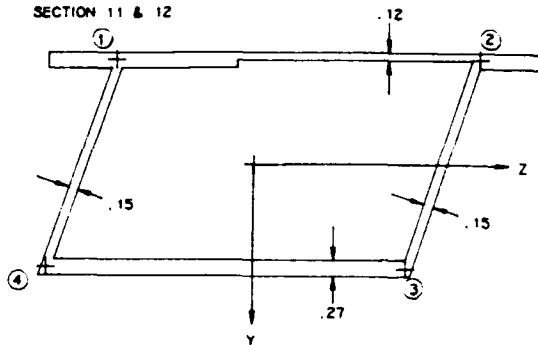
Figure A-2. Cross-Sections on Model of Existing Structure [Ref. 1,14].

SECTION 9 & 10



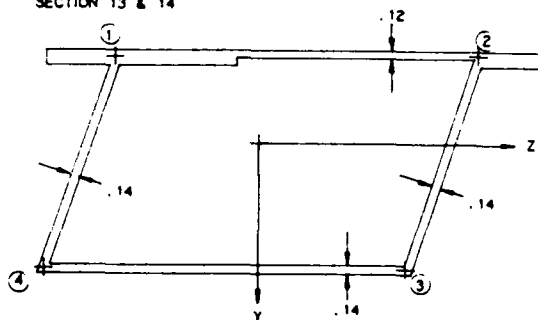
$$\begin{aligned} A &= 2.12 \text{ in}^2 \\ I_{YY} &= 3.25 \text{ in}^4 \\ I_{ZZ} &= 2.70 \text{ in}^4 \\ I_{YZ} &= -0.91 \text{ in}^4 \\ A_1 &= 11.1 \text{ in}^2 \end{aligned}$$

SECTION 11 & 12



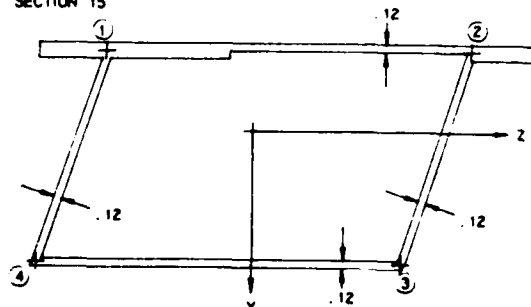
$$\begin{aligned} A &= 3.85 \text{ in}^2 \\ I_{YY} &= 20.82 \text{ in}^4 \\ I_{ZZ} &= 8.48 \text{ in}^4 \\ I_{YZ} &= -2.11 \text{ in}^4 \\ A_1 &= 19.0 \text{ in}^2 \end{aligned}$$

SECTION 13 & 14



$$\begin{aligned} A &= 3.17 \text{ in}^2 \\ I_{YY} &= 18.64 \text{ in}^4 \\ I_{ZZ} &= 6.68 \text{ in}^4 \\ I_{YZ} &= -1.64 \text{ in}^4 \\ A_1 &= 19.0 \text{ in}^2 \end{aligned}$$

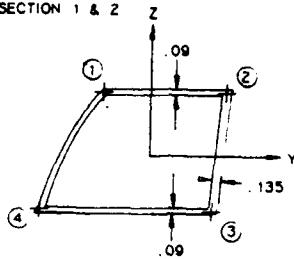
SECTION 15



$$\begin{aligned} A &= 2.92 \text{ in}^2 \\ I_{YY} &= 17.27 \text{ in}^4 \\ I_{ZZ} &= 6.12 \text{ in}^4 \\ I_{YZ} &= -1.48 \text{ in}^4 \\ A_1 &= 19.1 \text{ in}^2 \end{aligned}$$

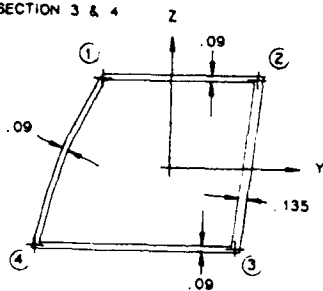
Figure A-2. (continued)

SECTION 1 & 2



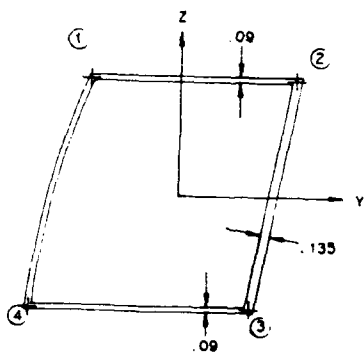
$$\begin{aligned} A &= 0.83 \text{ in}^2 \\ I_{YY} &= 0.44 \text{ in}^4 \\ I_{ZZ} &= 0.88 \text{ in}^4 \\ I_{YZ} &= 0.14 \text{ in}^4 \\ A_1 &= 11.8 \text{ in}^2 \end{aligned}$$

SECTION 3 & 4



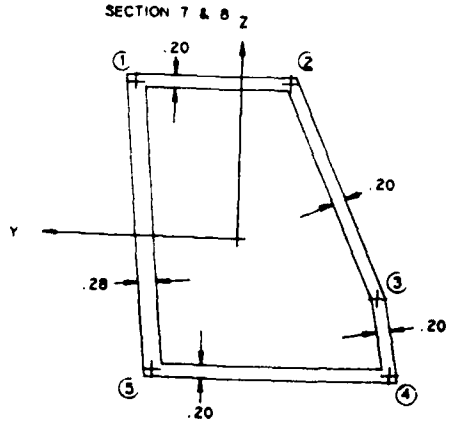
$$\begin{aligned} A &= 1.06 \text{ in}^2 \\ I_{YY} &= 1.13 \text{ in}^4 \\ I_{ZZ} &= 1.48 \text{ in}^4 \\ I_{YZ} &= 0.27 \text{ in}^4 \\ A_1 &= 7.29 \text{ in}^2 \end{aligned}$$

SECTION 5 & 6



$$\begin{aligned} A &= 1.38 \text{ in}^2 \\ I_{YY} &= 2.57 \text{ in}^4 \\ I_{ZZ} &= 2.86 \text{ in}^4 \\ I_{YZ} &= 0.59 \text{ in}^4 \\ A_1 &= 11.8 \text{ in}^2 \end{aligned}$$

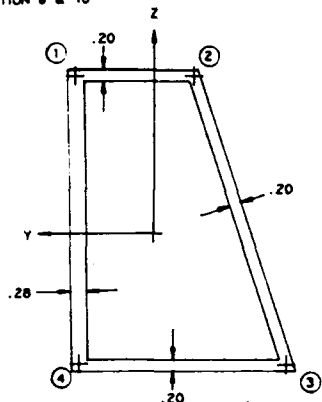
SECTION 7 & 8



$$\begin{aligned} A &= 3.38 \text{ in}^2 \\ I_{YY} &= 9.32 \text{ in}^4 \\ I_{ZZ} &= 6.77 \text{ in}^4 \\ I_{YZ} &= 2.01 \text{ in}^4 \\ A_1 &= 14.0 \text{ in}^2 \end{aligned}$$

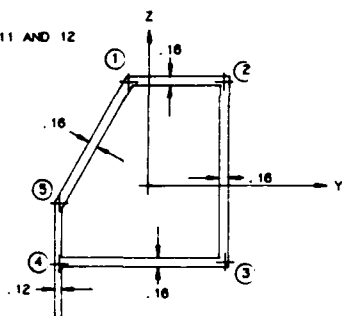
Figure A-3. Cross-Sections of Modified Structure Model.

SECTION 9 & 10



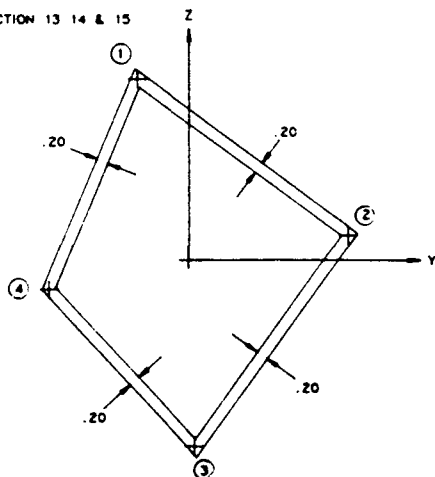
$$\begin{aligned} A &= 3.60 \text{ in}^2 \\ I_{YY} &= 12.24 \text{ in}^4 \\ I_{ZZ} &= 6.33 \text{ in}^4 \\ I_{YZ} &= -2.13 \text{ in}^4 \\ A_1 &= 14.4 \text{ in}^2 \end{aligned}$$

SECTION 11 AND 12



$$\begin{aligned} A &= 1.90 \text{ in}^2 \\ I_{YY} &= 2.93 \text{ in}^4 \\ I_{ZZ} &= 2.44 \text{ in}^4 \\ I_{YZ} &= -0.84 \text{ in}^4 \\ A_1 &= 11.1 \text{ in}^2 \end{aligned}$$

SECTION 13 14 & 15



$$\begin{aligned} A &= 3.36 \text{ in}^2 \\ I_{YY} &= 11.74 \text{ in}^4 \\ I_{ZZ} &= 7.94 \text{ in}^4 \\ I_{YZ} &= -0.50 \text{ in}^4 \\ A_1 &= 17.2 \text{ in}^2 \end{aligned}$$

Figure A-3. (continued)

Table A.1 - Material Properties

	Magnesium AZ91C-T6 (Ref. 10)	Aluminum 7075-T6 (Ref. 10)	Gr/EP 0° (Ref. 11)	Gr/EP ±45° (Ref. 11)	Kevlar/EP Bias Weave (Ref. 12)
$S_x^l$ (psi)	16.0E+3	67.0E+3	94.0E+3	14.4E+3	25.0E+3
$S_y^l$ (psi)	16.0E+3	66.0E+3	3.4E+3	14.4E+3	25.0E+3
$S_x^c$ (psi)	16.0E+3	68.0E+3	85.0E+3	15.3E+3	15.0E+3
$S_y^c$ (psi)	16.0E+3	71.0E+3	17.0E+3	15.3E+3	15.0E+3
$S^s$ (psi)	8.8E+3	38.0E+3	7.7E+3	36.7E+3	27.0E+3
$S^i$ (psi)	NA	NA	8.5E+3	8.5E+3	7.5E+3
$E_x^l$ (psi)	6.5E+6	10.3E+6	21.0E+6	2.0E+6	0.94E+6
$E_y^l$ (psi)	6.5E+6	10.3E+6	1.5E+6	2.0E+6	0.94E+6
$E_x^c$ (psi)	6.5E+6	10.5E+6	21.0E+3	2.0E+6	0.85E+6
$E_y^c$ (psi)	6.5E+6	10.5E+6	1.5E+6	2.0E+6	0.85E+6
$G_{xy}$ (psi)	2.4E+6	3.9E+6	0.55E+6	5.5E+6	2.5E+6
$\mu_{xy}$	0.35	0.33	0.30	0.83	0.75
$\rho$ (#/in <sup>3</sup> )	0.065	0.101	0.057	0.057	0.048
$\alpha_x$ (1/°F)	14.0E-6	12.9E-6	-0.30E-6	1.27E-6	1.1E-6
$\alpha_y$ (1/°F)	14.0E-6	12.9E-6	19.5E-6	1.27E-6	1.1E-6
$V_f$	NA	NA	0.60	0.60	0.50

Effective properties were used for the model of the existing structure to account for the combination magnesium-aluminum walls. The properties were scaled to those of an all-magnesium structure based on the modulus ratio of the magnesium and aluminum. The properties of the composite sections were based on the in-plane longitudinal and shear moduli of the panels.

Boundary conditions of the models assumed that the aft hinge pins had enough clearance to allow rotation in any direction. Rotations of the elements in this area were very small, validating this assumption. Load cases considered were all symmetric or anti-symmetric about the centerline. The first six load cases were representative of loads transmitted to the aft structure from the side rails during closed canopy operation. Load cases 7 through 9 were

representative of the loads transmitted by the side rails during open canopy operation. The load cases are summarized in Table A.2. The direction and location of application of these forces is also indicated in Figure A-4. Although the first six cases simulated closed canopy loads, the side rail was not constrained in the models, as it would be by latches for actual operation. Since the models were used only for the evaluation of loads transmitted to the aft structure, the side rails were not fixed at the latch locations so that a known applied load would be reacted entirely by the aft structure.

Table A.2 - Load Cases

Case	Original Canopy			Modified Canopy		
	Load	Direction	Location	Load	Direction	Location
1	1000 lb "	force +X " -X	sec 9 sec 10	1000 lb "	force +X " -X	sec 11 sec 12
2	" "	" +X " -X	sec 9 sec 10	" "	" +X " -X	sec 11 sec 12
3	" "	" +Z " -Z	sec 9 sec 10	" "	" +Z " -Z	sec 11 sec 12
4	1000 in-lb "	moment +X " -X	sec 9 sec 10	1000 in-lb "	moment +X " -X	sec 11 sec 12
5	" "	" +Y " -Y	sec 9 sec 10	" "	" +Y " -Y	sec 11 sec 12
6	" "	" +Z " -Z	sec 9 sec 10	" "	" +Z " -Z	sec 11 sec 12
7	10 lb/in "	force +Y " -Y	rail rail	10 lb/in "	force +Y " -Y	rail rail
8	" "	" +Y " +Y	rail rail	" "	" +Y " +Y	rail rail
9	" "	" +Z " -Z	rail rail	" "	" +Z " -Z	rail rail

Figure A-4 shows the displaced configurations for the nine load cases. Deflections of both the existing and proposed structures are shown for comparison. The figures show that the overall deflection of the proposed structure is less than that of the existing structure. The deflection of



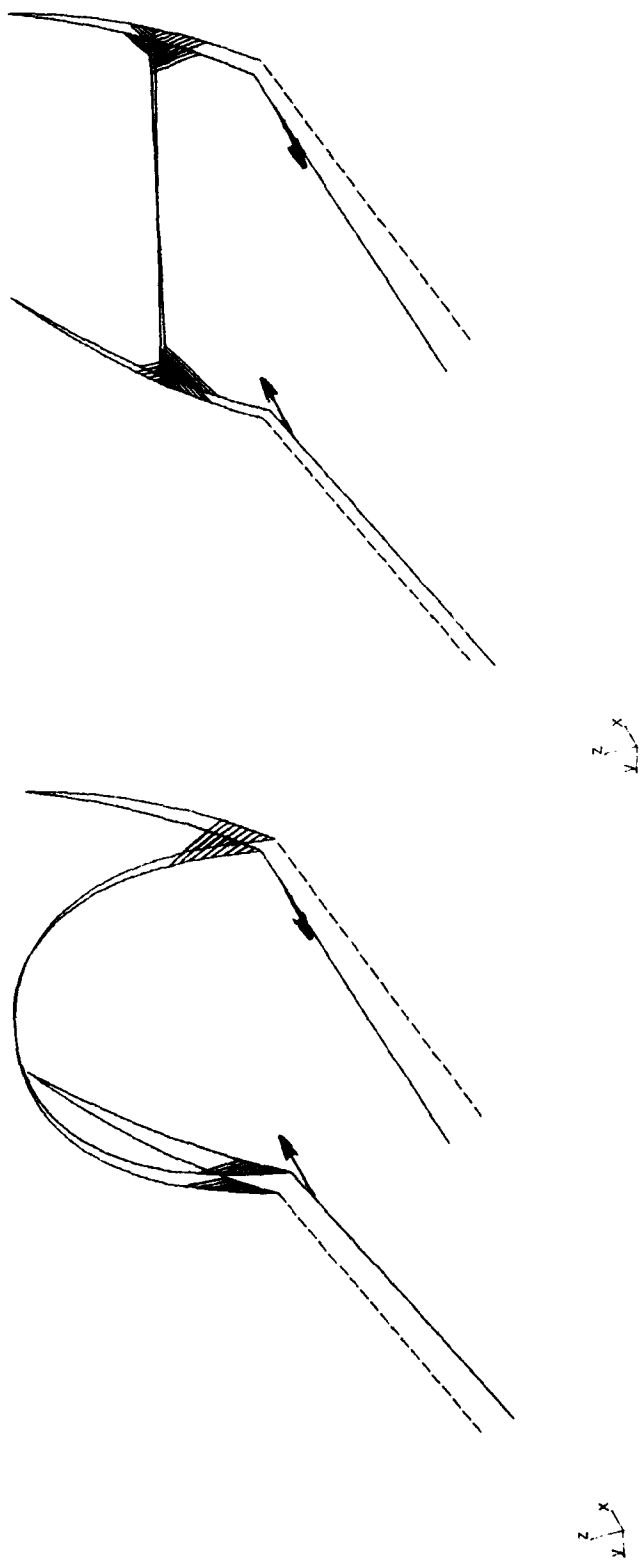


Figure A-4(a). Displacements Due to Load Case 1.

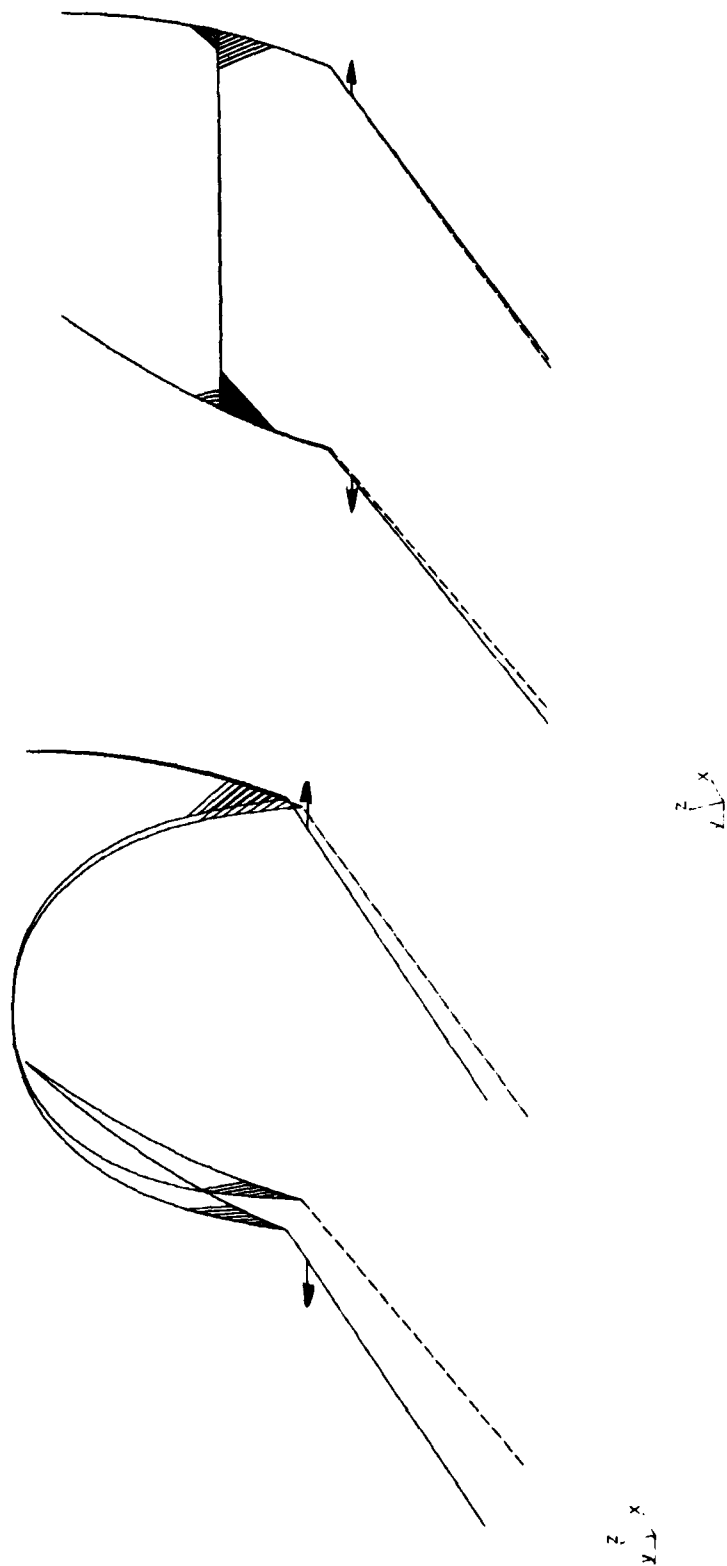


Figure A-4(b). Displacements Due to Load Case 2.

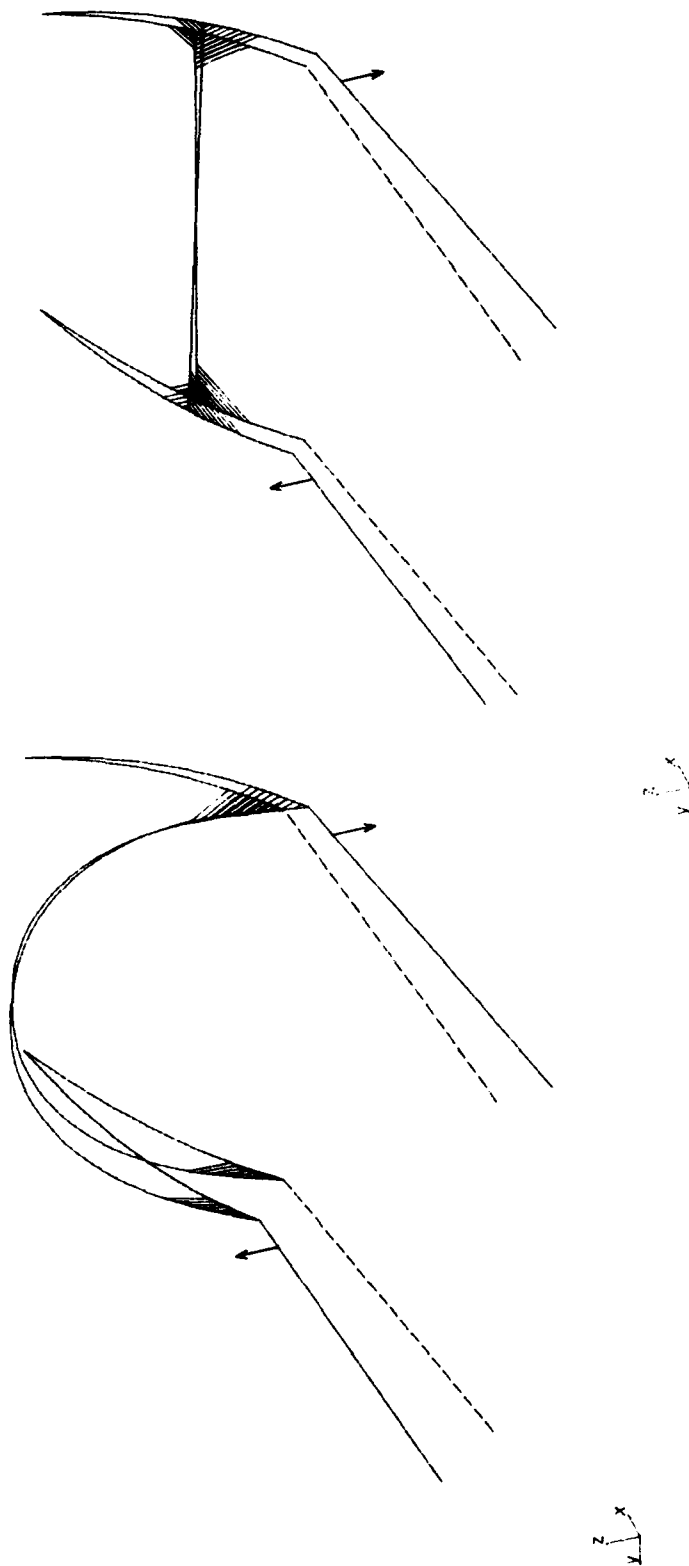


Figure A-4(c). Displacements Due to Load Case 3.

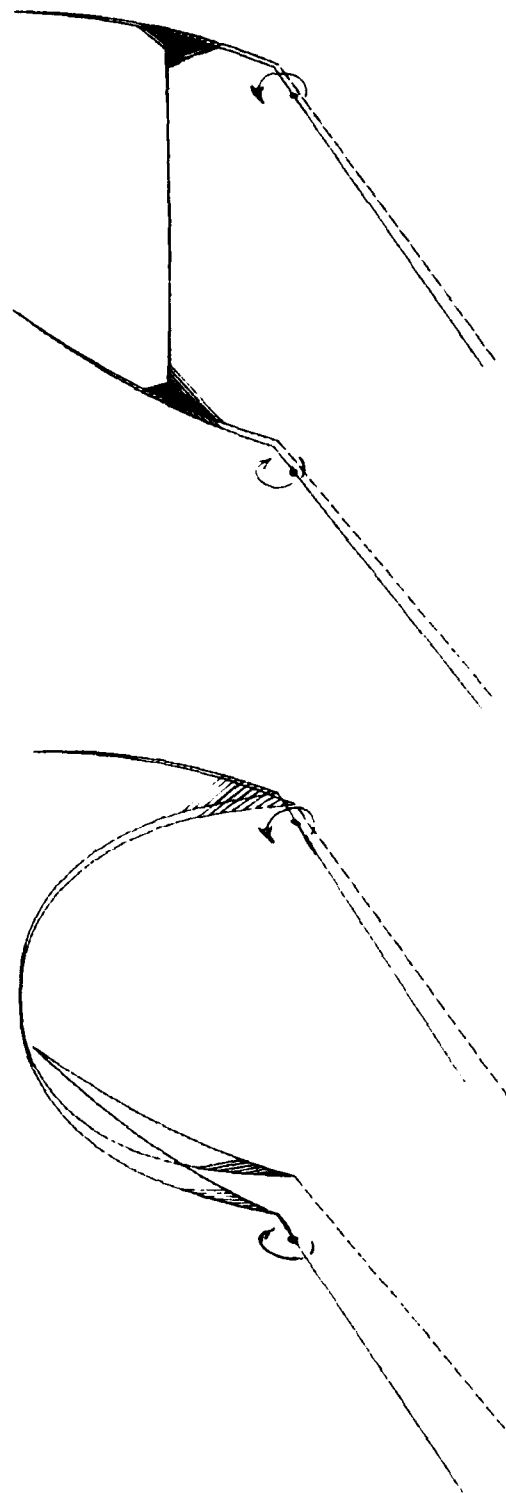


Figure A-4(d) Displacements Due to Load Case 4.

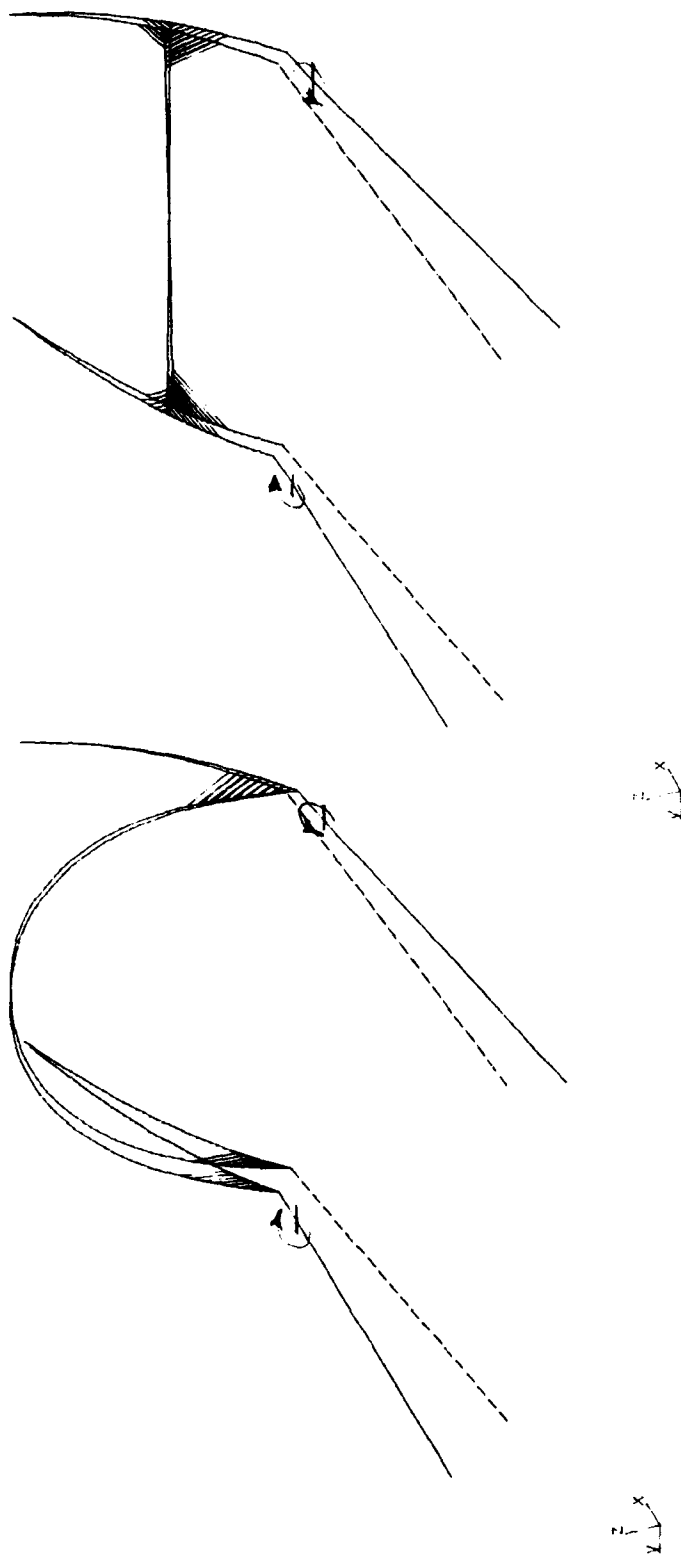


Figure A-4(e). Displacements Due to Load Case 5.

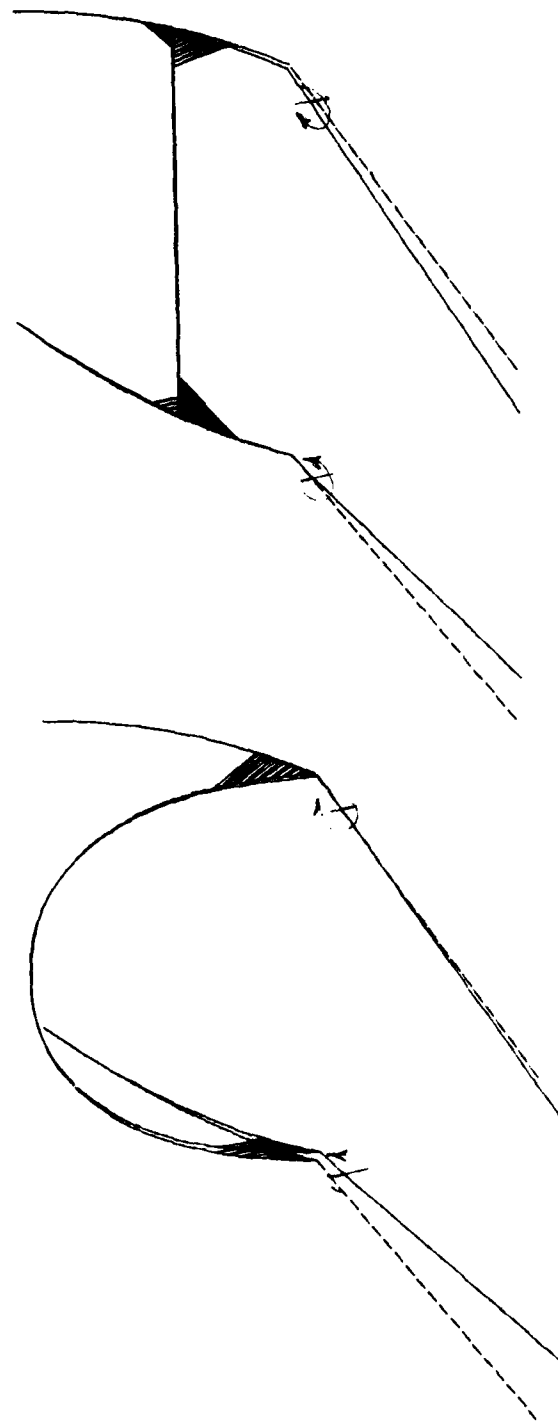


Figure A-4(f). Displacements Due to Load Case 6.

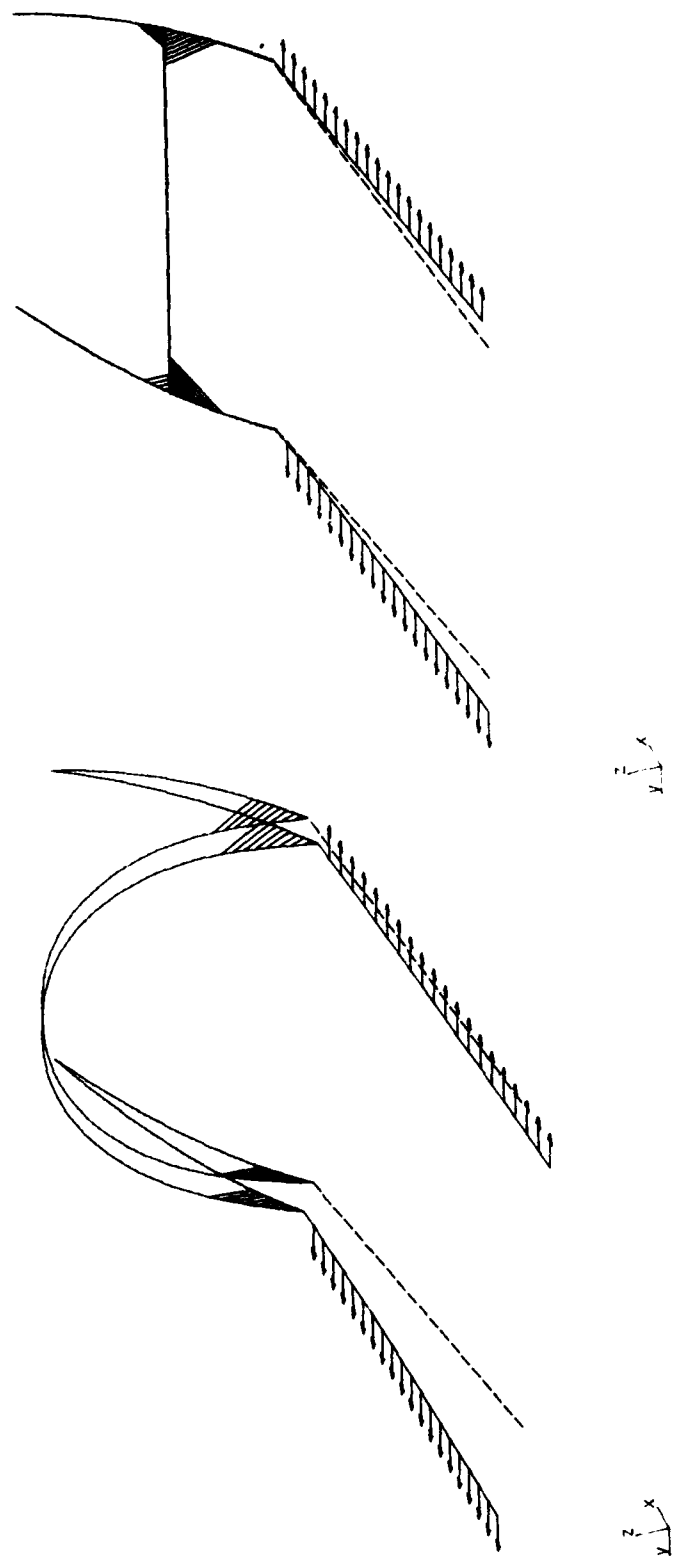


Figure A-4(g). Displacements Due to Load Case 7.

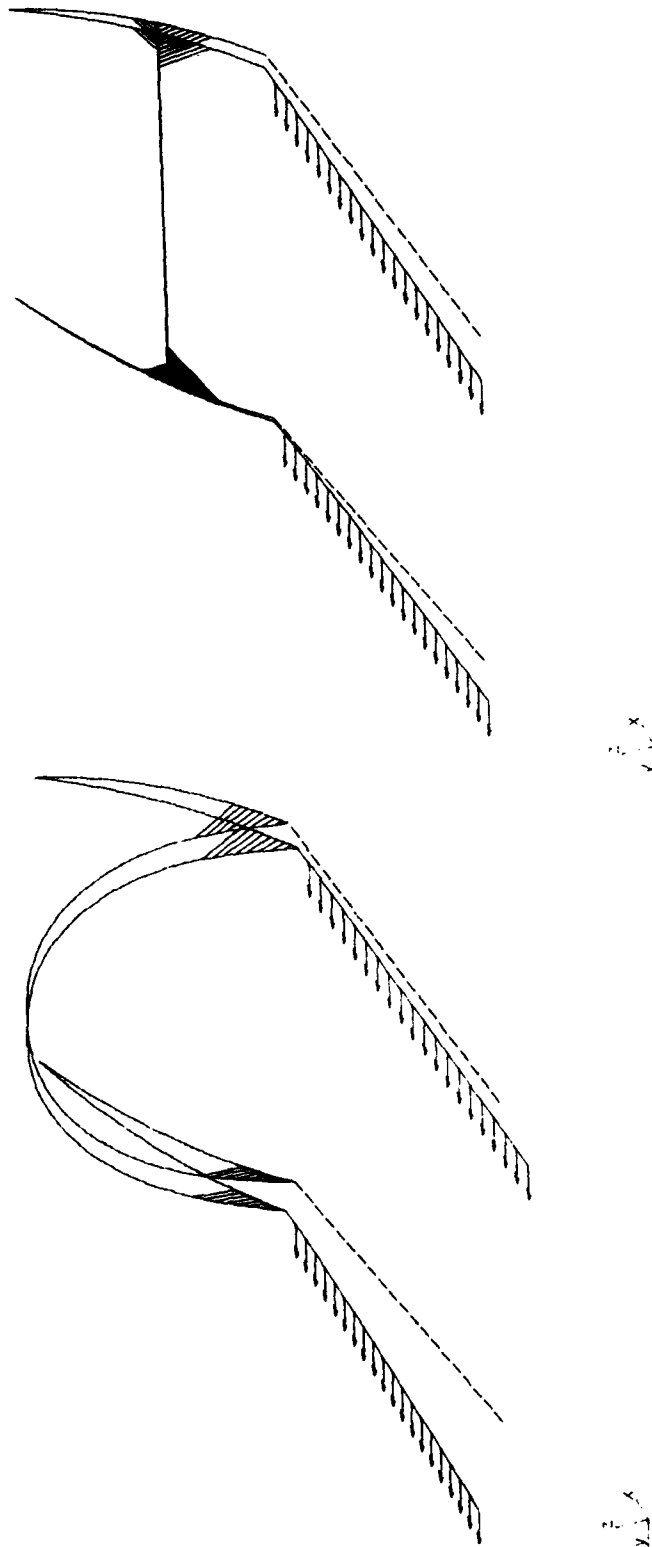


Figure A-4(h). Displacements Due to Load Case 8.



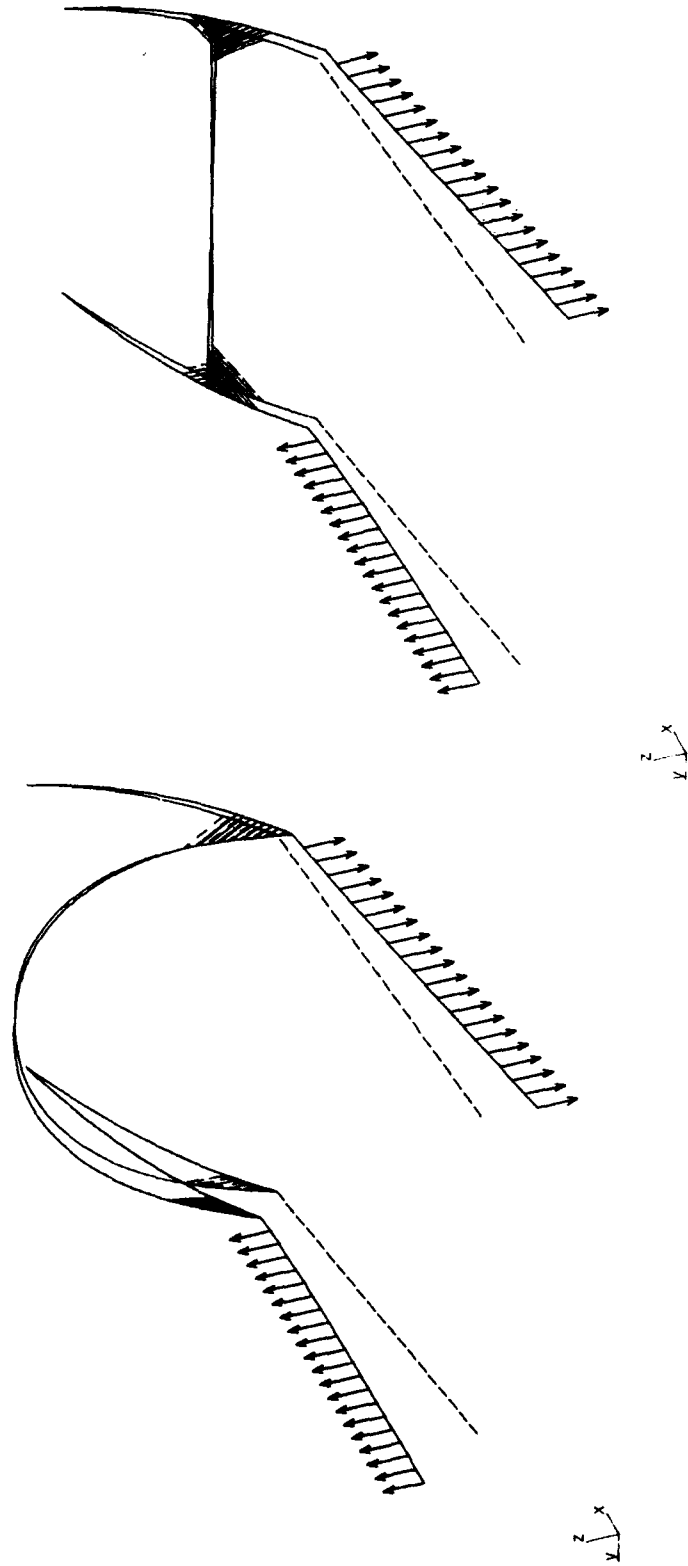


Figure A-4(i). Displacements Due to Load Case 9.

the points of load application (for cases 1 through 6) or the deflection of the forward point on the side rail (for cases 7 through 9) are summarized in Table A.3. Deflections listed are in the same direction as the applied load. For all nine cases, the proposed structure deflects less than the existing structure in the direction of the applied load.

Table A.3 - Summary of Displacements

Case	Direction	Original Canopy Deflection		Modified Canopy Deflection	
		L/H	R/H	L/H	R/H
1	$U_x$	0.143 in	-0.145 in	0.0951 in	-0.0969 in
2	$U_y$	0.195 in	-0.195 in	0.0193 in	-0.0193 in
3	$U_z$	0.281 in	-0.284 in	0.138 in	-0.138 in
4	$\theta_x$	0.0089 rad	-0.0089 rad	0.0046 rad	-0.0046 rad
5	$\theta_y$	0.0055 rad	-0.0054 rad	0.0046 rad	-0.0047 rad
6	$\theta_z$	0.0048 rad	-0.0048 rad	0.0045 rad	-0.0045 rad
7	$U_y$ (tip)	2.87 in	-2.87 in	1.82 in	-1.82 in
8	$U_y$ (tip)	4.84 in	4.85 in	2.66 in	2.71 in
9	$U_z$ (tip)	3.47 in	-3.51 in	2.56 in	-2.61 in

In general, there is a greater coupling of displacements in one direction due to loads in another for the existing structure than for the proposed structure. This occurs because of the difference in the manner in which the load is transferred from one side of the structure to the other (either by the existing arch or the proposed straight tube). Thus, displacements for directions not listed in Table A.3 are also smaller for the proposed structure than for the existing structure. Since any possible load can be generated from a linear combination of the first six load cases, the proposed structure will have a smaller deflection for any possible load. (It is stiffer than the existing structure.)

Force and moment resultants calculated by the FE program were converted to stresses at the cross-sections identified in Figure A-1. Stresses were calculated for these cross-sections at the locations identified in Figures A-2 and A-3. The cross-sections chosen for stress evaluation are located near changes in wall thickness or load path. The equations used for calculating

stresses are based on linear beam theory assumptions [15,16]. The stresses  $\sigma_x$  and  $\tau$  can be calculated from cross-section properties  $I_{xx}$ ,  $I_{yy}$ ,  $\theta$ ,  $A$ ,  $A_p$  and  $t$ , and the load resultants  $F_x$ ,  $V_y$ ,  $V_z$ ,  $T_x$ ,  $M_y$ , and  $M_z$ . Positive directions for these variables are shown in Figure A-5. Equations used for the calculations are:

$$M_p = M_y \cos(\theta) + M_z \sin(\theta) \quad (A.1)$$

$$M_q = -M_y \sin(\theta) + M_z \cos(\theta) \quad (A.2)$$

$$I_{xy} = 1/2 (I_y - I_z) \tan(2\theta) \quad (A.3)$$

$$I_{pp} = 1/2 (I_y + I_z) + [(I_y - I_z)^2/4 + I_{xy}^2]^{1/2} \quad (A.4)$$

$$I_{qq} = 1/2 (I_y + I_z) - [(I_y - I_z)^2/4 + I_{xy}^2]^{1/2} \quad (A.5)$$

$$p = (y - y_c) \cos(\theta) + (z - z_c) \sin(\theta) \quad (A.6)$$

$$q = -(y - y_c) \sin(\theta) + (z - z_c) \cos(\theta) \quad (A.7)$$

$$\sigma_x = M_p p / I_{pp} - M_q q / I_{qq} + F_x / A \quad (A.8)$$

$$\tau = T_x / (2tA_p) \pm k_1 V_y / A \pm k_2 V_z / A \quad (A.9)$$

The sign of the terms in Equation A.9 is determined by the direction of shear flow at the location under consideration. Assuming that the stresses are constant across the width of the beam wall, the margin of safety can be calculated using the Tsai-Wu criteria [9]:

$$MS = -b/2a + [(b/2a)^2 + 1/a]^{1/2} - 1 \quad (A.10)$$

where  $a$  and  $b$  are calculated from the stresses and material strengths:

$$a = \sigma_x^2 / (S_x^t \cdot S_x^c) + \sigma_y^2 / (S_y^t \cdot S_y^c) + \tau^2 / (S^s)^2 - 1/2 \sigma_x \sigma_y / (S_x^t \cdot S_x^c \cdot S_y^t \cdot S_y^c)^{1/2}$$

$$b = \sigma_x \cdot (1/S_x^t - 1/S_x^c) + \sigma_y \cdot (1/S_y^t - 1/S_y^c)$$

For the evaluation of the isotropic materials,  $\sigma_y = 0$  and  $\sigma_x$  and  $\tau$  are calculated from Equations A.8 and A.9. Equation A.10 gives the same results as the von Mises criteria for isotropic materials. For the evaluation of laminated composites, the stresses determined from beam theory must be converted to stresses on the axes of each layer using laminated plate theory calculations [9].

A summary of margins of safety for the weakest sections of the existing and proposed structures is given in Table A.4. Margins of safety for the proposed composite structure were

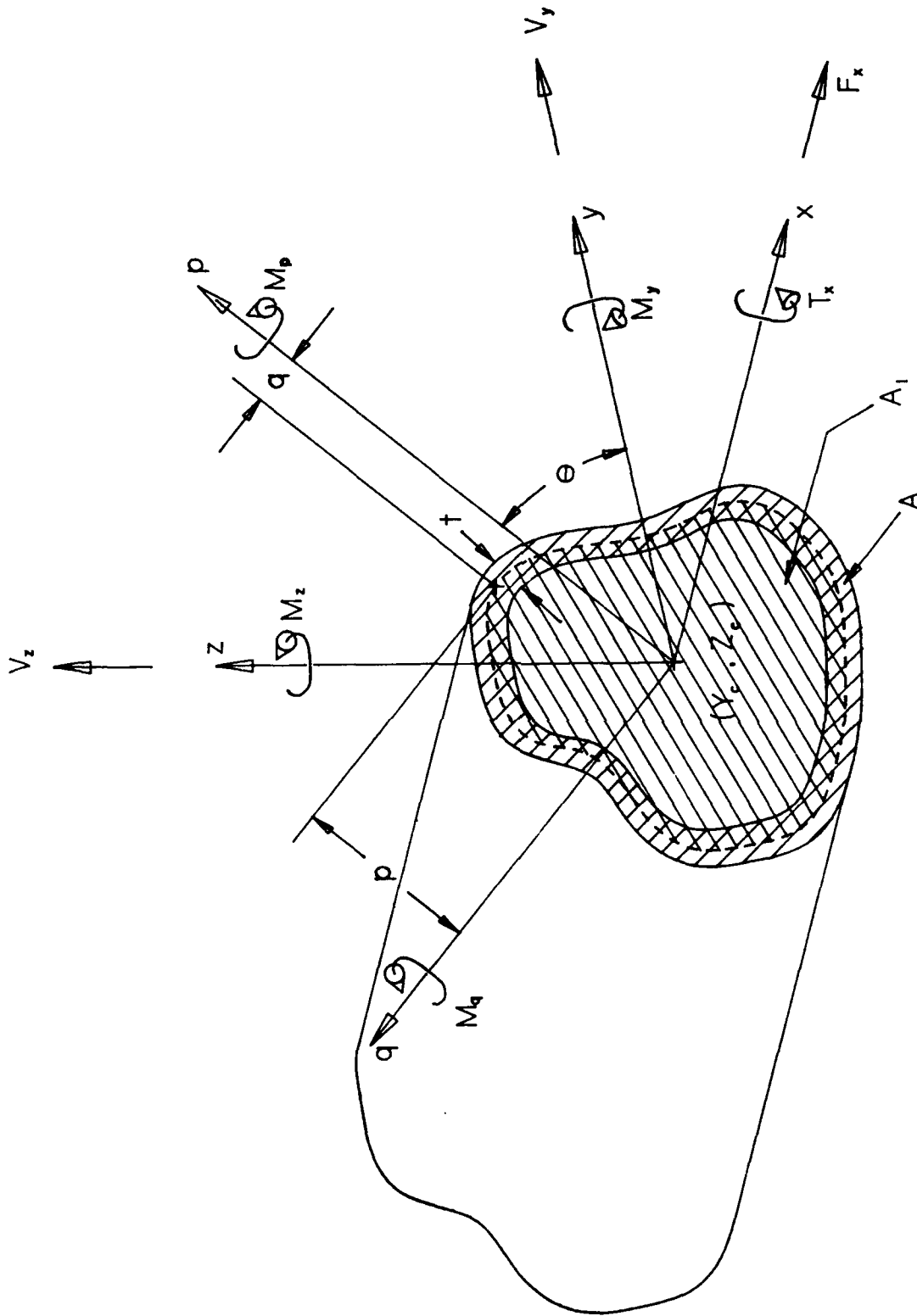


Figure A-5. Symbols Used in Stress Calculation.

based on a first-ply failure; i.e., the stress which causes the weakest ply for the given load condition to fail. This gave a conservative estimate of the strength of the proposed structure.

Table A.4 - Strength Comparison

Case	Original Structure			Modified Structure		
	Section Number	Location Number	Margin of Safety	Section Number	Location Number	Margin of Safety
1	4	2	1.2	5	2	2.1
2	2	4	1.4	5	4	6.5
3	2	2,3	1.2	5	3	2.7
4	9,10	all	36	7	3	47
5	9,10	1	17	11,12	1	17
6	9,10	4	23	11,12	4	23
7	9,10	4	160	11,12	1	170
8	5,14	2	95	13	2	120
9	9,10	1	120	11,12	1	120

For each of the nine load cases, the margin of safety for the modified structure matched or exceeded that of the existing structure. It should be noted that the smallest margin of safety for several of the load cases occurred in the side rail (sections 9 and 10 for the existing structure or sections 11 and 12 for the proposed structure). In cases where the smallest margin of safety occurs at the side rail, failure will occur at the joint (current design) which connects the aft structure and the side rail.

For the linear analysis considered here, any load from the side rail to the aft structure can be expressed as a combination of the first six load cases. Also, the average value of the stress across the wall thickness is a superposition of the stresses from each of those load cases. While the stress at failure of individual lamina in the composite is not a linear function of the components of the load, the use of first-ply failure theory and the high margins of safety for load cases where failure does not occur at the side rail indicates that the proposed structure is stronger than the existing structure for any load condition.

### A.3 PRESSURE PANEL

The composite pressure panel was analyzed for strength and stiffness under a 5-psi cockpit pressure load. The lower and upper portions of the panel were analyzed separately. The lower section is stiffer than the existing pressure panel and has a high margin of safety under cockpit pressure. The upper portion of the panel was designed to prevent excessive deflection under pressure. This section also has an acceptable margin of safety.

The lower portion of the pressure panel was designed to match the bending stiffness of the ribbed panel which it replaces. The ribs on the existing panel are composed of 7075-T6 aluminum, which has a yield strength of  $S=66,000$  psi. The cross-section of the existing panel and layup of the proposed panel are shown in Figure A-6. The cross-section shown is one of six ribs spaced 4 inches apart. The average stiffness of the panel along the direction of the ribs is  $54,000 \text{ lbf-in}^2/\text{in}$ . The allowable bending resultant on the section is calculated using:

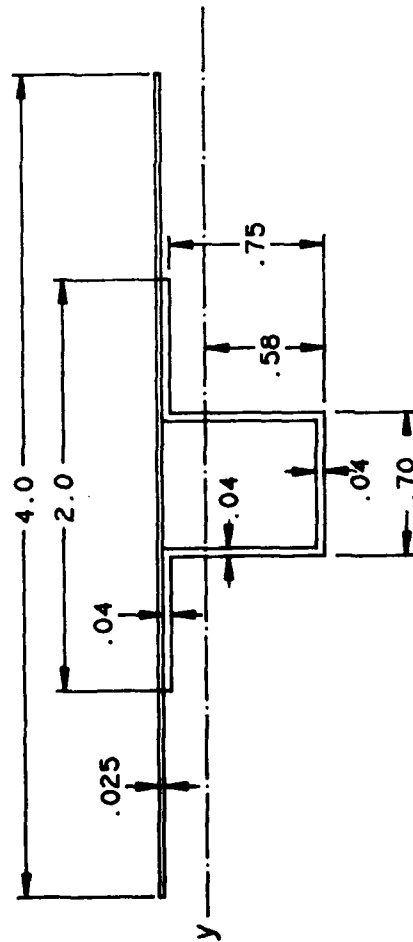
$$M_{\max} = S \cdot I / y \quad (\text{A.11})$$

For this section,  $M_{\max} = 610 \text{ in-lbf/in}$ . Based on laminated plate theory the bending stiffness of the proposed composite is  $68,000 \text{ lbf-in}^2/\text{in}$  along the axis aligned with the ribs. Using the Tsai-Wu criteria (Equation A.10), the allowable bending resultant is  $M_{\max} = 620 \text{ in-lbf/in}$ . Thus, the composite panel is both stiffer and stronger than the existing panel along the primary axis.

The simple beam theory analysis used above gave no information on the strength of the composite panel for bending in the transverse direction. To check the transverse bending strength of the panel, a simple finite element model was created using the COSMOS program. The model used orthotropic layered-shell elements. One-half of the symmetric panel model is shown in Figure A-7. Since the panel is less stiff than the structure to which it is attached, rotations and displacements were fixed around the boundary of the model. A 5-psi pressure (representing the highest normal in-flight pressure) was applied to the surface of the model. Figures A-7 and A-8 show the model of half of the pressure panel. Displacement contours are shown in Figure A-7. Stresses in the outer ply in the X-direction are shown in Figure A-8.

Using laminated plate theory to calculate the stresses in each ply, the margin of safety was calculated using Equation A.10. Force resultants over the entire plate were negligible. The highest bending resultants occurred at the location of the 600 psi stress in Figure A-7. The bending resultants were:  $M_x = -65.2 \text{ in-lbf/in}$ ,  $M_y = -1.0 \text{ in-lbf/in}$ ,  $M_{xy} = -0.1 \text{ in-lbf/in}$ . The

Existing Pressure Panel



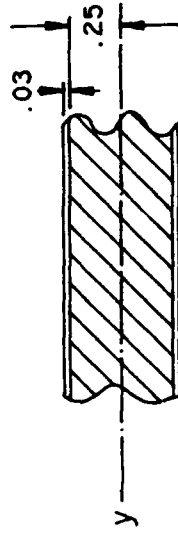
7075-T6 Aluminum

For Unit Width:

$$EI = 54 \times 10^3 \text{ lb-in}^2/\text{in}$$

$$I/Y = 0.00922 \text{ in}^3/\text{in}$$

Composite Panel



$$[(0_C)_2(45_C)(-45_C)(0_C)_2(0_N)_1]_s$$

$$C = 0.005 \text{ inch E25 Graphite Epoxy}$$

$$N = 1/4 \text{ inch Nomex-1/8 cell-2 gauge}$$

$$EI = 68 \times 10^3 \text{ lb-in}^2/\text{in}$$

Figure A-6. Cross-Sections of Lower Pressure Panels.

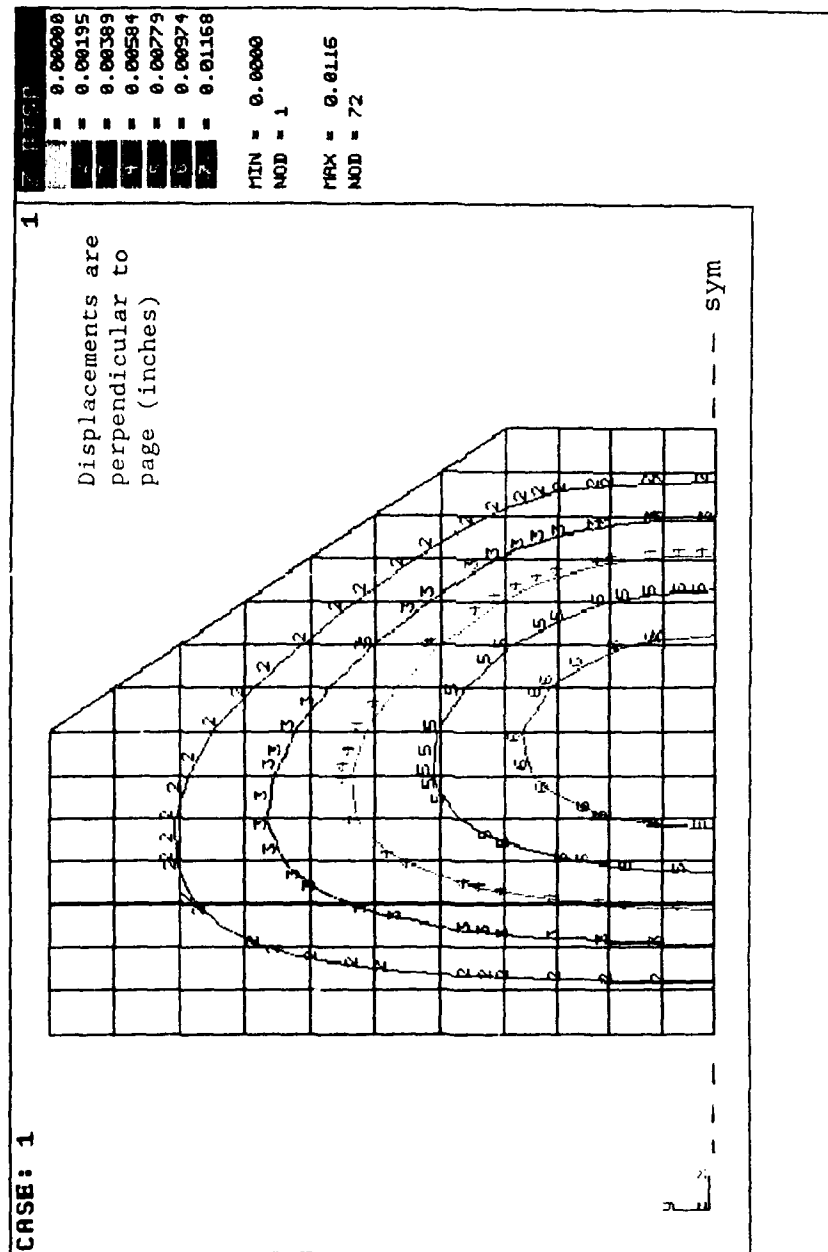


Figure A-7. Displacements in Lower Composite Panel Under 5-psi Pressure Load.



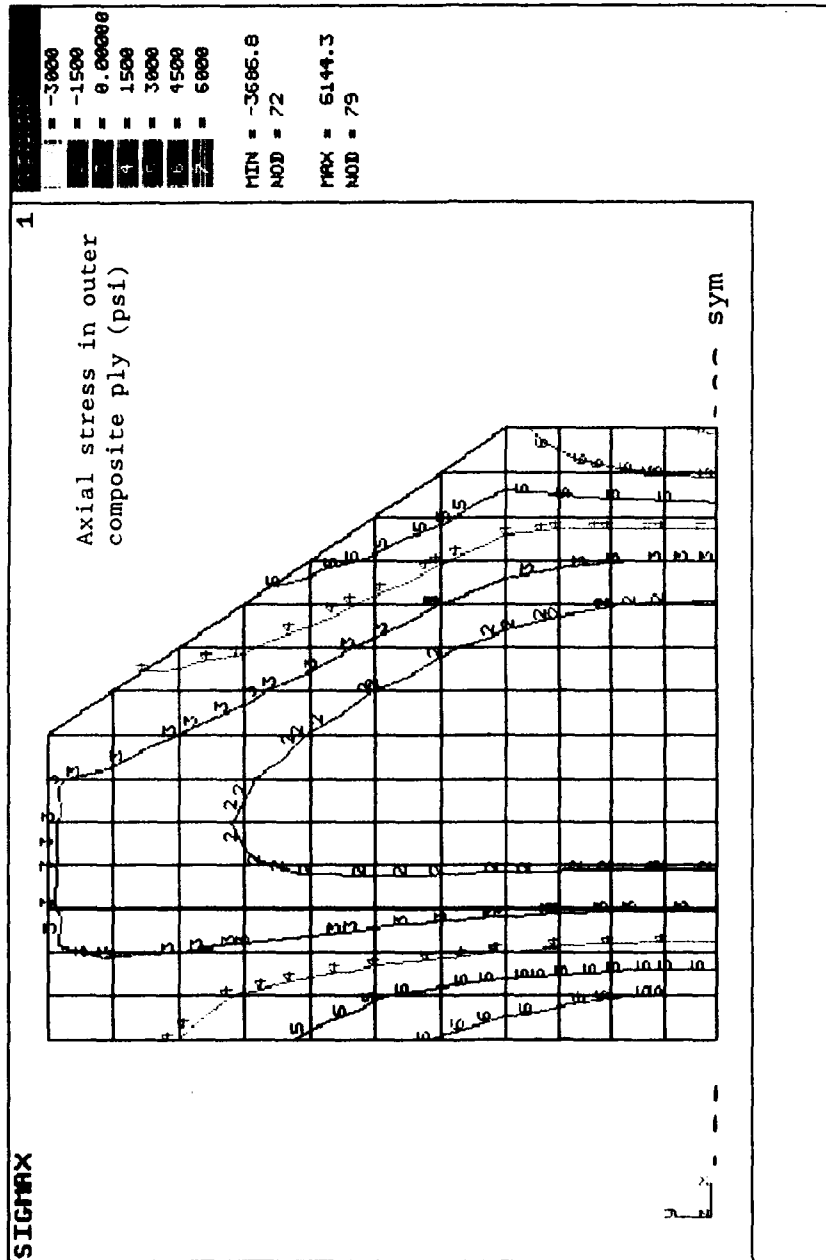


Figure A-8. Longitudinal Stress in Outer Ply of Panel for 5-psi Pressure Load.

minimum margin of safety also occurred at this location in the transverse plies. The minimum margin of safety was 6.9.

The upper portion of the pressure panel was designed for bending stiffness under pressure load. The nominal clearance between the aft edge of the canopy and the adjacent fuselage is 0.18 inch. The pressure panel was designed to deflect less than the nominal clearance under a 5-psi pressure load.

The upper pressure was more flexible than the existing structure. Allowing the upper portion of the pressure panel to be more flexible than the upper portion of the current aft frame increased the transparency displacement in this region. However, the evaluation of transparency stresses in Section 3 showed that a flexible upper structure would not increase the canopy stresses.

The upper portion of the pressure panel has a geometry similar to that of the lower portion shown in Figure A-6. The stacking sequence is  $[(0_c)_3(45_c)(-45_c)(90_c)(-45_c)(0_c)(0_n)]_s$ . Material designations are the same as in Figure A-6.

The deflection of this panel was evaluated using the orthotropic layered shell elements in the COSMOS FE program. One-half of the symmetric model is shown in Figure A-9. In this model, the translation displacements were fixed along the edges where the upper panel meets the skin and lower portion of the panel. Also, rotation displacements were fixed at the location where the panel is bolted to the canopy counterbalance. Since there is actually some additional resistance to rotation where the upper panel meets the lower panel, these boundary conditions are more flexible than is realistic. Also, the stiffness of the beam used for transparency attachment was neglected, further increasing the flexibility of the model. Hence, these results are conservative.

Displacement contours for the panel under a 5-psi pressure load are shown in Figure A-10. The maximum displacement of the panel is 0.114 inch, which is 58% less than the maximum allowable. Figure A-11 shows the stress in the X-direction for the outer ply of the panel. A large stress concentration can be seen at the location of the counterbalance. However, using the Tsai-Wu criteria, the margin of safety for first-ply failure is 0.95.

The same model was also analyzed with a 5-psi pressure load on the surface and a -25-lbf/inch load along the free edge. The edge load simulated the force of the canopy on the panel due to the internal pressurization. The constant force along the edge was estimated from

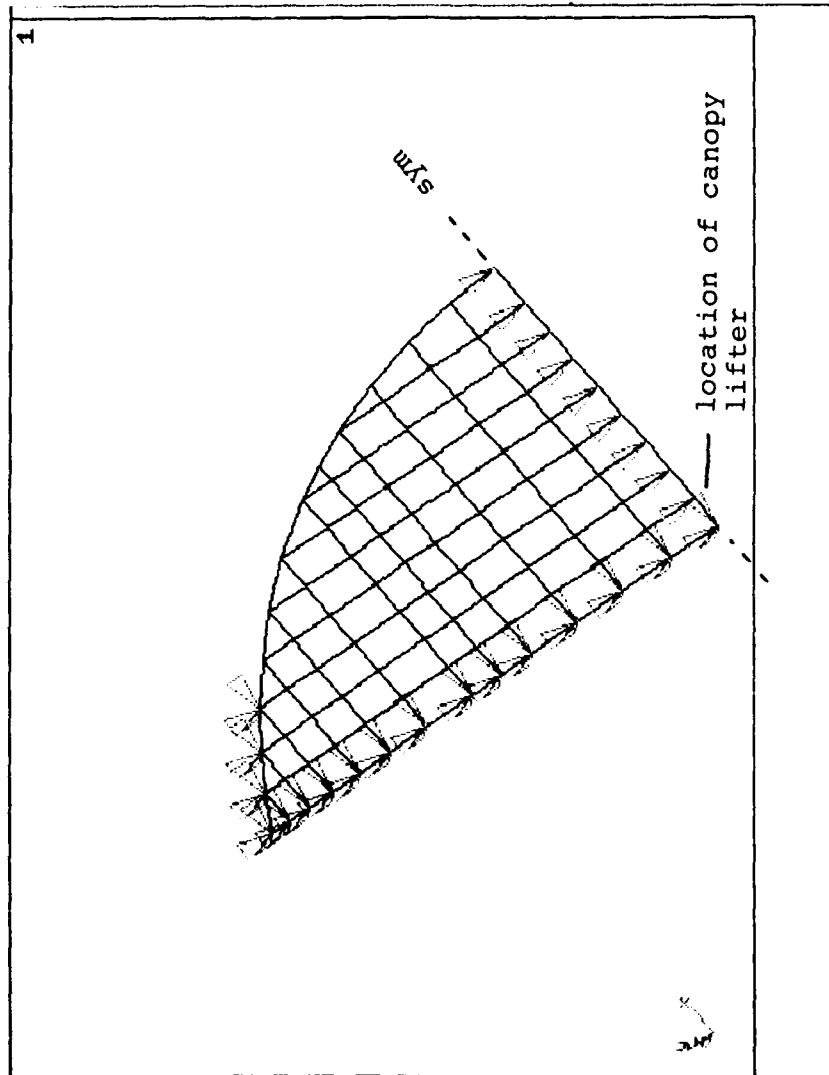


Figure A-9. Geometry and Boundary Conditions of Upper Composite Panel Model.

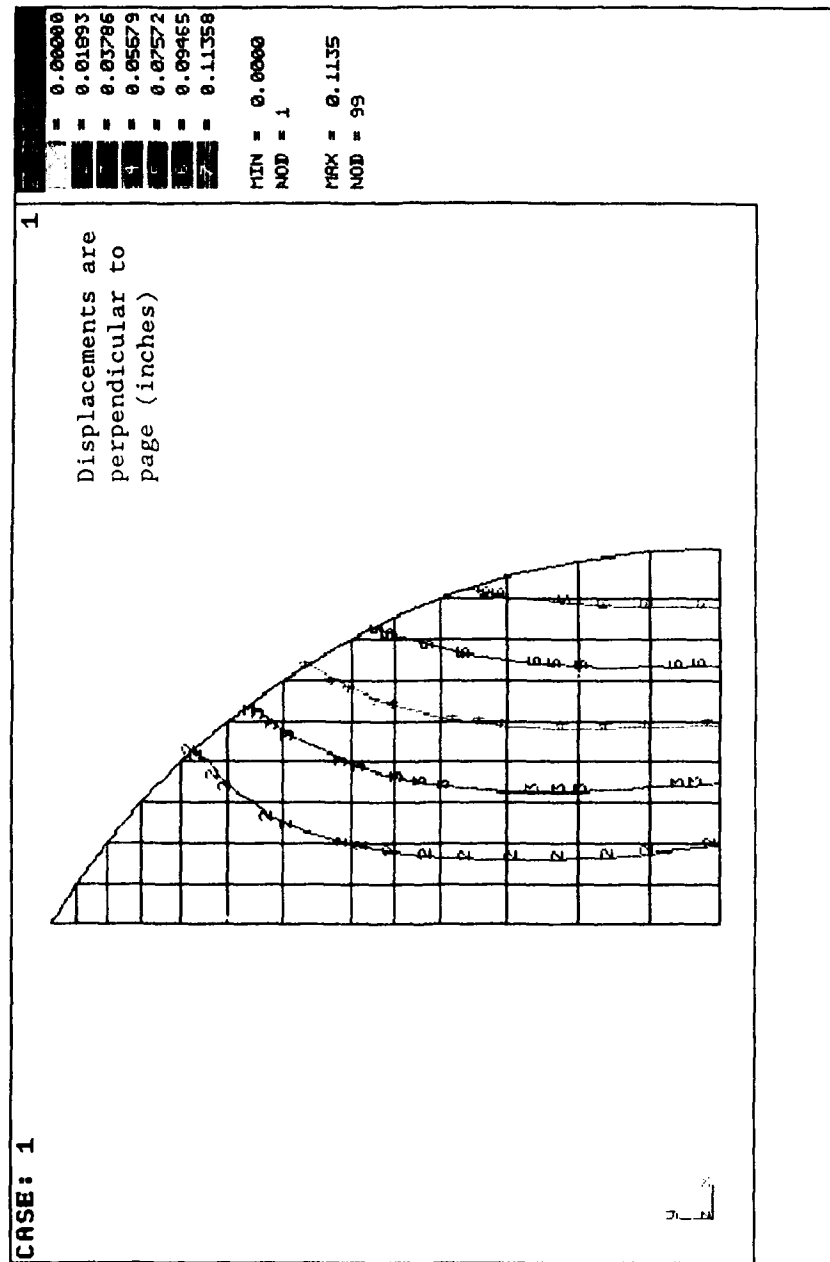


Figure A-10. Deflections of Upper Composite Panel for 5-psi Pressure Load.

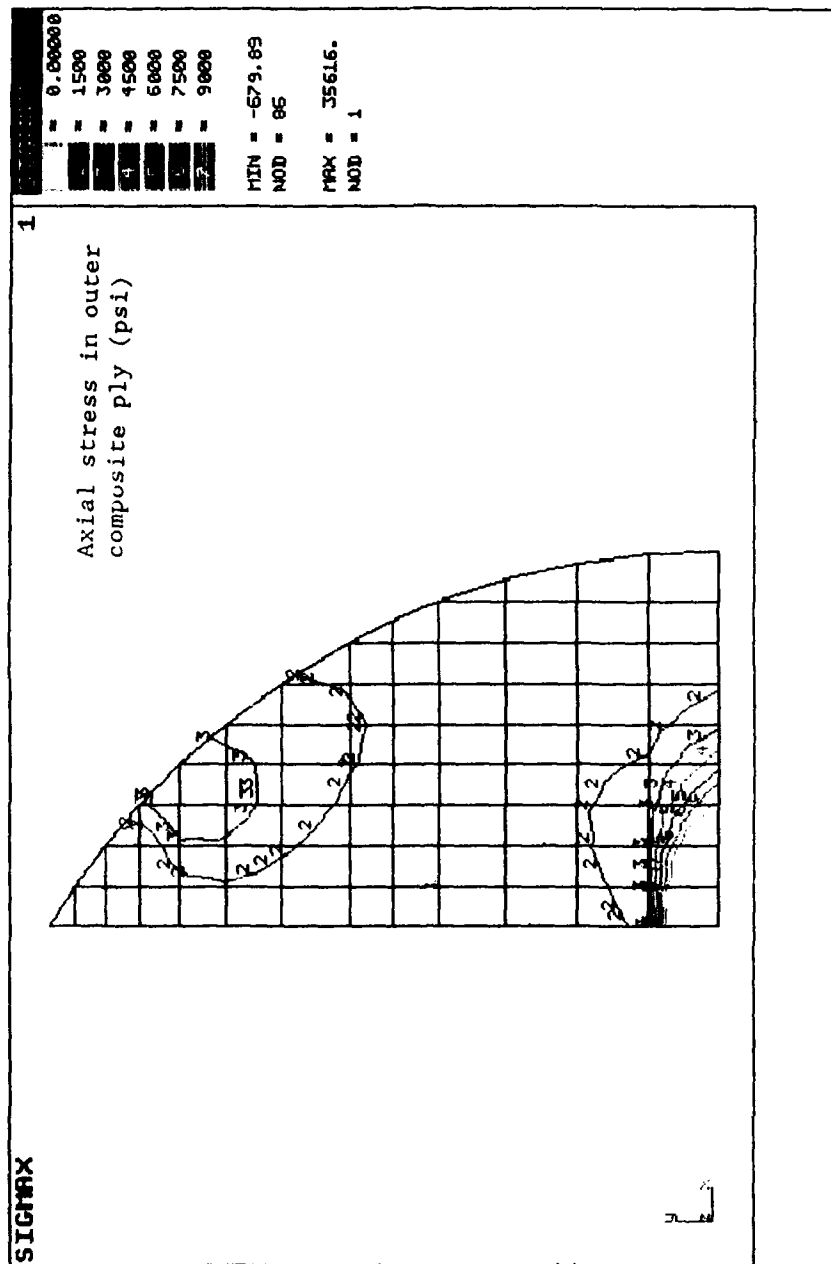


Figure A-11. Longitudinal Stress in Outer Ply of Composite Panel for 5-psi Pressure Load.

the canopy stress evaluation in Section 3. Displacement contours for this load condition are shown in Figure A-12. The maximum displacement is 0.028 inches, much less than the allowable. The stresses in the X-direction on the outer ply of the panel are shown in Figure A-13. Again, a large stress concentration is seen at the location of the lifter. Using the Tsai-Wu criteria, the margin of safety for first-ply failure is 5.5.

#### A.4 BONDED JOINTS

An analysis of the two critical joints is summarized in this section. These joints are the attachment of the canopy hinge pin adapter to the composite side-tube and the attachment of the cross-tube to the side-tube. Two methods were used for the analysis of each of these joints: finite element analysis and analytic methods [11]. Design loads for the joints are based on the failure loads of the surrounding structure. Only elastic deformation of the adhesive was considered. Since plastic deformation of the adhesive gives bonded joints a much higher strength than that predicted by elastic analysis [11], this represents a conservative analysis.

##### A.4.1 Composite Tube - Hinge Pin Adapter Joint

The attachment of the hinge pin adapter to the composite side-tube is shown in Figure A-14. The design loads for this bonded attachment were developed from the designed failure load of the hinge pins. The bolts are designed to fail in torsion in the range  $T = 800$ -1150 in-lbf [18]. Assuming the torsion is reacted only by the upper and lower surfaces of the composite tube, the load on the upper (narrower) surface is

$$\begin{aligned} N &= \frac{T}{L \cdot w} \\ &= \frac{1150 \text{ in}\cdot\text{lb}}{1.55 \text{ in} \cdot 1.7 \text{ in}} \\ &= 436 \text{ lb/in} \end{aligned} \tag{A.12}$$

The bolt narrows in diameter in the region of failure to a diameter  $d = 0.3125$  in. An upper bound on the shear strength of this bolt is found by assuming no plastic deformation during torsion and no stress concentration in the narrowed region. The shear strength is:

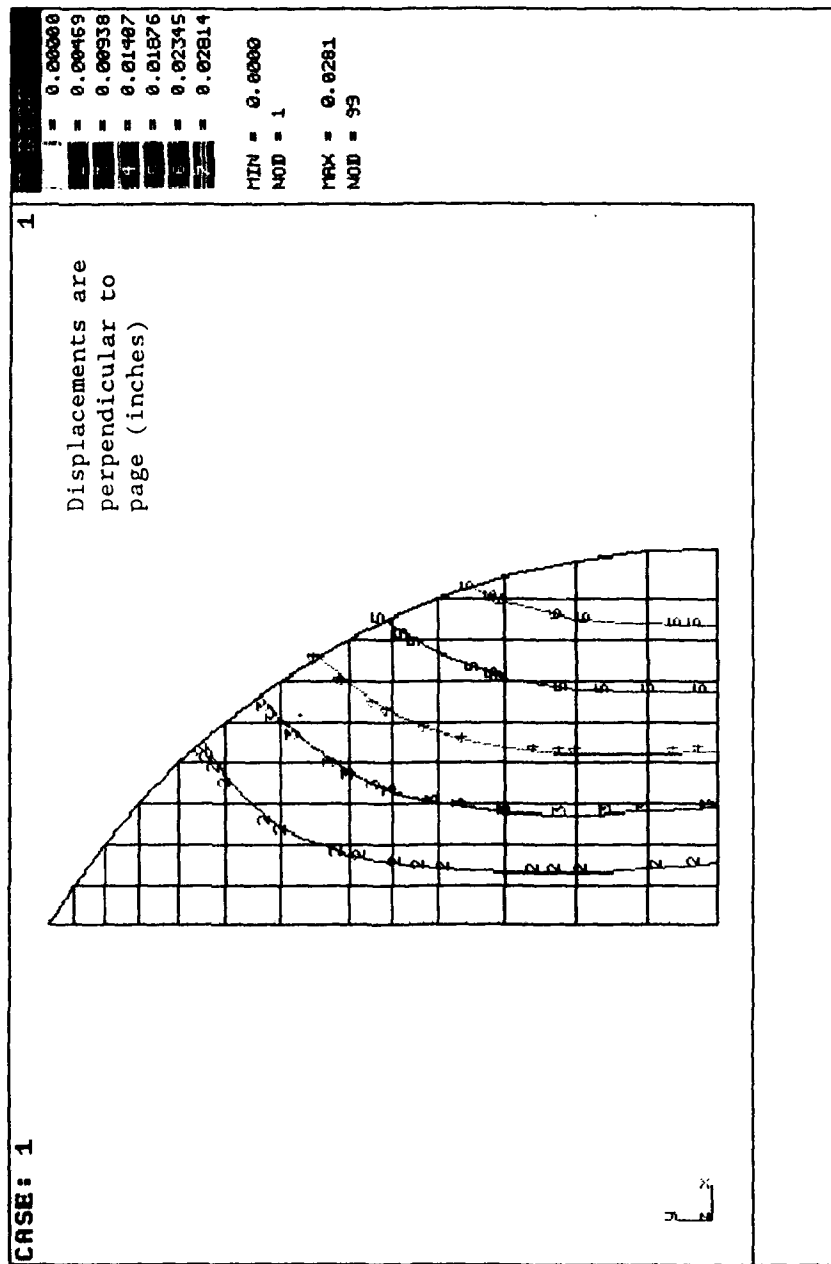


Figure A-12. Deflections of Upper Composite Panel for 5-psi Pressure and -25-lb/in Edge Load.

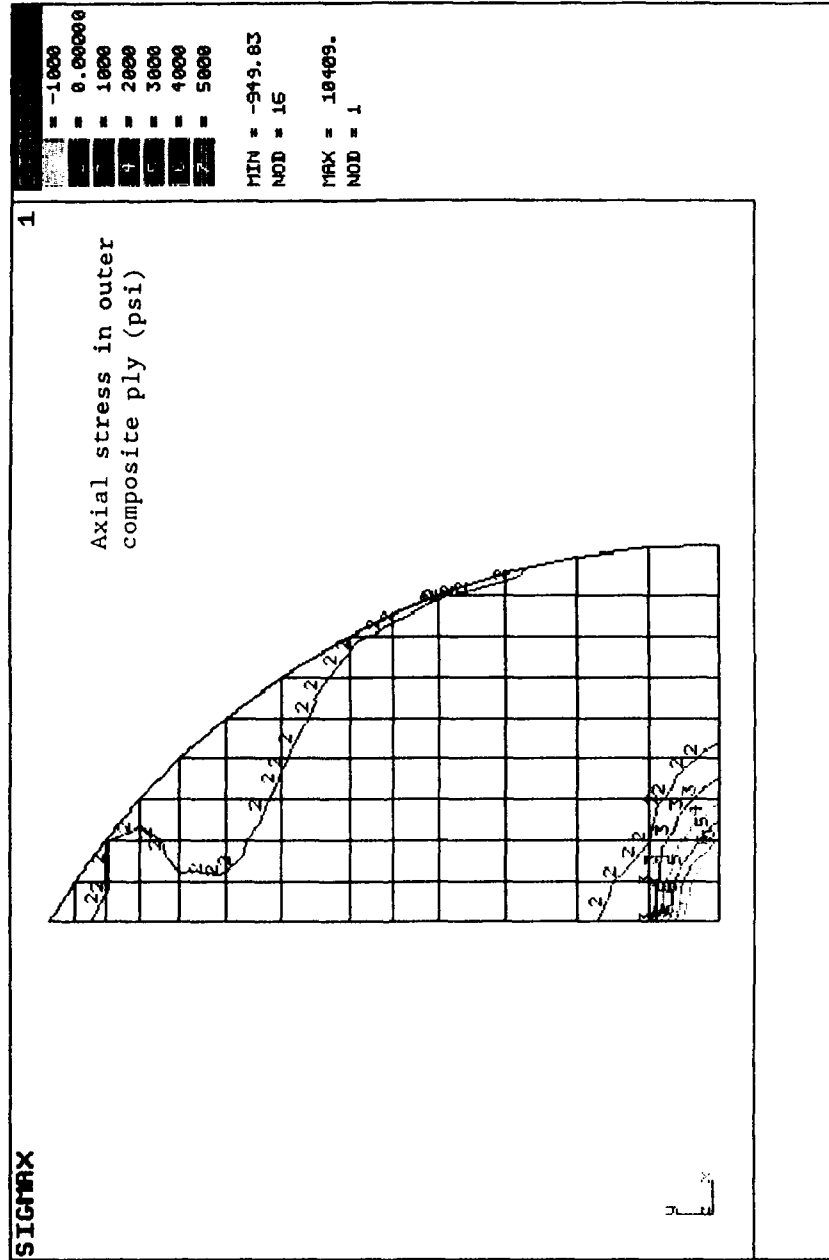


Figure A-13. Longitudinal Stress in Outer Ply of Composite Panel for 5-psi Pressure and -25-lb/in Edge Load.



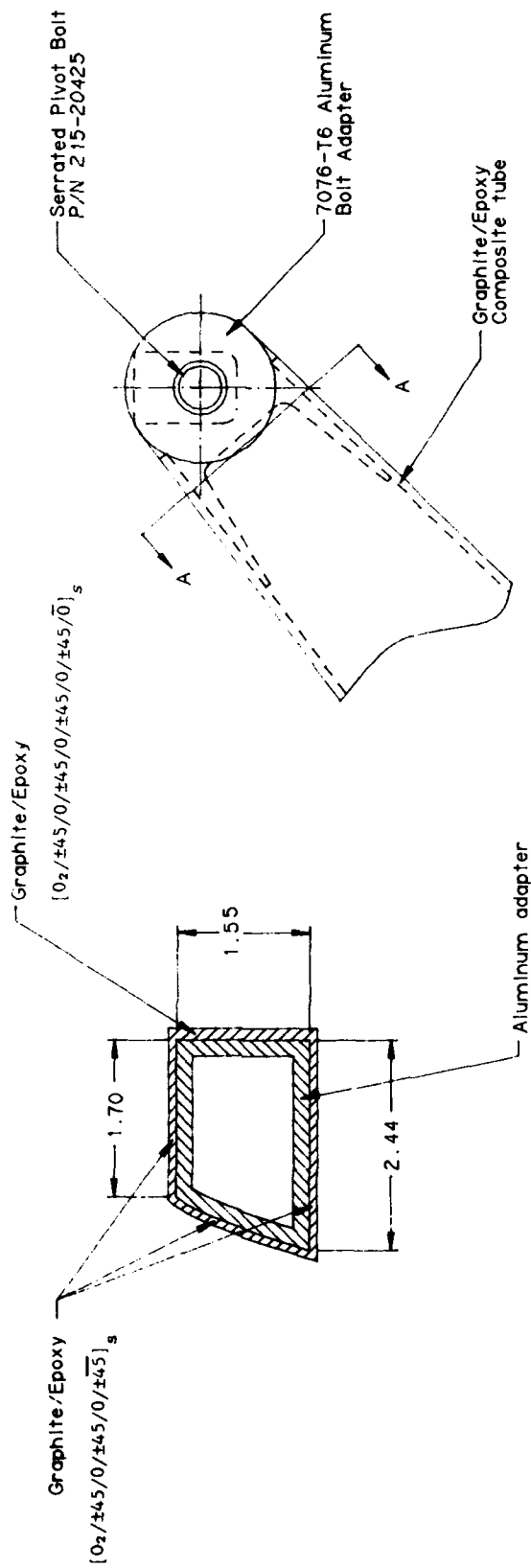


Figure A-14. Serrated Pivot Bolt Adapter Joint.

$$\begin{aligned}
 S_s &= \frac{T \cdot d/2}{J} \\
 &= \frac{1150 \cdot 0.3125/2}{\pi \cdot d^4/32} \\
 &= 192,000 \text{ psi.}
 \end{aligned}
 \tag{A.13}$$

Pure shear in the bolt causes a load to the composite tube of

$$\begin{aligned}
 F &= S_s \cdot \pi \cdot d^2 / 4 \\
 &= 190000 \cdot \pi \cdot 0.3125^2 / 4 \\
 &= 14,700 \text{ lbf.}
 \end{aligned}
 \tag{A.14}$$

The axial stress for this load is:

$$\begin{aligned}
 \sigma &= F / A \\
 &= 14700 / 0.79 \\
 &= 18,600 \text{ psi.}
 \end{aligned}
 \tag{A.15}$$

This stress is less than the compressive strength of 27,000 psi of this laminate and much less than the tensile strength of 50,300 psi. This load will be distributed to the walls of the composite tube in proportion to their thickness.

$$\begin{aligned}
 N &= \sigma \cdot t \\
 t = 0.090: \quad N &= 18600 \cdot 0.090 = 1670 \text{ lbf/in} \\
 t = 0.135: \quad N &= 18600 \cdot 0.135 = 2510 \text{ lbf/in.}
 \end{aligned}
 \tag{A.16}$$

The load required to shear the bolt is higher than for torsion failure of the bolt and is the critical design load.

To determine the allowable load on the interface, the joint was analyzed as two balanced adherends. The actual and modeled joints are shown in Figure A-15. The model joint

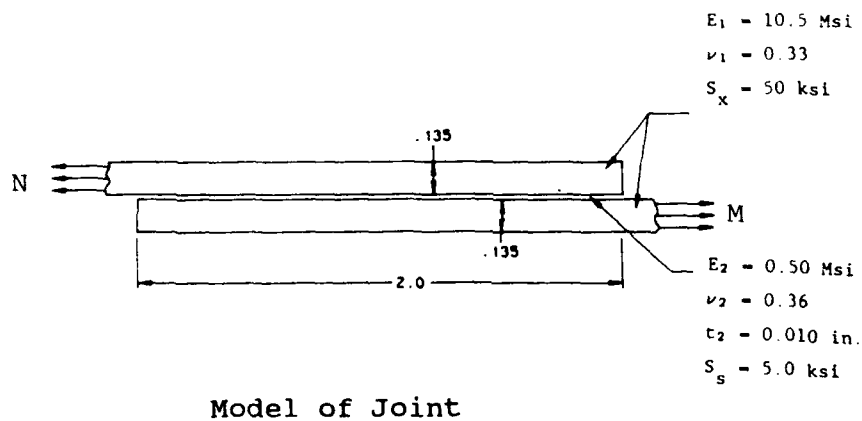
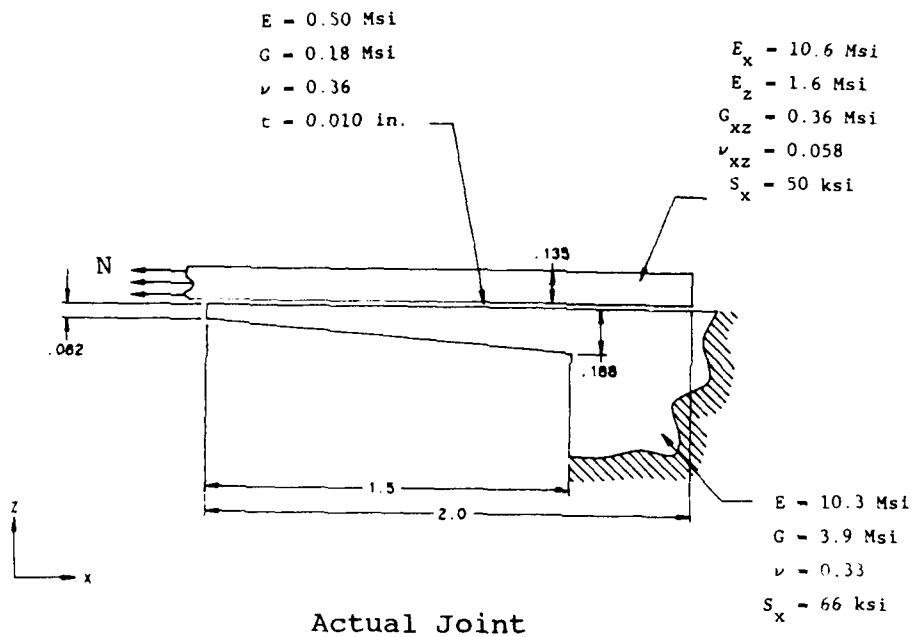


Figure A-15. Analytic Model of Pivot Bolt Adapter Joint.

assumes that the adherends are free to displace in the Z-direction. Since the box beams actually restrict displacement in this direction, this model is conservative. Effective uniform composite properties were determined from the lamina properties as in Reference 19. The adhesive properties shown in Figure A-15 were for Reduc K-6 [20]. Moduli for the balanced adherends were an average of the properties for the aluminum and the composite. The axial strength of the adherends was based on the in-plane strength of the composite laminate, which was weaker than the aluminum. The allowable force on the joint was calculated as follows: [11]:

$$\begin{aligned}
 a &= \left[ \frac{12 \cdot N \cdot (1 - \nu^2)}{E_1 \cdot t_1^2} \right]^{1/2} \\
 &= \left[ \frac{12 \cdot N \cdot (1 - 0.33^2)}{10.5E6 \cdot 0.135^2} \right]^{1/2} \\
 &\approx 0.0203 \cdot N^{1/2}.
 \end{aligned} \tag{A.17}$$

$$\begin{aligned}
 b &= \left[ 1 + \frac{L \cdot a}{2} + \frac{L^2 \cdot a^2}{24} \right]^{-1} \\
 &= \left[ 1 + \frac{L \cdot a}{2} + \frac{4 \cdot a^2}{24} \right]^{-1} \\
 &= \left[ 1 + 0.0203 \cdot N^{1/2} + 0.0000690 \cdot N \right]^{-1}
 \end{aligned} \tag{A.18}$$

$$\begin{aligned}
 N &= \frac{t_1 \cdot S_x}{1 + 3 \cdot b \cdot (1 + t_2/t_1)} \\
 &= \frac{0.135 \cdot 50000}{1 + 3 \cdot b \cdot (1 + 0.010/0.135)} \\
 &\approx \frac{6750}{1 + 3.222 \cdot b}
 \end{aligned} \tag{A.19}$$

Solving Equations A.18 and A.19 gives an allowable force resultant of  $N = 2790$  lbf/in. Thus, the margin of safety for the force resultant was:

$$MS = \frac{2790}{2510} - 1 = 0.11.$$

The analytical development did not give any information about the shear stress distribution in the adhesive. To determine this distribution, an FE model was generated using orthotropic plate elements from the COSMOS [13] FE program. As in the analytic model, the joint was treated as a plane stress problem, and the composite laminate was assumed to have uniform properties through the thickness. The geometry, loads, and material properties for the model are shown in Figure A-16. Shear stress concentrations occur in the adhesive at both ends of the bond. The peak value occurs at the tapered end of the aluminum adapter. The peak shear stress is 4370 psi. The highest shear stress at the thick end of the aluminum adapter was 4090 psi. Thus, the FE model showed a margin of safety for the adhesive in shear of:

$$MS = \frac{5000}{4370} - 1 = 0.14.$$

The model also shows that the stresses in both the composite and aluminum are much lower than their allowable strengths.

Both the analytic and FE model of the joint showed that the adhesive bond would remain in the elastic range up to the failure load of the hinge pins. Thus, the joint has a much higher strength than the surrounding structure.

#### A.4.2 Side-Tube - Cross-Tube Joint

Again, two models were used to evaluate this connection. The intersection of the cross-tube and side-tube is shown in Figure A-17. The figure shows the overlap of the walls of the cross-tube onto the side-tube to transfer load in shear. Clips were used on the inside of the cross-tube to transfer some of the load. Webs were used on the inside of the side-tube to prevent local deformation of the walls at this intersection. Not shown on the figure is the gusset used to reduce flexing between the two tubes. For a conservative analysis, the additional strength of the gusset was not included.

Torsion in the side-tube is reacted as bending in the cross-tube. The failure load due to torsion in the side-tube at the forward edge of the gusset (cross-section 7 of the modified structure in Figure A-1) is 65,800 in-lbf. This load is reacted primarily by the upper and lower overlaps of the tubes. The load in the lower, narrower flange is:

$E_x = 10.6 \text{ Msi}$   
 $E_z = 1.6 \text{ Msi}$   
 $G_{xz} = 0.36 \text{ Msi}$   
 $\nu_{xz} = 0.058$

$E = 0.50 \text{ Msi}$   
 $G = 0.18 \text{ Msi}$   
 $\nu = 0.36$   
 $t = 0.010 \text{ in.}$

$E = 10.3 \text{ Msi}$   
 $G = 3.9 \text{ Msi}$   
 $\nu = 0.33$

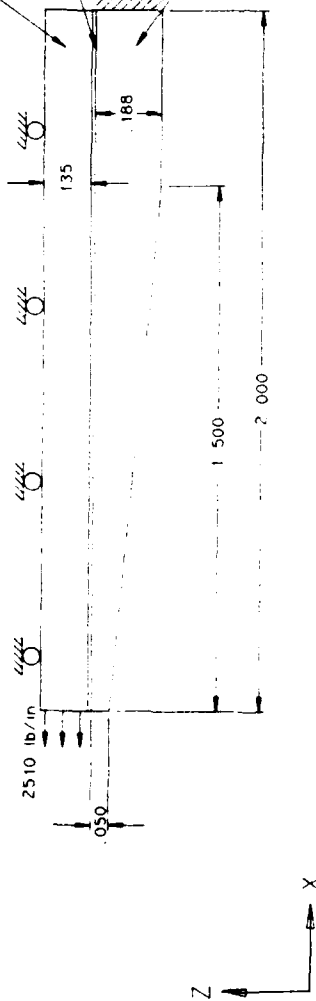


Figure A-16. Geometry and Materials for FE Model of Pivot Bolt Adapter Joint.

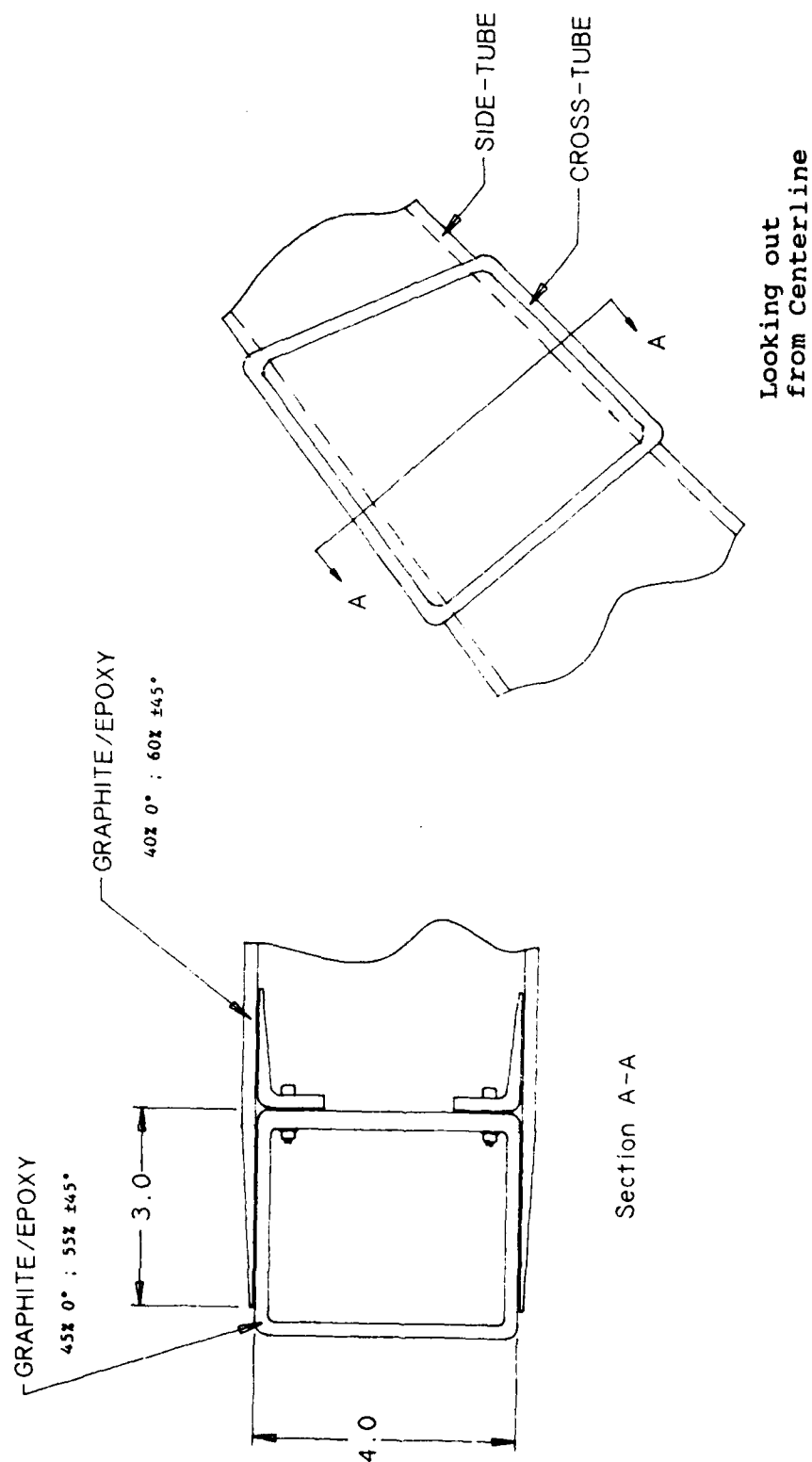


Figure A-17. Intersection of Cross-Tube and Side-Tube.

$$\begin{aligned}
 N &= \frac{T}{L \cdot w} \\
 &= \frac{65800}{4.0 \cdot 3.8} \\
 &= 4330 \text{ lbf/in}
 \end{aligned}
 \tag{A.20}$$

This is below the in-plane compressive strength of the laminate of 4950 lbf/in and well below the in-plane tensile strength of 9300 lbf/in.

Analytical evaluation of the joint used equations developed in Reference 11 for unbalanced adherends. The side-tube was conservatively modeled as being infinitely stiff. Geometry and material properties for the analytic model are shown in Figure A-18. Adhesive properties are for Redux K-6 [20]. Composite material properties are effective in-plane properties for the laminate. The adhesive failure load for this geometry is:

$$\begin{aligned}
 N &= [8 \cdot \tau_p \cdot t_2 \cdot (\gamma_e/2 + \gamma_p) \cdot E_1 \cdot t_1]^{1/2} \\
 &= [8 \cdot 5000 \cdot 0.010 \cdot (0.027/2 + \gamma_p) \cdot 9.6E6 \cdot 0.200]^{1/2} \\
 &= 27700 \cdot (0.013 + \gamma_p)^{1/2}
 \end{aligned}
 \tag{A.21}$$

To achieve the load of 4330 lbf/in required to react the torque at failure of the side-rail, the adhesive must deform plastically. The plastic strain  $\gamma_p$  for this load is:

$$\begin{aligned}
 N &= 4330 = 27700 (0.013 + \gamma_p)^{1/2} \\
 \gamma_p &= \left[ \frac{4330}{27700} \right]^2 - 0.013 = 0.011
 \end{aligned}
 \tag{A.22}$$

This amount of plastic strain is relatively small compared to the 140 percent shear strain for failure of the adhesive [20].

Verification of the effects of tapering the flanges and adding the clips was performed using linear, static FE analysis. The model used orthotropic plate elements from the COSMOS FE program [13]. Model geometry, boundary conditions, and material properties are defined in Figure A-18. This model shows two areas of high shear stress in the adhesive: (1) the narrow ends of the clip, and (2) the inner edge of the side-rail. These locations are shown in



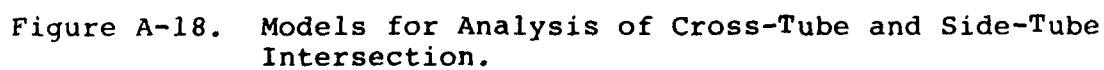


Figure A-18. The highest shear stress occurs at the narrow end of the clip and has a value of 4570 psi. This gives a margin of safety for shear in the joint of

$$MS = \frac{5000}{4570} - 1 = 0.09.$$

The model also shows a high tensile stress concentration on the epoxy just below the fillet. The model shows a peak tensile stress of 10,700 psi in this area. This exceeds the 8,300 psi tensile strength of the adhesive.

To reduce the stress in the adhesive at this point, the clips should be fastened to the side-tube with mechanical fasteners, as shown in Figure A-18. The model was run with fixed conditions on the portion of the clip which will be bolted to the side-tube. The model showed nearly identical results in all three areas of peak stress. Thus, mechanically fastening the clips to the side-tube will not eliminate plastic deformation near the fillet. However, the fasteners will limit the extent of deformation to a small area.

The analytical and FE models showed that a small amount of plastic deformation would occur in this joint at the failure load of the surrounding structure. Thus, a ductile adhesive is suggested to prevent fatigue. Use of an adhesive with properties similar to those used in this analysis and mechanical fasteners to limit deformation of the clips will produce a joint which is stronger than the surrounding structure.

**APPENDIX B**  
**MODIFIED CANOPY AFT FRAME DRAWINGS**

This section presents detailed drawings of the proposed structure.

Drawing notes:

- 1 Longitudinal (0°) orientation for lay-up of composite structures, if not specified, are parallel to beam centerline for beams or parallel to fuselage station axis for panels.
- 2 Materials referenced in composite lay-ups:  
C - E25 unidirectional Graphite/epoxy, 0.0050 in/layer  
K - K49 woven Kevlar cloth/epoxy, 0.010 in/layer  
N - 2 gage, 1/8 cell Nomex core, 0.25 in/layer.
- 3 For secondary bonding of cured parts use adhesive with properties similar to Redux K-6:  

E = 500 ksi	G = 180 ksi
F <sub>x</sub> = 8.0 ksi (min ultimate)	F <sub>s</sub> = 5.0 ksi (min shear yield).
- 4-10 Omitted
- 11 Graphite/epoxy lay-up (see note 2):  
[0<sub>2</sub>/(45/-45/0)<sub>5</sub>/0]<sub>T</sub>.
- 12 Graphite/epoxy lay-up (see note 2):  
[0<sub>2</sub>/(45/-45/0)<sub>6</sub>]<sub>S</sub>.
- 13 Continue plies from thinner portion along entire length of beam. Alternate additional plies between continuous plies to form thicker section. Distribute ply drop-offs along 2.0-inch section to provide similar ratio of 0° to ±45° plies along tapered section.

- 14 Bond in place 10-32 threaded bushing, 0.625 dia x 0.040 thick baseplate, anodized 7075-T6 aluminum. (P/N CB5005-A-3-A-150-N, Click Bond Inc., Carson City, Nevada, 89706).
- 15 Graphite/epoxy lay-up (see notes 2,50):  
[50/-50/0<sub>3</sub>/90/0<sub>3</sub>/90/0<sub>2</sub>]<sub>S</sub>.
- 16 Graphite/epoxy lay-up (see notes 2,50):  
[0/90/0<sub>3</sub>/90/0<sub>3</sub>/90/0<sub>2</sub>]<sub>S</sub>.
- 17 Graphite/epoxy lay-up (see note 2):  
[(0/90/45/-45)<sub>3</sub>]<sub>S</sub>  
Longitudinal fiber axis parallel to forward edge of web. Fold outer 2 plies to form lower 2 plies on attached flanges.
- 18 Graphite/epoxy lay-up (see notes 2,50):  
[30/-30/0<sub>3</sub>/90/0<sub>3</sub>/90/0<sub>2</sub>]<sub>S</sub>.
- 19 Pivot bolt adapter - material 7075-T6 aluminum and anodize.
- 20 Kevlar/epoxy lay-up (see note 2): [0<sub>15</sub>]<sub>T</sub>.  
Longitudinal fiber axis parallel to transparency edge. Extend lower 10 plies to form transparency attachment. Extend top 5 plies to form outer surface. Use additional layers between plies to fill shape.
- 21 Kevlar/epoxy lay-up (see note 2): [0<sub>14</sub>]<sub>T</sub>.  
Longitudinal fiber axis parallel to transparency edge. Extend lower 10 plies aft to form edge for pressure panel. Trim upper 4 plies to fill triangular shape.
- 22 Graphite/epoxy lay-up (see note 2): [90<sub>2</sub>/0/90<sub>2</sub>]<sub>S</sub>.  
Longitudinal fiber axis parallel to edge of transparency. Bond in place (see note 3).

- 23 Graphite/epoxy lay-up (see note 2):  $[(0/90/45/-45)_3]_S$ .  
Bond in place after curing (see note 3).
- 24 Graphite/epoxy lay-up (see note 2):  $[0/(0/45/-45)_3]_{2S}$ .
- 25 Composite lay-up (see note 2):  
 $[0_K/0/45_C/-45_C/90_C/(0_C/45_C/-45_C)/0_K]_S$ .  
Wrap inner 18 plies around core. Extend outer 11 plies to form flange.
- 26 Composite lay-up (see note 2):  
 $[0_K/0_C/45_C/-45_C/90_C/(0_C/45_C/-45_C)_2]_S$ .
- 27 Extend outer 11 plies from each wall to form flange. Add resin at corner to prevent voids.
- 28 Bond 8-32 x 0.50 long composite inserts in composite sandwich (P/N FIEGE0836, Tiodize Co., Inc., Huntington Beach, California, 92649). Align with rivet holes in existing hardware.
- 29 Use existing rubber seal and hardware. Attach to panel with 8-32 screws, replacing rivets.
- 30 Use existing hardware P/N 215-20428-1.
- 31 Composite lay-up (see note 2):  
 $[(90_C)/45_C/-45_C/(90_C)/0_N]_S$ .  
Longitudinal fiber axis parallel to transverse axis of aircraft.
- 32 Composite lay-up (see note 2):  
 $[(90_3)_C/45_C/-45_C/0_C/(90_2)_C/0_C/45_C/-45_C/(90_3)_C/0_N]_S$ .  
Longitudinal fiber axis parallel to transverse axis of aircraft.

- 33 Drill 0.51 in honeycomb panel. Bond 1/2 OD x 13/64 ID x 0.64 long titanium bushing in honeycomb panel. Install 10-32-NF-3B bolt and nut with nylon lock.
- 34 Drill 0.51 in honeycomb panel. Bond 1/2 OD x 17/64 ID x 0.60 long titanium bushing in honeycomb panel. Machine bushing flush with surface. Install 1/4-20-NF-3B bolt and nut with nylon lock.
- 35 Install 0.25 DIA x 0.35 long titanium shaft blind fastener. P/N MBF2111-8-350, Monogram Aerospace Fasteners, Los Angeles, California, 90022)
- 36 Kevlar/epoxy lay-up (see note 20: [0/45]<sub>S</sub>). Longitudinal fiber axis aligned with fuselage station axis. Extend these 4 plies over entire skin surface.
- 37 Kevlar/epoxy lay-up (see note 2): [0/45/45/0]<sub>S</sub>. Longitudinal fiber axis aligned with fuselage station axis. Outer 4 plies are extension of overall skin.
- 38 Nominal bond thickness 0.005 inches. See note 3.
- 39 Extend plies from transparency attachment (see note 21) to aft edge of section. Use additional plies as necessary to fill triangular section.
- 40 Taper flange from 0.20 to 0.080. Distribute ply drop-outs to retain nearly constant ratio of 0° and ±45° plies. Stagger ply drop-outs through thickness to prevent voids and minimize stress concentrations.
- 41 Graphite /epoxy lay-up (see note 2):  
[0<sub>2</sub>/(45/-45/0)<sub>4</sub>]<sub>S</sub>.
- 42 Graphite /epoxy lay-up (see note 2):  
[0<sub>2</sub>/(45/-45/0)<sub>2</sub>/(0/-45/45)<sub>2</sub>]<sub>2S</sub>.

- 43 Continue plies from thinner portion along entire length of beam. Alternate additional plies between continuous plies to form thicker section. Distribute ply drop-offs along 2.0 inch section to provide similar ratio of  $0^\circ$  to  $\pm 45^\circ$  plies along tapered section.
- 44 Machine Nomex core to taper both sides. Reduce thickness from 0.50 to 0.42 over upper 2.00 inches of lower panel. Extend plies of upper panel (see note 32) below corner. Drop out plies not needed for lower panel (see note 31) at rate of 4 plies/in in each face.
- 45 Graphite/epoxy lay-up (see note 2):  $[0_2/(45/-45/0)_6]_S$ .  
Lay-up tube around web. Co-cure tube and web.
- 46 Ream aluminum 0.6250X0.0005. Install NAS-537-8P-105. Press flush with inner surface. Ream bushing 0.500X0.0025. Countersink outer surface  $100^\circ \times 0.68$  dia.
- 47 Kevlar/epoxy lay-up (see note 2):  $[0_6]_T$ . Longitudinal fiber axis along axis of beam. Build up on outer surface of Gr/Ep tube before curing.
- 48 0.010 thick bond. See note 3. Use 0.010 glass beads to ensure constant bond-line thickness.
- 49 Graphite/epoxy lay-up (see note 2):  $[0/90/45/45]_{3S}$ .  
Fold over outer 8 plies on either side of web to form 1.50 wide by 0.040 thick flange on inner surface of tube. Co-cure web with tube.
- 50 Longitudinal fiber axis parallel to adjacent edge of web. Fold outer 2 plies on either side of web to form lower 2 plies on flange.
- 51 Machine outer surface of Nomex before lay-up to reduce core thickness to 0.375 inches. Fill any gaps at free edge of panel with epoxy after curing panel.

- 52 Install 0.198 dia x 0.25 long titanium shaft blind fastener (P/N MBF2111-6-250, Monogram Aerospace Fasteners, Los Angeles, California, 90022)
- 53 Drop 0° K/Ep and 90° Gr/Ep layers from side rail section. Extend remaining layers aft along beam. Alternate additional plies between continuous plies to achieve proper lay-ups (see notes 12, 42). Add plies at corner.
- 54 Install 0.198 dia x 0.45 long titanium shaft blind fastener (P/N MBF2111-6-450, Monogram Aerospace Fasteners, Los Angeles, California, 90022)
- 55 Graphite/epoxy lay-up (see note 2): [(0/90)<sub>10</sub>]<sub>S</sub>.  
Use 0/90 lay-up in upper and lower flanges of gusset. Fold over plies to create angles plies against walls of tubes. Use continuous plies in upper and lower flanges. Splice plies along walls of tube.
- 56 Install 0.198 DIA x 0.50 long titanium shaft blind fastener(P/N MBF2111-6-500, Monogram Aerospace Fasteners, Los Angeles, California, 90022)



Y  
13.00

0.014 THICK SKIN  
SEE NOTE 54

SEE NOTE 55

PRESS OUT ADHESIVE  
TO FILL CORNERS

0.005 ADHESIVE BOND  
SEE NOTE 38

SECTION H-H

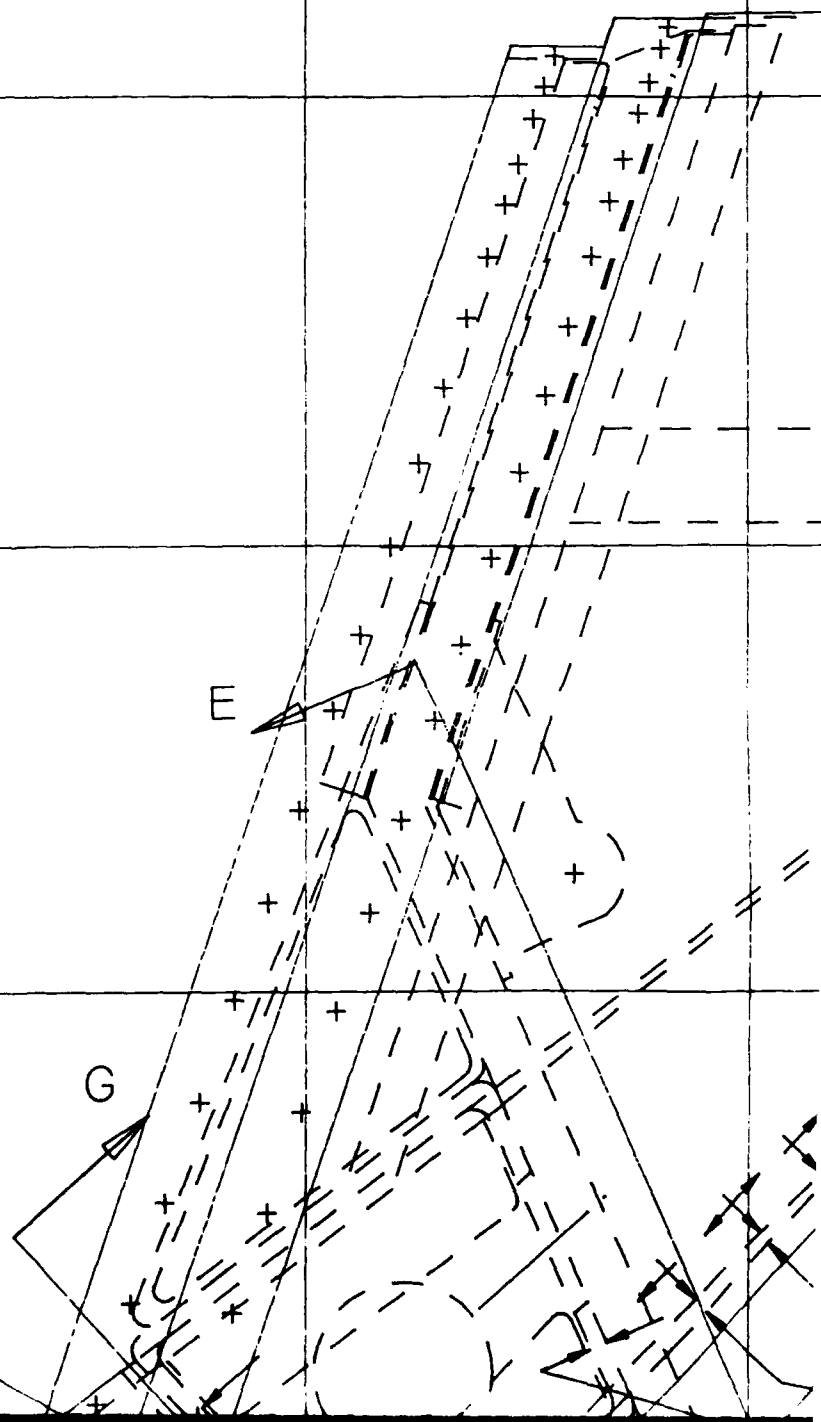
0.20 THICK WE  
SEE NOTE 4

DRILL 1 - 53 PLACE  
SPOTFACE 0.656 - 0.050 DEEP  
BOND NUTPLATE FLUSH WITH SURFACE  
SEE NOTE 14

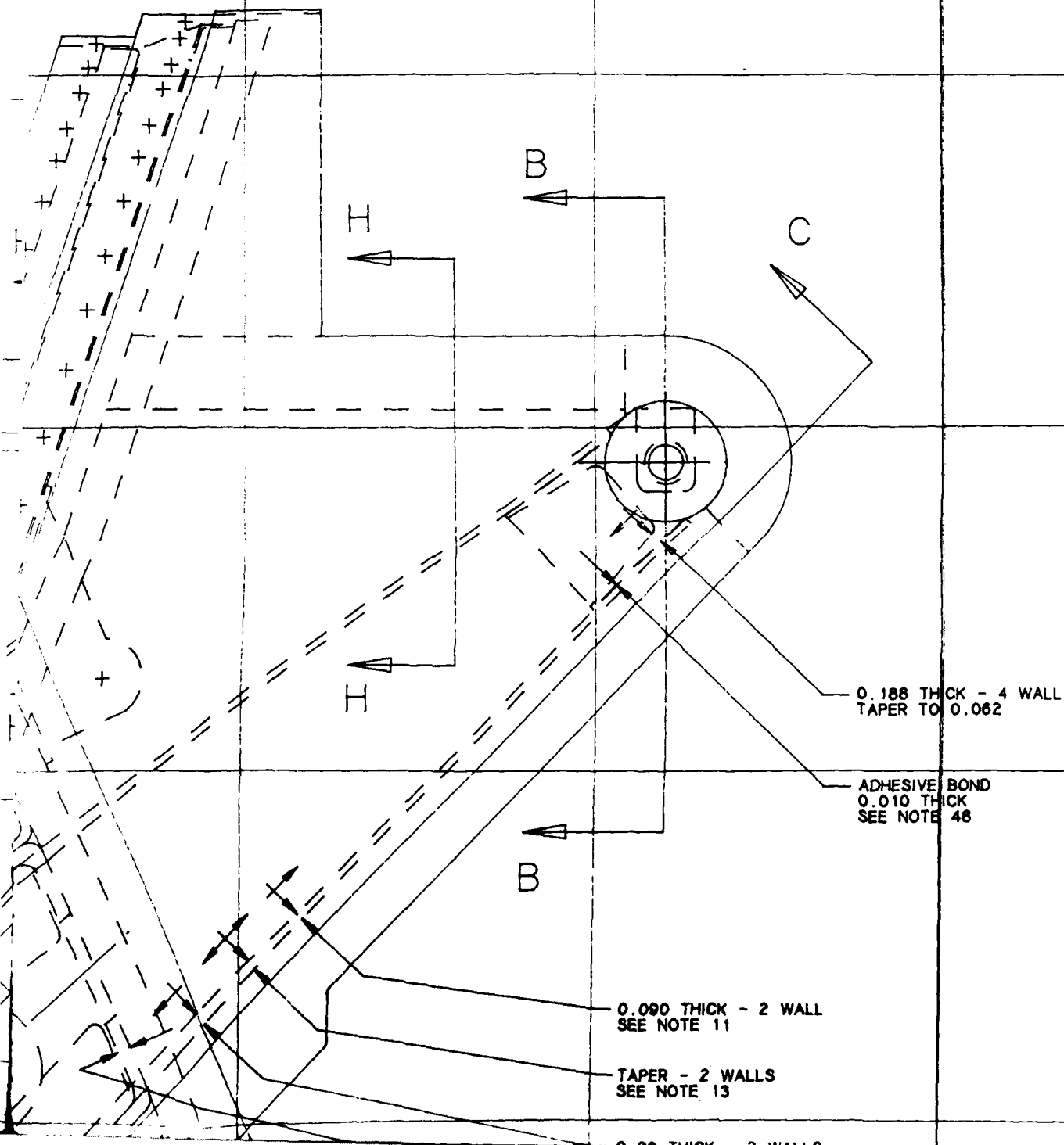
SEE NOTE 55

0.20 THICK WEB  
SEE NOTE 45

DRILL 1 - 53 PLACE  
FACE 0.656 - 0.050 DEEP  
PLATE FLUSH WITH SURFACE  
SEE NOTE 14



Z 140



Z 130

0.005 ADHESIVE BOND  
SEE NOTE 38

SECTION H-H

DRILL 1 - 53  
SPOTFACE 0.656 - 0.054  
BOND NUTPLATE FLUSH WITH SA  
SEE NOTE 53

SEE NOTE 53 -

DRILL ON ASSEMBLY - 42 PLACE  
INSTALL 0.198 DIA BLIND FASTENER - 42 REQ'D  
SEE NOTE 52

Y  
15.00

1.62 DIA CORE HOLE

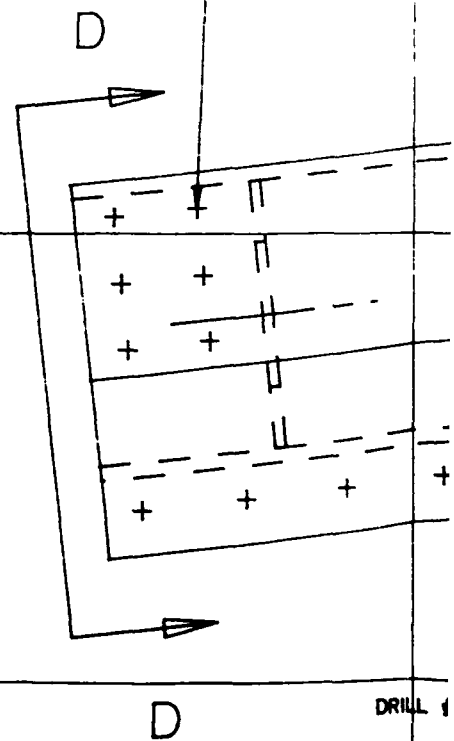
SEE NOTE 27

0.16 THICK - 5 WALLS  
SEE NOTE 25

0.12 THICK  
SEE NOTE 26

SECTION D-D

X280



THICK  
NO

0.20 THICK WEB  
SEE NOTE 45

DRILL 1 - 53 PLACE  
SPOTFACE 0.656 - 0.050 DEEP  
BOND NUTPLATE FLUSH WITH SURFACE  
SEE NOTE 14

SEE NOTE 53

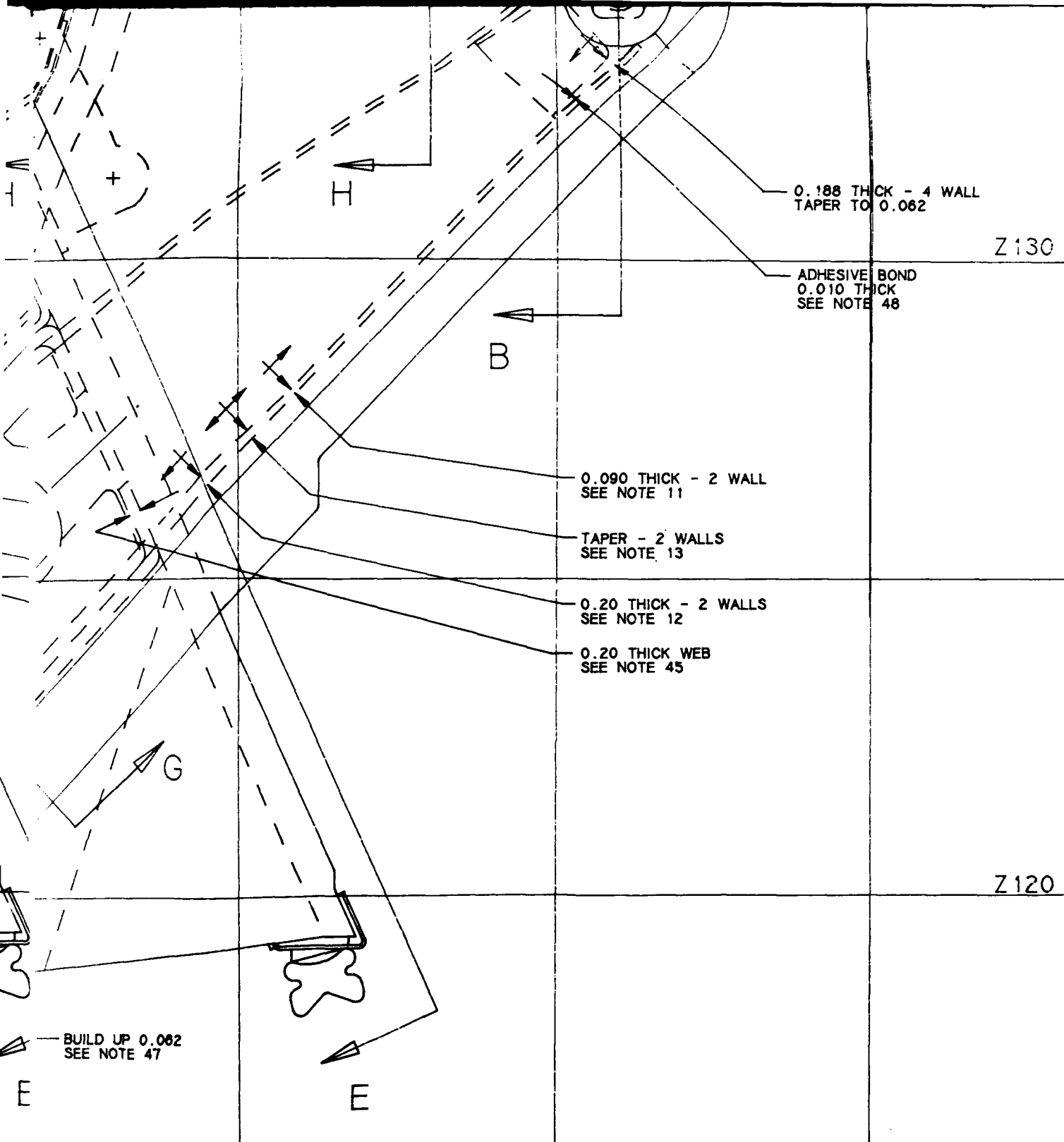
BUILD UP 0.062  
SEE NOTE 47

DRILL 1, 0.20 DEEP - 54 PLACE  
SPOTFACE 0.656, 0.050 DEEP  
BOND NUTPLATE FLUSH WITH SURFACE  
SEE NOTE 14

DRILL #9 ON ASSEMBLY - 16 PLACE

X290

X300



UNIVERSITY OF DAYTON RESEARCH INSTITUTE

PART

REVISED A-7 AFT CANOPY FRAME

SIDE VIEW, SECTION D-D, SECTION H-H

DRAWN BY

J. RODERER

DATE

15-JUN-90

CHECKED

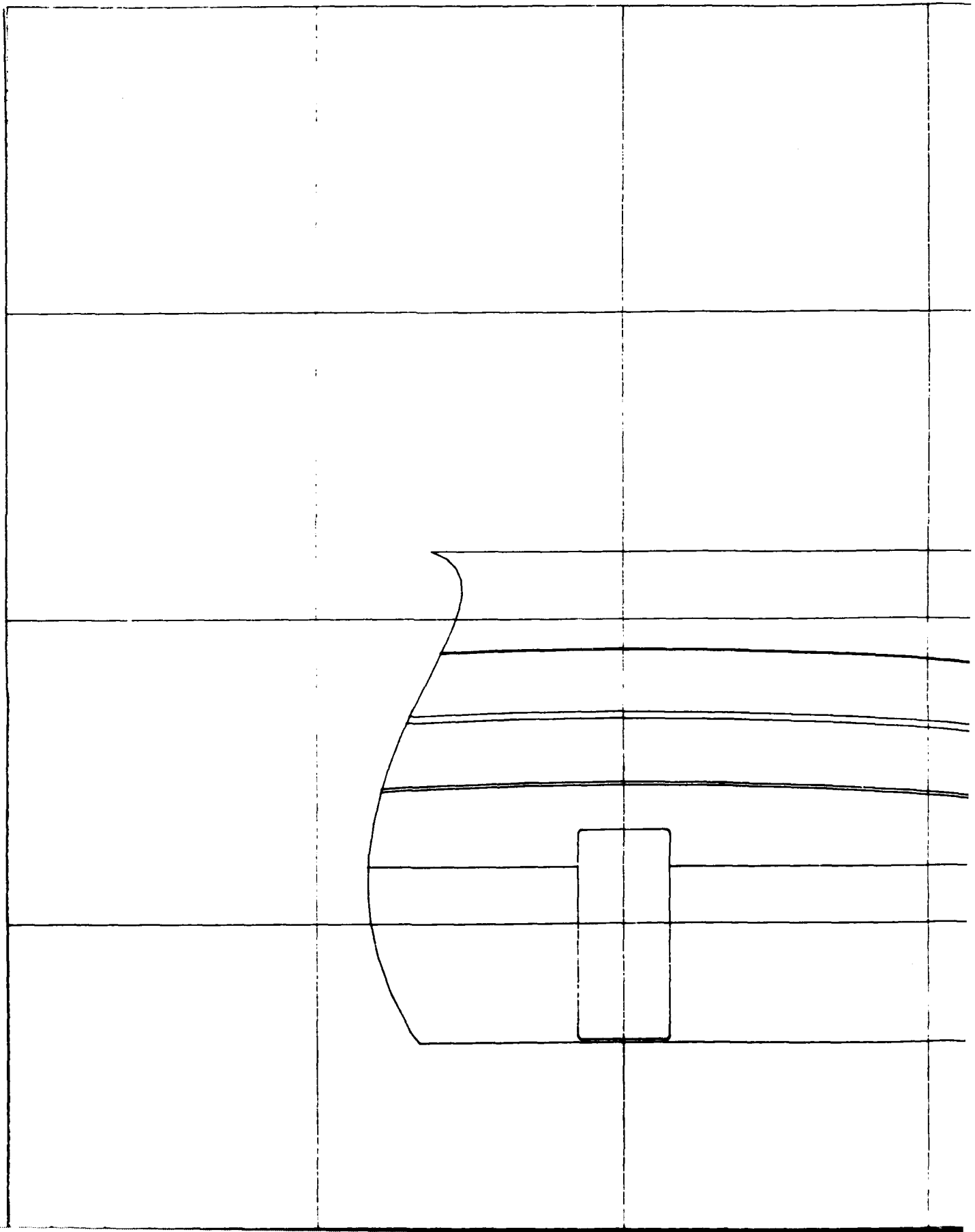
G.J. FRANK

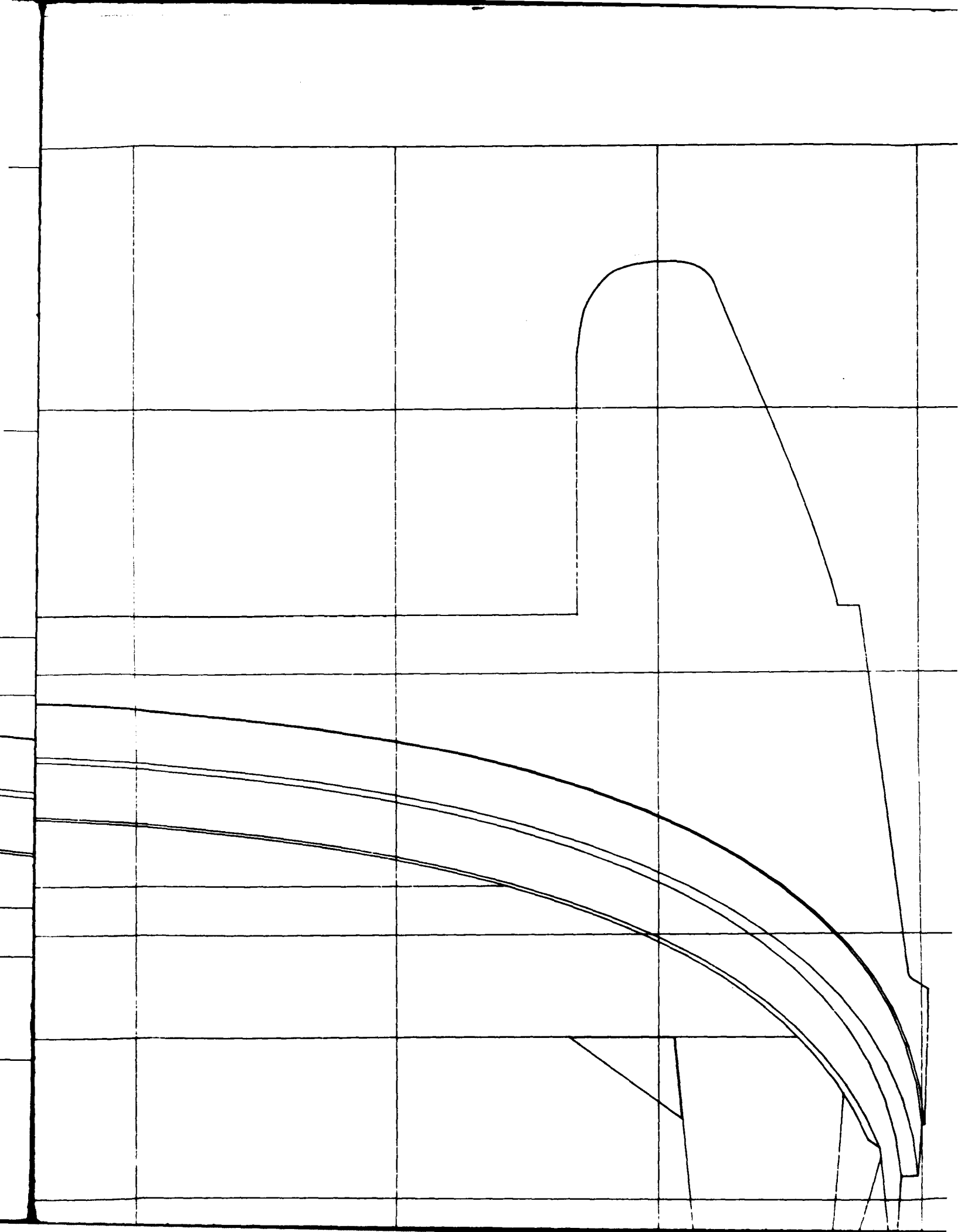
SCALE

1/2

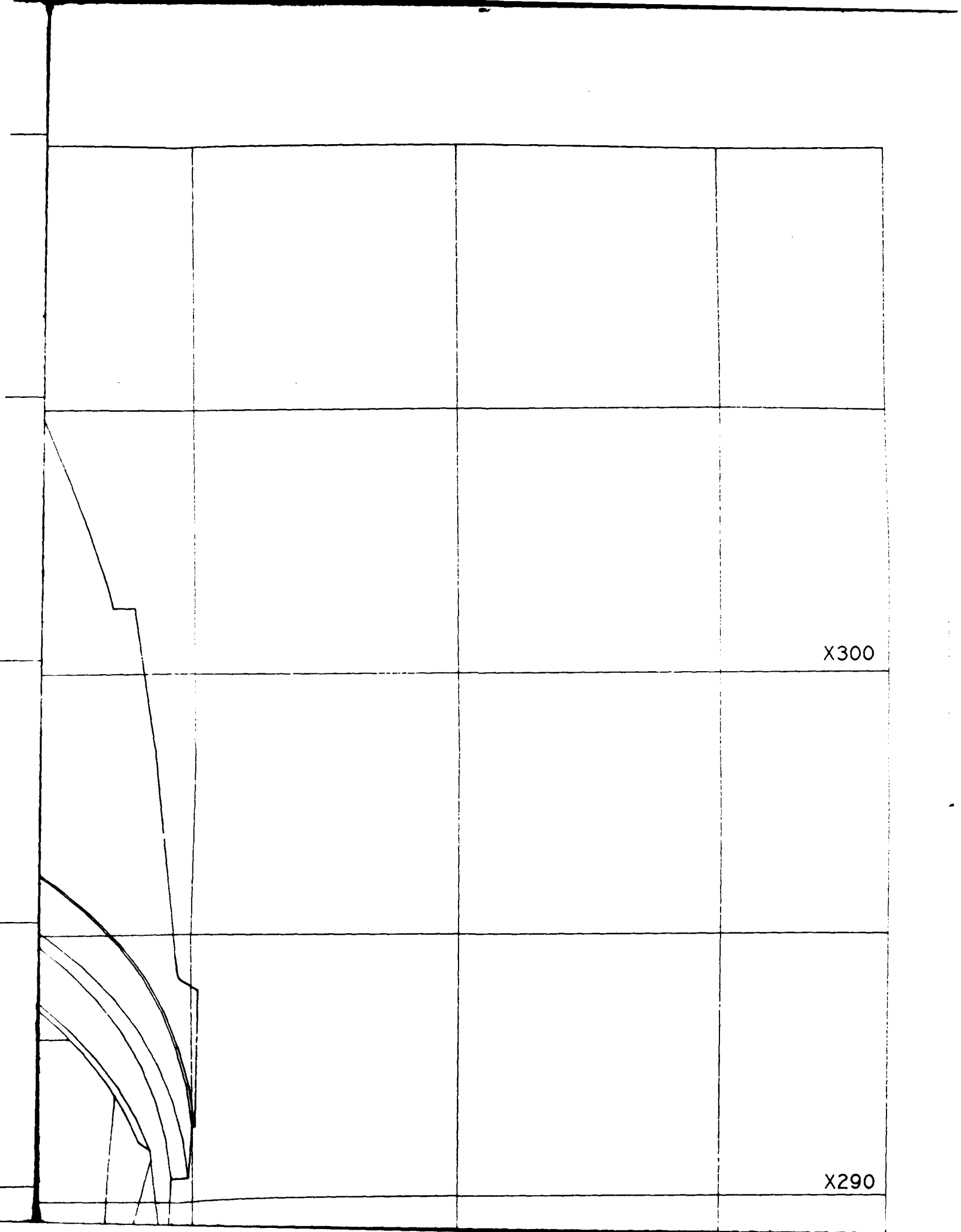
SHEET

1



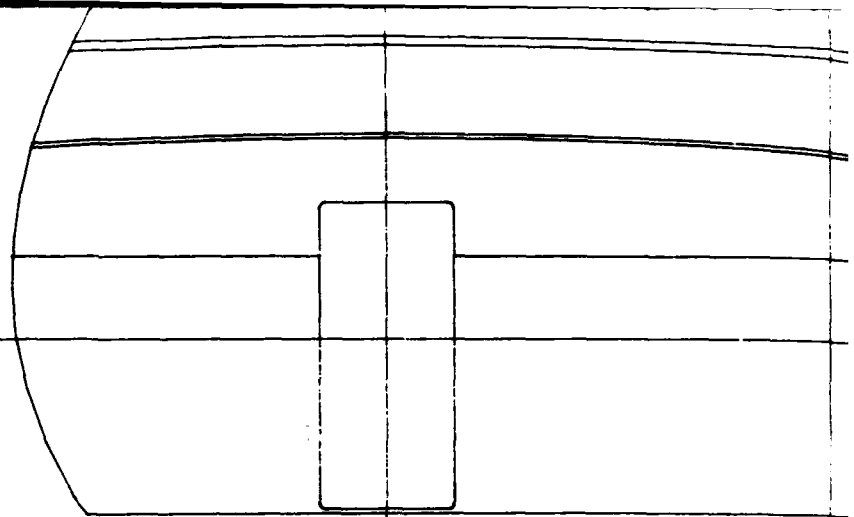




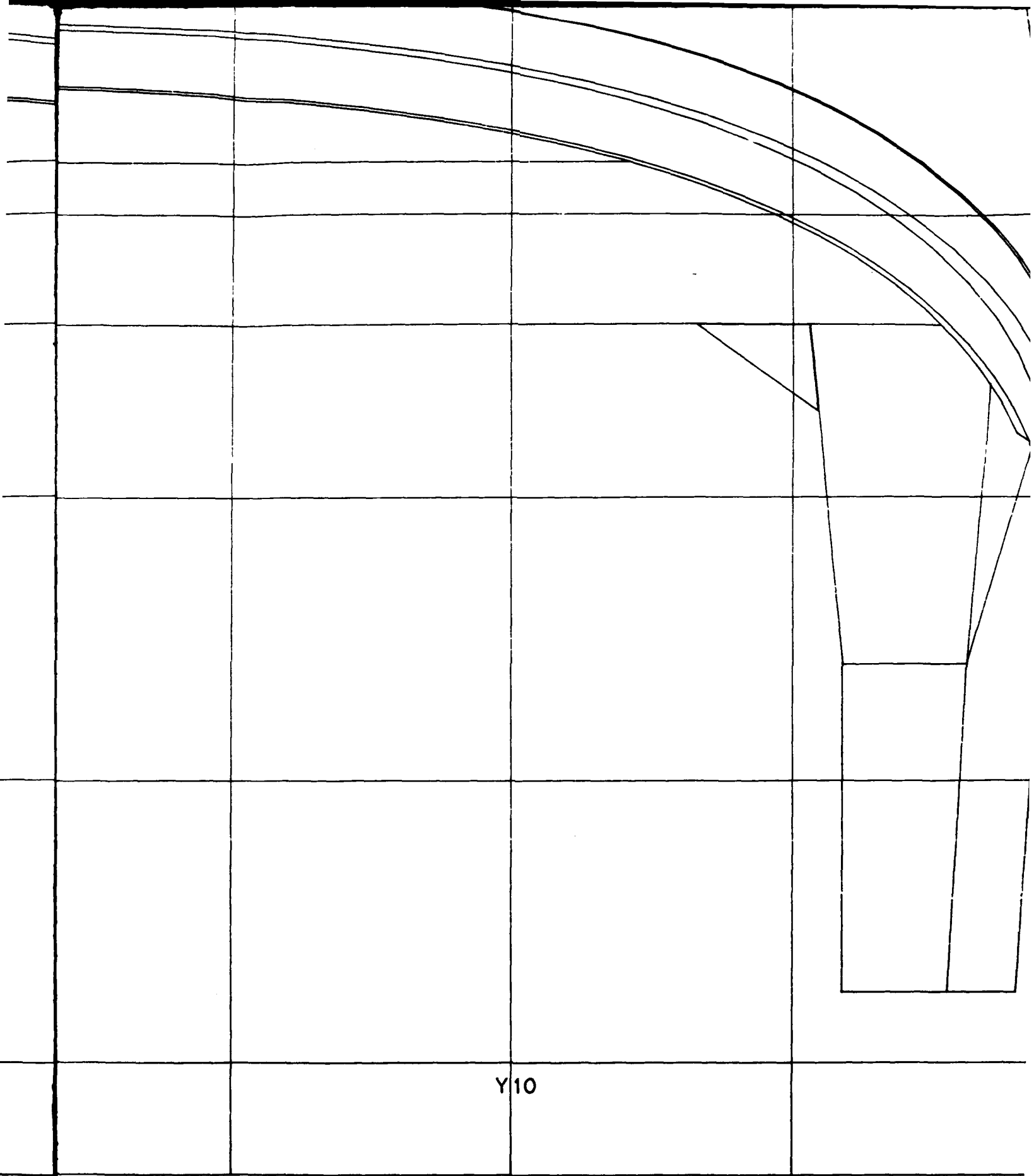


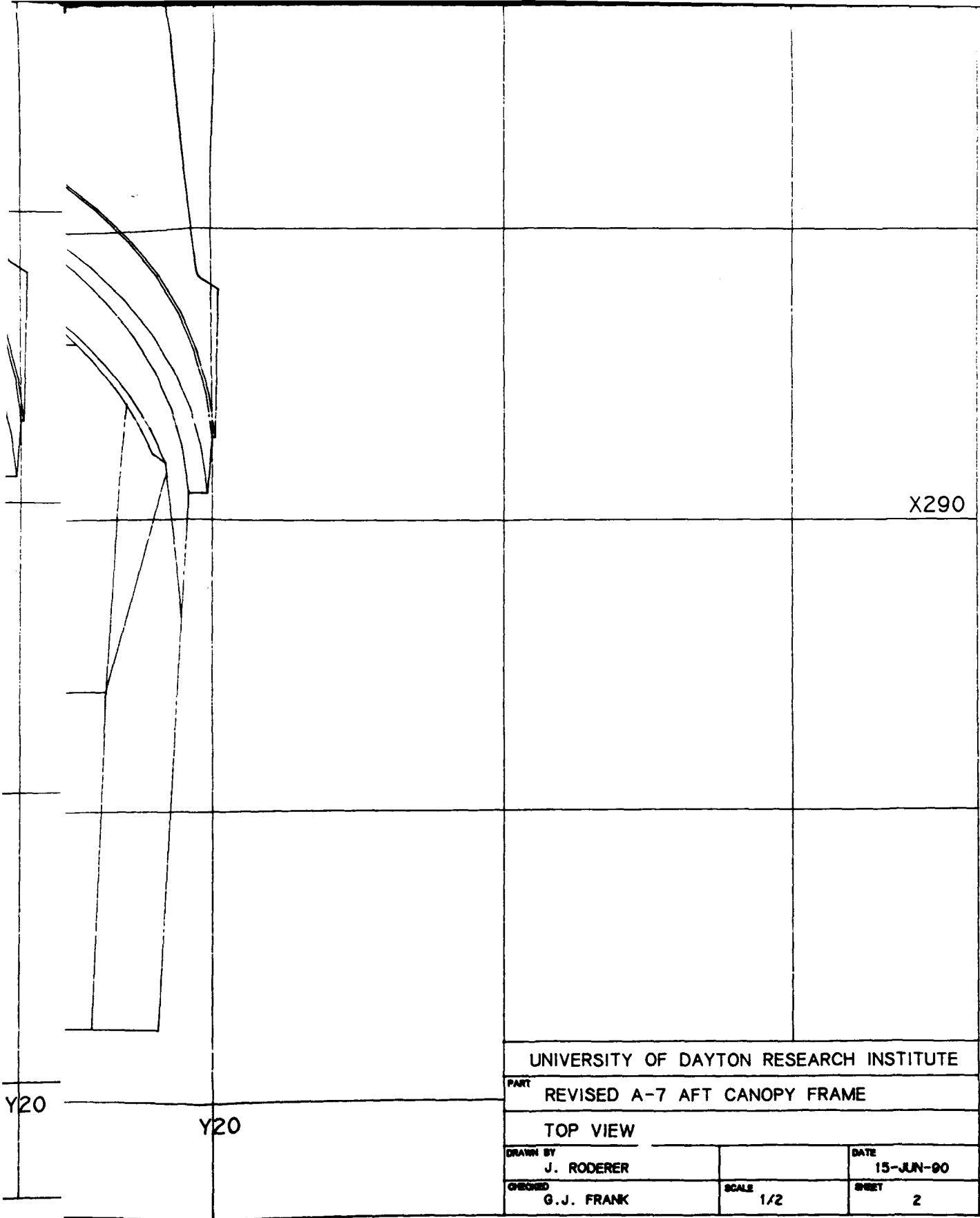
X300

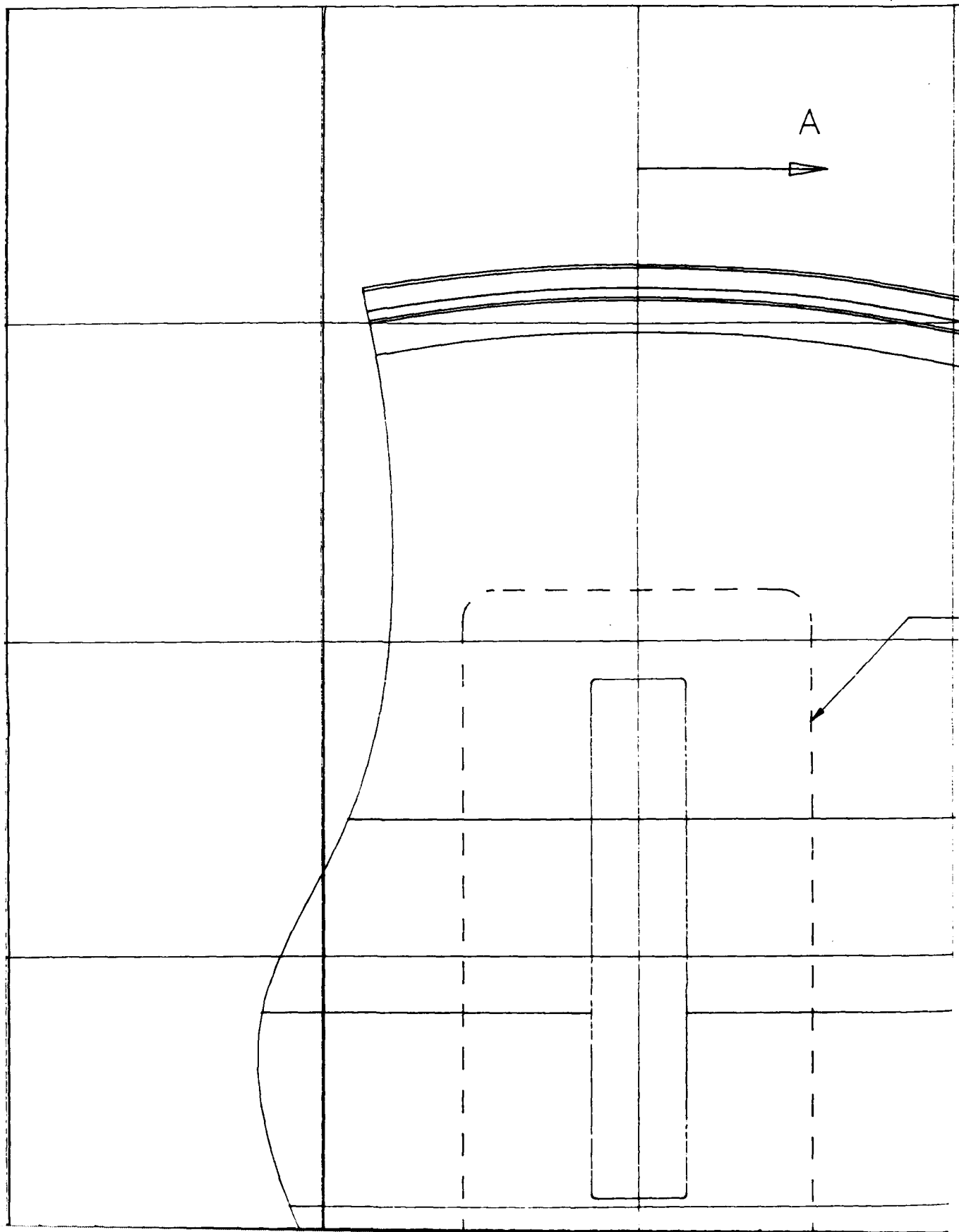
X290



YO





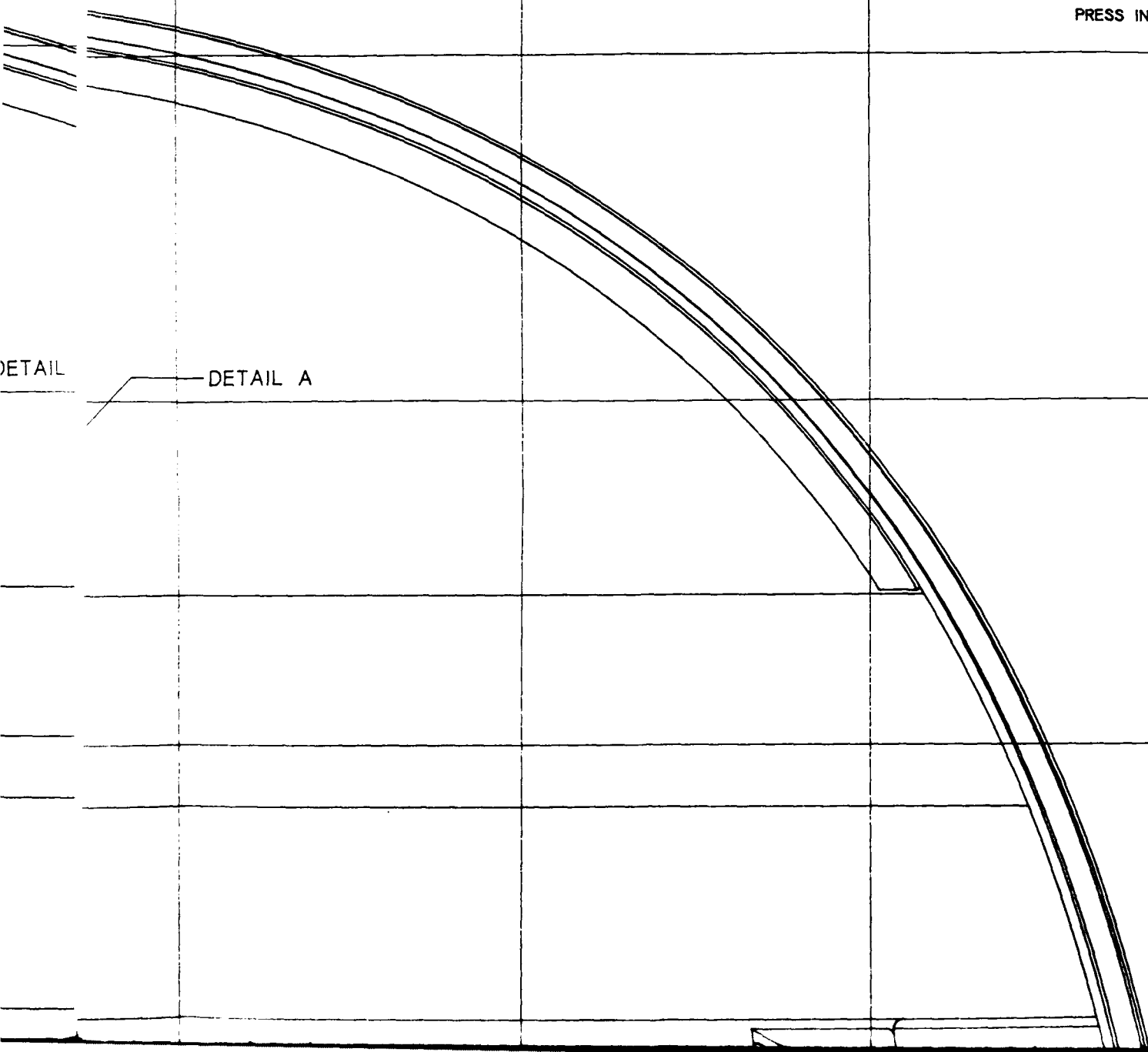


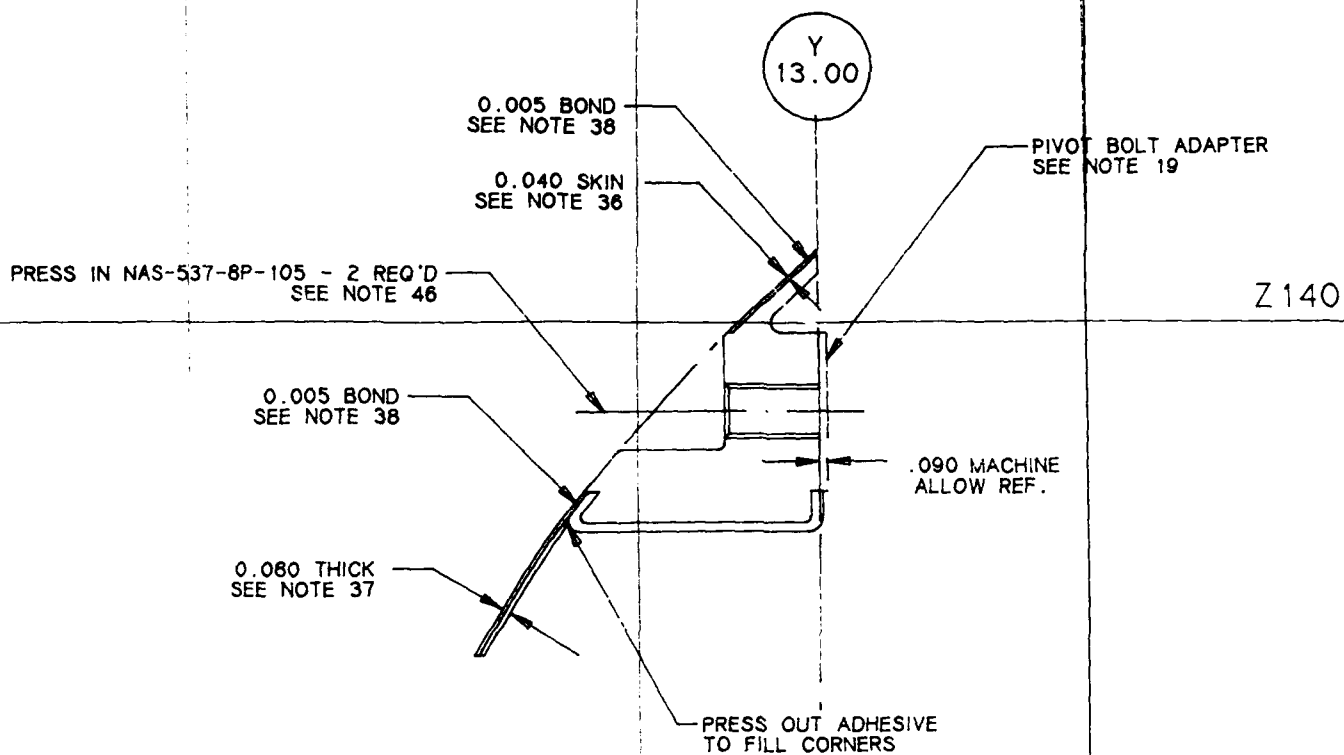
PRESS IN NAS-537-8F

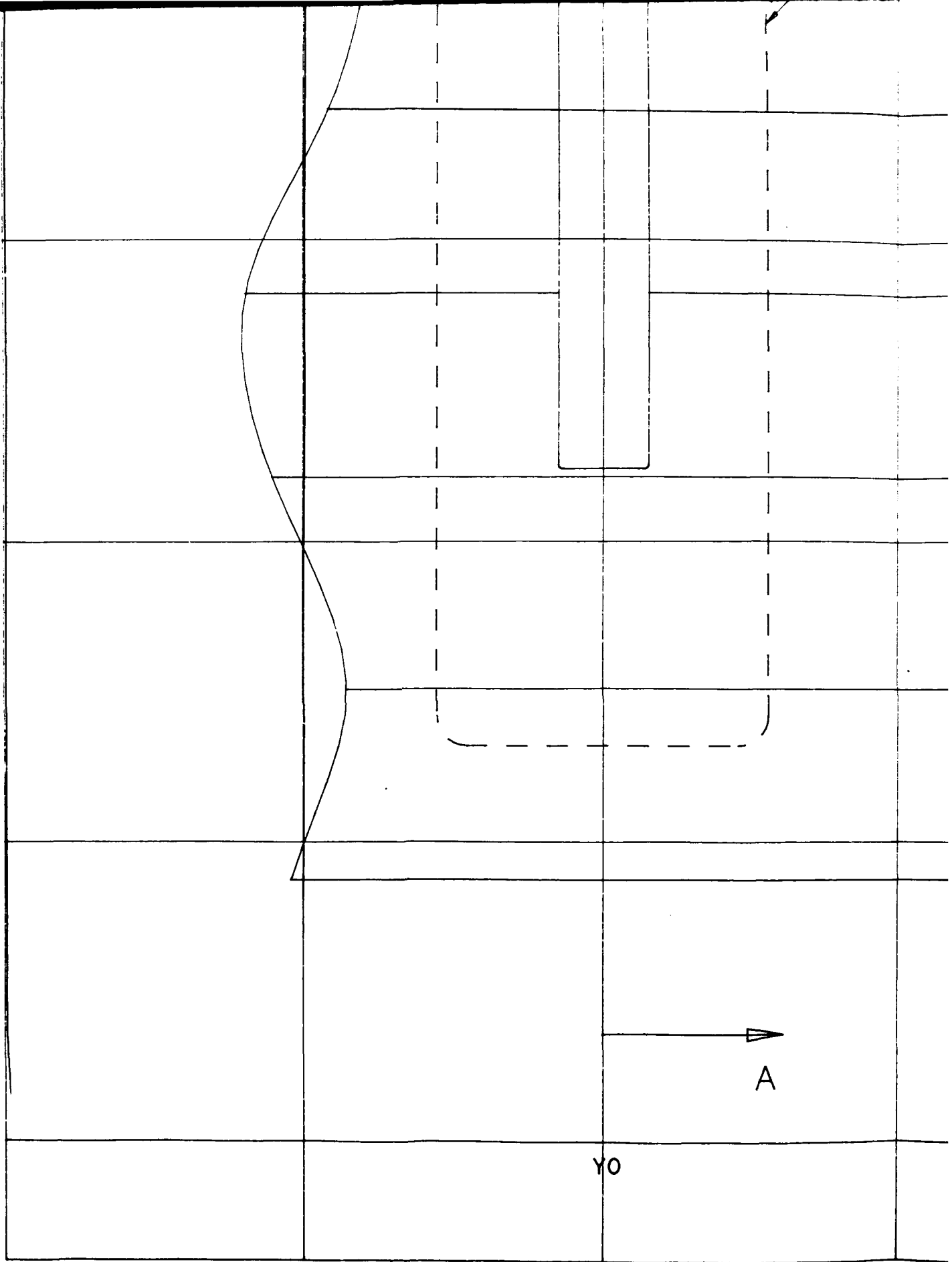
O  
SE

DETAIL

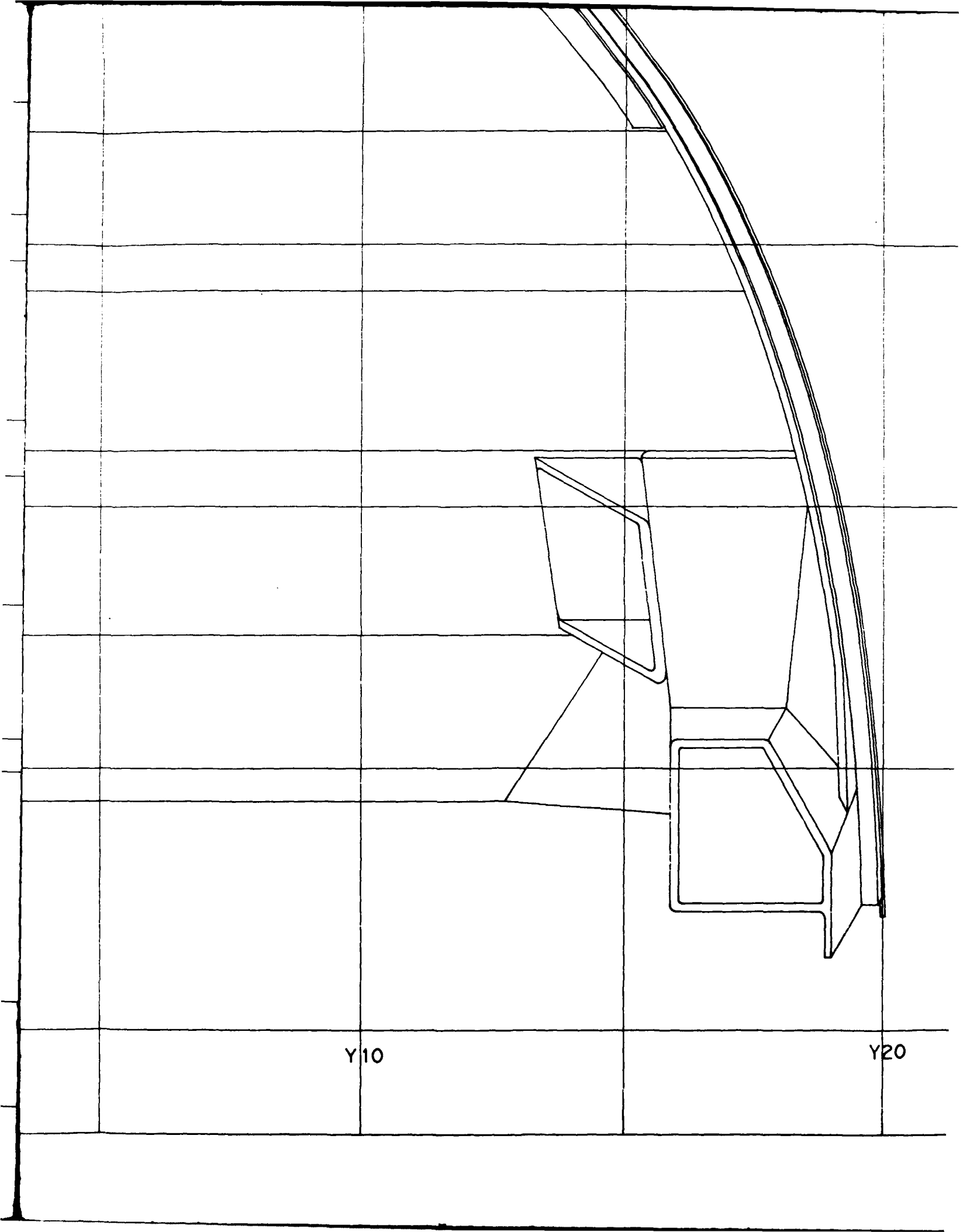
DETAIL A











Y10

Y20

# SECTION B-B

Z130

Z120

Y20

UNIVERSITY OF DAYTON RESEARCH INSTITUTE

PART

REVISED A-7 AFT CANOPY FRAME

FRONT VIEW, SECTION B-B

DRAWN BY

J. RODERER

DATE

15-JUN-90

CHECKED

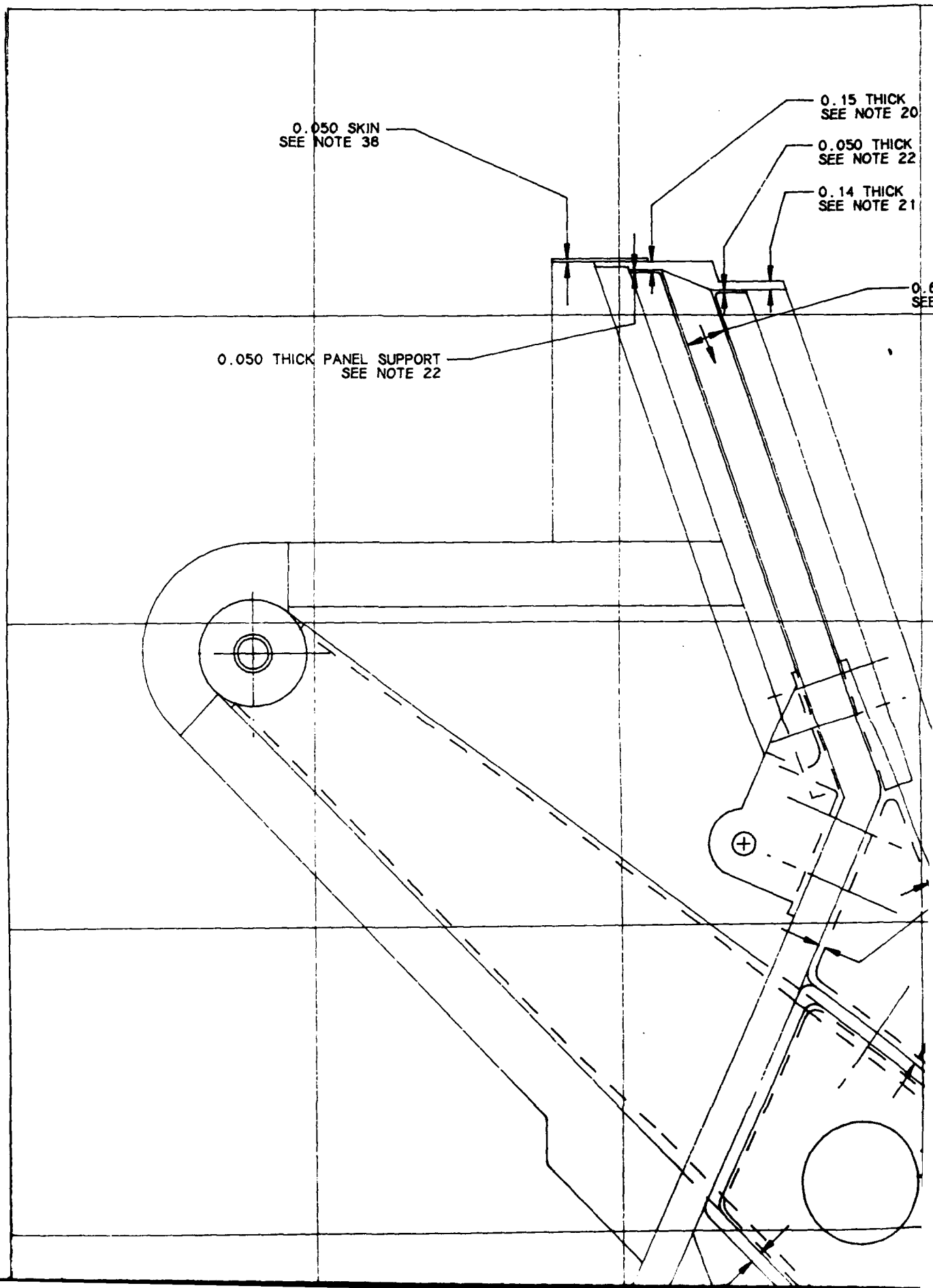
G.J. FRANK

SCALE

1/2

SHEET

3



0.15 THICK  
SEE NOTE 20

0.050 THICK  
SEE NOTE 22

0.14 THICK  
SEE NOTE 21

THICK  
SEE 3:

0.64 THICK  
SEE NOTE 32

0.12 THICK FLANGE  
SEE NOTES 16.50

0.12 THICK FLANGE  
SEE NOTES 15.50

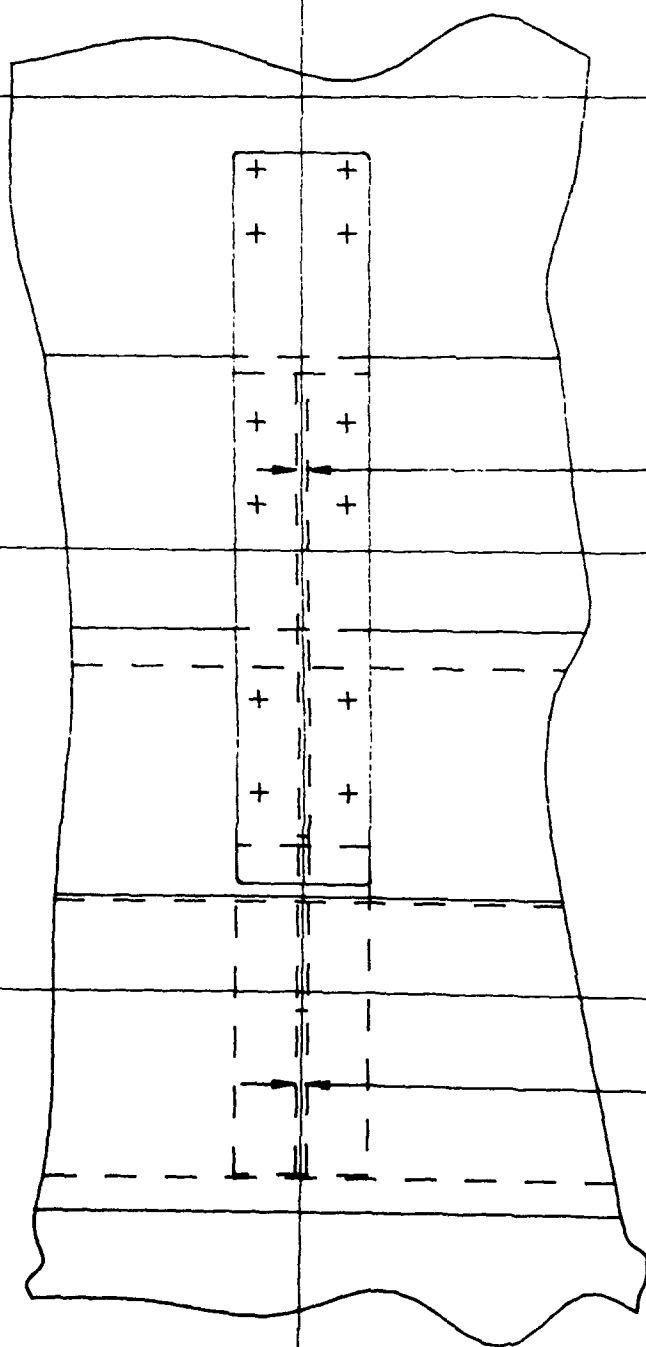
0.12 THICK FLANGE  
SEE NOTES 18.50

DRILL G - 4 PLACE  
INSTALL 1/4 DIA x 0.35 LONG  
BLIND BOLT 4 REQ'D  
SEE NOTE 35

0.040 THICK - 4 PLACE  
SEE NOTE 49

2.00 DIA CORE HOLE

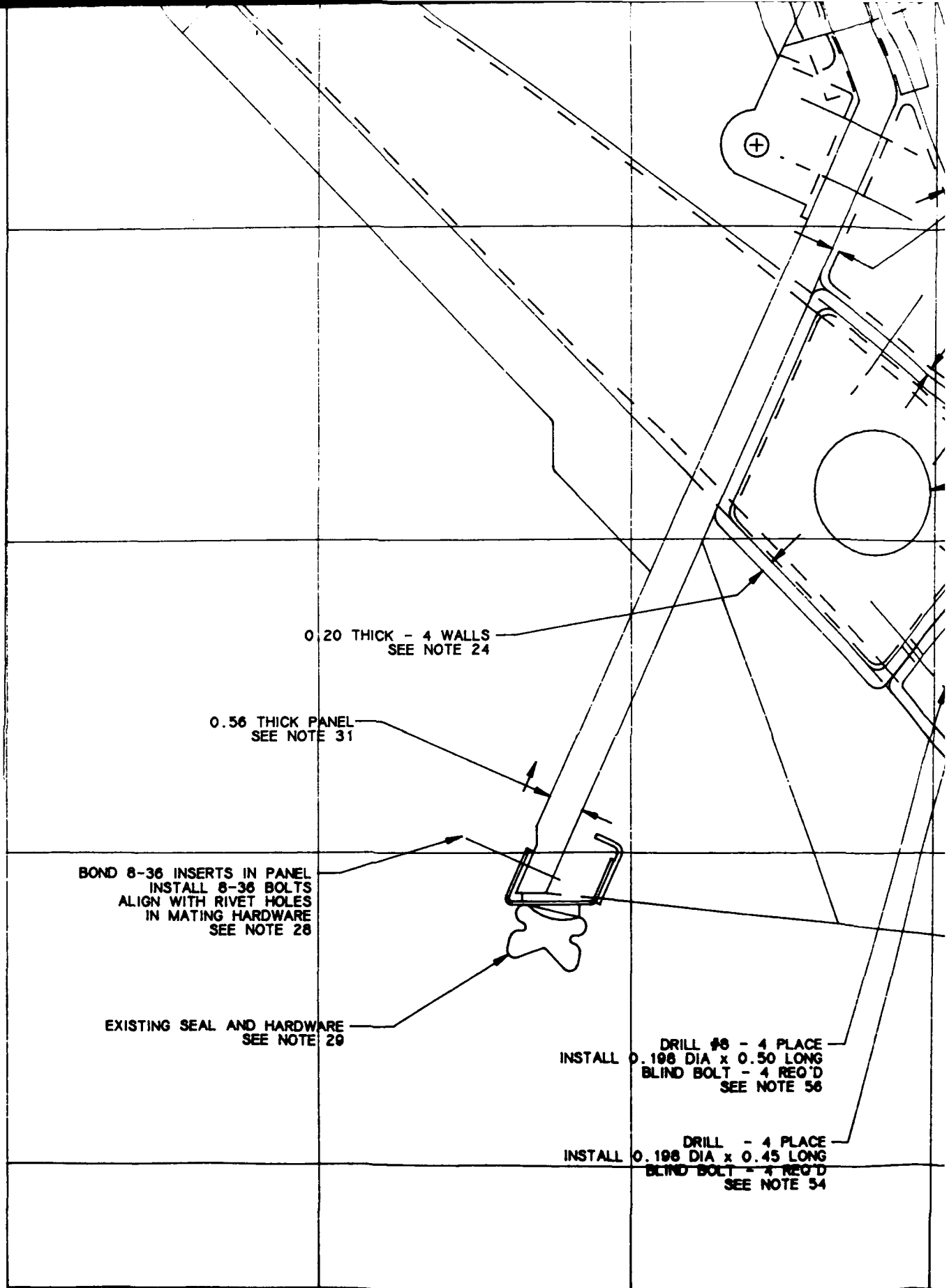
0.010 THICK BOND  
SEE NOTE 48



0.12 THICK WEB  
SEE NOTE 17

0.12 WEB  
SEE NOTE 49

DETAIL A



0.12 THICK FLANGE  
SEE NOTES 16.50

0.12 THICK FLANGE  
SEE NOTES 15.50

0.12 THICK FLANGE  
SEE NOTES 18.50

DRILL G - 4 PLACE  
INSTALL 1/4 DIA x 0.35 LONG  
BLIND DOLT 4 REQ'D  
SEE NOTE 35

0.040 THICK - 4 PLACE  
SEE NOTE 49

2.00 DIA CORE HOLE

0.010 THICK BOND  
SEE NOTE 48

0.20 THICK  
SEE NOTE 55

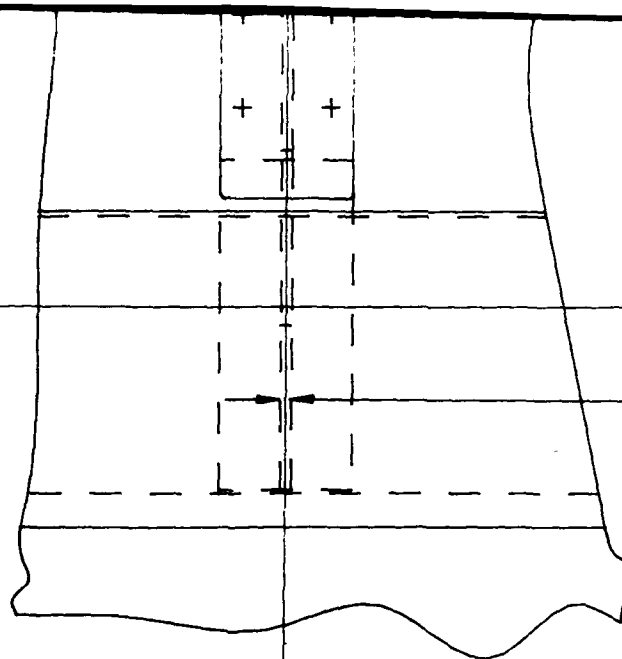
0.12 THICK WEB  
SEE NOTE 23

SECTION A-A

CE  
NG  
D  
56

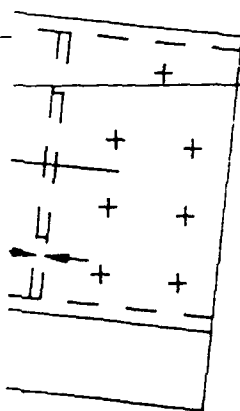
ACE  
DNG  
D  
54

EC



0.12 WEB  
SEE NOTE 49

DETAIL A



UNIVERSITY OF DAYTON RESEARCH INSTITUTE

PART

REVISED A-7 AFT CANOPY FRAME

SECTION A-A. DETAIL A

DRAWN BY

J. RODERER

DATE

15-JUN-90

CHECKED

G.J. FRANK

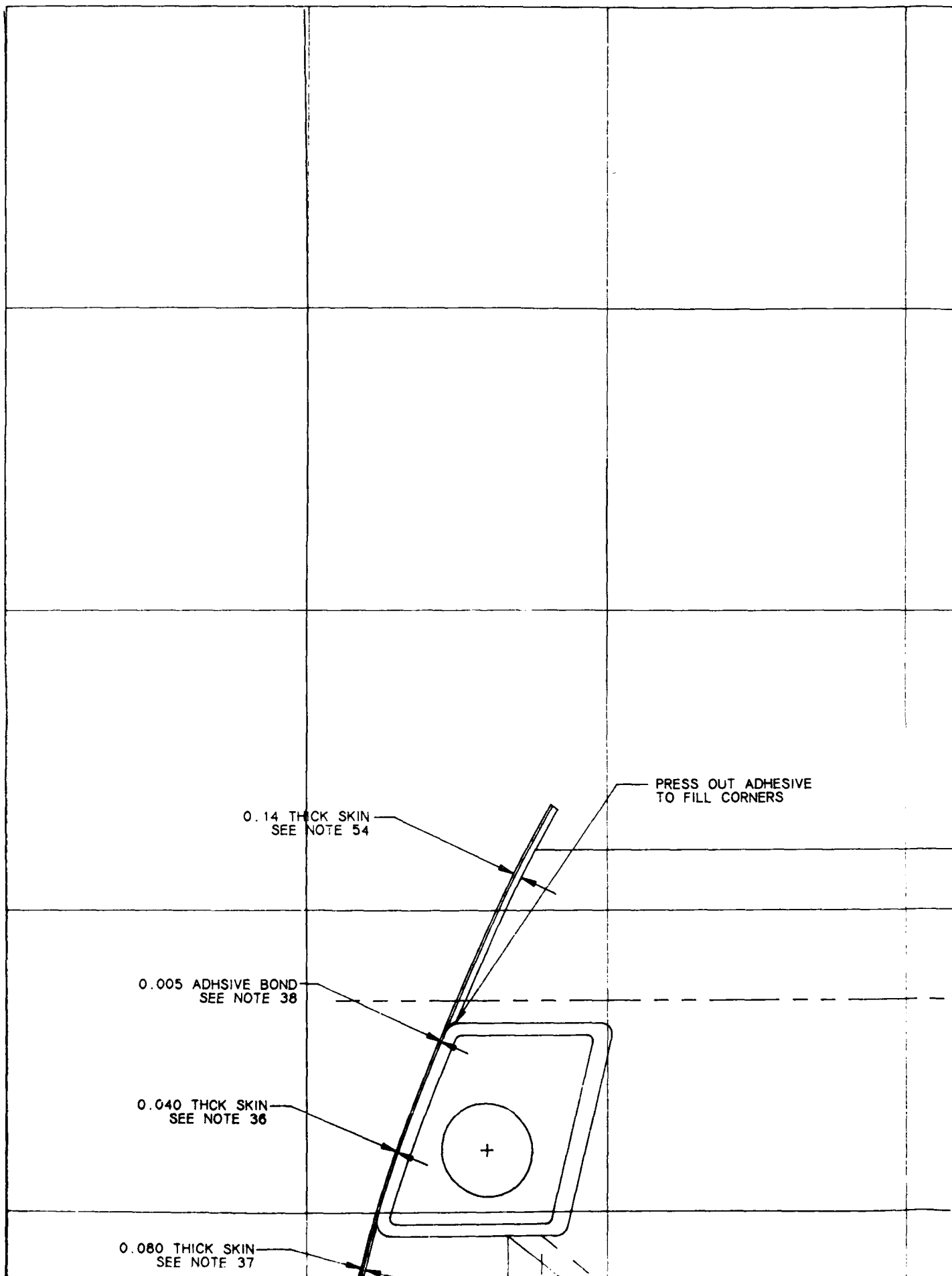
SCALE

1/2

SHEET

4

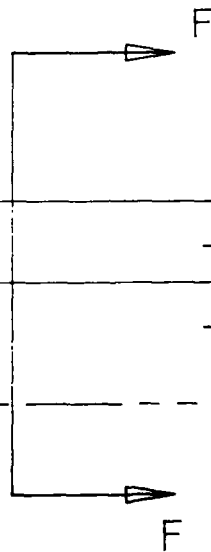




0.64

1  
s

0.56



BOND BUSHING IN PANEL - 4 PLACE  
INSTALL 10-32 BOLT & NUT -- 4 REQ'D  
SEE NOTE 33

0.64 THICK PANEL  
SEE NOTE 32

SEE NOTE 30

TAPER PANEL  
SEE NOTE 44

0.56 THICK PANEL  
SEE NOTE 31

## SECTION F-F

BOND BUSHING IN PANEL - 4 PLACE  
INSTALL 10-32 BOLT AND NUT - 4 REQ'D  
SEE NOTE 34

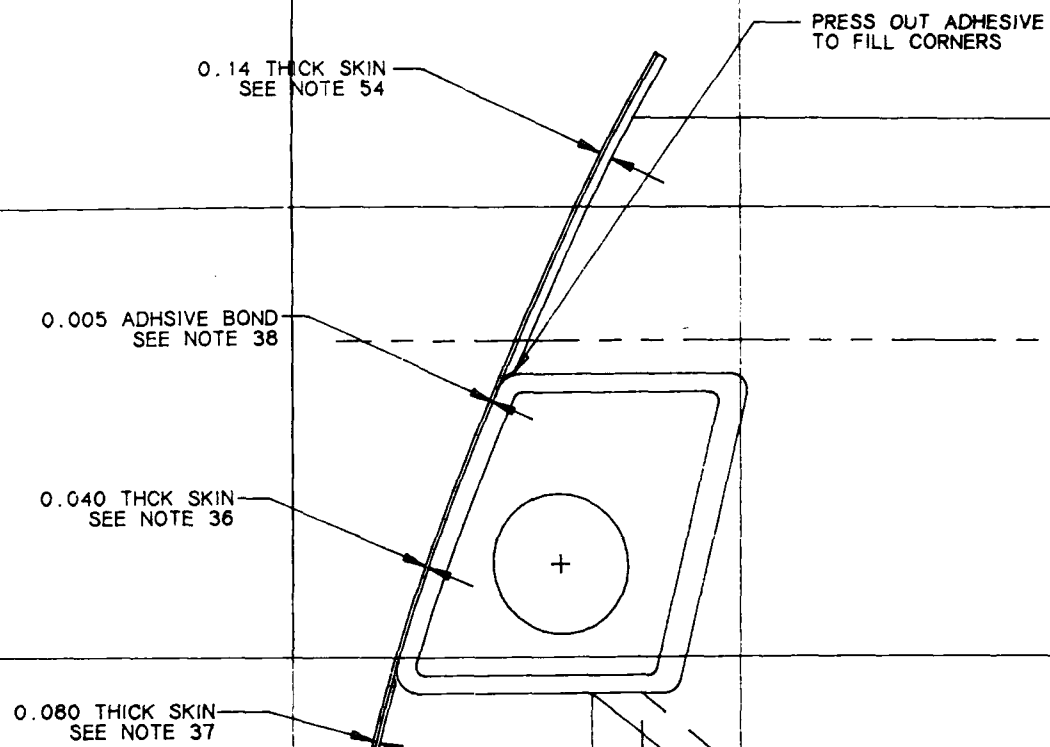
TRACE OF Z130

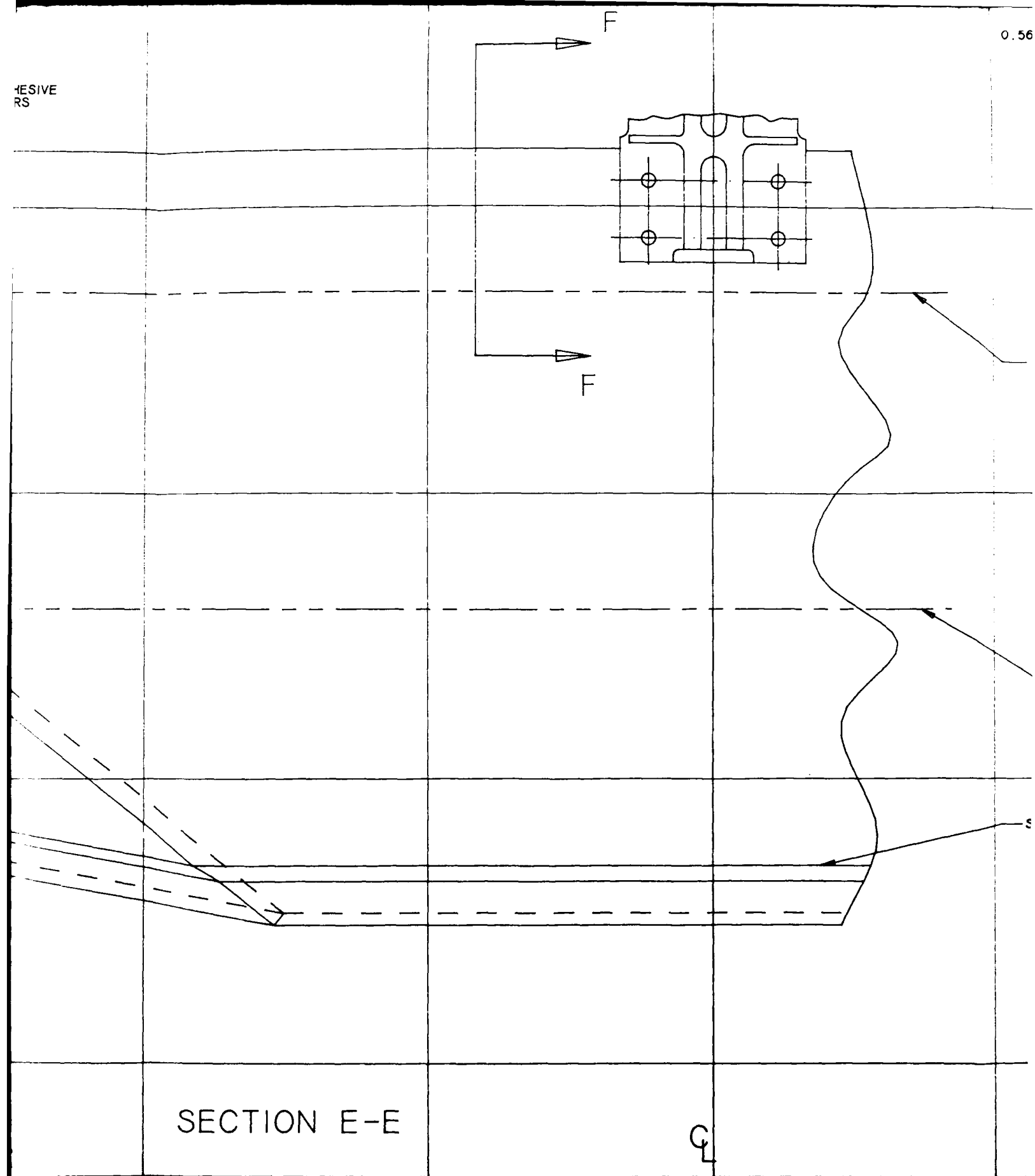
W PANEL  
NOTE 32

R PANEL  
NOTE 44

ICK PANEL  
NOTE 31

CE OF Z1



RESISTIVE  
RS

CK  
N

0.56 THICK PANEL  
SEE NOTE 31

# SECTION F-F

BOND BUSHING IN PANEL - 4 PLACE  
INSTALL 10-32 BOLT AND NUT - 4 REQ'D  
SEE NOTE 34

ICE

TRACE OF Z130

TRACE OF Z125

NO

SEE NOTE 51

UNIVERSITY OF DAYTON RESEARCH INSTITUTE

PART

REVISED A-7 AFT CANOPY FRAME

SECTION E-E, SECTION F-F

DRAWN BY

J. RODERER

DATE

15-JUN-90

CHECKED

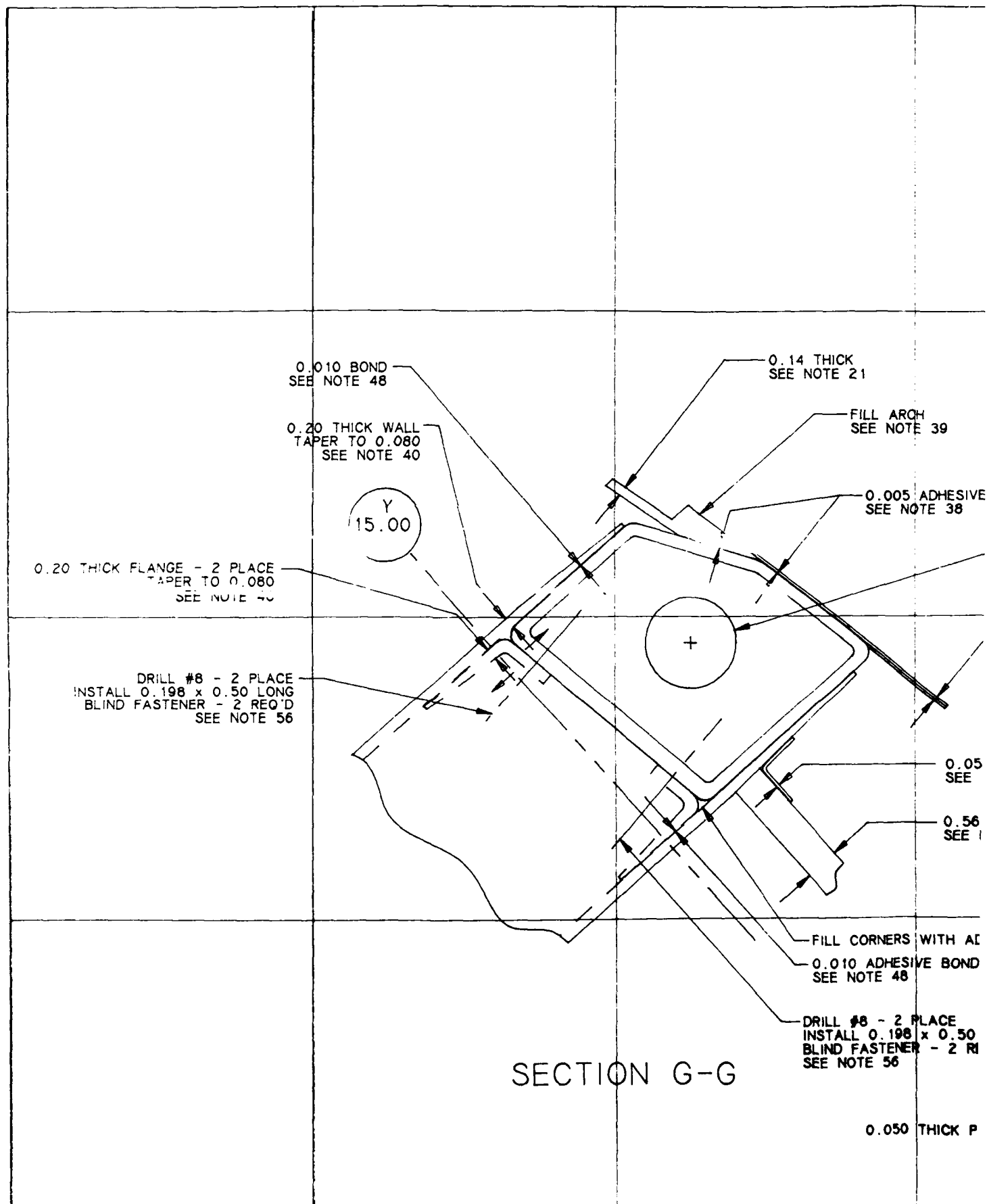
G.J. FRANK

SCALE

1/2

SHEET

5



THICK  
NOTE 21

FILL ARCH  
SEE NOTE 39

ND 0.005 ADHESIVE BOND  
SEE NOTE 38

1.50 1.50 DIA CORE HOLE  
0.080 THICK  
SEE NOTE 37

THICK  
NOTE 22 0.050 THICK PANEL SUPPORT  
SEE NOTE 22

CK P.  
31 0.56 THICK PANEL  
SEE NOTE 31

0.090 THICK  
SEE NOTE 11

TAPER WALL  
SEE NOTE 13

0.20 THICK  
SEE NOTE 12

VE FILL CORNERS WITH ADHESIVE  
0.010 ADHESIVE BOND  
SEE NOTE 48

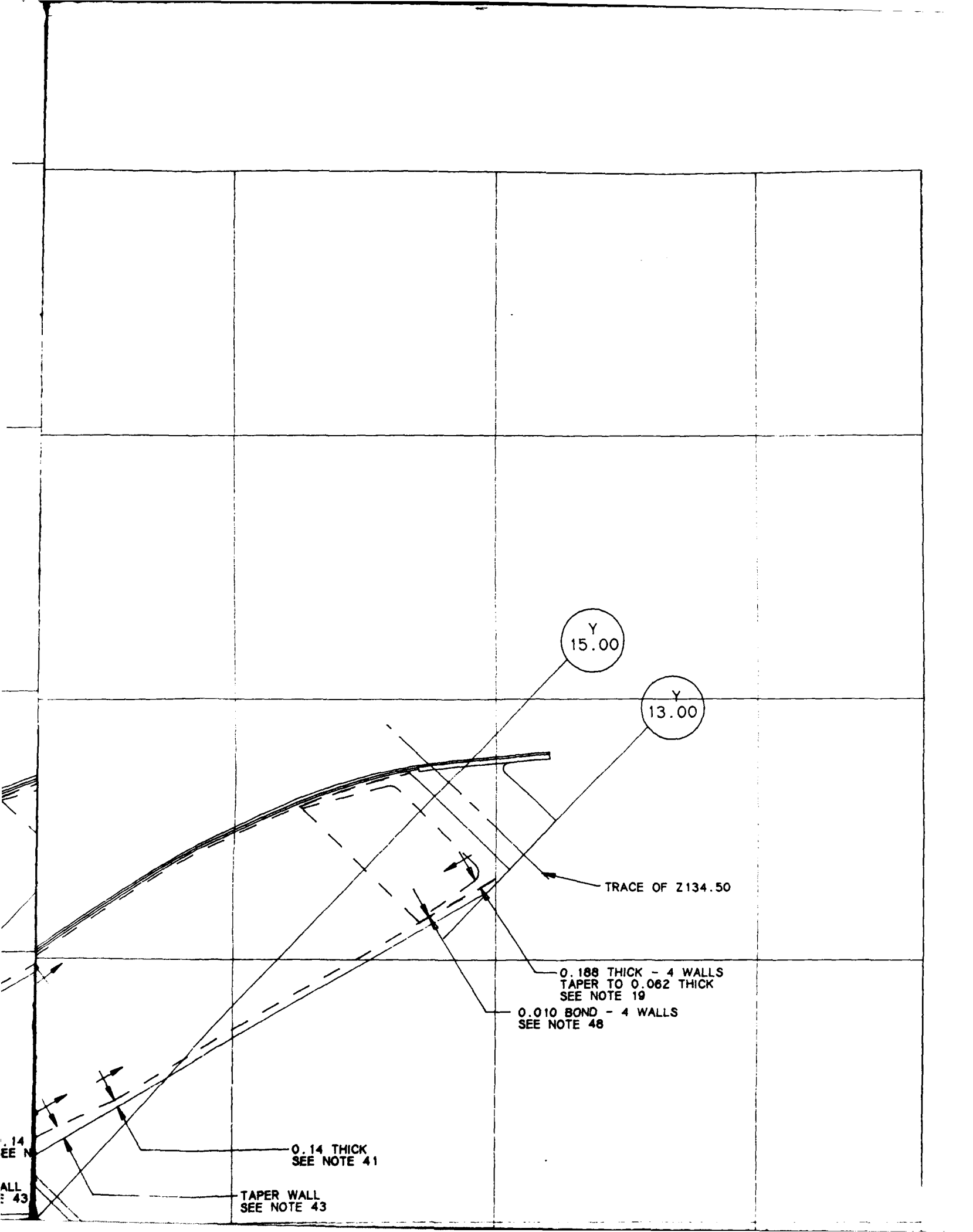
3 DRILL #8 - 2 PLACE  
INSTALL 0.198 x 0.50 LONG  
BLIND FASTENER - 2 REQ'D  
SEE NOTE 56

0.20 THICK WEB  
SEE NOTE 45

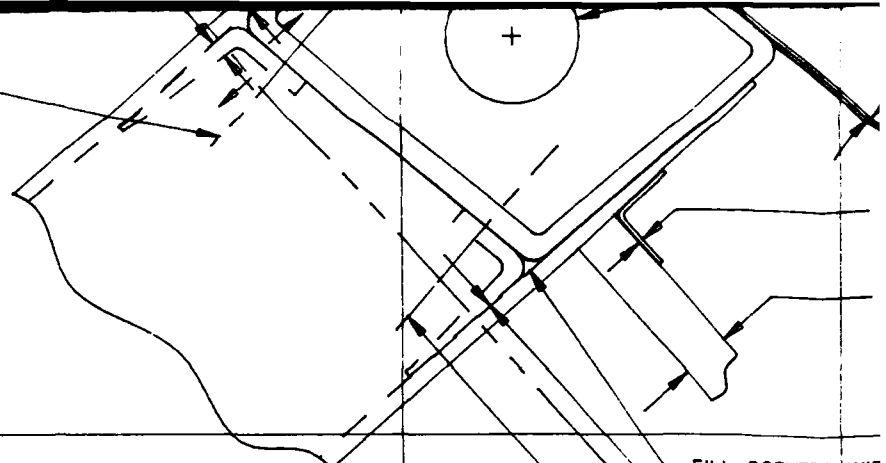
SUP  
NOT 0.050 THICK PANEL SUPPORT  
SEE NOTE 22

TAP  
SEE





DRILL #8 - 2 PLACE  
INSTALL 0.198 x 0.50 LONG  
BLIND FASTENER - 2 REQ'D  
SEE NOTE 56



FILL CORNERS WITH  
0.010 ADHESIVE  
SEE NOTE 48

DRILL #8 - 2 PLACE  
INSTALL 0.198 x 0.50 LONG  
BLIND FASTENER - 2 REQ'D  
SEE NOTE 56

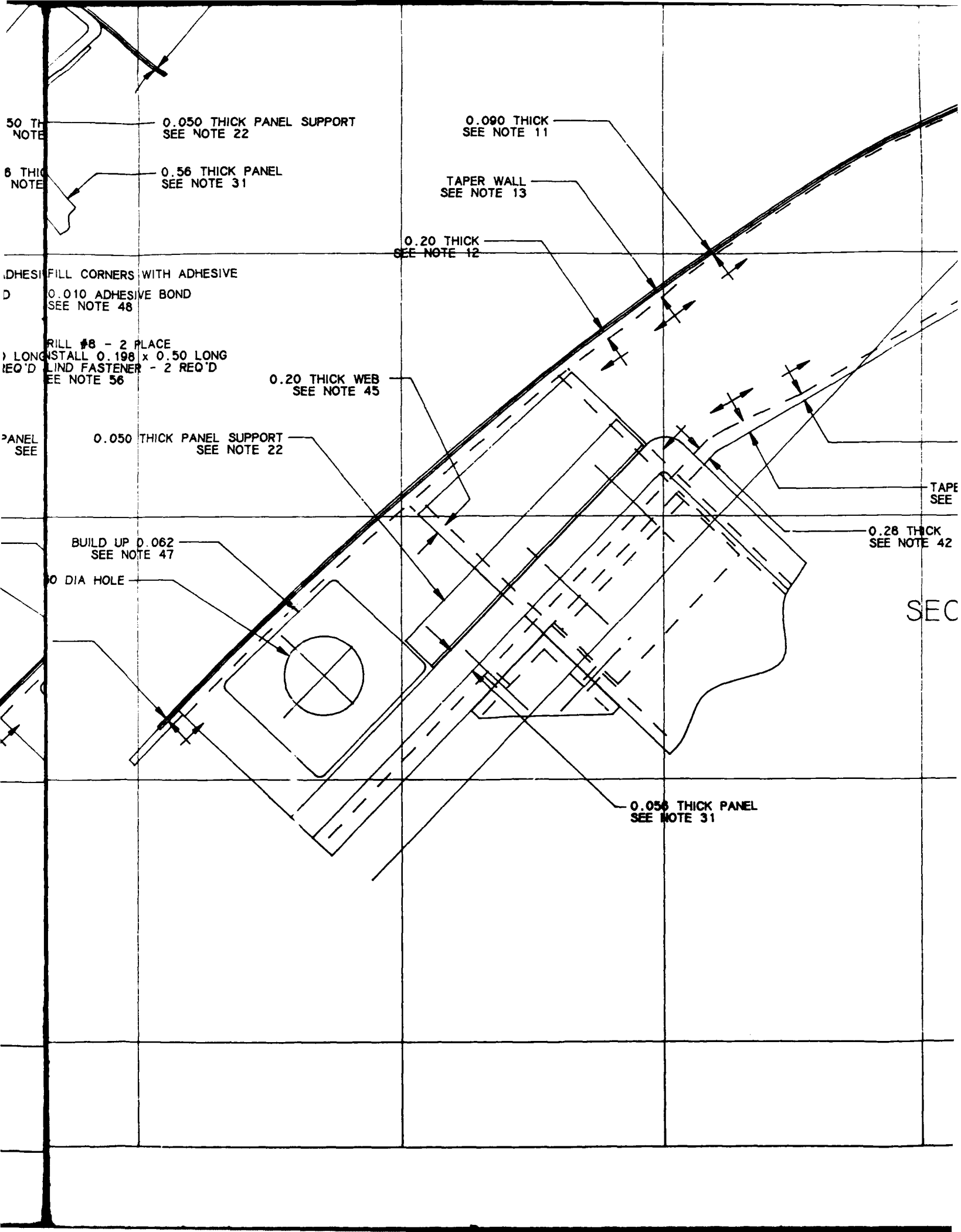
## SECTION G-G

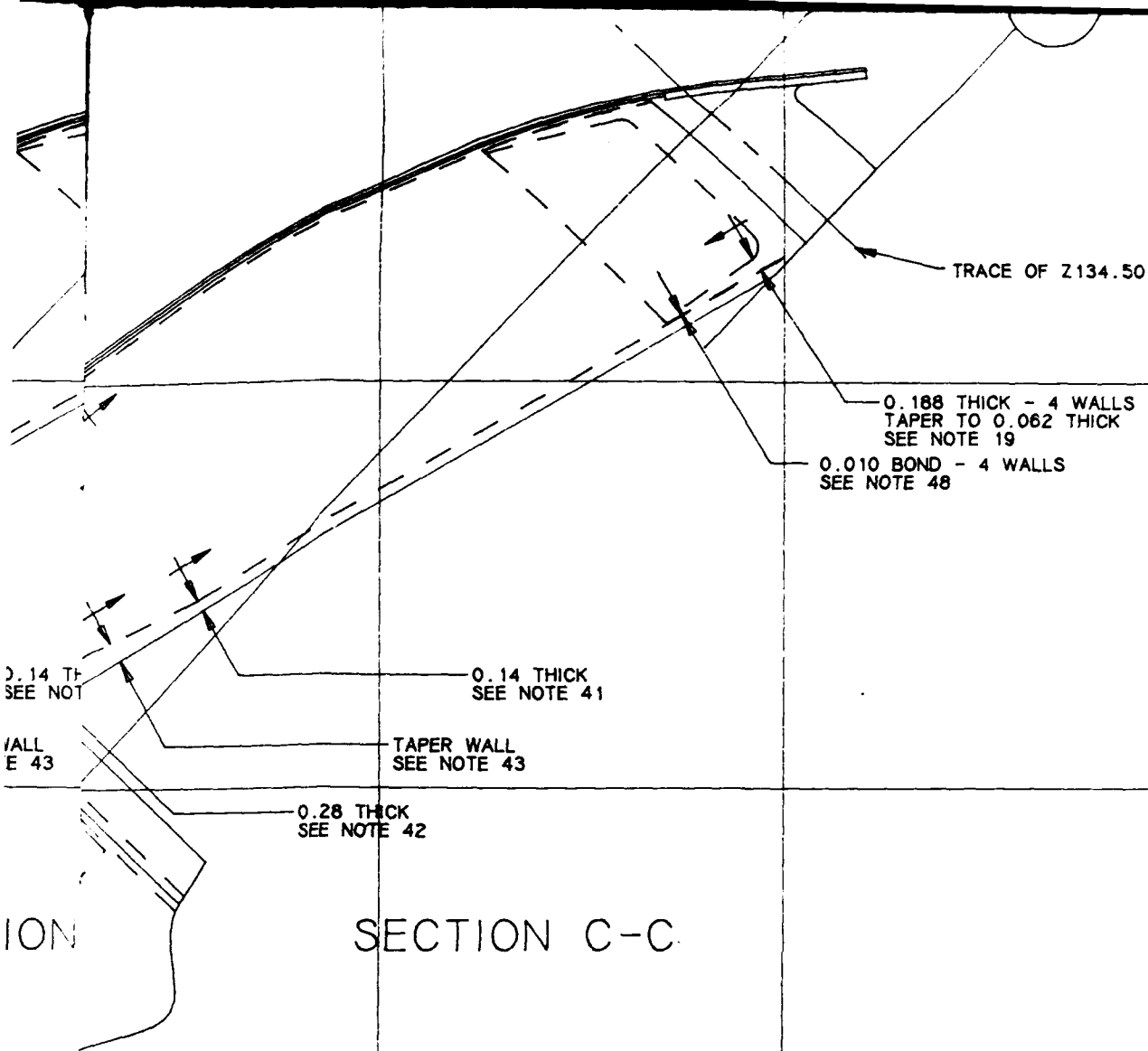
0.050 THICK

BUILD UP 0.010  
SEE NOTE 48

1.50 DIA HOLE

0.080 THICK





## SECTION C-C

PANEL

UNIVERSITY OF DAYTON RESEARCH INSTITUTE

PART

REVISED A-7 AFT CANOPY FRAME

SECTION C-C, SECTION G-G

DRAWN BY

J. RODERER

DATE

15-JUN-90

CHECKED

G.J. FRANK

SCALE

1/2

SHEET

6